UNIVERSITY OF CALIFORNIA
SANTA CRUZ

EVOLUTION OF TROPICAL PACIFIC OCEAN DYNAMICS: SURFACE TO SUBSURFACE TEMPERATURE VARIABILITY FROM THE PLIOCENE TO PRESENT

A dissertation submitted in partial satisfaction
of the requirements for the degree of

DOCTOR OF PHILOSOPHY

in

OCEAN SCIENCES

by

Heather L. Ford

June 2013

The Dissertation of Heather L. Ford is approved:

_____
Professor A. Christina Ravelo, chair

_____
Professor Andrew M. Moore

_____
Professor James C. Zachos

_____
Research Scientist Adina Paytan

_____

Tyrus Miller
Vice Provost and Dean of Graduate Studies

Table of Contents

Table of Figures

Table of Tables

Abstract

EVOLUTION OF TROPICAL PACIFIC OCEAN DYNAMICS:
SURFACE TO SUBSURFACE TEMPERATURE VARIABILITY
FROM THE PLIOCENE TO PRESENT

HEATHER L. FORD

The tropical Pacific is a significant component of the ocean's climate system and a source of considerable global climate variability, including El Niño events. Tightly coupled sea surface and thermocline dynamics influence tropical climate on a variety of spatial and temporal scales. Today, the tropical Pacific is characterized by a western warm pool with warm sea surface temperatures (SSTs) and a deep thermocline and an eastern "cold tongue" with cold SSTs and a shallow thermocline. Records of past climate surface and subsurface temperature variability, on long and short times scales, may aid in identifying the radiative and dynamic forcing important to tropical climate during different global climate states. During the Pliocene warm period (3.0-4.3 Ma) and Last Glacial Maximum (LGM, ~0.020 Ma) the global mean state was substantially different and may have influenced the behavior and strength of various processes and mechanisms that determine tropical climate. In this dissertation, I use geochemical techniques, including the novel application of the magnesium-calcite ratio of individual planktonic foraminifera, to investigate the different processes that determine tropical change on different time scales and background climate states.

In the first project, I generated stable isotope and minor element records using a subsurface dwelling planktonic foraminifera from a transect of sites across the

Pacific cold tongue. Using subsurface temperatures as a proxy for thermocline depth, my records suggest there was a gradual shoaling of the eastern equatorial Pacific thermocline from the early Pliocene to present day. This pronounced change in the background state of the cold tongue region influenced SSTs and implies dynamic processes, including atmospheric circulation and global heat balance, may have operated differently during the Pliocene warm period and contributed to global warmth.

In the second and third projects, I use the minor element ratio of individual surface and subsurface dwelling foraminifera to monitor the SST and subsurface temperature background state, high resolution variability and radiative and dynamic processes that determine tropical climate. The results suggest the tropical western Pacific has responded primarily to pCO_2-radiative forcing on glacial-interglacial time scales since the early Pliocene. In contrast, the eastern Pacific has responded to changes in dynamic and radiative forcing during the last glacial period, which influenced the background spatial pattern of the cold tongue region. Additionally, changes in individual foraminifera variability suggest a decrease in El Niño Southern Oscillation during the most recent glacial period in comparison to the Holocene. These records show that different scales of variability (i.e. long-term, glacial-interglacial, and seasonal/interannual) may illuminate the processes and mechanisms important to paleoclimate interpretations on various temporal and spatial scales.

Acknowledgements

While at Santa Cruz, I received an immense amount of financial, scholarly, and emotional support. Above all, Christina Ravelo has shared her expertise and encouraged me to develop a holistic approach to science and life. I am grateful for her guidance and patience. Thank you for your generous support.

I was fortunate to receive many sources of funding while at UCSC. In addition to teaching assistant positions through the Ocean Sciences Department and graduate student researcher funding through National Science Foundation grants awarded to A.C. Ravelo, I received fellowships from The Consortium of Ocean Leadership's Schlanger Fellowship, ARCS Foundation, and the University of California President's Dissertation-Year Fellowship. I also received research funding from the Institute of Geophysics and Planetary Physics Research Grant and several travel grants from the Graduate Student Association.

My thesis benefited from the comments of Andrew Moore, James Zachos and Adina Paytan. Andy often asked difficult questions to ground my interpretations and my research has benefitted from his influence. Jim was instrumental in procuring the laser system at UCSC. Additionally, I benefitted from countless beer hour conversations where topics meandered from science, career advice and pop culture. Adina has been an honest supporter and has continuously assured me that life and career always sort themselves out. She also encouraged me to participate in the high school summer research program. Mentoring Sahil Chopra for two summers was a rewarding experience and I am inspired by his hard work and potential.

Many individuals provided research assistance and companionship. My co-author Steven Hovan at Indiana University at Pennsylvania provided useful feedback on the Ford et al., 2012 manuscript. Pratigya Polissar at Lamont-Doherty Earth Observatory contributed immensely to my research providing code, analyses and figures. I was also very fortunate to sail with him in the equatorial Pacific on two separate occasions. He has been thoroughly encouraging and provided thoughtful feedback on manuscripts and research proposals. Rob Franks provided tremendous analytical support and was exceptionally valuable in establishing the laser ablation system at UCSC. Though I was often frustrated, Rob gently guided me through the tough analytical patches and gave me the confidence I needed to succeed. Linda Anderson has been an amazing friend and mentor. Her bright smile and encouraging words have been a constant source of support. She is a gifted artist and scientist and has been an inspiration to me. Andrea Erhardt has been my constant companion through graduate school. In addition to supporting me through the trials and tribulations of classes and research, she allowed me to become a small part of her family while here at Santa Cruz.

Past and present members of the Ravelo Lab have contributed to my success. Jonathan LaRiviere has been my sounding board throughout graduate school. Petra Dekens, Michael Wara, Dyke Andreasen, Mea Cook and Kelsey Dyez have provided endless advice and research support. Shiloh Schlung challenged my conventions and was an excellent traveling companion. I thank Karla Knudson, Fabian Batista, Sarah

White, Allison Myers Crimmins, Paul Talmadge, Sheela Zybkousky, Max Tung, and Joey Hermosillo for their effort and support.

The Ford, Dorman and Dalal families have provided constant support through my graduate studies. Daniel Zerbino has tirelessly supported me in Santa Cruz and from afar. I don't think I could have made it through the last year without Daniel. I look forward to many more adventures with you. Merci mon amour. *"Le cœur a ses raisons que la raison ne connaît point." ~ Blaise Pascal*

The text of this dissertation includes a reprint of the following published material: Ford, H., Ravelo, A., and Hovan, S. (2012). A deep Eastern Equatorial Pacific thermocline during the early Pliocene warm period. *Earth and Planetary Science Letters*, *355-356*, 152–161, doi: 10.1016/j.epsl.2012.08.027. This article is reproduced by permission by Elsevier. The co-authors listed in this publication directed and supervised the research which forms the basis for the dissertation

Chapter 1: Introduction

The tropical Pacific plays a vital role in global climate through heat and vapor transport via the atmospheric and oceanic circulations, and small variations in the mean state and variability have global consequences (Curtis, 2008). Two distinct features in the modern distribution of sea surface temperatures (SSTs) in the tropical Pacific are the western warm pool and the eastern cold tongue (Figure 1.1). In the western equatorial Pacific (WEP), warm SSTs drive vapor and latent heat transport toward the subtropics while in the eastern equatorial Pacific (EEP), cold waters absorb a significant amount of heat that contributes to the global heat budget. In the EEP wind driven upwelling and a relatively shallow thermocline deliver cold, nutrient rich water to the surface. Across the tropical Pacific, the basin wide surface SST and thermocline gradients are a prominent feature of the atmospheric and oceanic circulation (e.g. Walker Circulation). A large source of tropical variability is El Niño-Southern Oscillation (ENSO). Through atmospheric teleconnections, ENSO is also significant source of global climate variability. Though the tropical mean state and variability are important components of the global climate system, the impacts of future climate change on the tropics is uncertain. Records of past climate can be used to better understand essential components in the climate system. Therefore, in this dissertation, I present long-term and short-term records of past climate from the tropical Pacific to understand the evolution of the background mean state, variability and the processes and mechanisms that have influenced tropical paleoclimate.

During an El Niño event, warm SSTs in the EEP alter oceanic and atmospheric circulation with global impacts, including rain in California and drought in Australia. In the WEP, SSTs cool slightly and the thermocline shoals while in the EEP, SSTs warm significantly and the thermocline deepens. Weakening of atmospheric winds and the deepening of the thermocline during an El Niño event disrupt normally favorable upwelling conditions, which has a negative impact on biological productivity and fisheries. The strength of ENSO varies with the mean state including wind strength, thermocline depth and vertical temperature gradients (Fedorov and Philander, 2001). Although most climate models project the tropical Pacific will become more El Niño-like in its mean state with anthropogenic climate change, the ability of climate models to predict ENSO varies widely (Meehl and Stocker, 2007). As the instrumental record is too short to observe feedbacks that occur over long time scales, records of past climate may provide insight into the fundamental processes that integrate changes in mean state and variability on a variety of time scales.

As the thermocline plays a vital role in the cold SST expression in the EEP, Chapter 2 "A deep Eastern Equatorial Pacific thermocline during the early Pliocene warm period" (Ford et al., 2012) chronicles the long-term evolution of subsurface temperatures within the cold tongue region. During the early Pliocene (3.0-4.6 Ma), warm SST in the EEP altered the mean state of the tropical Pacific such that it resembled the SST pattern of a modern El Niño event (Wara et al., 2005). This permanent El Niño-like mean state impacted global atmospheric and oceanic

circulation and may have contributed to global warmth during this time (Brierley et al., 2009). During the Pliocene, warm SST in the EEP may have been caused by a weaker winds and cold water upwelling, or by a relatively deep thermocline compared to today. Using a latitudinal transect approach, subsurface temperatures reconstructed from the Mg/Ca values of the planktonic foraminifera *Globorotalia tumida* from Ocean Drilling Program (ODP) locations within (ODP Site 848 and 849) and outside (ODP Site 853) of the cold tongue extension along 110°W were used as a proxy for thermocline depth. During the early Pliocene, the thermocline was deep and between 4.8 to 4.0 Ma, closure of the Panama Seaway impacted regional ocean circulation such that the thermocline steeply shoaled. This event brought cold water to the surface, a precondition to cooling of the cold tongue region (Lawrence et al., 2006) and prompting various positive feedbacks to further cool SSTs and subsurface temperatures. These dynamic changes influenced the long-term mean state of the tropical Pacific and contributed to the transition from the warm Pliocene to the cold Pleistocene.

Changes in the background mean state affect the modes of variability and the positive and negative feedbacks that influence the time, space and intensity of variability (Fedorov and Philander, 2001). Today, the major modes of variability in the tropical Pacific (Figure 1.2) are seasonal and interannual (e.g. ENSO). In the western Pacific, variability is small (~0.5 °C) and dominated by the seasonal cycle. In contrast, in the eastern Pacific, variability is large and the seasonal cycle and interannual variability are similar in magnitude (~1.5 °C, each). As tropical climate

varies on many scales and the interaction of radiative and dynamic processes determine tropical response on different temporal and spatial dimensions. Here, radiative processes refer to changes in CO_2 and related feedbacks while dynamic processes refer to changes in atmospheric and oceanic circulation, like those that influence ENSO.

In Chapter 3 "Reduced ENSO during the Last Glacial Maximum" and Chapter 4 "Long-term stability and sensitivity of the Western Equatorial Pacific warm pool to radiative forcing" I examine changes in variability with a markedly different background states. In Chapter 3, I investigate ENSO behavior during the Last Glacial Maximum across the tropical Pacific. The feedbacks that govern modern ENSO behavior (Guilyardi et al., 2009) and the background state of the Last Glacial Maximum (Otto-Bliesner et al., 2009) are intensely studied, but the ability of climate models to project ENSO during the LGM background state is poorly constrained. In Chapter 4, I investigate the warm pool variability on glacial-interglacial time scales from the Pliocene to present day. Here I use novel techniques and the marine sediment archive to untangle high-resolution variability from the past.

Traditional Mg/Ca based temperature reconstructions use several foraminifera (n=20-30 specimens) and this proxy has contributed considerably to the understanding of long-term mean climate evolution. Specimens are homogenized to reconstruct a mean temperature that correlates well with mean annual SST (see Anand et al., 2003 and many others), however temperature variability recorded throughout an individual foraminifera lifespan (~2-4 weeks) and growth season is

homogenized in this process. Recently developed laser ablation techniques using the final chamber of individual foraminifera show good agreement with modern seasonal temperatures (Wit et al., 2010). With application to the marine sediment record, seasonal and decadal modes (e.g. ENSO, Pacific Decadal Oscillation) of variability are integrated due to slow accumulation rates and bioturbation, but changes in variability can still be accessed. By comparing the reconstructed temperature distributions from populations of foraminifera from discrete sediment samples, changes in radiative and dynamic forcing can be determined. Simple changes in radiative forcing (and related feedbacks) are unlikely to affect temperature distributions, as changes in radiative forcing would roughly impact all seasons equally and result in a mean shift in temperatures (Gastineau et al., 2009). In contrast, changes in dynamic forcing are likely to impact temperature distributions. For example, since ENSO events appear as extreme warm or cold events, changes in ENSO amplitude impact the tails of a temperature distribution. With the application of statistical techniques (Q-Q plots, Monte Carlo), changes in the distribution of individual foraminifera variability can be evaluated to identify important climatological processes and mechanism that may vary over time.

In Chapter 3, individual foraminifera temperature variability records were constructed from the WEP (ODP Site 806) and EEP (ODP Site 849) to investigate tropical variability from the Holocene and LGM. The LGM was a period of sustained cooling, and studying the LGM provides an opportunity to examine changes in variability during a different background mean climate state (e.g. ice extent, CO_2

levels). Using surface (*Globigerinoides sacculifer*) and subsurface (*G. tumida*) dwelling foraminfera to construct SST and subsurface temperature variability, I find that the WEP responds primarily to radiative forcing (e.g. CO_2 and related feedbacks) while the EEP responds to radiative and dynamic forcing (e.g. upwelling, winds). In the EEP, the temperature distribution changes between the Holocene and glacial samples are suggestive of a decrease in ENSO activity during the last glacial. Furthermore, an analysis of published SST records throughout the EEP reveals spatial heterogeneity; the magnitude of temperature decrease within the cold tongue is less than in the eastern warm pool during the LGM in comparison to the Holocene. Pacific basin zonal temperature gradient reconstructions are often used as an approximation for atmospheric and oceanic circulation strength. During the glacial period, the reduced zonal SST gradient is related to the dynamic changes that affect variability in the EEP cold tongue. Currently, no model simulations match the mean state and variability suggested by this study. However, this paleodata provides a benchmark for future climate model studies to determine the balance of feedbacks that will reproduce the LGM mean state and variability.

During the early Pliocene, SST records and climate modeling suggest the warm pool was greatly expanded compared to the present and gradually contracted as the climate transitioned to the cold Pleistocene. Although the global climate drastically changed over the Plio-Pleistocene, SST data from the warm pool suggest long-term stability (Wara et al., 2005). In the modern, the western Pacific warm pool acts as a global heat engine and is thought to largely respond to radiative forcing on

orbital time scales over the last three million years (Medina-Elizalde and Lea, 2010). Here I examine the long-term mean state and temperature variability of the warm pool on glacial-interglacial scales to evaluate the warm pool response to different climate forcing. In Chapter 4, long-term SST stability from ODP Site 806 suggests temperatures did not exceed present day. On glacial-interglacial time scales, though the means are offset, individual foraminifera SST variability has been constant since the early Pliocene. Long-term subsurface temperature records indicate the thermocline was deep during the Pliocene and gradually shoaled to its present position. Although the mean background state of the tropical thermocline has changed over the last four million years, the glacial-interglacial individual foraminifera subsurface temperature variability has been constant. These glacial-interglacial mean temperatures from the surface and subsurface suggest the warm pool has responded to radiative forcing since the early Pliocene.

This thesis contributes to the growing body of knowledge that explores tropical climate change on various time and space scales to constrain the radiative and dynamic factors that influence paleoclimate. This work reveals long-term changes in the basin-wide tropical thermocline, an element that is integral to several dynamic feedbacks. In addition to changes in the mean climate state, this work demonstrates high-resolution individual foraminifera temperature variability on a several time scales. These new observations from past climate records of mean state and variability will benefit paleoceanographers and climate modelers alike.

REFERENCES

Anand, P., Elderfield, H., and Conte, M., 2003, Calibration of Mg/Ca thermometry in planktonic foraminifera from a sediment trap time series: Paleoceanography, v. 18, no. 2, p. 1050, doi: 10.1029/2002KPA000846.

Brierley, C.M., Fedorov, A.V., Liu, Z., Herbert, T.D., Lawrence, K.T., and Lariviere, J.P., 2009, Greatly Expanded Tropical Warm Pool and Weakened Hadley Circulation in the Early Pliocene: Science, v. 323, no. 5922, p. 1714–1718, doi: 10.1126/science.1167625.

Curtis, S., 2008, The El Niño–Southern Oscillation and Global Precipitation: Geography Compass, v. 2, no. 3, p. 600–619, doi: 10.1111/j.1749-8198.2008.00105.x.

Fedorov, A.V., and Philander, S., 2001, A Stability Analysis of Tropical Ocean-Atmosphere Interactions: Bridging Measurements and Theory for El Nino: Journal of Climate, v. 14, p. 3086–3101.

Ford, H., Ravelo, A., and Hovan, S., 2012, A deep Eastern Equatorial Pacific thermocline during the early Pliocene warm period: Earth and Planetary Science Letters, v. 355-356, p. 152–161, doi: 10.1016/j.epsl.2012.08.027.

Gastineau, Li, and Le Treut, 2009. The Hadley and Walker Circulation Changes in Global Warming Conditions Described by Idealized Atmospheric Simulations. Journal of Climate, v. 22 p. 3993–4013. doi:10.1175/2009JCLI2794.1

Guilyardi, E., Wittenberg, A., Fedorov, A., Collins, M., Wang, C., Capotondi, A., van Oldenborgh, G.J., and Stockdale, T., 2009, Understanding El Niño in Ocean–Atmosphere General Circulation Models: Progress and Challenges: Bulletin of the American Meteorological Society, v. 90, no. 3, p. 325–340, doi: 10.1175/2008BAMS2387.1.

Lawrence, K., Liu, Z., and Herbert, T., 2006, Evolution of the eastern tropical Pacific through Plio-Pleistocene glaciation: Science, v. 312, no. 5770, p. 79–83, doi: 10.1126/science.1120395.

Medina-Elizalde, M., and Lea, D.W., 2010, Late Pliocene equatorial Pacific: Paleoceanography, v. 25, p. PA2208, doi: 10.1029/2009PA001780.

Meehl, G., and Stocker, T.F., 2007, Global Climate Projections: Global Climate Projections. In: Climate Change 2007: The Physical Science Basis. Contribution of Working Group I to the Fourth Assessment Report of the Intergovernmental Panel on Climate Change,, p. 747–846.

Otto-Bliesner, B.L., Schneider, R., Brady, E.C., Kucera, M., Abe-Ouchi, A., Bard, E., Braconnot, P., Crucifix, M., Hewitt, C.D., Kageyama, M., Marti, O., Paul, A., Rosell-Mele, A., Waelbroeck, C., et al., 2009, A comparison of PMIP2 model simulations and the MARGO proxy reconstruction for tropical sea surface temperatures at last glacial maximum: Climate Dynamics, v. 32, no. 6, p. 799–815, doi: 10.1007/s00382-008-0509-0.

Wara, M., Ravelo, A., and Delaney, M., 2005, Permanent El Nino-like conditions during the Pliocene warm period: Science, v. 309, no. 5735, p. 758–761, doi: 10.1126/science.1112596.

Wit, J.C., Reichart, G.-J., A Jung, S.J., and Kroon, D., 2010, Approaches to unravel seasonality in sea surface temperatures using paired single-specimen foraminiferal δ18O and Mg/Ca analyses: Paleoceanography, v. 115, no. 4, p. PA4220, doi: 10.1029/2009PA001857.

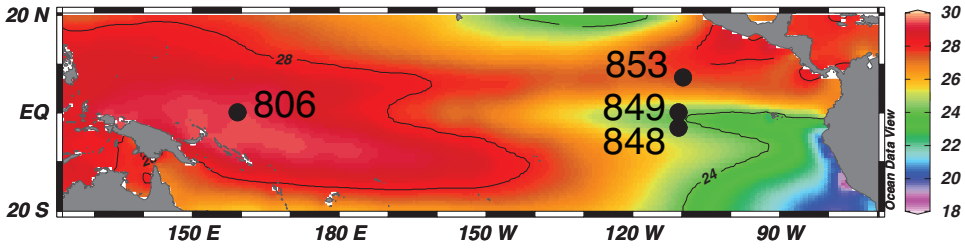

Figure 1.1: Sea Surface Temperature Overview of the Tropical Pacific
Mean annual sea surface temperature (WOA09 plotted with Ocean Data Viewer) showing the western warm pool and eastern cold tongue. Locations for Ocean Drilling Program Sites 806, 848, 849, 853 used in this dissertation and plotted.

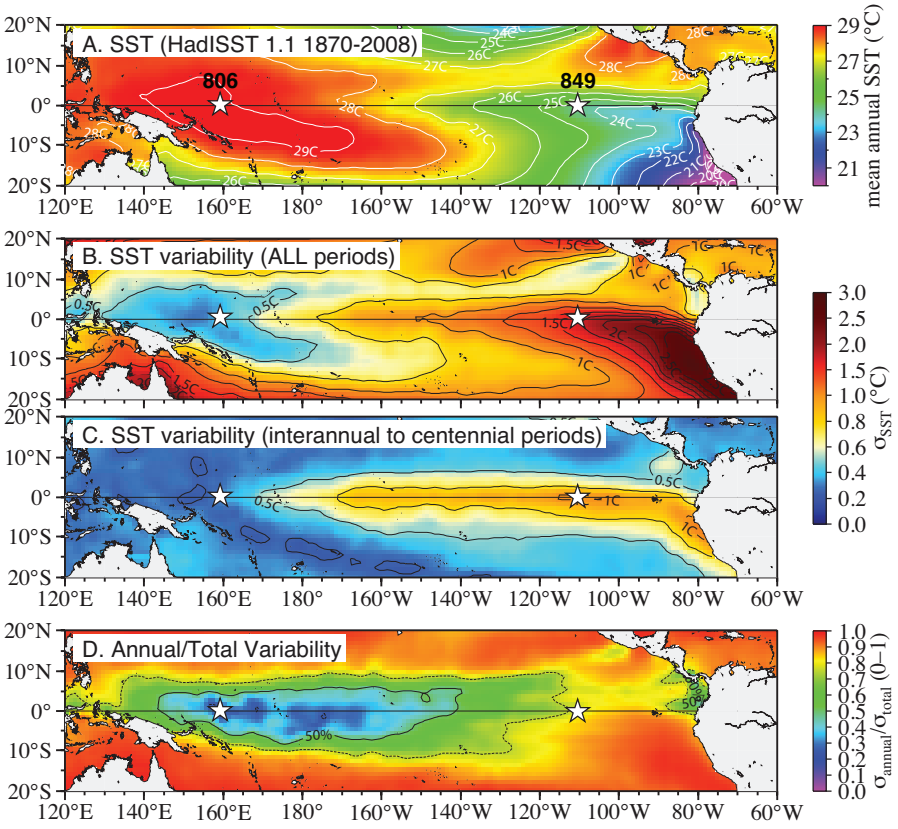

Figure 1.2: Modes of Variability in the Tropical Pacific
Mean annual sea surface temperatures (calculated from Rayner et al., 2003) (A). Variability of monthly sea surface temperatures 1870 – 2008 (B) and monthly values with the annual cycle removed (C), calculated as standard deviations and the proportion of total SST variability due to the annual cycle (D). Cool colors are regions dominated by interannual and centennial variations while warm colored regions are dominated by the annual cycle.

Chapter 2: A deep Eastern Equatorial Pacific thermocline during the early Pliocene warm period

Data published in this chapter is archived at the National Oceanic and Atmospheric Administration National Climate Data Center:

http://www.ncdc.noaa.gov/paleo/paleocean.html

Earth and Planetary Science Letters 355-356 (2012) 152–161

Contents lists available at SciVerse ScienceDirect

Earth and Planetary Science Letters

journal homepage: www.elsevier.com/locate/epsl

A deep Eastern Equatorial Pacific thermocline during the early Pliocene warm period

Heather L. Ford [a,*], A. Christina Ravelo [a], Steven Hovan [b]

[a] Ocean Sciences Department, University of California, Santa Cruz, 1156 High Street, Santa Cruz, CA 95064, USA
[b] Department of Geoscience, Indiana University of Pennsylvania, Walsh Hall, 302 East Walk, Indiana, PA 15705, USA

ARTICLE INFO

Article history:
Accepted 22 August 2012
Editor: P. DeMenocal

Keywords:
Pliocene
thermocline
Eastern Equatorial Pacific
foraminiferal Mg/Ca

ABSTRACT

During the early Pliocene warm period (~4.6–4.2 Ma) in the Eastern Equatorial Pacific upwelling region, sea surface temperatures were warm in comparison to modern conditions. Warm upwelling regions have global effects on the heat budget and atmospheric circulation, and are argued to have contributed to Pliocene warmth. Though warm upwelling regions could be explained by weak winds and/or a deep thermocline, the temporal and spatial evolution of the equatorial thermocline is poorly understood. Here we reconstruct temporal and spatial changes in subsurface temperature to monitor thermocline depth and show the thermocline was deeper during the early Pliocene warm period than it is today. We measured subsurface temperature records from Eastern Equatorial Pacific ODP transect Sites 848, 849, and 853 using Mg/Ca records from *Globorotalia tumida*, which has a depth habitat of ~50–100 m. In the early Pliocene, subsurface temperatures were ~4–5 °C warmer than modern temperatures, indicating the thermocline was relatively deep. Subsurface temperatures steeply cooled ~2–3 °C from 4.8 to 4.0 Ma and continued to cool an additional 2–3 °C from 4.0 Ma to present. Compared to records from other regions, the data suggests the pronounced subsurface cooling between 4.8 and 4.0 Ma was a regional signal related to restriction of the Isthmus of Panama, while continued cooling from 4.0 Ma to present was likely related to global processes that changed global thermocline structure. Additionally, the spatial evolution of the equatorial thermocline along a N–S transect across ODP Sites 853, 849 and 848 suggests an intensification of the southeast trades from the Pliocene to present. Large-scale atmospheric and oceanographic circulation processes link high and low latitude climate through their influence on equatorial thermocline source water regions and consequently the equatorial thermocline. Through these low latitude/high latitude linkages, changes in the equatorial thermocline and thermocline source water played an important role in the transition from the warm Pliocene to the cold Pleistocene.

1. Introduction

During the Pliocene (5.4–2.4 Ma), small nascent glaciers existed in the Northern Hemisphere (Haywood et al., 2000), global mean temperature was ~3 °C warmer than today (Haywood and Valdes, 2004), and atmospheric carbon dioxide concentrations (pCO_2) were similar to or slightly above modern values (350–400 ppm, Pagani et al., 2010; Seki et al., 2010). A modeling study suggests that high-latitude warmth in the Pliocene could be explained by high pCO_2 and reduced high-latitude ice and sea ice coverage (Haywood and Valdes, 2004). Another distinctive feature of Pliocene climate was warmer than modern upwelling regions (by ~3–9 °C, Dekens et al., 2007) and reduced zonal and meridional sea surface temperature (SST) gradients (Brierley et al., 2009). Reduced gradients affected large-scale atmospheric circulation (e.g. Hadley and Walker circulation), global cloud cover and water vapor content, and as such, provide an additional explanation for high latitude warmth and the suppression of ice sheet growth (Brierley and Fedorov, 2010). The transition from warm Pliocene climate to the cold climate of the Pleistocene is marked not just by the development of large Northern Hemisphere ice sheets, but also by cooling in tropical and subtropical upwelling regions, for example in the Eastern Equatorial Pacific and the Peruvian and California Margins (Dekens et al., 2007; Lawrence et al., 2006). Fedorov et al. (2006) proposed that during the global cooling transition and onset of Northern Hemisphere glaciation, high and low latitude climate changes were linked through the global thermocline.

Indirect support that global thermocline conditions changed through the Pliocene and Pleistocene comes from an examination of paleoceanographic conditions in upwelling regions (Dekens et al., 2007), where the thermocline structure plays an important role in determining SST. Upwelling regions are highly productive because upwelling favorable winds bring cold, nutrient rich water from

* Corresponding author.
E-mail addresses: hford@ucsc.edu (H.L. Ford), acr@ucsc.edu (A.C. Ravelo), hovan@iup.edu (S. Hovan).

0012-821X/$ - see front matter © 2012 Elsevier B.V. All rights reserved.
http://dx.doi.org/10.1016/j.epsl.2012.08.027

shallow thermocline depths to the surface. Warm SSTs in upwelling regions during the Pliocene could be explained by weaker winds and/or changes in thermocline conditions. Even with strong upwelling favorable winds, SSTs would be warm if the thermocline was sufficiently deep. Dekens et al. (2007) point out that in the early Pliocene, changes in SST and in biological productivity were decoupled indicating that weaker wind-driven upwelling cannot entirely explain why SSTs were warm in upwelling regions. Additional processes, like changes in the thermocline temperature and/or depth, are necessary to explain warm upwelling regions in the Pliocene.

Past studies of subsurface temperature and thermocline depth in the Pliocene suggest that the thermocline was deeper than today in the Eastern Tropical Pacific (EEP) during the earliest Pliocene (Steph et al., 2006, 2010). However, the records from these past studies do not directly and primarily reflect changes in equatorial upwelling, rather, they are affected by processes occurring in the East Pacific Warm Pool and in coastal upwelling regions, making it more difficult to directly compare them to previously generated SST records from open ocean equatorial upwelling regions (Dekens et al., 2007; Lawrence et al., 2006). In this study, we generated subsurface temperature records from ODP Sites 848, 849, and 853. These sites constitute a north–south transect across the East Equatorial Pacific upwelling 'cold tongue'. We use the long-term trend found at all sites to evaluate changes in the mean thermocline conditions. In addition, we use differences in trends between sites to assess how the spatial pattern of changes in thermocline conditions may have been influenced by changes in the local wind-field.

2. Hydrography

The EEP lies between the subtropical gyres of the North and South Pacific. It is characterized by a distinct cold tongue, situated along the equator, and a warm pool to the north (Fig. 1). The EEP cold tongue is climatically important due to its role in the global heat budget and the carbon cycle, and its influence on atmospheric circulation and meridional and zonal gradients across the Pacific basin (Lavin et al., 2006). This region is extremely productive because of wind driven upwelling along the equator, which brings cold nutrient rich water from a shallow thermocline (~20–60 m) to the surface (Fiedler and Talley, 2006). Additionally, the prevailing winds cause westward advection of coastally upwelled water, which also delivers nutrients to the region.

In the EEP region, water that occupies subsurface depths, which upwells along the cold tongue and on the coast of Peru, originates from subtropical regions from the North and South Pacific (for a comprehensive review, see Fiedler and Talley, 2006); water from

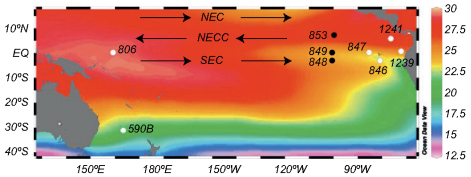

Fig. 1. Sites in this study (black dots) Site 848 (3856 m water depth), Site 849 (3839 m water depth) and Site 853 (3714 m black depth) and sites with previously generated data (white dots) Sites 590B, 806, 846, 847, 1239, and 1241 overlaid on a modern sea surface temperature map. Major equatorial currents, North Equatorial Current (NEC), North Equatorial Counter Current (NNEC) and South Equatorial Current (SEC), are denoted with arrows.

these extratropical regions is source water for the equatorial thermocline. The primary subsurface water mass along the equator at ~100 m depth, the Subtropical Underwater (STUW), is mostly comprised of South Pacific Subtropical Surface Water subducted between 150 °W and 90 °W and south of 20 °S (O'Connor et al., 2002). A smaller component is North Pacific Subtropical Water which is subducted north of 20 °N and meets STUW at ~10 °N (O'Connor et al., 2002). Below STUW, subducted South Pacific and North Pacific mode waters occupy thermocline water depths. South Pacific Eastern Subtropical Mode Water (SPESTMW) is ventilated over a wide area and subducts in the southeastern subtropical Pacific (Wong and Johnson, 2003). North Pacific Eastern Subtropical Mode Water (NPESTMW) originates northeast of Hawaii near the boundary of the subtropical and subpolar water masses (Hautala and Roemmich, 1998). Additionally, Subantarctic Mode Water is also known to contribute to EEP thermocline water (Toggweiler et al., 1991). Although a large component of equatorial thermocline waters are sourced in the South Pacific, anthropogenic tracers suggest some water is also sourced in the North Pacific (Fine et al., 2001; Jenkins, 1996). These EEP subsurface waters, which originate in extratropical regions, define the equatorial thermocline structure.

Changes in source water characteristics (e.g. temperature and nutrients) affect the structure of the equatorial thermocline. For example, extratropical temperature and salinity variations modify the density structure of the equatorial thermocline and ultimately the water that upwells in the EEP cold tongue (Fedorov et al., 2007, 2004; Gu and Philander, 1997). In addition, changes in nutrient distributions in thermocline source water regions have downstream influences on equatorial productivity and consequently the carbon cycle (Lawrence et al., 2006). Monitoring equatorial thermocline behavior not only reveals climatic conditions within the equatorial Pacific, but also teleconnections to extratropical climate.

3. Materials and methods

To investigate changes in EEP thermocline structure though the Pliocene to Pleistocene, low-resolution (~30,000 yr) subsurface temperature and stable-isotope records were generated from well-dated (Shackleton et al., 1995) Leg 138 drilling sites: ODP Sites 848 (2°59.63′S, 110°28.79′W, 3856 m water depth), 849 (0°10.99′N, 110°31.17′W, 3839 m water depth), and 853 (7°12.66′N, 109°45.80′W, 3714 m water depth; (Fig. 1). An age model for each site was constructed using high-resolution GRAPE density measurements correlated to an orbital insolation record (Shackleton et al., 1995). Located within the southern margin (ODP Site 848), core (ODP Site 849) and northern margin (ODP Site 853) of the equatorial cold tongue extension, this transect of sites along 110 °W is excellent for monitoring the temporal and spatial development of the regional EEP thermocline. Though some zonal (~4° longitude) and meridional (~1° latitude) movement of the ocean crust occurred over the last 5 million years, the sites' backtrack paths (Duncan and Clague, 1985; van Andel et al., 1975) indicate these sites have remained within similar modern temperature zones.

To reconstruct subsurface properties, we analyzed specimens of *Globorotalia tumida* (355–425 μm, ~10–25 specimens, but in a few cases as few as five specimens), a planktonic foraminifera with a mean calcification depth of ~50–100 m (Ravelo and Fairbanks, 1992; Schweitzer and Lohmann, 1991). Sediment core top $\delta^{18}O$ (where $\delta^{18}O=((^{18}O/^{16}O_{sample}/^{18}O/^{16}O_{standard})-1)\times 1000$) analyses indicate there is no latitudinal difference in *G. tumida* calcification depth, despite a variety of hydrographic zones throughout the EEP (Rincón-Martínez et al., 2011). Before analysis, specimens were crushed, weighed, and split for minor element and stable isotope analyses. Minor element splits were cleaned using a modified "Boyle

protocol", i.e. crushed samples were rinsed and sonicated in Milli-Q and methanol, subjected to reductive and oxidative cleaning steps, and transferred into 1.5 mL acid cleaned vials for a weak acid leach and final rinse before minor-element analysis (Boyle and Keigwin, 1985; Lea and Boyle, 1993). Minor-element ratios were measured using a PerkinElmer Optima 8300 inductively coupled plasma optical emission spectrometer (ICP-OES, see Wara et al., 2003). Long term Mg/Ca mmol/mol reproducibility for a liquid consistency standard and foraminifera standards are 0.0254 mmol/mol (1 s, $n=144$) and 0.176 mmol/mol (1 s, $n=63$) respectively.

Though a *G. tumida*-specific calibration exists for the Atlantic (Regenberg et al., 2009), has been approximated for the Pacific (Rickaby and Halloran, 2005), and a multi-species deep-dwelling foraminifera calibration also exists (Cléroux et al., 2008), comparison of Site 848, 849 and 853 core-tops and modern hydrographic data suggest the calculated subsurface temperatures given by these calibrations are much too cold, and imply a *G. tumida* calcification depth of around 500 m. This is well outside of known *G. tumida* calcification depths (~50–300 m, Farmer et al., 2007; Mekik and François, 2007; Ravelo and Fairbanks, 1992; Rincón-Martínez et al., 2011; Schweitzer and Lohmann, 1991). Since no species-specific temperature calibration from the Pacific Ocean is available for *G. tumida*, we employed the same equation as Steph et al. (2010). Specifically, *G. tumida* Mg/Ca values were converted to paleotemperature using the multispecies Mg/Ca-temperature calibration of Anand et al. (2003) and a core depth dissolution correction factor *G. sacculifer* from Dekens et al. (2002) for the Pacific: $Mg/Ca = 0.38\exp 0.09[T - 0.36(\text{core depth in km}) - 2.0\ ^{\circ}C]$.

Though *G. tumida* is known to calcify at a variety of depths (Farmer et al., 2007; Mekik and François, 2007; Ravelo and Fairbanks, 1992; Rincón-Martínez et al., 2011; Schweitzer and Lohmann, 1991), temperature estimates from Mg/Ca measurements of *G. tumida* from the coretops at our study sites are most consistent with a mean calcification depth of ~50–100 m. The relative distribution of *G. tumida* calcification temperatures, warmest at Site 853, coolest at Site 849, and in between at Site 848, is consistent with modern observations of temperatures above 100 m, and is inconsistent with modern observations below 100 m.

Similar to Steph et al. (2010), we consider that *G. tumida* and *G. sacculifer* have different Mg/Ca-carbonate dissolution sensitivity (Brown and Elderfield, 1996), which would impact absolute temperature estimates. We are interested in the relative change in subsurface temperature through time in order to monitor thermocline depth; the fact that there are no long-term changes or perturbations in nannofossil preservation and $\%CaCO_3$, suggests that our Mg/Ca based temperature estimates are not affected by changes in dissolution (Farrell et al., 1995). The multi-species calibrations (Anand et al., 2003; Cléroux et al., 2008; Rickaby and Halloran, 2005) and the *G. tumida*-specific calibration (Regenberg et al., 2009) have different Mg/Ca-temperature sensitivities (9.0 mmol/mol change in Mg/Ca for 1 °C vs. 4.0 mmol/mol change in Mg/Ca for 1 °C, respectively) Here, we assume a *minimum* change in subsurface temperature by applying the same equation as Steph et al. (2010) with a multi-species Mg/Ca-temperature sensitivity (9.0 mmol/mol change in Mg/Ca for 1 °C) with a standard error between ±1.2 and 1.4 °C (Anand et al., 2003; Dekens et al., 2002).

Crushed stable isotope splits from Site 848, 849, and 853 were analyzed for carbon and oxygen stable-isotope values using a Fisons Prism dual inlet gas source ratio mass spectrometer with an automated common acid bath carbonate preparation system. Long-term reproducibility of NBS-19 and an in-house standard are better than ±0.05‰ for $\delta^{13}C$ (where $\delta^{13}C = (({}^{13}C/{}^{12}C_{sample}/{}^{13}C/{}^{12}C_{standard}) - 1) \times 1000$) and ±0.07‰ for $\delta^{18}O$ (relative to Vienna Pee Dee Belemnite, V-PDB).

4. Results

Specimens of *G. tumida* were analyzed for minor element and stable isotope ratios from ODP Sites 848, 849 and 853 in order to monitor changes in subsurface water properties. Generally, in the early Pliocene (~5 Ma), subsurface temperatures were ~4–5 °C warmer than modern conditions. From 4.8 to 4.0 Ma, there was a pronounced subsurface temperature decrease of ~2–3 °C (Fig. 2 and Fig. 3). EEP subsurface temperatures in general continued to cool gradually by an additional ~2–3 °C from 4.0 Ma to present (Fig. 2 and Fig. 3).

Comparison between regional subsurface temperature records from Sites 848, 849 and 853 shows the temporal and spatial evolution of the eastern equatorial thermocline (Discussion Section 5.3). In the earliest part of the record, temperature was warmer at Site 848 than at Sites 849 and 853. Sites 848 and 853 have a similar magnitude of cooling between 4.8 and 4.0 Ma, ~2 °C, while equatorial Site 849 cools by ~3 °C. Between the early Pliocene (4–5 Ma) and the Late Pleistocene (0–1 Ma), subsurface temperature at Site 848 has the greatest magnitude of cooling, ~5 °C. From 4 Ma to ~2 Ma, subsurface temperatures at Site 848 continue to gradually cool, overlapping with subsurface temperatures at Site 849 from ~2 to 3 Ma. At ~3 Ma, Site 848 subsurface temperatures cooled below those at Site 853. At Site 848 there is a brief warming around 2 Ma and then subsurface temperatures continue to cool to present. Throughout most of the record, subsurface temperatures at Site 849 were the coolest and cooled ~4.0 °C between the early Pliocene and the Late Pleistocene. Between 3 and 4 Ma, subsurface temperatures at Site 849 were relatively constant, and then gradually cooled from 3 Ma to present. Site 853 subsurface temperatures had the least magnitude of cooling, ~3.4 °C. Between ~2 and 4 Ma, subsurface temperatures at Site 853 were relatively constant, and then gradually cooled from ~2 Ma to present.

At the beginning of the Pliocene, $\delta^{18}O$ values of *G. tumida* were ~1‰ lower than the Late Pleistocene (Fig. 3a). This is comparable to the ~1‰ shift in $\delta^{18}O$ values of benthic foraminifera and consistent with reduced global ice volume (Lisiecki and Raymo, 2005) and warmer temperatures as indicated by the Mg/Ca-based estimates. At the beginning of the $\delta^{18}O$ record, Site 853 is ~0.5‰ lower than Site 848 and 849, and from ~4.2 Ma onwards, the records have similar trends. There was a small change in $\delta^{13}C$ values such that *G. tumida* $\delta^{13}C$ values were ~0.25‰ lower during

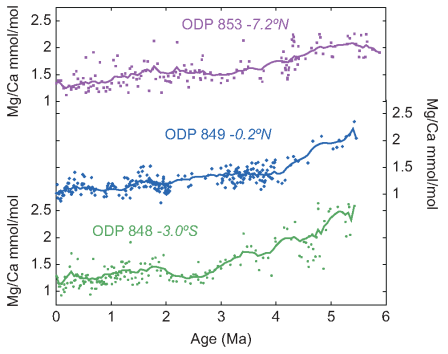

Fig. 2. Mg/Ca mmol/mol records from Sites 848 (green circles), 849 (blue diamonds) and 853 (purple squares) generated from Mg/Ca values of *G. tumida*. Thick lines are locally weighted (±10%) least squares smoothing. (For references to color in this figure legend, the reader is requested to refer the web version of this article.)

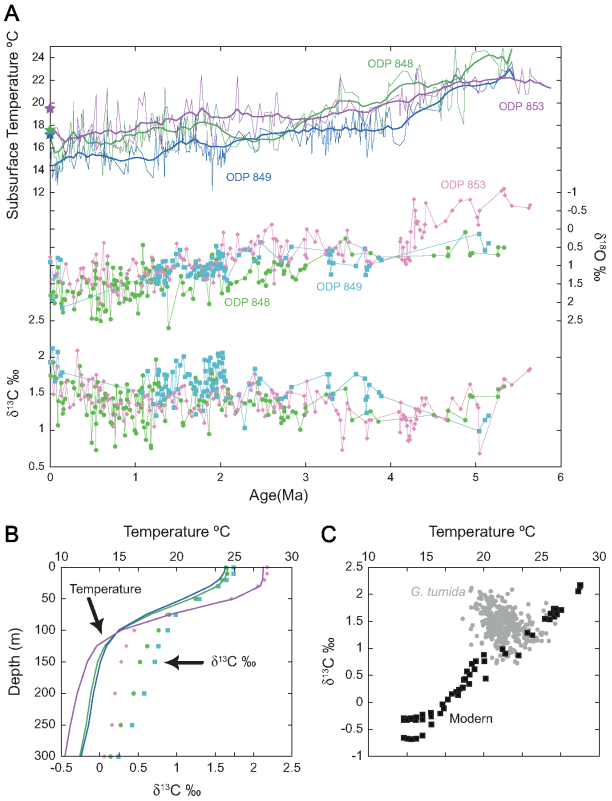

Fig. 3. Subsurface temperature and stable isotope records from Sites 848 (dark green line/light green circles), 849 (dark blue line/light blue squares) and 853 (dark purple line/light purple diamonds) generated from *G. tumida* (A). Modern subsurface temperatures are 75 m (World Ocean Atlas 2009) are denoted in green, blue and purple stars for Sites 848, 849, and 853 respectively. Subsurface temperatures were warm during the early Pliocene to comparison to present day. Carbon isotope records show a moderately increasing trend from the early Pliocene to present day. Oxygen isotope records show an increasing trend from Pliocene to present day, which is consistent with cooling global temperatures and increasing ice volumes. Modern temperature and δ^{13}C (calculated from modern PO_4 data using the relationship $\delta^{13}C = 2.4 - PO_4 \times 0.93$, (Charles and Fairbank, 1990)) profiles from World Ocean Atlas 2009 (B). The modern temperature and δ^{13}C mixing line (black squares) are plotted along with *G. tumida* subsurface temperature and δ^{13}C values (C). If subsurface temperature change from the Pliocene to present was simply related to a change in calcification depth, *G. tumida* values would plot along the modern relationship. Instead, coupled subsurface temperature and δ^{13}C values appear unrelated. (For references to color in this figure legend, the reader is requested to refer the web version of this article.)

the early Pliocene in comparison to the Late Pleistocene. Though the record is sparse, there appears to be a moderately increasing trend in δ^{13}C from the early Pliocene to ~2.5 Ma, which is comparable to the trend found in *G. tumida* from Site 851 (Cannariato and Ravelo, 1997). From ~2 Ma onward the δ^{13}C values between Sites were similar, though values at Site 849 may be slightly higher. δ^{13}C values decreased moderately from ~1 to 1.5 Ma and then increased from 1 Ma to present day, which is similar to the trend found in a high resolution benthic δ^{13}C record from Site 849 (Mix et al., 1995).

When *G. tumida* δ^{13}C values are compared to the paleotemperature estimates, they are inconsistent with a change in depth habitat of *G. tumida*. Due to the biological export of isotopically light carbon, in the modern ocean there is a δ^{13}C gradient between the surface ocean (relatively high δ^{13}C values) and subsurface ocean (relatively low δ^{13}C values). If temperature changes recorded by *G. tumida* were simply related to a change in depth habitat, δ^{13}C values would co-vary linearly with temperature (Fig. 3b), as predicted by the mixing line representing the upper water column (Fig. 3c); however, in our *G. tumida* records there is no relationship with time between temperature and δ^{13}C (i.e. values do not fall on the mixing line), suggesting that temperature variations recorded by *G. tumida* are not related to a simple change in calcification depth. During the Pliocene, *G. tumida* data record warm temperatures and low δ^{13}C values compared to the Late Pleistocene. This is the opposite of what would be expected from a simple change in depth habitat where specimens recording warm temperatures would also have high δ^{13}C values. Therefore, changes in calcification temperatures of *G. tumida* should be interpreted as changes in subsurface temperature at ~50–100 m.

5. Discussion

5.1. Eastern Equatorial thermocline depth and restriction of the Panama Seaway

Our subsurface temperature records, combined with previously generated *G. tumida* Mg/Ca and stable isotope records from the East Equatorial Pacific show strikingly similar histories and collectively indicate restriction of the Panama Seaway had a significant impact on the regional thermocline (Cannariato and Ravelo, 1997; Steph et al., 2006, 2010; Wara et al., 2005, Fig. 4). Throughout the Pliocene, equatorial subsurface temperatures were warmer than modern conditions and from 4.8 to 4.0 Ma there was a pronounced decrease in subsurface temperature of ~2–3 °C. The timing of this regional event suggests it is related to restriction of the Panama Seaway (this study; Steph et al., 2006, 2010, Fig. 4).

Though small passages likely existed until ~1.8 Ma (Keller et al., 1989), significant closure of the Panama Seaway occurred at ~2.6–2.7 Ma, when land mammals exchanged between North and South America (Marshall et al., 1982; Webb and Rancy, 1996); however, ocean faunal and geochemical evidence indicate the Caribbean and Pacific Basins were isolated from one another much earlier. For instance, subsurface temperature cooling in our records prior to 4.8 Ma may be related to early emergence of the Panama archipelago ~12 Ma (Coates et al., 2003) which impacted water masses on either side of the isthmus (Molnar, 2008). A comparison of δ^{18}O values of *G. sacculifer* from ODP Site 851 (Equatorial Pacific) and ODP Site 999 (Caribbean) shows an inferred increase in Caribbean surface salinity between 4.7 and 4.2 Ma, suggesting the two basins became isolated from ocean surface water exchange at that time (Haug et al., 2001). Similarly, at Site 1241, Mg/Ca and δ^{18}O values of *G. sacculifer* demonstrate the development of a distinct EEP hydrographic region between 4.8 and 2.4 Ma (Groeneveld et al., 2006). In the subsurface, EEP *G. tumida* Mg/Ca records (this study; Steph et al., 2006, 2010) exhibit a decrease in temperature of ~2–3 °C while Mg/Ca and δ^{18}O records from Caribbean ODP Sites 999 and 1000 generated from thermocline dwelling *Neogloboquadrina dutertrei* exhibit an increase in temperature of ~6 °C from 4.8 to 4.0 Ma (Steph et al., 2010). The divergence of subsurface trends in the Caribbean and Pacific basins further points to significant reorganization of thermocline waters related to restriction of the Panama Seaway at this time (Steph et al., 2010).

Additional records from the EEP indicate subsurface reorganization from 4.8 to 4.0 Ma. For instance, between 4.5 and 4.0 Ma,

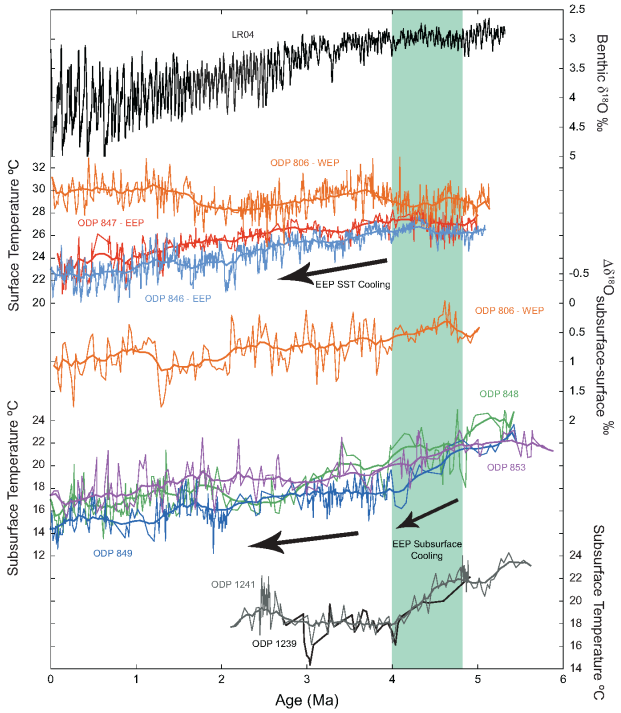

Fig. 4. Global ice volume and tropical temperature records. Global benthic foraminifera stack from Lisiecki and Raymo (2005). WEP SST record from Wara et al. (2005) (orange) and EEP SST records from Dekens et al. (2007) (red) and Lawrence et al. (2006) (light blue). Subsurface temperature records from WEP Site 806 (orange, LaRiviere et al., in press) and EEP Sites 848, 849, 853 (green, blue, purple, this study), 847, 1241 (gray, Steph et al., 2006), and 1239 (black, Steph et al., 2010). Thick lines are locally weighted (±10%) least squares smoothing. The green band highlights the steep subsurface cooling regional the EEP subsurface. (For references to color in this figure legend, the reader is requested to refer the web version of this article.)

rapid planktonic foraminifera faunal turnover suggests a rapidly changing subsurface environment at ODP Site 851 (Chaisson and Ravelo, 2000). Additionally, oxygen stable isotope evidence of subsurface dwelling *G. tumida* from Site 851 shows a shift in values of ~0.6‰ between 4.6 and 4.2 Ma (Cannariato and Ravelo, 1997). Subsurface *G. tumida* Mg/Ca and $\delta^{18}O$ records from ODP Sites 1241, 1239 (Steph et al., 2006, 2010) show a remarkably similar trend as Sites 848, 849 and 853 suggesting the pronounced shift in subsurface temperature and $\delta^{18}O$ values are pervasive throughout the EEP. Furthermore, Sites 1241 (Steph et al., 2006) and 853, which are located well outside of the EEP upwelling zone, share similar subsurface temperature trends as those sites located within the upwelling zone. This indicates that the subsurface temperature changes from 4.8 to 4.0 Ma are not related to simple changes in upwelling location and structure, but a fundamental shift in the EEP thermocline (this study; Steph et al., 2006, 2010).

A SST record from southwest Pacific ODP Site 590B indicates surface waters were cooling and freshening at 4.6–4.0 Ma, concurrent with restriction of the Panama Seaway (Karas et al., 2011), possibly related to "heat piracy" of the Northern Hemisphere from the Southern Hemisphere due to closure of the Panama Seaway (e.g. enhanced surface meridional heat transport to northern high latitudes, Lunt et al., 2008). Since the south Pacific is a potential source water region for the equatorial thermocline, cooling in the Southern Hemisphere related to restriction of the Panama Seaway could provide a mechanism for the pronounced subsurface temperature cooling in the EEP records from 4.8 to 4.0 Ma. Likewise, modeling results (Steph et al., 2010; Zhang et al., 2012) indicate there is a direct relationship between closure of the Panama Seaway and the equatorial Pacific thermocline shoaling. Consequently, Steph et al. (2010) hypothesize there is an intimate connection between the strength of the Atlantic Meridional Overturning Circulation (AMOC) and the position of the equatorial thermocline. As such, when AMOC strengthened the equatorial thermocline shoaled, and vice versa. For example, Site 1241 has a subsurface warming event at ~2.5 Ma, which coupled with benthic $\delta^{13}C$ records from the Caribbean ODP Site 1000 and Mid Atlantic ODP Site 925, was used to infer changes in Upper/Lower NADW ventilation, AMOC strength and teleconnections to the equatorial thermocline. Steph et al. (2010) proposed that when there was a weakening of the AMOC around 2.5 Ma, there was a corresponding deepening of the equatorial Pacific thermocline. Conversely, here we suggest that the AMOC-equatorial thermocline depth hypothesis proposed by Steph et al. (2010) is inconsistent with long-term subsurface trends from the Western Equatorial Pacific (WEP) and other EEP subsurface records.

A $\Delta\delta^{18}O_{subsurface-surface}$ record from Western Equatorial Pacific (WEP) ODP Site 806 (LaRiviere et al., in press), constructed from stable isotope measurements from *G. tumida* and *G. sacculifer* as a proxy for thermocline depth (Nathan and Leckie, 2009; Wara et al., 2005), indicates the thermocline steadily shoaled from the early Pliocene to present. The dramatic shoaling between 4.8 and 4.0 Ma present in all EEP records is absent in the WEP record, though this could be attributed to differences in *G. tumida* as a subsurface temperature recorder between the east and west. That is, in the EEP, there is enhanced sensitivity of *G. tumida* as a subsurface temperature recorder because the thermocline is relatively shallow, and consequently *G. tumida* probably lives within a steep thermal gradient, in comparison to the WEP where the thermocline is relatively deep. However, subsurface warming at 2.5 Ma described by Steph et al. (2010) in support of the AMOC-equatorial thermocline depth hypothesis is not present at Sites 806 (LaRiviere et al., in press), 848, 849, and 853 (this study).

Though Sites 848 and 849 are located within the EEP cold tongue and subsurface temperatures may be influenced by other factors (e.g. upwelling processes and advection), Site 853 is located at 7°N, well outside of the cold tongue region, and similarly situated to record tropical thermocline position as Site 1241 (Steph et al., 2006, 2010), yet does not indicate thermocline deepening at 2.5 Ma. Likewise, deepening of the equatorial thermocline is not apparent in WEP Site 806 (LaRiviere et al., in press). This suggests thermocline deepening interpreted at Site 1241 ~2.5 Ma (Steph et al., 2006, 2010) was related to local processes and that Site 1241 does not represent broad scale changes in the equatorial thermocline depth.

On glacial–interglacial time scales, the position of the Atlantic equatorial thermocline is known to adjust to changes in AMOC strength (Lopes dos Santos et al., 2010). Similarly, a model indicates there are global adjustments to the thermocline in relation to AMOC strength on centennial time scales (Huang et al., 2000). On longer time scales however, the Steph et al. (2010) AMOC-equatorial thermocline depth hypothesis appears inconsistent with basin-scale changes in the equatorial thermocline from the early Pliocene to present day, as described above; we instead propose changes in the Pacific equatorial thermocline appear related to changes in global heat balance and source water regions (Section 5.2.3, Fedorov et al., 2006). In particular, closure of the Panama Seaway impacted heat balance between the northern and southern hemisphere and consequently influenced EEP thermocline source water regions (Lunt et al., 2008; Karas et al., 2011). Though the thermocline shoaling in the EEP is poorly captured by modeling results (Zhang et al., 2012), closure of the Panama Seaway significantly impacted subsurface temperatures in the EEP and preconditioned SST cooling in the region starting at ~4 Ma (Fig. 4, this study; Steph et al., 2006, 2010). The appearance of cool SSTs in the EEP further altered the global heat balance and as a result global climate transitioned from the warm Pliocene to the cool Pleistocene (Fedorov et al., 2006).

5.2. Gradual subsurface cooling from 4.0 ma to present

From 4.0 Ma to present, subsurface temperatures gradually cool by ~2–3 °C (Figs. 3 and 4). Several climatically important events occurred throughout this period, such as initiation of high latitude cooling and Northern Hemisphere Glaciation (~3.6 Ma, Mudelsee and Raymo, 2005), and intensification of Northern Hemisphere Glaciation (~2.75 Ma, Haug et al., 1999); our subsurface temperature records from Sites 848, 849 and 853 exhibit no dramatic response to any of these events suggesting subsurface temperature cooling was a gradual process. Several factors discussed below could be related to further subsurface cooling after 4.0 Ma including final closure of the Panama Seaway, constriction of the Indonesian Seaway, and changing source waters.

5.2.1. Further restriction and closure of the panama seaway

Several paleoceanographic studies (summarized by Molnar, 2008) indicate changing properties of Caribbean and EEP surface and subsurface waters between ~2 and 4 Ma with a complete isthmus emerging ~2.6–2.7 Ma. However, closure of the Panama Seaway does not explain further subsurface temperature cooling from ~2 Ma onwards. Though restriction of the Panama Seaway is a likely source for the changing properties in subsurface water between 4.8 and 4.0 Ma as discussed above (Section 5.1), closure cannot entirely explain continued subsurface cooling from 4.0 Ma to recent.

5.2.2. Constriction of the Indonesian throughflow

Rodgers et al. (2000) postulate that the northward movement of New Guinea would constrict surface ocean circulation and could change the composition of thermocline water for the Indian

and Pacific Ocean. This constriction impacts Indonesian throughflow waters, which feed Indian Ocean thermocline waters, and subsequently the Equatorial Undercurrent that feeds EEP thermocline waters. Cane and Molnar (2001) propose the aridification of Africa at approximately 3–4 Ma was the result of cooling Indian Ocean thermocline and SSTs due to the constriction of the Indonesian Throughflow. Although not discussed by Cane and Molnar (2001), it may be that the constriction of the Indonesian Throughflow influenced Subantarctic Mode Water, which is known to contribute to the modern thermocline waters that upwell in the EEP (Toggweiler et al., 1991). Karas et al. (2011) point out subsurface cooling at Southwest Pacific Ocean DSDP Site 590B from ~3.5 to 2.5 Ma may reflect an increased cooling or northward movement of Subantarctic Mode Water due to the constriction of the Indonesian Throughflow. Thus, the gradual cooling in the EEP subsurface temperature records could reflect an increased contribution of Subantartic Mode Water to the EEP thermocline due to this constriction. However the DSDP Site 590B record stops at ~2.5 Ma so the continued influence of Subantarctic Mode Water continued on the EEP thermocline from 2.5 Ma to present is unknown.

5.2.3. *Changing source waters and shoaling of the equatorial thermocline*

Reconstruction of the meridional and zonal SST gradient for the Pacific Ocean indicates the tropical warm pool was expanded during the early Pliocene (Brierley et al., 2009). In addition to global impacts on atmospheric circulation and ocean heat uptake (Brierley et al., 2009; Brierley and Fedorov, 2010), an expanded warm pool would directly influence mid-latitude regions where equatorial thermocline waters are sourced. Subsurface temperature *G. tumida* records in the EEP (this study; Steph et al., 2006, 2010) and WEP (LaRiviere et al., in press) suggest extratropical conditions had reduced horizontal gradients, which resulted in a deeper thermocline.

Extratropical changes that may help to explain subsurface conditions in the EEP include: (1) the temperature and salinity properties of the source water, which would influence the density (Fedorov et al., 2007, 2004; Gu and Philander, 1997), (2) a shift in location or preferred pathway of the source water (Huang and Qiu, 1998; Karstensen and Quadfasel, 2002; Suga et al., 2004; Zhang and Liu, 1999) and/or (3) the relative contributions of North and South Pacific source waters (Cane and Molnar, 2001; Fine et al., 2001; Johnson and McPhaden, 1999; O'Connor et al., 2002; Toggweiler et al., 1991). Intimately related to changes in equatorial thermocline source water regions is a change in the equatorial thermocline and possibly global thermocline (Philander and Fedorov, 2003). Changes within these thermocline source water regions (Karas et al., 2011) and their impact on the equatorial thermocline and EEP SST may have been an important factor in the transition out of the warm Pliocene and into the cold Pleistocene climate (Brierley and Fedorov, 2010).

During the early Pliocene, an altered global heat budget resulted in a deep global thermocline and may explain the Pliocene warm period (Fedorov et al., 2006). Alkenone based SST reconstructions from the upwelling regions of California, Peru and the EEP, indicate low latitude upwelling regions were 3–9 °C warmer than today during the early Pliocene, suggesting the global thermocline was deep in comparison to its modern position (Dekens et al., 2007; Fedorov et al., 2006). Our new subsurface temperature records provide direct evidence that EEP thermocline was deep during the early Pliocene. Due to the deep thermocline, the EEP gained less heat during the Pliocene warm period. In order to balance the global heat budget, others suggest that the ocean absorbed heat over a larger area and, in the absence of evidence for significantly warmer than present SSTs in the WEP, that this would require higher vertical mixing rates (Brierley et al., 2009; Brierley and Fedorov, 2010; Fedorov et al., 2006), perhaps due to increased hurricane activity (Fedorov et al., 2010). This change in the global heat budget and the accompanying alterations in atmospheric and ocean circulation, as well as changes in greenhouse gases (water vapor, CO_2) may explain the Pliocene warm period.

Fedorov et al. (2006) hypothesize that at approximately 3 Ma, the global thermocline sufficiently shoaled, cool waters upwelled along the equator and subtropical upwelling zones, and global climate transitioned from the warm Pliocene to the cool Pleistocene. However, we propose that the balance of observational data indicate that the transition began at ~4 Ma. Warm SSTs in the EEP (Dekens et al., 2007; Lawrence et al., 2006; Wara et al., 2005) coupled with subsurface temperature records generated for this study and others (Steph et al., 2006, 2010) suggest the EEP thermocline shoaled sufficiently to influence and cool SSTs ~4 Ma (Fig. 4). Restriction of the Panamanian Seaway played a pivotal role in this transition because regional EEP thermocline shoaling between 4.8 and 4.0 Ma by effectively bringing cold waters closer to the surface to be upwelled by wind-driven processes. This set up air–sea feedbacks to further cool the EEP, shoal the thermocline and alter the global heat budget. It is interesting to note our subsurface temperature records do not have significant steps or events correlating with climatically important events such as initiation (~3.6 Ma, Mudelsee and Raymo, 2005) and intensification (~2.75 Ma, Haug et al., 1999) of Northern Hemisphere Glaciation. No abrupt transitions would be expected if the Pacific wide thermocline was mainly adjusting to gradual changes in its source water regions in mid-latitudes, which were not strongly impacted by the high latitude conditions that changed dramatically during glaciation.

5.3. *Development of regional subsurface temperature structure*

Wind forcing determines much of the surface and subsurface temperature gradients and thermocline structure in the EEP (Fig. 5a). Along the equatorial thermocline transect from 3°S to 7°N (captured at ODP Sites 848, 849 and 853), the spatial evolution of the subsurface temperature records suggest intensification of the southeast trades from the Pliocene to present in the EEP. Today, west of 110 °W, the atmospheric circulation is generally zonal, but east of 110 °W the trades and wind jets through Central America influence the complex oceanographic structure of the EEP (for a comprehensive review, see Kessler, 2006). The westward flowing South Equatorial Current (SEC, Fig. 5a) bifurcates in the far eastern EEP. It has two main branches at 3°N and 3°S and is relatively weak on the equator. The northern boundary of the SEC appears as a sharp SST front that separates the cold tongue from the EEP warm pool. Immediately below the SEC, the Equatorial Undercurrent (EUC, Fig. 5b) and thermocline are deepest in the west and tilt to shallower depths toward the east. As the thermocline forms an east–west oriented ridge along the equator, the EUC and upper thermocline are the primary source of upwelling water. In addition, strong southeast trade winds (Fig. 5a) strengthen upwelling to the south of the equator. To the north, a thermocline trough centered at 5 °N and a thermocline ridge centered at 10 °N limit the eastward flowing North Equatorial Counter Current (NECC) (Fig. 5a).

In a modern meridional cross section (Fig. 5c), the dynamic position of the thermocline (20 °C isotherm) and ODP Sites 848, 849 and 853 are plotted. Recent subsurface temperatures from Sites 849 and 848 have the coolest temperatures because they are centered on a thermocline ridge and Site 853 has the warmest temperatures because it is located near a thermocline trough. In Fig. 5d, subsurface temperature is averaged over one million-yr time intervals and plotted along latitude. The most striking

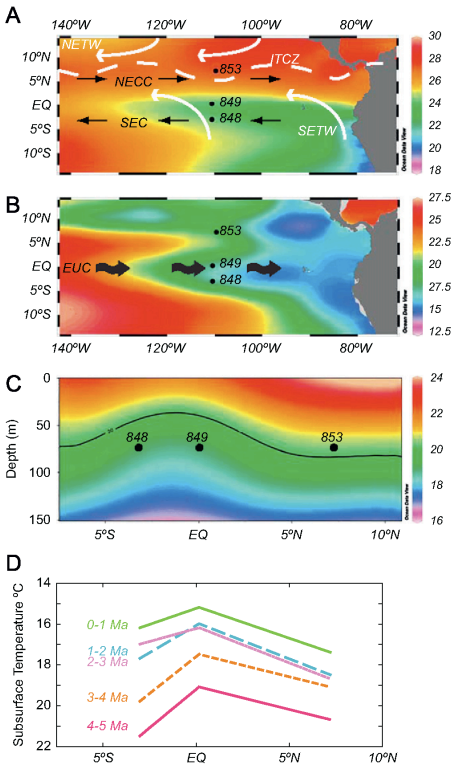

Fig. 5. Regional changes in subsurface temperature profiles. Map view (A) of modern sea surface temperatures, equatorial currents denoted in black arrows and atmospheric features denoted in white lines (Intertropical Convergence Zone—ITCZ, Southeast Trade Winds—SETW, Northeast Trade Winds—NETW). Map view (B) of modern subsurface temperatures at ~75 m depth, the approximate calcification depth of *G. tumida*, Equatorial Undercurrent (EUC) denoted with a black arrow. Cross section view (C) along transect at approximately 110 °W longitude, 20 °C isotherm denoted with black line. Average subsurface temperature binned in one million year intervals (D) for Sites 848, 849 and 853. Axis is plotted in reverse to compare with the structure of the 20 °C isotherm.

feature of Fig. 5d is that the same subsurface temperature structure present in Fig. 5c is present though the Pleistocene and early Pliocene. A similar stable pattern of sedimentation rates (Farrell et al., 1995) and atmospheric circulation (Hovan 1995) is observed from ~4.5 Ma to present day. For example, eolian dust grainsize data indicate the Intertropical Convergence Zone (ITCZ) has been north of the equator since the early Pliocene (Hovan, 1995). Similarly, light $\delta^{18}O$ values from Site 853, which we interpret as an increased fresh water flux in comparison to Sites 848 and 849, suggest there was a northward displacement of the ITCZ during the early Pliocene in comparison to modern, which is also consistent with eolian flux records (Hovan, 1995). Although each site has a different cooling history and magnitude of cooling, the thermocline structure is maintained, suggesting general patterns of oceanic and atmospheric forcing have been present since at least the early Pliocene.

Although subsurface temperature cooled at all sites from the early Pliocene to late Pleistocene, a different magnitude of cooling occurred at each site: 5.4 °C, 4.0 °C and 3.4 °C for ODP Sites 848, 849 and 853, respectively. At the start of the record, in the early Pliocene, subsurface temperature at ODP Site 848 was noticeably warmer than at ODP Site 853, but around 3 Ma, it became cooler. The relatively enhanced cooling of subsurface temperatures at ODP Site 848 over the last 4 myr, must have occurred due to increasing advection of coastally upwelled water and/or the expanding influence of regional upwelling due to the strengthening of the southeast trade winds (Hovan, 1995). Specifically, increased southeast trade winds would strengthen the SEC and Ekman transport resulting in advection of coastally upwelled water, and in enhanced local upwelling, which would further shoal and broaden the equatorial thermocline just south of the equator. The comparatively warmer subsurface temperatures at ODP Site 853 and Site 1241 (Steph et al., 2006, 2010) are related to the development of the doldrums, the ITCZ, and the evolution of a stable eastern tropical warm pool.

From ~2 to 3 Ma subsurface temperatures at Sites 848 and 849 are comparable, seen as a flattening of the reconstructed thermocline depth between the two sites in Fig. 5d. An increased thermocline subsurface contribution from cooler South Pacific or Subantarctic Mode waters or enhanced southeast trade strength which would further shoal the thermocline and could explain cool temperatures at Site 848 between 2 and 3 Ma. However, additional eolian data (as a proxy for wind strength) and temperature reconstructions for thermocline source water regions are necessary to determine a cause. Interestingly, at ~2 Ma, when modern-like basin-wide zonal and meridional SST gradients were established (Etourneau et al., 2009; Martinez-Garcia et al., 2010), the relative subsurface temperatures trend stabilized such that 853 was the warmest, 849 was the coolest and 848 was in between (though ~0.4 Ma subsurface temperatures at Site 853 and 848 temporarily overlap). This suggests that in addition to stable SST gradients, the thermocline source water regions and overall wind forcing components stabilized as well. In summary, while the general EEP thermocline structure has been present since at least the early Pliocene, regional atmospheric and oceanic changes, such as a strengthening of the southeast trade winds and its influence on surface water (i.e. advection of water, local upwelling) were also important for establishing the modern thermocline structure at ~2 Ma.

6. Summary

Subsurface temperatures in the EEP show a long cooling history from the early Pliocene warm period to modern. Between 4.8 and 4.0 Ma, the Panama Seaway restriction preconditioned sea surface temperature cooling in the EEP starting at ~4 Ma by dramatically altering subsurface temperature and thermocline water structure (this study; Steph et al., 2006, 2010). Closure of the Panama Seaway enhanced meridional heat transport to the northern hemisphere (Lunt et al., 2008), altering EEP thermocline source water regions (Karas et al., 2011) which cooled EEP subsurface temperatures. From 4.0 Ma to present, subsurface temperatures in the EEP continued to cool gradually, appearing unaffected by major climatic shifts. More broadly, it appears that changes in source water regions and the global heat budget influenced the depth of the equatorial thermocline, perhaps globally (Fedorov et al., 2006). In addition, regional differences in evolution of subsurface temperature structure indicate regional changes in atmospheric and oceanic forcing.

Although the subsurface temperature records presented here are only representative of the EEP, the EEP thermocline depth and the global heat budget are intimately related—the global oceanic

heat budget is balanced by equal heat loss at high latitudes and heat gain in low latitudes where the thermocline outcrops at the ocean's surface (Fedorov et al., 2006). Though high latitude processes such as reduced ice cover and sea ice are likely important for maintaining early Pliocene warmth, warm sea surface temperatures in upwelling regions, a direct consequence of a deep thermocline, are an additional factor. Specifically, the development of meridional temperature gradients between low latitudes (e.g. upwelling zones) and mid-latitudes (thermocline source water regions) is particularly important for the transition from warm Pliocene to the cold Pleistocene via atmospheric teleconnections (Brierley and Fedorov, 2010).

The gradual change in the EEP thermocline position, which is governed by mid-latitude subsurface and thermocline water source regions, supports the idea that mid-latitude regions are important for connecting low and high latitudes (Brierley et al., 2009; Dekens et al., 2007; Fedorov et al., 2007). Generating sea surface temperature records from these areas is necessary to understand the complete global climate transition from the warm Pliocene to the cold Pleistocene.

Acknowledgement

We would like to thank L. Anderson, J. LaRiviere, K. Dyez, D. Rossiter, and E. Randall-Goodwin for their helpful discussions and reviewing initial drafts of this manuscript. Additionally, we would like to thank four anonymous reviewers whose comments greatly improved the quality of this manuscript. R. Franks and D. Andreasen provided analytical support and members of the Ravelo laboratory group assisted with sample preparation and processing. This research used samples and/or data provided by the Ocean Drilling Program (ODP) and Integrated Ocean Drilling Program (IODP). This work was support by NSF Grants OCE-0902047 and OCE-623419, IUP Senate Fellowship Program, and Consortium for Ocean Leadership Schlanger Fellowship.

References

Anand, P., Elderfield, H., Conte, M.H., 2003. Calibration of Mg/Ca thermometry in planktonic foraminifera from a sediment trap time series. Paleoceanography 18, 1050.

Boyle, E.A., Keigwin, L.D., 1985. Comparison of Atlantic and Pacific paleochemical records for the last 215,000 years—changes in deep ocean circulation and chemical inventories. Earth Planet. Sci. Lett. 76, 135–150.

Brierley, C., Fedorov, A., Liu, Z., Herbert, T., Lawrence, K., Lariviere, J., 2009. Greatly expanded tropical warm pool and weakened Hadley circulation in the early Pliocene. Science 323, 1714–1718.

Brierley, C.M., Fedorov, A.V., 2010. Relative importance of meridional and zonal sea surface temperature gradients for the onset of the ice ages and Pliocene–Pleistocene climate evolution. Paleoceanography 25, PA2214.

Brown, S.J., Elderfield, H., 1996. Variations in Mg/Ca and Sr/Ca ratios of planktonic foraminifera caused by postdepositional dissolution: evidence of shallow Mg-dependent dissolution. Paleoceanography 11, 543–551.

Cane, M., Molnar, P., 2001. Closing of the Indonesian seaway as a precursor to east African aridi@cation around 3–4 million years ago. Nature 411, 157–162.

Cannariato, K., Ravelo, A., 1997. Plio-Pleistocene evolution of eastern tropical Pacific surface water circulation and thermocline depth. Paleoceanography 12, 805–820.

Chaisson, W., Ravelo, A., 2000. Pliocene development of the east-west hydrographic gradient in the equatorial Pacific. Paleoceanography 15, 497–505.

Charles, C.D., Fairbanks, R.G., 1990. Glacial–interglaciacl changes in the isotopic gradients of Southern Ocean surface water. In: Bleil, U., Thiede, J. (Eds.), The Geologic History of Polar Oceans: Arctic vs. Antarctic, NATO ASI Series, vol. 308. Kluwer Academic, Norwell, Massachusetts, pp. 519–538.

Cléroux, C., Cortijo, E., Anand, P., Labeyrie, L., Bassinot, F., Caillon, N., Duplessy, J.C., 2008. Mg/Ca and Sr/Ca ratios in planktonic foraminifera: proxies for upper water column temperature reconstruction. Paleoceanography 23, 1–16.

Coates, A.G., Aubry, M.-P., Berggren, W.A., Collins, L.S., Kunk, M., 2003. Early Neogene history of the Central American arc from Bocas del Toro, western Panama. Geol. Soc. Am. Bull. 115, 271–287.

Dekens, P., Ravelo, A., McCarthy, M., 2007. Warm upwelling regions in the Pliocene warm period. Paleoceanography 22, 12.

Dekens, P., Lea, D., Pak, D., Spero, H., 2002. Core top calibration of Mg/Ca in tropical foraminifera: Refining paleotemperature estimation. Geochem. Geophys. Geosyst, p. 3.

Duncan, R.A., Clague, D.A., 1985. Pacific plate motion recorded by linear volcanic chains. In: Nairn, A.E.M., Stehli, F.G., Uyeda, S. (Eds.), The Ocean Basins and Margins: The Pacific Ocean. Plenum, New York, pp. 89–121.

Etourneau, J., Martinez, P., Blanz, T., Schneider, R., 2009. Pliocene–Pleistocene variability of upwelling activity, productivity, and nutrient cycling in the Benguela region. Geology 37, 871–874.

Farmer, E.C., Kaplan, A., de Menocal, P.B., Lynch-Stieglitz, J., 2007. Corroborating Ecological Depth Preferences of Planktonic Foraminifera in the Tropical Atlantic with the Stable Oxygen Isotope Ratios of Core Top Specimens.

Farrell, J.W., Murray, D.W., McKenna, V.S., Ravelo, A.C., 1995. Upper ocean temperature and nutrient contrasts inferred from Pleistocene planktonic foraminifer d18O and d13C in the Eastern Equatorial Pacific. Proc. Ocean Drilling Program Sci. Results 138, 289–319 (13, Leg 138).

Fedorov, A., Barreiro, M., Boccaletti, G., Pacanowski, R., Philander, S., 2007. The freshening of surface waters in high latitudes: effects on the thermohaline and wind-driven circulations. J. Phys. Oceanogr. 37, 896–907.

Fedorov, A., Dekens, P., McCarthy, M., Ravelo, A., deMenocal, P., Barreiro, M., Pacanowski, R., Philander, G., 2006. The Pliocene paradox (mechanisms for a permanent El Nino). Science 312, 1485–1489.

Fedorov, A.V., Brierley, C.M., Emanuel, K., 2010. Tropical cyclones and permanent El Niño in the early Pliocene epoch. Nature 463, 1066–1070.

Fedorov, A.V., Pacanowski, R., Philander, S., Boccaletti, G., 2004. The effect of salinity on the wind-driven circulation and the thermal structure of the upper ocean. J. Phys. Oceanogr. 34, 1949–1966.

Fiedler, P.C., Talley, L.D., 2006. Hydrography of the eastern tropical Pacific: a review. Prog. Oceanogr. 69, 143–180.

Fine, R.A., Maillet, K.A., Sullivan, K.F., Willey, D., 2001. Circulation and ventilation flux of the Pacific Ocean. J. Geophys. Res. Oceans 106, 22159–22178.

Groeneveld, J., Steph, S., Tiedemann, R., Garbe-Schönberg, D., Nürnberg, D., Sturm, A., 2006. 13. Pliocene Mixed-Layer Oceanography for Site 1241, Using Combined Mg/Ca and 18 O Analyses of Globigerinoides sacculifer. In: Tiedemann, R., Mix, A., Richter, C., Ruddiman, W. (Eds.), Proceedings of the Ocean Drilling Program, Scientific Results, vol. 202; 2006, pp. 1–27.

Gu, D.F., Philander, S.G.H., 1997. Interdecadal climate fluctuations that depend on exchanges between the tropics and extratropics. Science 275, 805–807.

Haug, G.H., Sigman, D.M., Tiedemann, R., Pedersen, T.F., Sarnthein, M., 1999. Onset of permanent stratification in the subarctic Pacific Ocean. Nature 401, 779–782.

Haug, G.H., Tiedemann, R., Zahn, R., Ravelo, A.C., 2001. Role of Panama uplift on oceanic freshwater balance. Geology 29, 207–210.

Huang, R.X., Cane, M.A., Naik, N., Goodman, P., 2000. Global adjustment of the thermocline in response to deepwater formation. Geophys. Res. Lett. 27, 759–762.

Hautala, S.L., Roemmich, D.H., 1998. Subtropical mode water in the Northeast Pacific Basin. J. Geophys. Res. Oceans 103, 13055–13066.

Haywood, A., Sellwood, B., Valdes, P., 2000. Regional warming: Pliocene (3 Ma) paleoclimate of Europe and the Mediterranean. Geology 28, 1063–1066.

Haywood, A.M., Valdes, P.J., 2004. Modelling Pliocene warmth: contribution of atmosphere, oceans and cryosphere. Earth Planet. Sci. Lett. 218, 363–377.

Hovan, S., 1995. 28. Late Cenozoic atmospheric circulation intensity and climatic history recorded by Eolian deposition in the Eastern Equatorial Pacific Ocean, Leg 138. In: Pisias, N., Mayer, L., Janecek, T., Palmer-Julson, A., van Andel, T. (Eds.), Proceedings of the Ocean Drilling Program, Scientific Results. Proceedings of the Ocean Drilling Program, Scientific Results, pp. 615–625.

Huang, R.X., Qiu, B., 1998. The structure of the wind-driven circulation in the subtropical South Pacific ocean. J. Phys. Oceanogr. 28, 1173–1186.

Jenkins, W., 1996. Tritium and 3He in the WOCE Pacific Programme. Int. WOCE Newsl. 23, 6–8.

Johnson, G.C., McPhaden, M.J., 1999. Interior pycnocline flow from the subtropical to the equatorial Pacific Ocean. J. Phys. Oceanogr. 29, 3073–3089.

Karas, C., Nürnberg, D., Tiedemann, R., Garbe-Schönberg, D., 2011. Pliocene climate change of the Southwest Pacific and the impact of ocean gateways. Earth Planet. Sci. Lett. 301, 117–124.

Karstensen, J., Quadfasel, D., 2002. Formation of southern hemisphere thermocline waters: water mass conversion and subduction. J. Phys. Oceanogr. 32, 3020–3038.

Keller, G., Zenker, C., Stone, S., 1989. Late Neogene history of the Pacific-Caribbean gateway. J. South Am. Earth Sci. 2, 73–108.

Kessler, W.S., 2006. The circulation of the eastern tropical Pacific: a review. Prog. Oceanogr. 69, 181–217.

LaRiviere, J.P., Ravelo, A.C., Crimmins, A., Dekens, P.S., Ford, H.L., Lyle, M., Wara, M.W., 2012. Late Miocene decoupling of oceanic warmth and atmospheric carbon dioxide forcing. Nature 486, 97–100.

Lavin, M.F., Fiedler, P.C., Amador, J.A., Ballance, L.T., Farber-Lorda, J., Mestas-Nunez, A.M., 2006. A review of eastern tropical Pacific oceanography: summary. Prog. Oceanogr. 69, 391–398.

Lawrence, K.T., Liu, Z.H., Herbert, T.D., 2006. Evolution of the eastern tropical Pacific through Plio-Pleistocene glaciation. Science 312, 79–83.

Lea, D., Boyle, E.A., 1993. Determination of carbonate-bound barium in foraminifera and corals by isotope-dilution plasma mass-spectrometry. Chem. Geol. 103, 73–84.

Lisiecki, L.E., Raymo, M.E., 2005. A Pliocene–Pleistocene stack of 57 globally distributed benthic delta O-18 records. Paleoceanography 20, PA1003.

Lopes dos Santos, R.A.L., Prange, M., Castañeda, I.S., Schefuß, E., Mulitza, S., Schulz, M., Niedermeyer, E.M., et al., 2010. Glacial–interglacial variability in Atlantic meridional overturning circulation and thermocline adjustments in the tropical North Atlantic. Earth Planet. Sci. Lett. 300, 407–414, http://dx.doi.org/10.1016/j.epsl.2010.10.030.

Lunt, D.J., Valdes, P.J., Haywood, A., Rutt, I.C., 2008. Closure of the Panama Seaway during the Pliocene: implications for climate and Northern Hemisphere glaciation. Climate Dyn. 30, 1–18.

Marshall, L.G., Webb, S.D., Sepkoski, J.J., Raup, D.M., 1982. Mammalian evolution and the Great American Interchange. Science 215, 1351–1357.

Martinez-Garcia, A., Rosell-Mele, A., McClymont, E.L., Gersonde, R., Haug, G.H., 2010. Subpolar link to the emergence of the modern equatorial pacific cold tongue. Science 328, 1550–1553.

Mekik, F., François, R., 2007. A novel approach to dissolution correction of Mg/Ca-based paleothermometry in the tropical Pacific. Paleoceanography.

Mix, A., Pisias, N., Rugh, W., Wilson, J., Morey, A., Hagelberg, T.K., 1995. Benthic foraminifer stable isotope record from Site 849 (0–5 Ma): local and global climate changes. Proc. Ocean Drilling Program Sci. Results 138, 371–412.

Molnar, P., 2008. Closing of the Central American Seaway and the Ice Age: a critical review. Paleoceanography 23, 15.

Mudelsee, M., Raymo, M.E., 2005. Slow dynamics of the Northern Hemisphere glaciation. Paleoceanography 20, PA4022.

Nathan, S., Leckie, R., 2009. Early history of the Western Pacific Warm Pool during the middle to late Miocene (~13.2–5.8 Ma): role of sea-level change and implications for equatorial circulation. Palaeogeogr. Palaeoclimatol. Palaeoecol. 274, 140–159.

O'Connor, B.M., Fine, R.A., Maillet, K.A., Olson, D.B., 2002. Formation rates of subtropical underwater in the Pacific Ocean. Deep-Sea Res. I Oceanogr. Res. Pap. 49, 1571–1590.

Pagani, M., Liu, Z., Lariviere, J., Ravelo, A., 2010. High Earth-system climate sensitivity determined from Pliocene carbon dioxide concentrations. Nat. Geosci. 3, 27–30.

Philander, S.G., Fedorov, A.V., 2003. Role of tropics in changing the response to Milankovich forcing some three million years ago. Paleoceanography 18, 12.

Ravelo, A.C., Fairbanks, R., 1992. Oxygen isotopic composition of multiple species of planktonic foraminifera: recorders of the modern photic zone temperature gradient. Paleoceanography 7, 815–831.

Regenberg, M., Steph, S., Nürnberg, D., Tiedemann, R., Garbe-Schönberg, D., 2009. Calibrating Mg/Ca ratios of multiple planktonic foraminiferal species with δ^{18}O-calcification temperatures: paleothermometry for the upper water column. Earth Planet. Sci. Lett. 278, 324–336.

Rickaby, R., Halloran, P., 2005. Cool La Nina during the warmth of the Pliocene? Science 307, 1948–1952.

Rincón-Martínez, D., Steph, S., Lamy, F., Mix, A., Tiedemann, R., 2011. Tracking the equatorial front in the eastern equatorial Pacific Ocean by the isotopic and faunal composition of planktonic foraminifera. Mar. Micropaleontol. 79, 24–40.

Rodgers, K.B., Latif, M., Legutke, S., 2000. Sensitivity of equatorial Pacific and Indian Ocean watermasses to the position of the Indonesian throughflow. Geophys. Res. Lett. 27, 2941–2944.

Shackleton, N.J., Crowhurst, S., Hagelberg, T., Pisias, N., Schneider, D., 1995. 6. A New Late Neogene Time Scale: Application to Leg 138 Sites. In: Pisias, N., Mayer, L., Janecek, T., Palmer-Julson, A., van Andel, T. (Eds.), Proceedings of the Ocean Drilling Program, Scientific Results, vol. 138; 1995, pp. 73–101.

Schweitzer, P.N., Lohmann, G.P., 1991. Ontogeny and habitat of modern menardiform planktonic foraminifera. J. Foraminiferal Res. 21, 332–446.

Seki, O., Foster, G.L., Schmidt, D.N., Mackensen, A., Kawamura, K., Pancost, R.D., 2010. Alkenone and boron-based Pliocene pCO_2 records. Earth Planet. Sci. Lett. 292, 201–211.

Steph, S., Tiedemann, R., Groeneveld, J., Sturm, A., Nürnberg, a., 2006. Pliocene changes in tropical East Pacific Upper Ocean stratification: response to tropical gateways? Proc. Ocean Drilling Program Sci. Results 202, 1–51.

Steph, S., Tiedemann, R., Prange, M., Groeneveld, J., Schulz, M., Timmermann, A., Nürnberg, D., Rühlemann, C., Saukel, C., Haug, G., 2010. Early Pliocene increase in thermohaline overturning: a precondition for the development of the modern equatorial Pacific cold tongue. Paleoceanography 25, PA2202.

Suga, T., Motoki, K., Aoki, Y., Macdonald, A.M., 2004. The North Pacific climatology of winter mixed layer and mode waters. J. Phys. Oceanogr. 34, 3–22.

Toggweiler, J.R., Dixon, K., Broecker, W.S., 1991. The Peru upwelling and the ventilation of the South-Pacific thermocline. J. Geophys. Res. Oceans 96, 20467–20497.

van Andel, Tj. H., Heath, G.R., Moore Jr., T.C., 1975. Cenozoic history and paleoceanography of the central equatorial Pacific Ocean. Geol. Soc. Am. Mem. 143, 134 p.

Wara, M., Anderson, L., Schellenberg, S., Franks, F., Ravelo, A., Delaney, M., 2003. Application of a radially viewed inductively coupled plasma-optical emission spectrophotometer to simultaneous measurement of Mg/Ca, Sr/Ca, and Mn/Ca ratios in marine biogenic carbonates. Geochem. Geophys. Geosyst. 4, 14.

Wara, M.W., Ravelo, A., Delaney, M.L., 2005. Permanent El Nino-like conditions during the Pliocene warm period. Science 309, 758–761.

Webb, S.D., Rancy, A., 1996. Late Cenozoic evolution of the neotropical mammal fauna. In: Jackson, J., Budd, A.F., Coates, A.G. (Eds.), Evolution and Environment in Tropical America. University of Chicago Press, Chicago, pp. 335–358.

Wong, A.P.S., Johnson, G.C., 2003. South Pacific eastern subtropical mode water. J. Phys. Oceanogr. 33, 1493–1509.

Zhang, R.H., Liu, Z.Y., 1999. Decadal thermocline variability in the North Pacific Ocean: two pathways around the subtropical gyre. J. Climate 12, 3273–3296.

Zhang, X., Prange, M., Steph, S., Butzin, M., Krebs, U., Lunt, D.J., Nisancioglu, K.H., Park, W., Schmittner, A., Schneider, B., Schulz, M., 2012. Changes in equatorial Pacific thermocline depth in response to Panamanian seaway closure: insights from a multi-model study. Earth Planet. Sci. Lett. 317–318, 76–84.

Chapter 3: Reduced ENSO during the Last Glacial Maximum

ABSTRACT

El Niño-Southern Oscillation is a major source of global interannual variability (Alexander et al., 2002) with far-reaching climatic effects (Curtis, 2008), but its behavior in the face of future global warming is largely unknown (Meehl and Stocker, 2007). Paleoclimate records from the Last Glacial Maximum can provide insight into ENSO behavior when important boundary conditions such as ice sheet extent and atmospheric *p*CO2 were different than today. We use Mg/Ca ratios of individual shells of planktonic foraminifera to reconstruct Last Glacial Maximum surface and sub-surface temperature variability at western and eastern equatorial Pacific sites. Uniformly cooler temperatures in the western equatorial Pacific suggest that *p*CO2-radiative forcing controlled seasonal and annual average temperatures there. In the Eastern Equatorial Pacific, a skewed and reduced range of surface temperatures suggests that both radiative pCO_2 and dynamic oceanic-atmospheric processes controlled temperature in that region. Further, the reduced range of surface temperatures suggests that the El Niño-Southern Oscillation was absent or greatly diminished in strength. The mean equatorial climate state during the Last Glacial Maximum included a weaker zonal temperature gradient, steeper equatorial thermocline tilt, and stronger Walker Circulation (Koutavas and Lynch-Stieglitz, 2003; Otto-Bliesner et al., 2003; DiNezio et al., 2011; Andreasen et al., 2001; Shin et al., 2003). How mean state changes affects the balance of positive and negative

feedbacks that determine ENSO amplitude is model dependent (Guilyardi, 2006). Our new results for the LGM provide observational constraints for the development and testing of models that could enhance their ability to project ENSO behavior in the future.

MAIN TEXT

The warm Western Equatorial Pacific (WEP), with a relatively deep thermocline, acts as a center of latent heat flux to the global climate system. In contrast, Eastern Equatorial Pacific (EEP) is characterized by a shallow thermocline and vigorous upwelling that brings cold water to the surface where a large amount of radiation is absorbed. Today, the equatorial east-west SST gradient and thermocline structure are tightly coupled and significantly influence the mean state and variability of the tropical Pacific (Guilyardi, 2006).

While the WEP seasonal variability is relatively small, seasonal variation in the EEP is large, reflecting the interplay between radiative heating and local to basin-wide atmospheric and oceanic forcing (Wang and McPhaden, 1999). Superimposed on the seasonal cycle is ENSO, which is dynamically influenced, both in initiation and strength, by the underlying processes that determine the seasonal cycle (Wang and McPhaden, 1999; Wang and McPhaden, 2000).

During the Last Glacial Maximum (LGM, ~21,000 years ago), tropical sea surface temperatures (SST) were ~2.7 °C cooler than modern day (Ballantyne, 2005), largely due to reduced radiative forcing by CO_2 (Lea, 2004). However, SST reconstructions suggest that the LGM was not uniformly cooler than today, and that the east-west SST gradient across the tropical Pacific was possibly weaker, neutral, or stronger than today (Lea et al., 2000; Hewitt et al., 2003; Patrick and Thunell, 1997; Koutavas et al., 2002). While some LGM climate models suggest that SST changes should be uniform and primarily controlled by radiative forcing, others predict

asymmetric SST changes related to strong dynamical controls on regional temperature (e.g. cloud/evaporation feedbacks, Walker Circulation , thermocline depth or upwelling, Hewitt et al., 2003). The net effect of these processes on the tropical Pacific mean state, oceanic structure and pattern is unknown but their interaction could inhibit or strengthen ENSO events in the past and future (Fedorov and Philander, 2001). Past records of climate are useful in understanding how the variability and mean state of tropical climate changed under different boundary conditions such as lower CO_2 concentrations.

We use temperature records from Ocean Drilling Program (ODP) Site 806 from the Western Pacific Warm Pool and ODP Site 849 from the Eastern Pacific Cold Tongue to reconstruct surface and subsurface temperature variability across the tropical Pacific, (Fig. 1). Unlike several previous reconstructions (e.g. Rein et al., 2005; Tudhope et al., 2001; Leduc et al., 2009), our sites are ideally located to directly monitor changes in SST and thermocline depth strongly associated with ENSO dynamics. Site 806 is located in the heart of the warm pool on the equator where SST variability is small and primarily in the interannual to decadal frequency. In contrast, Site 849 is located on the equator in the EEP cold tongue extension where variability is relatively large and dominated equally by seasonal and ENSO frequencies (Wang and Fiedler, 2006), away from the influence of advection of waters from the Peru upwelling system. Sediment samples from these sites integrate several hundreds of years of variability. While secular SST trends over the timespan represented by a sample could influence reconstructed variability at these sites, the

relatively small SST changes over <1000 years documented in these cores suggests that seasonal and interannual frequencies of variation will dominate our reconstructions. To reconstruct tropical variability, we use Mg/Ca of individual surface and subsurface dwelling foraminifera (*Globigerinoides sacculifer* without sac-like final chamber and *Globorotalia tumida*, respectively) from the west and east during the late Holocene and LGM. In addition, we analyzed one glacial sample ~1000 years older then our LGM sample at EEP site 849. The Mg/Ca-derived ocean temperature populations are compared to each other and to modern hydrographic data using statistical methods for detecting differences in frequency distribution functions (Supplementary Material).

In comparison to the late Holocene, LGM surface and subsurface temperatures in the Western Equatorial Pacific (WEP) were uniformly cooler by ~2.3 to 2.4 ˚C with no apparent change in variability (Figure 3.2a and 3.2d). Cooler subsurface temperatures during the LGM could be interpreted as a colder or shallower thermocline (Sagawa et al., 2011), however modeling (DiNezio et al., 2011), faunal (Andreasen and Ravelo, 1997) and geochemical (Xu et al., 2010) studies suggest that the thermocline was actually deeper during the LGM. Thus, cooler subsurface temperatures must reflect that the whole ocean, particularly in the source region of the thermocline waters, was colder during the LGM. As average surface and subsurface temperature cooling occurred without a change in individual foraminifera temperature variability, this is consistent with pCO_2 radiative forcing as the main agent of WEP SST change (Medina-Elizalde and Lea, 2005; Lea et al., 2000). While unlikely,

dynamical processes that did not change the temperature distribution, such as changes in year-round upwelling, cannot be ruled out as a possible contributor to WEP cooling during the LGM.

In the Eastern Equatorial Pacific (EEP), the average SST was ~1.2-1.3˚C cooler during the glacial period in comparison to the late Holocene reflecting greater cooling of warm SSTs and minimal cooling of cold SSTs (i.e. a cooler warm season, Figure 3.2b/c). In the modern ocean, EEP surface variability is controlled by locally wind-forced upwelling, with weakest upwelling and warmest SST occurring during the boreal spring (Wang and McPhaden, 1999). The warm season during the LGM was ~2˚C cooler than today consistent with reduced pCO_2 forcing and possibly stronger upwelling-favorable winds. In contrast, cool season temperatures during the Glacial period were similar to today; thus, cooling due to lower pCO_2 must have been countered by less intense upwelling. Overall, EEP SST variability during the glacial period was reduced in comparison to modern. Analysis of modern hydrographic data (Supplementary Material) provides insight into the interpretations of this reduction and indicates that the amplitude of ENSO was greatly reduced during the glacial period. Our reconstruction of the EEP cold tongue variability, which directly records a reduction in ENSO strength, is supported by auxiliary data from sediment (Rein et al., 2005), coral (Tudhope et al., 2001) and foraminiferal (Leduc et al., 2009) records which suggest ENSO was weak during past glacial periods.

Our results contrast with those of Koutavas and Joanides (2012) who use the variance of individual surface dwelling *Globigerinoides ruber* $\delta^{18}O$ values at site

V21-30 in the east equatorial Pacific, to suggest an increase in ENSO activity during the glacial period. However, changes to ENSO preferentially affect the tails of the $\delta^{18}O$ distribution while variance integrates both ENSO and seasonal cycle variability. We examined the Koutavas and Joanides dataset using our statistical methods and found that the $\delta^{18}O$ distributions are not consistent with an increase in ENSO activity, but rather suggestive of an increase in seasonality during the last glacial period in comparison to the Late Holocene (Supplementary Material).

In the EEP, the subsurface average temperature was ~0.3˚C cooler, and the variability was higher during the glacial period in comparison to the late Holocene (Figure 3.2e/f). As discussed above, the SST data from the EEP indicates that ENSO variability was reduced during the glacial period, and therefore, the relatively high subsurface variability must be related to processes that alter subsurface variability independently. In the modern ocean, subsurface variability in the EEP thermocline is forced locally and remotely by seasonal winds (Wang et al., 2000); here we attribute higher subsurface variability to increased vertical migration of the thermocline responding to seasonal variations in basin-wide pressure gradient and/or remote winds. Alternatively, a tighter thermocline during the glacial period, that is, a steeper change in temperature with depth within the habitat of the subsurface dwelling foraminifera, could also explain enhanced subsurface variability. Our data indicates a combination of dynamical and radiative processes may have influenced EEP variability, SST and subsurface temperature response during the LGM. In contrast, the response of the WEP may have been primarily radiative.

The understanding as to how the mean state, seasonal cycle and ENSO cycle interact with one another on long time scales is incomplete. Some models indicate an inverse relationship between the intensity of the seasonal cycle and ENSO (Fedorov and Philander, 2001; Timmermann et al., 2007); that is when the seasonal cycle is strong, ENSO is weak. For the EEP, reconstructions at Site 849 indicate ENSO was weak while our reanalysis of the V21-31 data (Koutavas and Joanides, 2012) may suggest enhanced seasonality. Similarly, the observation of greater subsurface variability in the EEP during the glacial period may suggest enhanced seasonality, particularly in the winds. Therefore, the inverse relationship between the seasonal cycle and ENSO strength may be a robust relationship over long time scales.

ENSO behavior is thought to be linked to the mean state of the tropical Pacific (Jin et al., 2006). Past studies have attempted to characterize the mean state during the LGM by measuring the WEP-EEP zonal gradient with mixed results (Lea et al., 2000; Hewitt et al., 2003; Patrick and Thunell, 1997; Koutavas et al., 2002) likely due to the fact that zonal gradient reconstructions are confounded by spatial heterogeneity in the amplitude of SST changes in the EEP. We compiled SST data in the EEP and WEP from the LGM and find that within the EEP the Eastern Pacific Warm Pool (EPWP) was ~2.3˚C cooler than today, while the cold tongue was only ~1.6˚C cooler (Figure 3.1c). The EPWP temperature change was similar to that of the WEP (~2.7˚C, Figure 3.1b) suggesting a largely radiative SST response to lower pCO_2 within both the WEP and EPWP. In contrast, the magnitude of temperature change within the cold tongue was muted by dynamic processes (e.g. wind and upwelling forces) related to changes

in seasonality and interannual variability as demonstrated from our single foraminiferal temperatures. Areally averaged, the amplitude of change in the EEP was less than in the WEP, and thus the equatorial WEP-EEP zonal gradient during the LGM was reduced overall in comparison to today.

Climate models ability to simulate the mean state, especially the tropical spatial pattern (Yin and Battisti, 2001), is particularly important to understanding coupled oceanic-atmospheric conditions and thus variability (Fedorov and Philander, 2001). During the LGM the zonal SST gradient was slightly reduced, the WEP thermocline was slightly cooler, but deeper, and the thermocline tilt between the WEP and EEP was steeper (Andreasen and Ravelo, 1997; Xu et al., 2010; Patrick and Thunell, 1997). The reduced zonal SST gradient has been associated with a reduction in Walker Circulation during the LGM (Koutavas et al., 2002), however, a steeper thermocline tilt during the LGM suggests that the Walker Circulation was, instead, stronger. Modeling simulations demonstrate that enhanced Walker Circulation is possible even when the SST gradient was reduced or unchanged during the LGM (DiNezio et al., 2011). These observed and modeled ocean structure conditions in the LGM, particularly the reduced zonal gradient and deeper thermocline, are consistent with weak and dampened ENSO activity (Jin et al., 2006; Fedorov and Philander, 2001) which could explain why ENSO is largely absent from LGM climate records.

Currently, climate model simulations of ENSO intensity are highly model dependent for the LGM (Otto-Bliesner et al., 2006) and future climate projections (Meehl and Stocker, 2007; Guilyardi, 2006) highlighting model dependence in how

changes in the mean state, feedbacks and teleconnections influence ENSO behavior. The balance of several positive and negative feedbacks (Wang and Picaut, 2004; An and Jin, 2001; Choi et al., 2011) determine the inception, propagation and dominant mode of oscillation of ENSO (Fedorov and Philander, 2001; Guilyardi et al., 2009), but there are large differences between models in how these feedbacks behave when the mean state changes. Our new data showing reduced ENSO, combined with observations of changes in the mean state during the LGM, can be used as a test of model performance including the feedbacks that are critically important to determining ENSO behavior.

REFERENCES

Alexander, M., Bladé, I., Newman, M., Lanzante, J., Lau, N., and Scott, J., 2002, The Atmospheric Bridge: The Influence of ENSO Teleconnections on Air–Sea Interaction over the Global Oceans: Journal of Climate, v. 15, p. 2205–2231.

An, S.-I., and Jin, F.-F., 2001, Collective role of thermocline and zonal advective feedbacks in the ENSO mode*: Journal of Climate, v. 14, no. 16, p. 3421–3432.

Andreasen, D., and Ravelo, A., 1997, Tropical Pacific Ocean thermocline depth reconstructions for the last glacial maximum: Paleoceanography, v. 12, no. 3, p. 395–413.

Andreasen, D., Ravelo, A., and Broccoli, A., 2001, Remote forcing at the last glacial maximum in the tropical Pacific Ocean: Journal Of Geophysical Research-Oceans, v. 106, no. C1, p. 879–897.

Ballantyne, A.P., 2005, Meta-analysis of tropical surface temperatures during the Last Glacial Maximum: Geophysical Research Letters, v. 32, no. 5, p. L05712–, doi: 10.1029/2004GL021217.

Choi, J., An, S.-I., and Yeh, S.-W., 2011, Decadal amplitude modulation of two types of ENSO and its relationship with the mean state: Climate Dynamics, v. 38, no. 11-12, p. 2631–2644, doi: 10.1007/s00382-011-1186-y.

Curtis, S., 2008, The El Niño–Southern Oscillation and Global Precipitation: Geography Compass, v. 2, no. 3, p. 600–619, doi: 10.1111/j.1749-8198.2008.00105.x.

DiNezio, P.N., Clement, A., Vecchi, G.A., Soden, B., Broccoli, A.J., Otto-Bliesner, B.L., and Braconnot, P., 2011, The response of the Walker circulation to Last Glacial Maximum forcing: Implications for detection in proxies: Paleoceanography, v. 26, no. PA3217, doi: 10.1029/2010PA002083.

Fedorov, A.V., and Philander, S., 2001, A Stability Analysis of Tropical Ocean-Atmosphere Interactions: Bridging Measurements and Theory for El Nino: Journal of Climate, v. 14, p. 3086–3101.

Guilyardi, E., 2006, El Niño–mean state–seasonal cycle interactions in a multi-model ensemble: Climate Dynamics, v. 26, no. 4, p. 329–348.

Guilyardi, E., Wittenberg, A., Fedorov, A., Collins, M., Wang, C., Capotondi, A., van Oldenborgh, G.J., and Stockdale, T., 2009, Understanding El Niño in Ocean–Atmosphere General Circulation Models: Progress and Challenges: Bulletin of the American Meteorological Society, v. 90, no. 3, p. 325–340, doi:

10.1175/2008BAMS2387.1.

Hewitt, C., Stouffer, R., Broccoli, A., Mitchell, J., and Valdes, P.J., 2003, The effect of ocean dynamics in a coupled GCM simulation of the Last Glacial Maximum: Climate Dynamics, v. 20, no. 2, p. 203–218.

Jin, F.-F., Kim, S.T., and Bejarano, L., 2006, A coupled-stability index for ENSO: Geophysical Research Letters, v. 33, no. 23, p. L23708, doi: 10.1029/2006GL027221.

Koutavas, A., and Joanides, S., 2012, El Niño–Southern Oscillation extrema in the Holocene and Last Glacial Maximum: Paleoceanography, v. 27, doi: 10.1029/2012PA002378.

Koutavas, A., and Lynch-Stieglitz, J., 2003, Glacial-interglacial dynamics of the eastern equatorial Pacific cold tongue-Intertropical Convergence Zone system reconstructed from oxygen isotope records: Paleoceanography, v. 18, no. 4, p. 1089, doi: 10.1029/2003PA000894.

Koutavas, A., Lynch-Stieglitz, J., Marchitto, T.M., Jr, and Sachs, J.P., 2002, El Nino-like pattern in ice age tropical Pacific sea surface temperature: Science, v. 297, no. 5579, p. 226–230, doi: 10.1126/science.1072376.

Lea, D., Pak, D., and Spero, H., 2000, Climate Impact of Late Quaternary Equatorial Pacific Sea Surface Temperature Variations: Science.

Lea, D.W., 2004, The 100 000-yr cycle in tropical SST, greenhouse forcing, and climate sensitivity: Journal of Climate, v. 17, no. 11, p. 2170–2179.

Leduc, G., Vidal, L., Cartapanis, O., and Bard, E., 2009, Modes of eastern equatorial Pacific thermocline variability: Implications for ENSO dynamics over the last glacial period: Paleoceanography, v. 24, p. PA3202, doi: 10.1029/2008PA001701.

Medina-Elizalde, M., and Lea, D., 2005, The Mid-Pleistocene Transition in the Tropical Pacific: Science, v. 310, no. 5750, p. 1009–1012, doi: 10.1126/science.1115933.

Meehl, G., and Stocker, T.F., 2007, Global Climate Projections: Global Climate Projections. In: Climate Change 2007: The Physical Science Basis. Contribution of Working Group I to the Fourth Assessment Report of the Intergovernmental Panel on Climate Change,, p. 747–846.

Otto-Bliesner, B., Brady, E., Shin, S., Liu, Z., and Shields, C., 2003, Modeling El Nino and its tropical teleconnections during the last glacial-interglacial cycle:

Geophysical Research Letters, v. 30, no. 23, p. 2198, doi: 10.1029/2003GL018553.

Otto-Bliesner, B.L., Brady, E.C., Clauzet, G., Tomas, R., Levis, S., and Kothavala, Z., 2006, Last glacial maximum and Holocene climate in CCSM3: Journal of Climate, v. 19, no. 11, p. 2526–2544.

Patrick, A., and Thunell, R., 1997, Tropical Pacific sea surface temperatures and upper water column thermal structure during the last glacial maximum: Paleoceanography, v. 12, no. 5, p. 649–657.

Rein, B., Luckge, A., Reinhardt, L., Sirocko, F., Wolf, A., and Dullo, W.C., 2005, El Niño variability off Peru during the last 20,000 years: Paleoceanography, v. 20, no. 4, p. A4003.

Sagawa, T., Yokoyama, Y., Ikehara, M., and Kuwae, M., 2011, Vertical thermal structure history in the western subtropical North Pacific since the Last Glacial Maximum: Geophysical Research Letters, v. 38, doi: 10.1029/2010GL045827.

Shin, S.I., Liu, Z., Otto-Bliesner, B., Brady, E., Kutzbach, J.E., and Harrison, S., 2003, A simulation of the Last Glacial Maximum climate using the NCAR-CCSM: Climate Dynamics, v. 20, no. 2-3, p. 127–151.

Timmermann, A., Lorenz, S.J., An, S.-I., Clement, A., and Xie, S.-P., 2007, The Effect of Orbital Forcing on the Mean Climate and Variability of the Tropical Pacific: Journal of Climate, v. 20, no. 16, p. 4147–4159, doi: 10.1175/JCLI4240.1.

Tudhope, A., Chilcott, C., McCulloch, M., Cook, E., Chappell, J., Ellam, R., Lea, D., Lough, J., and Shimmield, G., 2001, Variability in the El Nino - Southern oscillation through a glacial-interglacial cycle: Science, v. 291, no. 5508, p. 1511–1517.

Wang, B., Wu, R., and Lukas, R., 2000, Annual adjustment of the thermocline in the tropical Pacific Ocean: Journal of Climate, v. 13, no. 3, p. 596–616.

Wang, C., and Fiedler, P., 2006, ENSO variability and the eastern tropical Pacific: A review: Progress In Oceanography, v. 69, no. 2-4, p. 239–266, doi: 10.1016/j.pocean.2006.03.004.

Wang, C., and Picaut, J., 2004, Understanding ENSO physics—a review, *in* Wang, C., Xie, S.-P., and Carton, J.A. eds., Geophysical Monograph Series, Geophysical Monograph Series, Earth's Climate: The Ocean-Atmosphere Interaction, Washington, D. C., p. 21–48.

Wang, W., and McPhaden, M.J., 1999, The Surface-Layer Heat Balance in the Equatorial Pacific Ocean. Part I: Mean Seasonal Cycle*: Journal of Physical Oceanography, v. 29, no. 8, p. 1812–1831.

Wang, W., and McPhaden, M.J., 2000, The Surface-Layer Heat Balance in the Equatorial Pacific Ocean. Part II: Interannual Variability*: Journal of Physical Oceanography, v. 30, no. 11, p. 2989–3008.

Xu, J., Kuhnt, W., Holbourn, A., Regenberg, M., and Andersen, N., 2010, Indo-Pacific Warm Pool variability during the Holocene and Last Glacial Maximum: Paleoceanography, v. 25, no. 4, p. PA4230, doi: 10.1029/2010PA001934.

Yin, J., and Battisti, D., 2001, The importance of tropical sea surface temperature patterns in simulations of last glacial maximum climate: Journal of Climate, v. 14, no. 4, p. 565–581.

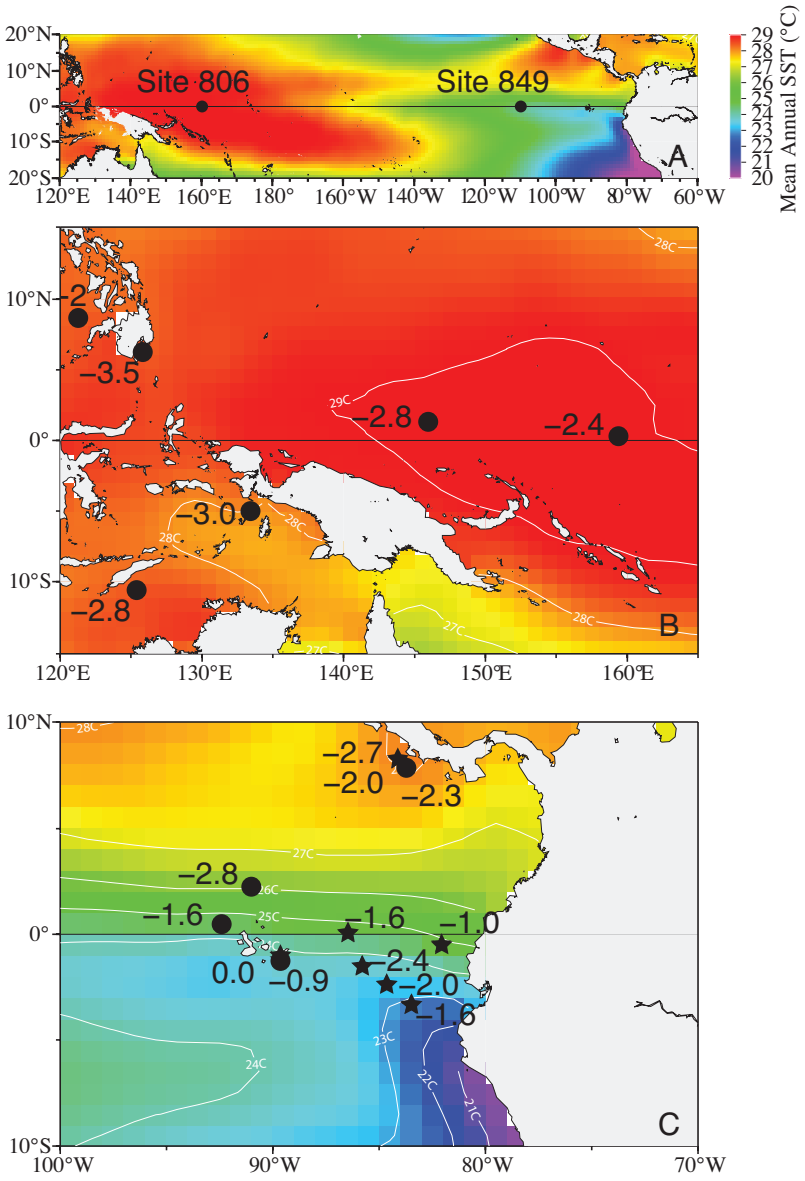

Figure 3.1: Reconstruction of the Zonal Holocene-LGM Temperature Gradient Ocean Drilling Program Site 806 and Site 849 indicated on a mean annual sea surface temperature map using the Met Office Hadley Centre's HadISST 1.1 data set (A, Rayner et al., 2003). Inset maps of WEP (B) and EEP (C) show analysis of published Holocene (4-6 ka) to LGM (18-20 ka) temperature changes to reconstruct the zonal SST gradient. Locations using Mg/Ca proxy are denoted in circles while locations using the alkenone proxy are denoted with stars. Generally, there was a reduced zonal temperature across the Pacific, though there is some spatial heterogeneity in the EEP. The WEP and EPWP have similar magnitude of cooling (~2.7˚C and ~2.3˚C, respectively) suggesting LGM cooling was largely dominated by radiative cooling. In contrast, the EEP cold tongue region had a small magnitude of cooling (~1.6˚C) indicating LGM cooling had radiative and dynamic components.

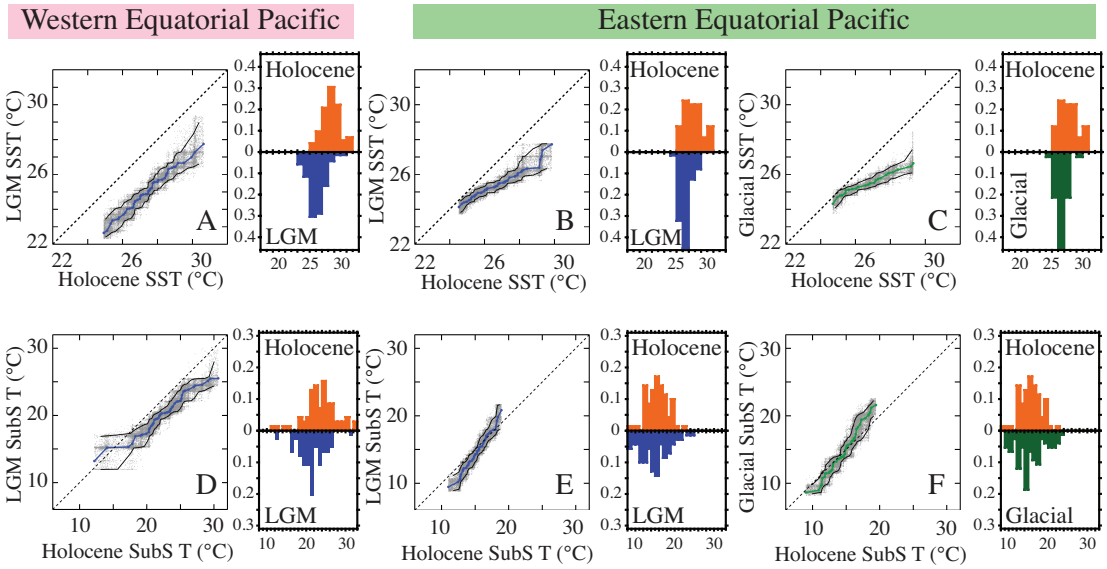

Figure 3.2: Reconstructing Temperature Variability from Individual Foraminifera

Q-Q Plots of WEP and EEP surface and subsurface temperature variability reconstructed from planktonic foraminifera. Resampling of pdf distribution (blue or green line), Monte Carlo simulation (grey dots) and 90% confidence limits (black lines) are shown (see Supplementary Material for further details). For each Q-Q Plot, the pdfs of each sample are plotted in "histogram" form with temperature on the horizontal axis and probability density on the vertical axis. WEP SST variability from Holocene (~3.0 ka, orange) and LGM (~19.0 ka, blue) comparison is uniformly shifted ~2.4˚C colder while EEP SST variability from the Holocene (~2.8 ka and ~5.6 ka, orange), LGM (~20.3 ka, blue), and glacial (21.5 ka, green) indicate a reduction in ENSO. WEP subsurface temperature variability from Holocene (~3.0 ka, orange) and LGM (~19.0 and ~20.0 ka, blue) comparison is mostly uniformly shifted ~2.3˚C colder while EEP subsurface temperature variability from the Holocene (~2.8 ka and ~5.6 ka, orange), LGM (~20.3 ka, blue) and glacial (21.5 ka, green) indicate greater variability, likely related to higher seasonality.

SUPPLEMENTARY MATERIALS

Site Locations

Ocean Drilling Program Site 806, located on the Ontong Java Plateau (0°N, 159°E, 2520 m water depth) is used to monitor the mean state and variability in the Western Equatorial Pacific Ocean. ODP Site 849, located within the core of the equatorial cold tongue extension (0°N, 110°W, 3839 m water depth) is used to monitor the mean state and variability in the Eastern Equatorial Pacific Ocean. Equatorial Pacific ODP Sites 806 (WEP) and 849 (EEP) were selected because these sites have large sources of interannual and centennial variability in the modern (Supplementary Material Figure 3.1). Age models for each site are based on high-resolution benthic isotope records (Bickert et al., 1993; Mix et al., 1995). Using Analyseries (Paillard et al., 1996) the previous age model for Site 849 (Mix et al., 1995) was slightly adjusted to better match with the LR04 Last Glacial Maximum and deglacial period. Ages for core-top samples were calculated using the average sedimentation rate for the last 100 kyrs (Supplementary Materials Table 3.1).

Foraminifera Analysis

In order to investigate climate variability from the mid-Holocene to the Last Glacial Maximum, surface and subsurface-dwelling individual foraminifera from Site 806 and 849 were analyzed. Individual shells of surface-dwelling *Globigerinoides sacculifer* (without final sac-like chamber) and subsurface-dwelling *Globorotalia tumida* were picked for analysis (Supplementary Materials Table 3.2). Due to their

preferred depth habitat, *G. sacculifer* were used to construct shallow mixed layer temperatures (~15 m), and *G. tumida* were used to construct subsurface temperatures (depth habitat ~100 m, independent of thermocline depth). Approximately 60-70 individuals of *G. sacculifer* and *G. tumida* were analyzed for minor elements and in some instances, depth intervals were combined (Supplementary Materials Table 3.2). To minimize size dependent ontogenetic/kinetic effects on geochemical composition, only individuals from restricted size range (355-425 μm) were analyzed. Individuals of *G. sacculfer* were analyzed via laser ablation on an Inductively Coupled Plasma-Mass Spectrometer (LA-ICP-MS) while individuals of *G. tumida* were analyzed via Inductively Coupled Plasma-Optical Emission Spectrometer (ICP-OES).

Due to their small size, *G. sacculifer* specimens were analyzed via laser ablation (Photon Machines Analyte.193 with HelEx sample cell) coupled with a Thermo ElementXS ICP-MS (LA-ICP-MS). Prior to analysis, samples were sonicated in deionized water for 5-10 seconds, rinsed with methanol and dried. The final chamber was severed from the whole of the foraminifera and mounted onto carbon tape. Between five-eight spots ~30 mm in diameter were analyzed for selected isotopes (^{11}B, ^{24}Mg, ^{25}Mg, ^{27}Al, ^{43}Ca, ^{44}Ca, ^{55}Mn, ^{66}Zn, ^{88}Sr) and integrated for a mean minor elemental signal. ^{27}Al, ^{55}Mn, ^{66}Zn were specifically monitored for clay and oxide contamination. Data acquisition was between 40-60s. NIST glass standards were analyzed at 4Hz and 4.1 laser fluence. Analytical reproducibility for NIST610 and NIST612 for Mg/Ca was 8.66 ± 0.14 and 1.31 ± 0.23, respectively (1s, n = 359 over 25 analytical days). Carbonate standards and samples were analyzed at 4Hz and

1.13 laser fluence. Carbonate standard reproducibility for JCt-1-Plug and MACS-3 for Mg/Ca was 1.35 ± 0.15 and 7.61 ± 0.47, respectively (1s, n=280 and 582). Specimens were analyzed from the inner shell surface to the outside to minimize surface heterogeneity during ablation. Average intra-test variability for Mg/Ca is 0.11 mmol/mol, which is comparable to previous study (Sadekov et al., 2008). Eggins et al., (2003) has shown that LA-ICP-MS can reliably determine the range and variability of modern and Holocene temperature from a population of cold-dwelling and tropical planktonic foraminifera such as *G. sacculifer*. *G. sacculifer* Mg/Ca values were converted to temperature using the Mg/Ca dissolution correction of Regenberg et al., (2006) and the temperature equation of Anand et al., (2003) $\Delta[CO_3^2]$ values for the Mg/Ca dissolution correction were calculated using the GLODAP ocean carbon (Key et al., 2004) and World Ocean Atlas temperature (Locarnini et al., 2010) datasets and estimated to be 5.692 mmol/kg and -13.055 mmol/kg for Site 806 and 849, respectively.

Individual *G. tumida* specimens were analyzed via ICP-OES. Crushed individual *G. tumida* were rinsed and sonicated in Milli-Q and methanol, cleaned with reductive and oxidative reagents, and transferred into 1.5mL acid cleaned vials for a weak acid leach and final rinse before minor-element analysis (Boyle and Keigwin, 1985; Martin and Lea, 2002). A PerkinElmer Optima 8300 ICP-OES was used to measure minor-element ratios (Wara et al., 2003). Long term Mg/Ca mmol/mol reproducibility for a liquid consistency standard and foraminifera standards are 3.318 ± 0.030 mmol/mol (1σ, n=401) and 3.737 ± 0.181 mmol/mol (1s, n=103)

respectively. Here we use the *G. tumida*-specific temperature calibration of Mohtadi et al., (2011), which results in a good match between ODP Site 806 and Site 849 core-tops Mg/Ca values and local modern hydrographic data.

Data Analysis

Probability Density Functions (pdfs) are generated from each data set and indicate the probability that a sample taken at random will fall within a given range of temperature values (Main Text Figure 3.2). As we are specifically interested in changes in seasonality and interannual variability, which typically impact the tails of a distribution, we are interested in how the tails of two distributions are different from one another. One way to investigate changes in distributions is a Q-Q plot (Quantile, see Supplementary Material Figure 3.2 for an example). The quantiles of each probability distribution are plotted against each other; that is, the quantile means of one distribution is on the horizontal axis and paired with the equivalent quantile mean of another distribution on the vertical axis creating a series of points. If the mean and variability of two samples are the same, they plot along the one-to-one line. Changes to the mean, without changes in distribution, uniformly shifts the Q-Q series parallel to the one-to-one line while changes in the distribution (e.g. skewness) pull the Q-Q series away from lines parallel to the one-to-one line. We estimate the uncertainty in distributions on these Q-Q plots using a Monte Carlo approach. The cumulative distribution function (CDF) of the observed temperature distributions was resampled. Treating the CDF as a continuous function, it was resampled using random numbers to yield a dataset with the same number of temperatures as the original dataset.

Quantiles (50 bins) were then generated from the resampled datasets and plotted over the original data (see Supplementary Material Figure 3.2 for an example). Due to the limited number of individual foraminiferas measured in each sample, this process was repeated 1000 times to produce an estimate of the variability in the Q-Q plot analysis (see Supplementary Material Figure 3.2 for an example, Monte Carlo in grey dots). 90% confidence limits along the Y-direction were calculated for each quantile along the X-direction thus defining a 90% contour of the Monte Carlo cloud of dots.

Due to low numbers of individuals in some depth intervals, data from adjacent stratigraphic intervals was combined to increase the number of individuals in the Holocene-LGM comparison (Supplementary Materials Table 3.1). Prior to this combination, Q-Q plots and Monte-Carlo uncertainties of the separate samples were used to ascertain whether these adjacent depth intervals had similar temperature distributions. In these analyses the number of quantile bins was reduced to 25 because the number of individual foraminifera analyzed ranged from N= 26-70. These comparisons are shown in Supplementary Material Figures 3.2, 3.3, 3.4, 3.5 and 3.6 and demonstrate samples have similar temperature distributions and may be combined for further analysis.

Comparison of Modern Hydrographic Data and Foraminifera Fluxes

Site 806: As a proxy for SST, the *G. sacculifer* derived temperature distribution from Site 806 matches well with SODA hydrographic data at 15 m water depth. As a proxy for subsurface temperature, *G. tumida* derived temperature distributions are generally cooler and have a broader distribution than SODA

hydrographic data at 97 m water depth. Though production and export for a certain season could explain temperature discrepancies, nearby sediment trap experiments indicate a relatively uniform export flux of *G. sacculifer* and *G. tumida* throughout the annual cycle (Kawahata et al., 2002). For *G. tumida*, a large subsurface temperature distribution may be attributed to a depth habitat that is partially within the upper thermocline, (e.g. an environment with a strong temperature gradient) and/or gametogenic calcite that precipitates as specimens fall through the water column. However, the benefit of comparing Holocene *G. tumida* temperature variability records to LGM *G. tumida* temperature variability records is these potential biases are inherent to both data sets are effectively minimized.

Site 849: As a proxy for SST, the *G. sacculifer* derived temperature distribution from Site 849 is generally warmer than SODA hydrographic data at 15 m water depth. Nearby in the Panama Basin, *G. sacculifer* has a maximum flux peak during the phytoplankton bloom when the mixed layer is deep and a secondary peak during the upwelling season (Thunell and Reynolds, 1984). Locally for Site 849, this corresponds, not with the temperature extremes, but with moderate temperatures. Note that while the minimum temperature recorded by *G. sacculifer* within this study is ~24˚C, *G. sacculifer* is not biologically limited to this temperature as *G. sacculifer* is known to precipitate shells within the EEP at ~21˚C (Dekens et al., 2002). As a proxy for subsurface temperature, *G. tumida* derived temperature distributions are generally cooler and have a normal distribution in comparison to the SODA hydrographic data at 97 m water depth, which is skewed toward warm subsurface

temperatures. Though not specifically discussed in sediment trap data from the Panama Basin, nonspinose foraminifera, such as *G. tumida*, have a maximum flux during the season of maximum upwelling (Thunell and Reynolds, 1984), which corresponds to moderate subsurface temperatures at Site 849. As with Site 806, though the *G. tumida* temperature variability reconstructions are limited, we chose to compare Holocene and LGM distributions to minimize these biases.

Q-Q Plots of Modern Hydrographic Data: The ENSO signal in the modern hydrographic data from Sites 806 (Supplementary Material Figure 3.7 a/c) and 849 (Supplementary Material Figure 3.7 b/d) was manipulated for ease of comparison of Q-Q plots. Monthly mean temperatures from 1958-2007 from the SODA v2.4 re-analysis dataset (Carton and Giese, 2008) were identified as Normal, El Nino or La Nina using the National Oceanic and Atmospheric Administration Climate Prediction Center Oceanic Nino Index (ONI) applied to the Niño 3.4 SST timeseries. For the "No ENSO" trace (red), months identified as El Nino or La Nina were removed and replaced by the normal climatological monthly mean. In contrast, for the "Increased ENSO" (pink), months identified as El Nino or La Nina, the average amplitude of the excursion from the normal climatological mean was increased by 50%. Similarly, for the seasonality, the average seasonal excursion from the normal climatological mean was increased (blue) or decreased (turquoise) by 50% and added to the temperature. Manipulation of the ENSO cycle clearly impacts the Q-Q trace, while changes in seasonality at the calcification depth of *G. sacculifer* do not clearly impact the Q-Q trace (i.e. the distributions fall on or near the one-to-one line).

Reanalysis of Koutavas and Joanides (2012)

In contrast to our study, a recent study by Koutavas and Joanides (2012) suggests ENSO variability increased during the LGM and glacial period in comparison to the Late Holocene. Their study differs from ours in three distinct ways. First, the study location, core V21–30 (1° 13′S, 89° 41′W, 617 m depth), may have a different dynamical response to glacial forcing due to its proximity to the Galapagos and shifts in the ITCZ. Second, individuals of *Globigerinoides ruber* were analyzed for oxygen stable isotope values ($\delta^{18}O$). Oxygen stable isotopes of foraminfera are influenced by temperature and $\delta^{18}O$ value of seawater, both of which vary seasonally and interannually. Reconstructed shifts in the ITCZ during the glacial period (Koutavas and Lynch-Stieglitz, 2003) and consequently changes in the salinity field may have influenced $\delta^{18}O$ of seawater through time making $\delta^{18}O$ of *G. ruber* difficult to constrain and interpret. Third, variance (squared standard deviation, σ^2) of the *G. ruber* populations from various horizons was used to characterize ENSO variability through time. However, variance may be a poor indicator of ENSO variability, as there may be changes in variance unrelated to the range of temperatures observed. Here we reanalyze the Koutavas and Joanides (2012) dataset using the statistical methods described above.

Similar to above, the SODA v2.4 modern hydrographic data from 5 m water depth was converted to predicted $\delta^{18}O_{calcite}$ values for ease of comparison with Q-Q plots (Supplementary Material Figure 3.8). $\delta^{18}O_{water}$ was estimated using a the gridded $\delta^{18}O$ database and salinity-$\delta^{18}O_{water}$ relationship of Legrande and Schmidt,

(2006) combined with salinity values from the SODA dataset. $\delta^{18}O_{calcite}$ values were estimated from $\delta^{18}O_{water}$ estimates and SODA temperatrues using the paleotemperature equation of Bemis et al., (1998). Mean $\delta^{18}O$ values and the distribution of $\delta^{18}O$ calcite values from individual foraminifera from the core top are consistent with a shallow calcification depth of *G. ruber* of ~5 m. In Supplementary Material Figure 3.8, manipulated modern hydrographic data shows changes in ENSO strength and seasonality have the same affect on the warm and cold tails of the distribution. Q-Q plots of the $\delta^{18}O$ values from *G. ruber* glacial samples compared to the core top sample from core V21–30 do not strongly support a change in distribution suggesting neither a change in seasonality nor in ENSO strength (Supplementary Material Figure 3.9, 40 quantile bins). In general, the $\delta^{18}O_{calcite}$ values along the mean adjusted one-to-one line indicate there was no change in $\delta^{18}O_{calcite}$ distributions between the Late Holocene and LGM and glacial intervals. Similar results for other Late Holocene intervals compared to LGM and glacial intervals were also found (figures not shown). However, the strong change in temperature distribution from Mg/Ca-based temperature variability reconstructions of *G. sacculifer* from Site 849 in our study do indicate a decrease in temperature variability suggesting a change in ENSO strength (e.g. Supplementary Material Figure 3.3). We attribute these apparent differences in temperature variability to the preferred calcification depth of *G. ruber* and *G. sacculifer*.

At the calcification depth of *G. ruber* (~5 m), and the location of V21-30, an increase or decrease in seasonality produce changes in the Q-Q distributions that are

similar to an increase or decrease in ENSO (Supplementary Material Figure 3.8), which means that it is not possible to distinguish a change in seasonality from ENSO using the Koutavas and Joanides (2012) data set. In contrast, at the calcification depth of *G. sacculifer* (~15 m), at the location of Site 849, changes in distribution are dominated by changes in ENSO (Supplementary Material Figure 3.7). A robust result among climate models that simulate ENSO activity indicates there is an inverse relationship between the seasonal cycle and ENSO (Fedorov and Philander, 2001; Timmermann et al., 2007). For example when ENSO intensity decreases, the seasonal cycle increases. Here we suggest that the decrease in variability found at Site 849 reflects a decrease in ENSO strength during the glacial period in comparison to the late Holocene (e.g. Supplementary Material Figure 3.3). The decrease in ENSO strength found at Site 849 may not be detectable at V21-30 because seasonality may have remained the same or increased, thereby masking a decrease in ENSO. The increase in seasonality may explain the observed increase in variance reported by Koutavas and Joanides (2012) and is further supported by the increase in seasonality found in subsurface records from *G. tumida* at Site 849.

Western Equatorial and Eastern Equatorial Pacific SST Gradients

In order to investigate how our observed individual foraminifera WEP and EEP variability may influence mean temperature records and WEP-EEP temperature gradient reconstructions, we compare our record to previously generated SST records (Supplementary Materials Table 3, Kienast et al., 2006; Koutavas and Sachs, 2008; Lea et al., 2000; Lea et al., 2006; Koutavas et al., 2002; Leduc et al., 2007; Benway et

al., 2006; De Garidel-Thoron et al., 2007; Rosenthal et al., 2003; Stott et al., 2007). Here we employ a time slice from the WEP and EEP from the Holocene (4-6 ka) and Last Glacial Maximum (18-20 ka). Note that our core top ages for our late Holocene samples are closer to ~3 ka, but these previously generated records have few ~3 ka measurements for comparison. Regardless, for this comparison, our combined Holocene samples from the EEP (~3 ka and ~5 ka) have similar variability distributions which supports our choice of the 4-6 ka time slice. Using the published age models, Mg/Ca and Uk37-derived temperatures we calculated the temperature difference from the LGM to Holocene, which are plotted on the modern SST field (Figure 3.1).

SUPPLEMENTARY MATERIALS REFERENCES

Anand, P., Elderfield, H., and Conte, M., 2003, Calibration of Mg/Ca thermometry in planktonic foraminifera from a sediment trap time series: Paleoceanography, v. 18, no. 2, p. 1050, doi: 10.1029/2002KPA000846.

Bemis, B., Spero, H., Bijma, J., and Lea, D., 1998, Reevaluation of the oxygen isotopic composition of planktonic foraminifera: Experimental results and …: Paleoceanography.

Benway, H.M., Mix, A.C., Haley, B.A., and Klinkhammer, G.P., 2006, Eastern Pacific Warm Pool paleosalinity and climate variability: 0-30 kyr: Paleoceanography, v. 21, no. 3, p. n/a–n/a, doi: 10.1029/2005PA001208.

Bickert, T., Berger, W.H., Burke, S., Schmidt, H., and Wefer, G., 1993, 24. Late Quaternary Stable Isotope Records of Benthic Foraminifers: Sites 805 and 806 Ontong Java Plateau, *in* Proceedings of the Ocean Drilling Program, Scientific Results, Volume 130.

Boyle, E., and Keigwin, L., 1985, Comparison of the Atlantic and Pacific Paleochemical Records for the Last 215,000 Years - Changes in Deep Ocean Circulation and Chemical Inventories: Earth and Planetary Science Letters, v. 76, no. 1-2, p. 135–150.

Carton, J.A., and Giese, B.S., 2008, A Reanalysis of Ocean Climate Using Simple Ocean Data Assimilation (SODA): Monthly Weather Review, v. 136, no. 8, p. 2999–3017, doi: 10.1175/2007MWR1978.1.

De Garidel-Thoron, T., Rosenthal, Y., Beaufort, L., Bard, E., Sonzogni, C., and Mix, A.C., 2007, A multiproxy assessment of the western equatorial Pacific hydrography during the last 30 kyr: Paleoceanography, v. 22, no. 3, p. PA3204, doi: 10.1029/2006PA001269.

Dekens, P., Lea, D., Pak, D., and Spero, H., 2002, Core top calibration of Mg/Ca in tropical foraminifera: Refining paleotemperature estimation: Geochemistry Geophysics Geosystems, v. 3, no. 4, doi: 10.1029/2001GC000200.

Eggins, S., Dedeckker, P., and Marshall, J., 2003, Mg/Ca variation in planktonic foraminifera tests: implications for reconstructing palaeo-seawater temperature and habitat migration: Earth and Planetary Science Letters, v. 212, no. 3-4, p. 291–306, doi: 10.1016/S0012-821X(03)00283-8.

Fedorov, A.V., and Philander, S., 2001, A Stability Analysis of Tropical Ocean-Atmosphere Interactions: Bridging Measurements and Theory for El Nino: Journal of Climate, v. 14, p. 3086–3101.

Kawahata, H., Nishimura, A., and Gagan, M.K., 2002, Seasonal change in foraminiferal production in the western equatorial Pacific warm pool: evidence from sediment trap experiments: Deep-Sea Research Part Ii-Topical Studies In Oceanography, v. 49, no. 13-14, p. 2783–2800.

Key, R.M., Kozyr, A., Sabine, C.L., Lee, K., Wanninkhof, R., Bullister, J.L., Feely, R.A., Millero, F.J., Mordy, C., and Peng, T.H., 2004, A global ocean carbon climatology: Results from Global Data Analysis Project (GLODAP): Global Biogeochemical Cycles, v. 18, no. 4, p. n/a–n/a, doi: 10.1029/2004GB002247.

Kienast, M., Kienast, S.S., Calvert, S.E., Eglinton, T.I., Mollenhauer, G., Francois, R., and Mix, A.C., 2006, Eastern Pacific cooling and Atlantic overturning circulation during the last deglaciation: Nature, v. 443, no. 7113, p. 846–849, doi: 10.1038/nature05222.

Koutavas, A., and Joanides, S., 2012, El Niño–Southern Oscillation extrema in the Holocene and Last Glacial Maximum: Paleoceanography, v. 27, doi: 10.1029/2012PA002378.

Koutavas, A., and Lynch-Stieglitz, J., 2003, Glacial-interglacial dynamics of the eastern equatorial Pacific cold tongue-Intertropical Convergence Zone system reconstructed from oxygen isotope records: Paleoceanography, v. 18, no. 4, p. 1089, doi: 10.1029/2003PA000894.

Koutavas, A., and Sachs, J.P., 2008, Northern timing of deglaciation in the eastern equatorial Pacific from alkenone paleothermometry: Paleoceanography, v. 23, no. 4, doi: 10.1029/2008PA001593.

Koutavas, A., Lynch-Stieglitz, J., Marchitto, T.M., Jr, and Sachs, J.P., 2002, El Nino-like pattern in ice age tropical Pacific sea surface temperature: Science, v. 297, no. 5579, p. 226–230, doi: 10.1126/science.1072376.

Lea, D. W., Pak, D. K., & Spero, H. J. (2000). Climate impact of late Quaternary equatorial Pacific sea surface temperature variations. Science, v. 289, p. 1719–1724.

Lea, D. W., Pak, D. K., Belanger, C. L., Spero, H. J., Hall, M. A., & Shackleton, N. J. (2006). Paleoclimate history of Galapagos surface waters over the last 135,000 yr. Quaternary Science Reviews, v. 25, p. 1152–1167.

Leduc, G., Vidal, L., Tachikawa, K., Rostek, F., Sonzogni, C., Beaufort, L., and Bard, E., 2007, Moisture transport across Central America as a positive feedback on abrupt climatic changes: Nature, v. 445, p. 908–911, doi: 10.1038/nature05578.

Legrande, A.N., and Schmidt, G.A., 2006, Global gridded data set of the oxygen

isotopic composition in seawater: Geophysical Research Letters, v. 33, no. 12, p. L12604, doi: 10.1029/2006GL026011.

Locarnini, A.R., Mishonov, A.V., Antonov, J.I., Boyer, T.P., Garcia, H.E., Baranova, O.K., Zweng, M.M., and Johnson, D.R., 2010, *World Ocean Atlas 2009* (S. Levitus, Ed.): U.S. Government Printing Office, Washington, D.C.

Martin, P.A., and Lea, D., 2002, A simple evaluation of cleaning procedures on fossil benthic foraminiferal Mg/Ca: Geochemistry Geophysics Geosystems, v. 3, no. 10, p. 8, doi: 10.1029/2001GC000280.

Mix, A., Pisias, N., Rugh, W., Wilson, J., Morey, A., and Hagelberg, T., 1995, 17. Benthic Foraminifer Stable Isotope Recond From Site 849 (0-5Ma): Local and Global Climate Changes: Proceedings of the Ocean Drilling Program, Scientific Results, v. 138, p. 371–412.

Mohtadi, M., oppo, D.W., Lückge, A., DePol-Holz, R., Steinke, S., Groeneveld, J., Hemme, N., and Hebbeln, D., 2011, Reconstructing the thermal structure of the upper ocean: Insights from planktic foraminifera shell chemistry and alkenones in modern sediments of the tropical eastern Indian Ocean: Paleoceanography, v. 26, no. 3, doi: 10.1029/2011PA002132.

Paillard, D., Labeyrie, L., and Yiou, P., 1996, Macintosh program performs time-series analysis: Eos, Transactions American Geophysical Union, v. 77, no. 39, p. 379–379.

Regenberg, M., Nuernberg, D., Steph, S., Groeneveld, J., Garbe-Schoenberg, D., Tiedemann, R., and Dullo, W.-C., 2006, Assessing the effect of dissolution on planktonic foraminiferal Mg/Ca ratios: Evidence from Caribbean core tops: Geochemistry Geophysics Geosystems, v. 7, p. –, doi: 10.1029/2005GC001019.

Rosenthal, Y., Oppo, D., and Linsley, B.K., 2003, The amplitude and phasing of climate change during the last deglaciation in the Sulu Sea, western equatorial Pacific: Geophysical Research Letters, v. 30, no. 8, p. 1428, doi: 10.1029/2002GL016612.

Sadekov, A., Eggins, S.M., De Deckker, P., and Kroon, D., 2008, Uncertainties in seawater thermometry deriving from intratest and intertest Mg/Ca variability in Globigerinoides ruber: Paleoceanography, v. 23, no. 1, p. PA1215, doi: 10.1029/2007PA001452.

Stott, L., Timmermann, A., and Thunell, R., 2007, Southern Hemisphere and Deep-Sea Warming Led Deglacial Atmospheric CO2 Rise and Tropical Warming: Science, v. 318, no. 5849, p. 435–438, doi: 10.1126/science.1143791.

Thunell, R., and Reynolds, L.A., 1984, Sedimentation of Planktonic-Foraminifera - Seasonal-Changes in Species Flux in the Panama Basin: Micropaleontology, v. 30, no. 3, p. 243–262.

Timmermann, A., Lorenz, S.J., An, S.-I., Clement, A., and Xie, S.-P., 2007, The Effect of Orbital Forcing on the Mean Climate and Variability of the Tropical Pacific: Journal of Climate, v. 20, no. 16, p. 4147–4159, doi: 10.1175/JCLI4240.1.

Wara, M.W., Anderson, L., Schellenberg, S., Franks, F., Ravelo, A., and Delaney, M., 2003, Application of a radially viewed inductively coupled plasma-optical emission spectrophotometer to simultaneous measurement of Mg/Ca, Sr/Ca, and Mn/Ca ratios in marine biogenic carbonates: Geochemistry Geophysics Geosystems, v. 4, no. 8, p. 14, doi: 10.1029/2003GC000525.

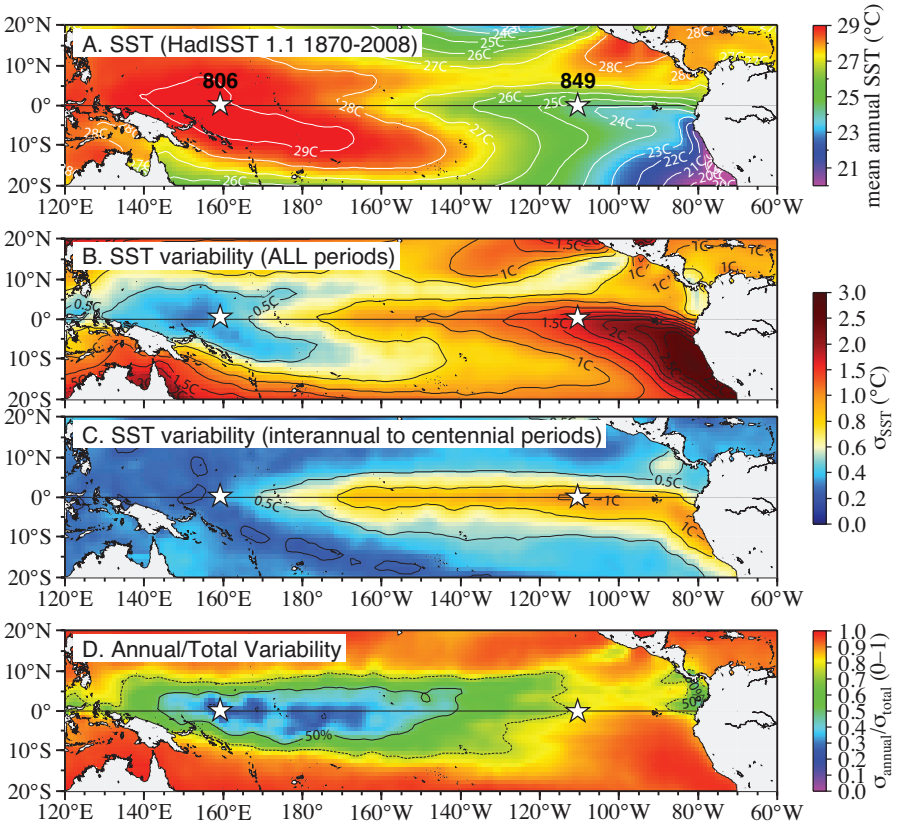

Supplementary Material Figure 3.1: Modes of Variability in the Tropical Pacific Mean annual sea surface temperatures (calculated from Rayner et al., 2003) (A). Variability of monthly sea surface temperatures 1870 – 2008 (B) and monthly values with the annual cycle removed (C), calculated as standard deviations and the proportion of total SST variability due to the annual cycle (D). Cool colors are regions dominated by interannual and centennial variations while warm colored regions are dominated by the annual cycle.

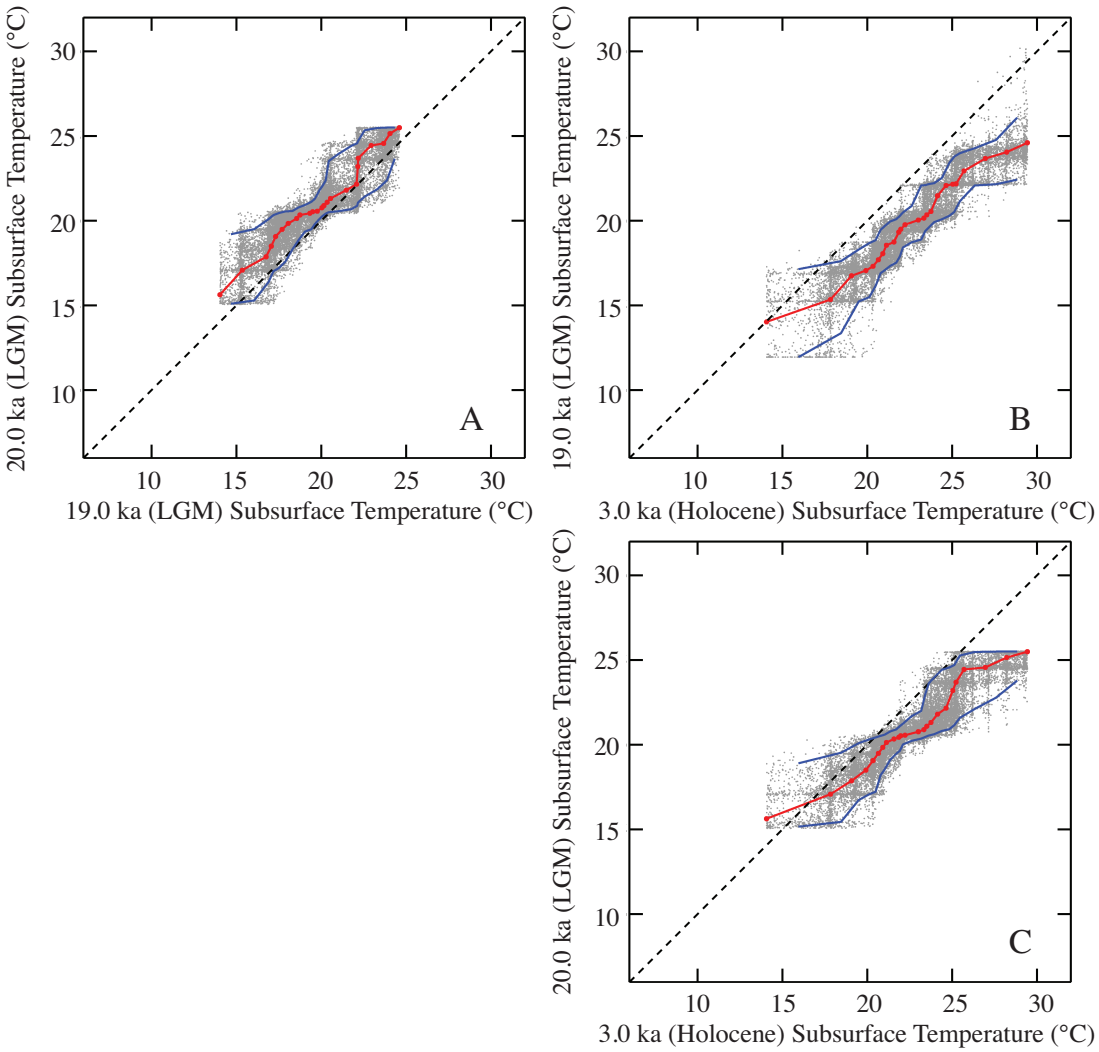

Supplementary Material Figure 3.2 Q-Q plots for subsurface dwelling *G. tumida* from the WEP

Depth intervals 0-2 cm (Holocene), 51-53 cm (LGM) and 53-55 cm (LGM) are compared in Q-Q plots. Resampling of pdf distribution (red line), Monte Carlo simulation (grey dots) and 90% confidence limits (blue lines) are shown. When the LGM samples are compared to each other (A) there is little difference in the distributions between the two populations. Similarly, when the LGM samples are compared to the Holocene sample (B and C), they have comparable distributions. Therefore, the two LGM samples are aggregated and compared to the Holocene sample.

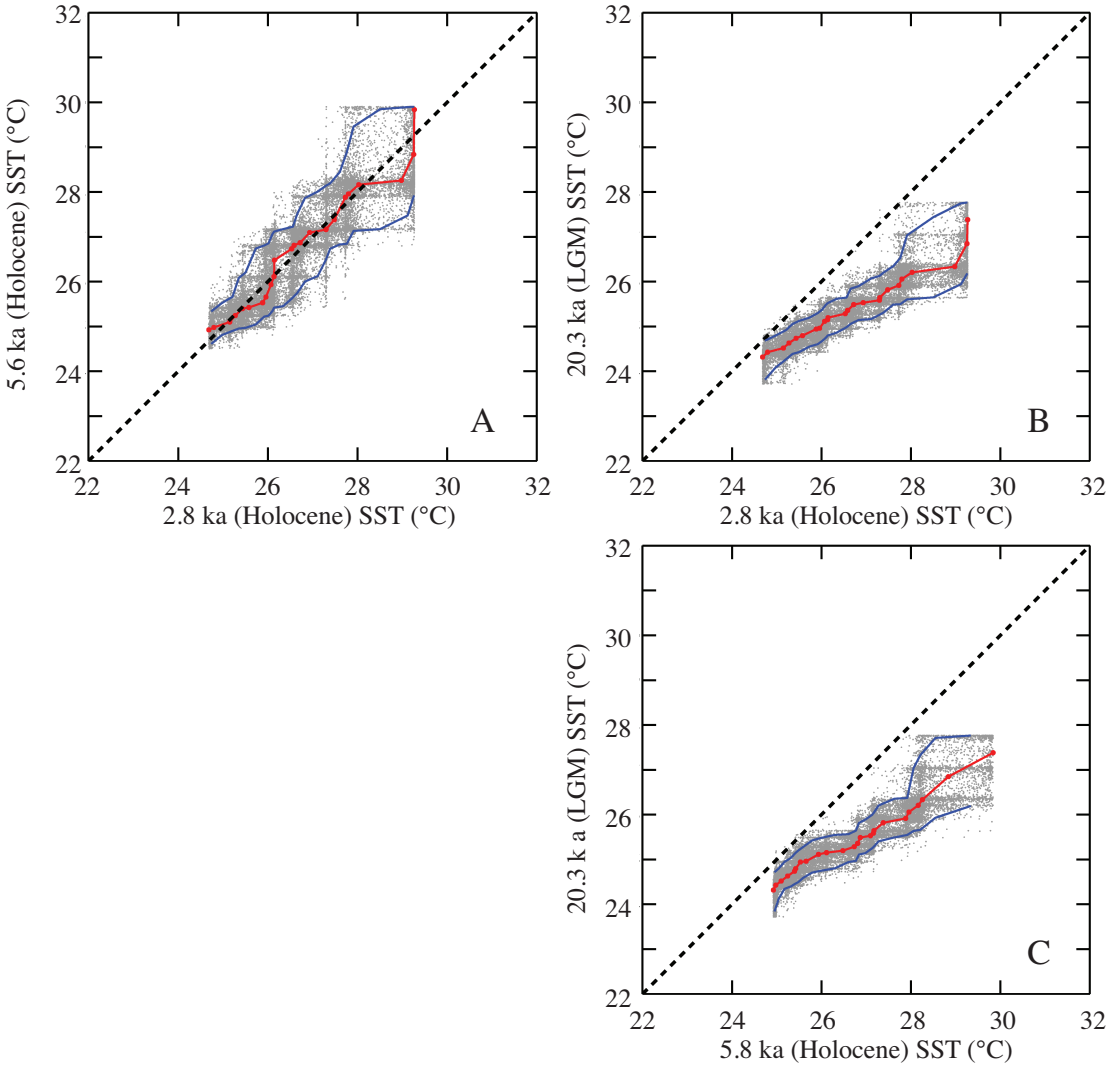

Supplementary Material Figure 3.3: Q-Q plots for surface dwelling *G. sacculifer* from the EEP Holocene and LGM

Depth intervals 6-8 cm (Holocene), 15-18 cm (Holocene), and 74-80 cm (LGM) are compared. Resampling of pdf distribution (red line), Monte Carlo simulation (grey dots) and 90% confidence limits (blue lines) are shown. When the Holocene samples are compared to each other (A) there is little difference in the distributions between the two populations. Similarly, when the Holocene samples are compared to the LGM sample (B and C), they have comparable distributions. Therefore, the two Holocene samples are aggregated and compared to the LGM sample.

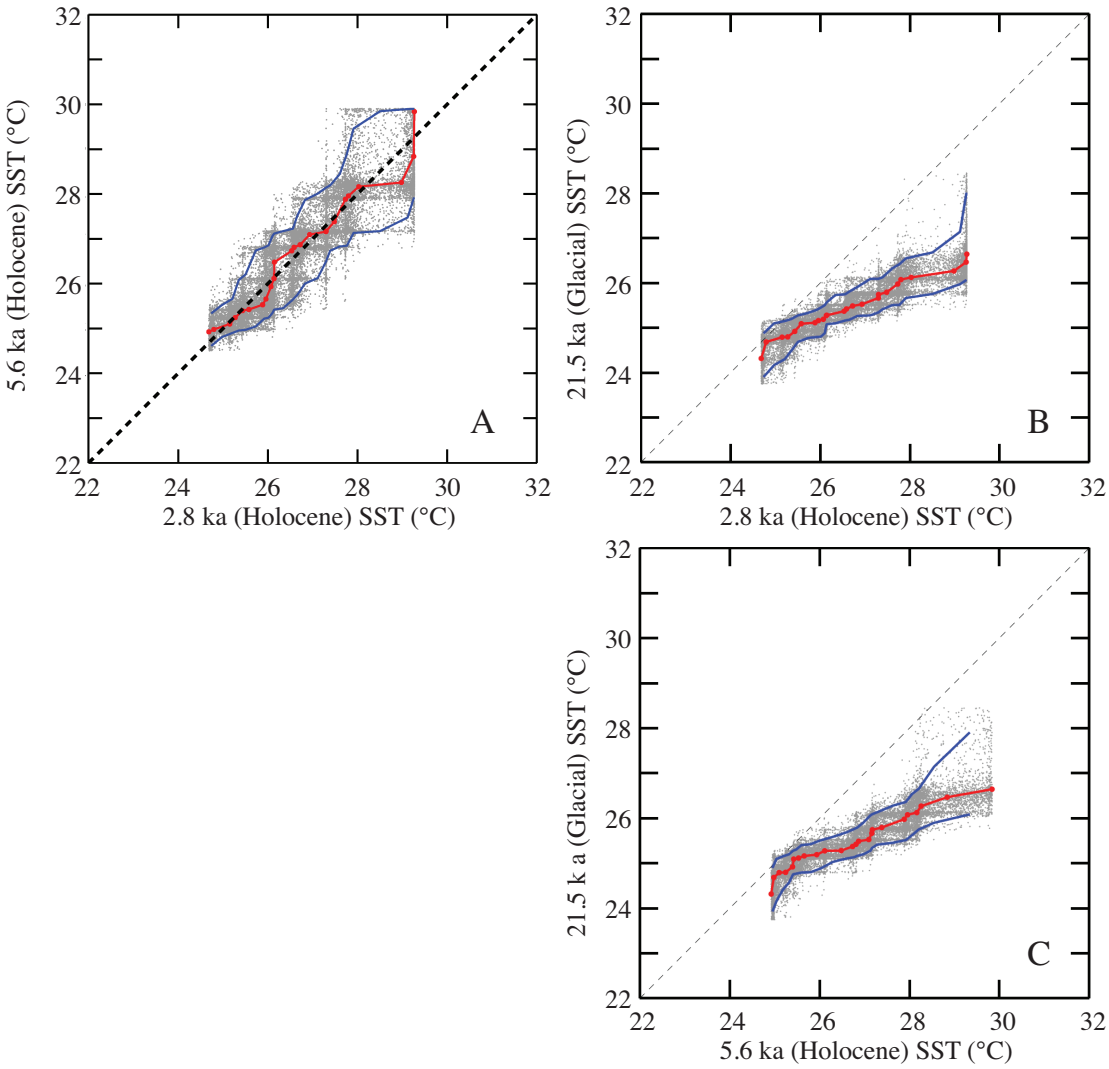

Supplementary Material Figure 3.4: Q-Q plots for surface dwelling *G. sacculifer* from the EEP Holocene and Glacial

Depth intervals 6-8 cm (Holocene), 15-18 cm (Holocene), and 85-87 cm (glacial) are compared. Resampling of pdf distribution (red line), Monte Carlo simulation (grey dots) and 90% confidence limits (blue lines) are shown. When the Holocene samples are compared to each other (A) there is little difference in the distributions between the two populations. Similarly, when the Holocene samples are compared to the glacial sample (B and C), they have comparable distributions. Therefore, the two Holocene samples are aggregated and compared to the glacial sample.

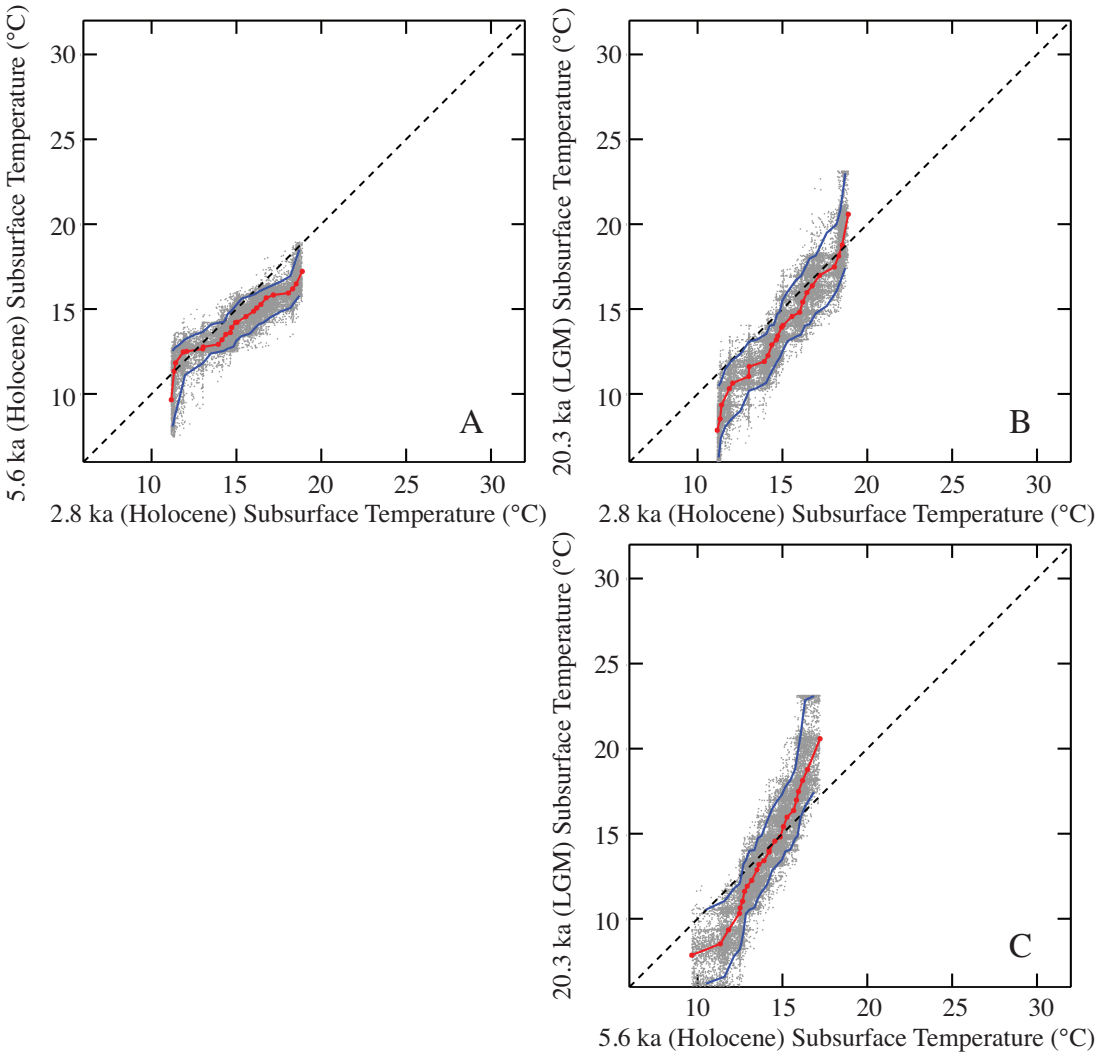

Supplementary Material Figure 3.5: Q-Q plots for surface dwelling *G. tumida* from the EEP Holocene and LGM

Depth intervals 6-8 cm (Holocene), 15-18 cm (Holocene), and 74-80 cm (LGM) are compared. Resampling of pdf distribution (red line), Monte Carlo simulation (grey dots) and 90% confidence limits (blue lines) are shown. When the Holocene samples are compared to each other (A) there is little difference in the distributions between the two populations. Similarly, when the Holocene samples are compared to the LGM sample (B and C), they have comparable distributions. Therefore, the two Holocene samples are aggregated and compared to the LGM sample.

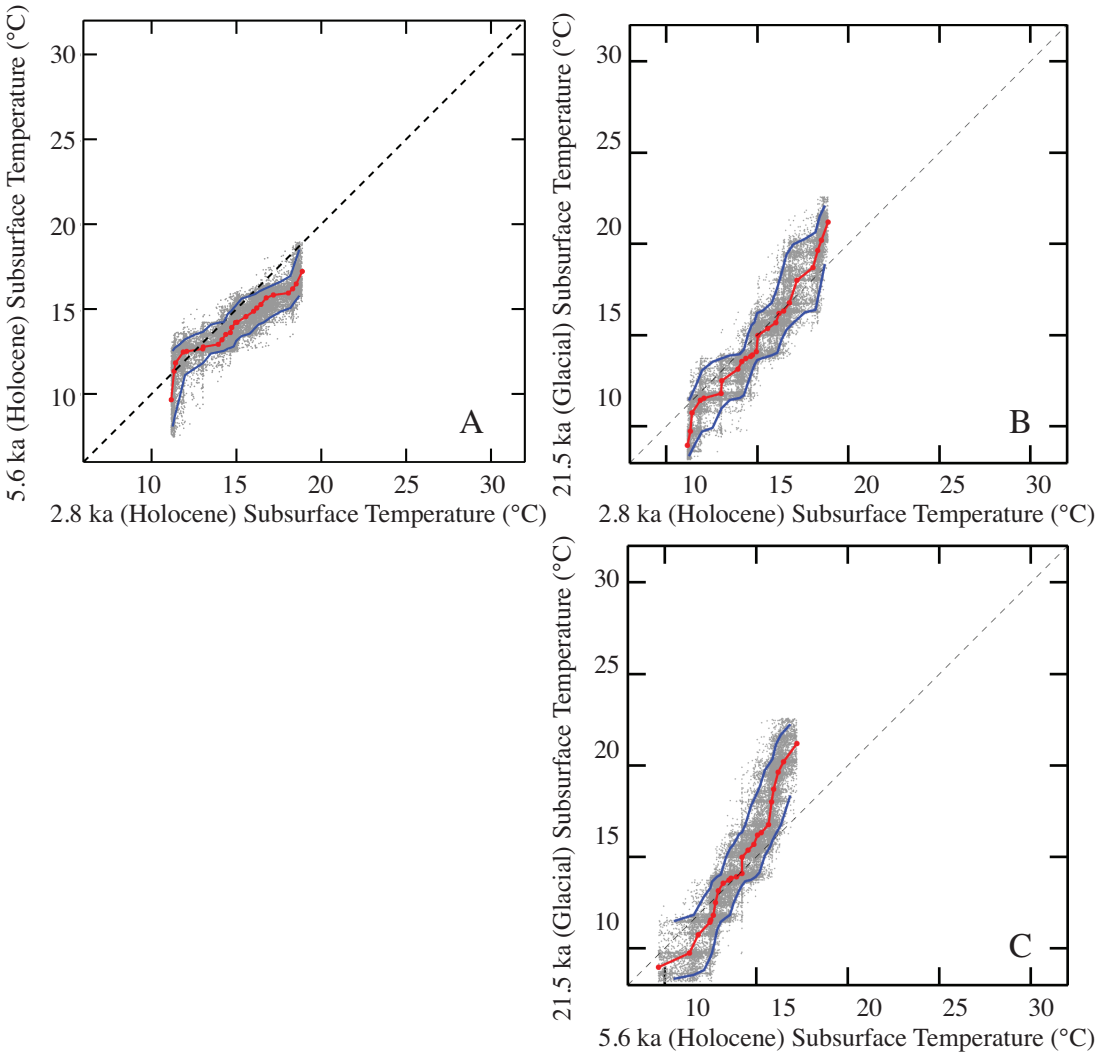

Supplementary Material Figure 3.6: Q-Q plots for surface dwelling *G. tumida* from the EEP Holocene and Glacial

Depth intervals 6-8 cm (Holocene), 15-18 cm (Holocene), and 85-87 cm (glacial) are compared. Resampling of pdf distribution (red line), Monte Carlo simulation (grey dots) and 90% confidence limits (blue lines) are shown. When the Holocene samples are compared to each other (A) there is little difference in the distributions between the two populations. Similarly, when the Holocene samples are compared to the glacial sample (B and C), they have comparable distributions. Therefore, the two Holocene samples are aggregated and compared to the glacial sample.

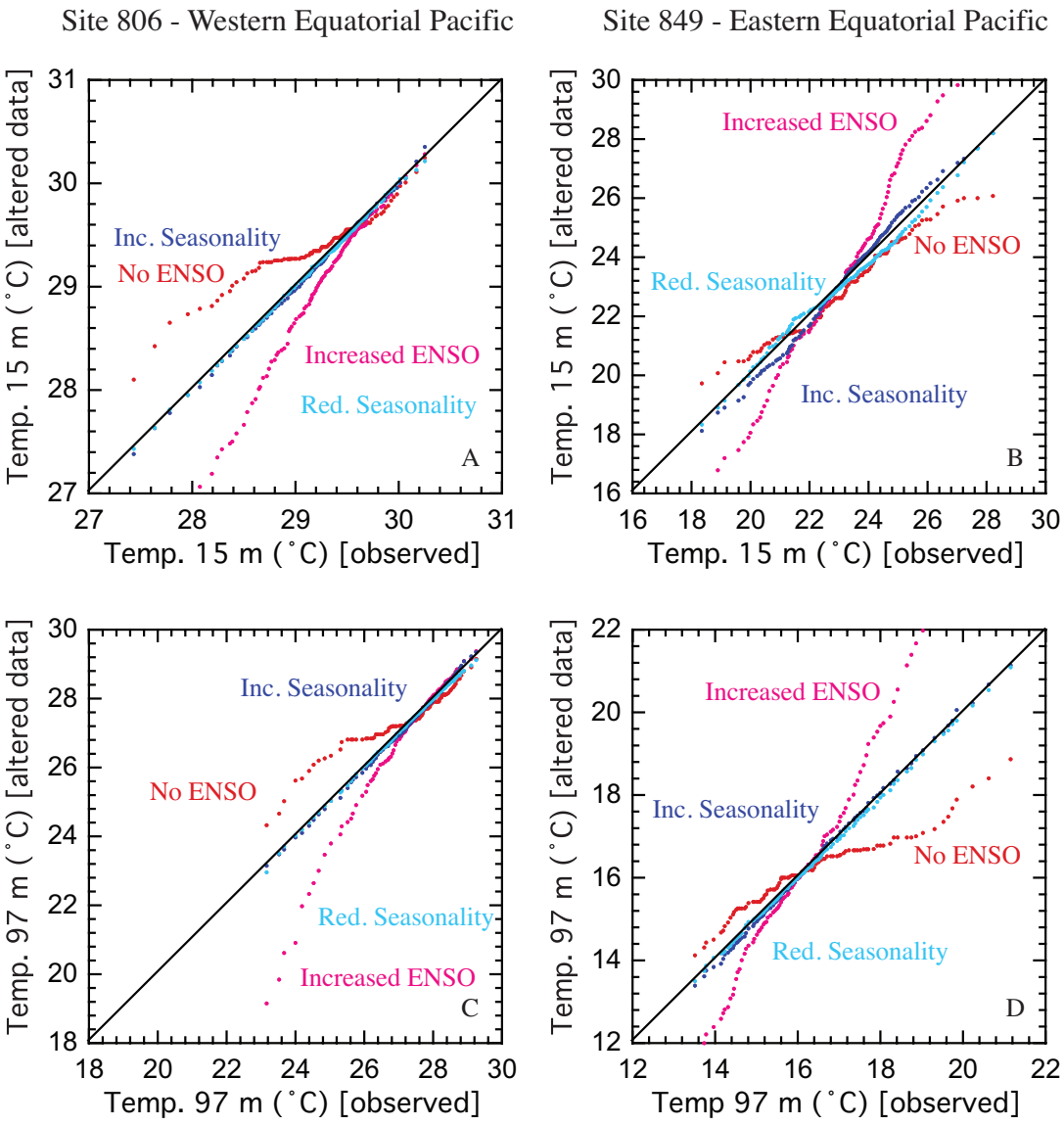

Supplementary Material Figure 3.7: Q-Q plots of altered modern hydrographic data from Sites 806 and 849

SODA v2.4 average monthly means are manipulated with no ENSO (red), Increased ENSO (pink), Increased Seasonality (blue) and Reduced Seasonality (turquoise). WEP Site 806 surface, 15 m (A) and subsurface, 97 m (C). EEP Site 849 surface, 15 m (B) and subsurface, 97 m (D).

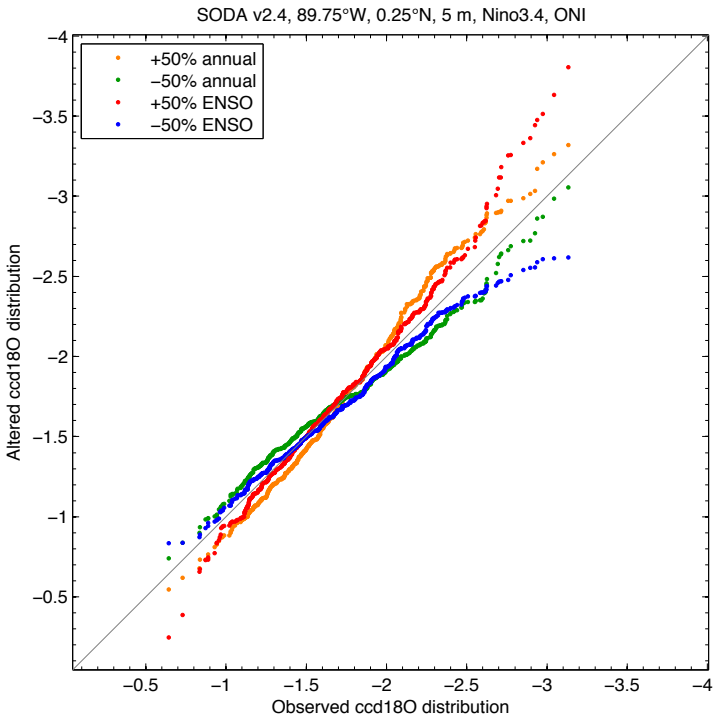

Supplementary Material Figure 3.8: Q-Q plots of altered modern hydrographic data from Site V21-30

SODA v2.4 average monthly means for Koutavas and Joanides (2012) core V21-30 manipulated with no ENSO (blue), Increased ENSO (red), Increased Seasonality (yellow) and Reduced Seasonality (green). Note that changes in seasonality and ENSO in the same direction (i.e. both increase in amplitude) have a similar impact on distributions and appear similar on the Q-Q plot.

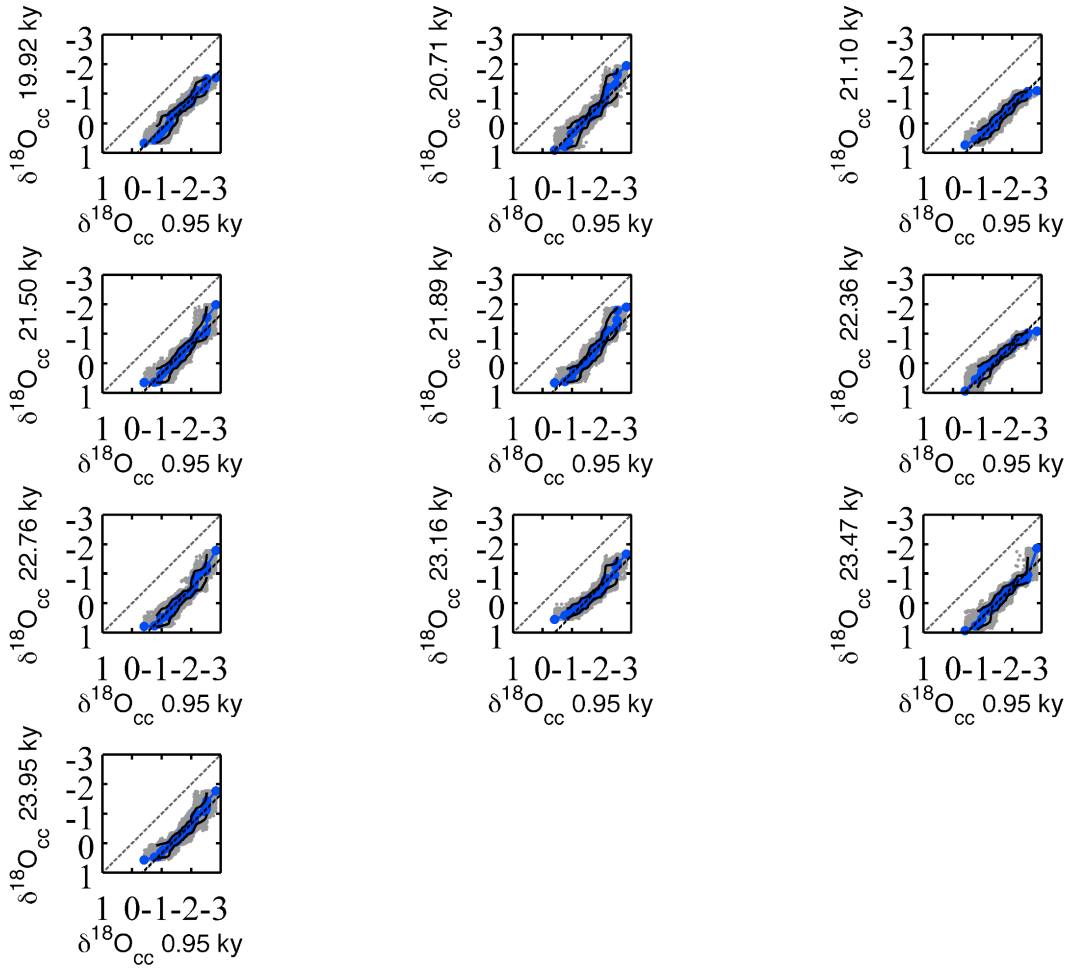

Supplementary Material Figure 3.9: Q-Q plots of Koutavas and Joanides (2012) $\delta^{18}O$ values of individual *G. ruber* from the Late Holocene core top in comparison to LGM and glacial intervals. Resampling of pdf distribution (blue line), Monte Carlo simulation (grey dots) and mean adjusted one-to-one line (black line).

Table 3.1: Site information and ages.

Leg	Site	H	Core	Type	Section	Top (cm)	Bottom (cm)	Depth (mbsf)	Depth (mcd)	Age (yrs)
130	806	A	1	H	1	0	2	0	0	3000
130	806	A	1	H	1	51	53	0.51	0.53	19000
130	806	A	1	H	1	53	55	0.53	0.55	20000
138	849	A	1	H	1	6	8	0.06	0.06	2800
138	849	B	1	H	1	15	18	0.15	0.15	5600
138	849	B	1	H	1	74	80	0.74	0.74	20300
138	849	B	1	H	1	85	87	0.85	0.85	21500

Table 3.2: Site information and depth intervals.

ODP Site	*Lat*	*Long*	*Depth (m)*	*mid-Holocene*	*Last Glacial Maximum*	*Glacial Period*
806	0	159°E	2520	806A 1H-1 0-2 cm	806A 1H-1 51-53 cm 806A 1H-1 53-55 cm*	
849	0	110°W	3839	849A 1H-1 6-8 cm 849B 1H-1 15-18 cm	849B 1H-1 74-80 cm	849B 1H-1 85-87 cm

*Intervals combined for *G. tumida* only.

Table 3.3: Previously generated SST records used to compare mean annual and WEP-EEP gradient reconstructions to our generated SST variability.

Reference	Region	Method	Site	Latitude	Longitude	Depth (m)	Holocene (4-6 ka) Mean	LGM (18-20 ka) Mean
Kienast et al, 2001	EEP	Uk37	ME0005A-24JC	Eq	93.5 W	2941	24.4	22.8
Koutavas & Sachs, 2008	EEP	Uk37	RC11-238	1.5 S	94.2 W	2573	24.3	21.9
Koutavas & Sachs, 2008	EEP	Uk37	V19-27	0.5 S	97.9 W	1373	25.4	24.4
Koutavas & Sachs, 2008	EEP	Uk37	V19-28	2.4 S	95.4 W	2720	23.5	21.5
Koutavas & Sachs, 2008	EEP	Uk37	V19-30	3.4 S	96.5 W	3091	22.3	20.7
Koutavas & Sachs, 2008	EEP	Uk37	V21-30	1.2 S	90.3 W	617	24.6	23.7
Lea et al., 2000	EEP	Mg/Ca	TR163-19	2.3 N	89.0 W	2348	25.9	23.1
Lea et al., 2006	EEP	Mg/Ca	TR163-22	0.5 N	87.6 W	2830	24.2	22.6
Koutavas et al., 2002	EEP	Mg/Ca	V21-30	1.2 S	90.3 W	617	22.0	21.9
Leduc et al., 2007	EPWP	Uk37	MD02-2529	8.2 N	95.9 W	1619	27.9	25.6
Benway et al., 2006	EPWP	Mg/Ca	ME0005A-43JC	7.9 N	96.4 W	1368	26.3	23.7
Benway et al., 2006	EPWP	Mg/Ca	ODP-1242	7.9 N	96.4 W	1364	26.2	24.3
de Garidel-Thoron et al, 2007	WEP	Mg/Ca	MD97-2138	1.3 N	146.1 E	1960	29.4	26.6
Rosenthal et al, 2003	WEP	Mg/Ca	MD97-2141	8.8 N	121.3 E	3600	28.8	26.8
Stott et al., 2007	WEP	Mg/Ca	MD98-2170	10.6 S	125.4 E	832	29.2	26.3
Stott et al., 2007	WEP	Mg/Ca	MD98-2176	5.0 S	133.4 E	2382	29.2	26.2
Stott et al., 2007	WEP	Mg/Ca	MD98-2181	6.3 N	125.8 E	2114	29.4	25.9
Lea et al., 2000	WEP	Mg/Ca	ODP-806B	0.3 N	159.4 E	2520	28.7	26.3

Chapter 4: Long-term stability and sensitivity of the Western Equatorial Pacific warm pool to radiative forcing

ABSTRACT

The Western Equatorial Pacific (WEP) warm pool is an important source of heat for the global climate system, and small variations in its sea surface temperature (SST) can alter cloud cover and atmospheric circulation with global consequences. From orbital resolution SST reconstructions over Pleistocene glacial cycles, previous studies have inferred that the WEP warm pool largely responded to pCO_2-radiative forcing (Medina-Elizalde and Lea, 2005; Dyez and Ravelo, 2012). However, these reconstructions do not provide information on the thermocline, which is important to tropical dynamics, and were based on measurements of pooled foraminiferal shells, which do not resolve short-term SST variability. To investigate changes in the mean state, we combine published low-resolution SST records with a newly generated subsurface temperature record to monitor the thermocline. Additionally, to monitor high-resolution variability, populations of individual surface and subsurface dwelling foraminifera were analyzed from glacial-interglacial (G-IG) pairs from four intervals since the early Pliocene. Throughout the last four million years long-term mean SSTs were similar to present day, and there were G-IG shifts of ~+0.6 to -2.0°C in the mean state relative to the Holocene. In contrast, subsurface temperatures in the early Pliocene were warm and gradually cooled to present day values, indicating a long-term shoaling or cooling of the tropical thermocline. Although the selected intervals show G-IG changes in mean surface and subsurface temperatures, the G-IG

temperature variability of single foramininfera measurements did not change since the early Pliocene. This implies that while the tropical long-term mean state (i.e. thermocline structure) and other boundary conditions (e.g. ice, pCO_2) have changed since the early Pliocene, the mechanism and feedbacks responsible for G-IG mean temperature changes are similar and consistent through time. We infer that changes in mean SST and subsurface temperatures on G-IG scales since the early Pliocene have responded largely to pCO_2 forcing and related feedbacks.

INTRODUCTION

The WEP warm pool acts as a global heat engine by supplying vapor and heat to the atmosphere, and small changes in its mean state and variability greatly impact global climate (McPhaden et al., 1998). With current global warming, temperatures in this region have risen ~0.2 to 1°C (Cravatte et al., 2009), likely related to anthropogenic pCO_2 inputs. However, from the short-term instrumental record, it is difficult to discern anthropogenic changes from natural variability. Records of past climate can be used to identify process that integrate natural variability in short and long-term feedbacks, as well as global changes that may affect climate.

The Pliocene warm period (~3.0 – 4.3 Ma, (Dowsett and Robinson, 2009; Wara et al., 2005) provides an opportunity for understanding warm climate behavior and validating models. During the early Pliocene warm period (4.0 – 4.3 Ma), the Northern Hemisphere was relatively ice-free (Haywood et al., 2000), the warm pool expanded into mid-latitudes (Brierley et al., 2009), and pCO_2 levels were similar to present day (Seki et al., 2010; Pagani et al., 2010). Following the initiation of

Northern Hemisphere glaciation at ~3.6 Ma (Mudelsee and Raymo, 2005), the mid-Pliocene warm period has been extensively studied through paleodata (Dowsett and Robinson, 2009) and climate modeling (Haywood et al., 2013) from the PRISM time slice (3.3 to 3.0 Ma). During the Pleistocene (2.6 to 0.01 Ma), climate oscillated between glacial and interglacial periods with the expansion and contraction of large ice sheets. The establishment of strong zonal and meridional gradients at ~2 Ma (Etourneau et al., 2009; Martinez-Garcia et al., 2010) marks the transition into a more modern global climate configuration. As the climate evolved from the warm Pliocene to the cold Pleistocene, radically different boundary conditions (e.g. pCO_2, ice sheets) may have impacted the long-term mean and variability of climate through various mechanisms and processes.

To monitor the response of the WEP mean state and variability to different boundary conditions (ice volume, pCO_2), we generated paleoproxy temperature records from Ocean Drilling Program Site 806, which is located in the core of the warm pool (Figure 4.1). To complement previously generated SST records (Wara et al., 2005), we constructed a long-term record of subsurface temperature to provide a complete view of the WEP upper ocean development over the last five million years. Additionally, glacial-interglacial (G-IG) pairs within four discrete time slices were chosen to reconstruct changes in G and IG mean state and in the distribution of temperatures recorded by single foraminifera shells (hereafter referred to as temperature distribution). Within each interval (eight total, from G-IG pairs from four time slices) we analyzed individual shells of surface and subsurface dwelling

foraminifera and using populations of foraminifera were able to reconstruct a G and IG mean state (average of the foraminifera populations) as well as temperature distribution (range and temperature distributions from population of foraminifera). In all, this study reconstructs variability on multiple time scales: long-term (over the last five million years), and for each interval G-IG means and temperature distribution. Identifying the mechanisms that control mean state and variability on multiple time scales (long-term, G-IG, and temperature distribution) in the WEP, particularly with different boundary conditions (e.g. pCO_2, ice sheets), will aid in understanding climate evolution on a global scale.

METHODS AND APPROACH

Site Location and Age Model: Located in the heart of the Western Equatorial Pacific (WEP), Ocean Drilling Program Site 806 (0°N, 159°E, 2520 m water depth) is used to monitor the mean state and temperature variability of the warm pool. Today, the WEP is characterized by warm SSTs (>27°C) and a relatively deep thermocline. The age model is based on a high-resolution benthic isotope (0-4 Ma, Bickert et al., 1993) and bulk density (>4 Ma, Mayer et al., 1993) record. For the glacial-interglacial (G-IG) comparisons, the Site 806 benthic isotope record and the LR04 benthic stack (Lisiecki and Raymo, 2005) were compared during target intervals (Holocene-Last Glacial Maximum, ~2 Ma, PRISM, ~4 Ma). High fidelity intervals (i.e. shape, peak, and trough matches) were chosen for further paired G-IG analysis.

Foraminiferal Minor Element Analysis: To reconstruct the mean state and temperature variability since the late Pliocene, subsurface and surface dwelling foraminifera from Site 806 were analyzed for minor element ratios. Samples from 2 to 3 cm intervals were washed, dried and picked for *Globorotalia tumida* and *Globigerinoides sacculifer* (without final sac-like chamber) from the 355-425 mm size fraction.

Subsurface-dwelling *G. tumida* (~100 m depth habitat, irrespective of thermocline depth Ravelo and Fairbanks, 1992) was used to reconstruct subsurface temperatures. In the modern ocean,h *G. tumida* calcifies at a relatively constant depth in a variety of hydrographic settings (Rincón-Martínez et al., 2011). Each sample was prepared using standard analytical techniques and analyzed via Inductively Coupled Plasma-Optical Emission Spectrometer (ICP-OES). A low-resolution, long-term subsurface mean temperature record was generated by crushing and homogenizing several *G.tumida* (~10-25 specimens). A high-resolution subsurface temperature variability record from G-IG pairs from four intervals (Holocene-LGM, 2 Ma, PRISM and 4 Ma) was generated from individual *G. tumida* (~70 individuals per G and IG). Samples were sonicated in Milli-Q and methanol, washed with reductive and oxidative reagents, and transferred to acid-cleaned vials (see Martin and Lea (2002) for a detailed description) for analysis on the ICP-OES (Wara et al., 2003). Reproducibility for a liquid consistency standard and foraminifera standards are 3.318 ± 0.030 mmol/mol (1σ, n=401) and 3.737 ± 0.181 mmol/mol (1σ, n=103) respectively. *G. tumida* Mg/Ca values were converted to temperature using the *G.*

tumida-specific temperature calibration of Mohtadi et al., (2011). The long-term Mg/Ca record constructed from *G. tumida* is reported in Figure 4.2 and the mean and variance of pooled individual *G. tumida* is reported in Table 4.1.

Surface-dwelling *G. sacculifer* was used to reconstruct shallow mixed layer (~0-50 m, Fairbanks et al., 1982) temperatures. Prior to analysis, individuals (~80 individuals per G and IG) were sonicated in deionized water for 20 seconds and rinsed with methanol, and the final chamber was mounted onto carbon tape for laser analysis. *G. sacculifer* specimens were analyzed by laser ablation (Photon Machines Analyte.193 with HelEx sample cell) coupled with a Thermo ElementXS Inductively Coupled Plasma-Mass Spectrometer (LA-ICP-MS), using methods similar to (Eggins et al., 2003; Sadekov et al., 2010). Approximately four spots, ~50 mm in diameter, were ablated and analyzed for selected isotopes (^{11}B, ^{24}Mg, ^{25}Mg, ^{27}Al, ^{43}Ca, ^{44}Ca, ^{55}Mn, ^{66}Zn, ^{88}Sr). ^{27}Al, ^{55}Mn, and ^{66}Zn were used as indicators of clay and oxide contamination, such that peaks in these elements were avoided when integrating data traces to compute mean minor elemental ratios. Specimens were analyzed from the inner shell surface to the outside, and data acquisition lasted 40-60s. NIST glass standards were analyzed at 4Hz and 4.1 laser fluence. Analytical reproducibility for NIST610 and NIST612 for Mg/Ca was 8.66 ± 0.14 and 1.31 ± 0.23, respectively (1σ, n = 359 over 25 analytical days). To monitor carbonate matrix effects, carbonate standards and samples were analyzed at 4Hz and 1.13 laser fluence. Carbonate standard reproducibility for JCt-1-Plug and MACS-3 for Mg/Ca was 1.35 ± 0.15 and 7.61 ± 0.47, respectively (1s, n=280 and 582). Average intra-test variability for

Mg/Ca is 0.11 mmol/mol. Mg/Ca values were converted to temperature using the Mg/Ca dissolution correction of Regenberg et al., (2006) and the multi-species temperature equation of Anand et al., (2003). For the Regenberg et al., (2006) dissolution correction, a $\Delta[CO_3^{2-}]$ value was calculated for Site 806 using proximal GLODAP ocean carbon (Key et al., 2004) and World Ocean Atlas temperature (Locarnini et al., 2010) datasets. The $\Delta[CO_3^{2-}]$ value is estimated to be 5.692 mmol/kg. The mean and variance of pooled individual *G. sacculifer* is reported in SOM Table 1. Mean bulk values (~20 specimens) of *G. sacculifer* were also generated from each interval using the same minor element techniques described to generate *G. tumida* records and show good correspondence with mean values calculated from pooled individual *G. sacculifer* (Table 4.2).

Data Analysis: The data analysis follows the statistical approach described in Chapter 3. In a Q-Q plot, the quantiles of probability distributions are plotted against one another to facilitate qualitative comparison (Figure 4.3). Intervals that have a distribution with the same quantiles will plot on the one-to-one line (dashed gray line), while samples that have the same distribution but different mean values, will plot in an offset line parallel to the one-to-one line (dashed black line). Samples that have different distributions will plot with a different slope or nonlinear to the one-to-one line (e.g. curved, s-shaped, and/or tangent depending on the distributions). Uncertainty was estimated using a Monte Carlo simulation (gray dots) to construct 90% confidence limits (black lines).

Modern Hydrographic Data, Foraminiferal Fluxes and High-Resolution Variability: With respect to modern monthly mean temperatures from 1958-2007 from the SODA v2.4 re-analysis dataset (Carton and Giese, 2008), *G. sacculifer* and *G. tumida* inhabit a broad range of depths, 0-50 m and 100-150 m, respectively. Foraminifera serially precipitate shell material over a 2-4 week lifespan, and the shell chemistry records water properties including temperature. Nearby sediment trap experiments show uniform export flux of *G. sacculifer* and *G. tumida* throughout the annual cycle (Kawahata et al., 2002), suggesting no seasonal bias in the sediment record. As the sediment record integrates several hundreds of years, our reconstructions likely reflect high-resolution variability, an integration of seasonal, interannual and sub-centennial variability. While secular changes in SST and subsurface temperature may occur within the timespan of a single sediment sample, seasonal and interannual frequencies of variation will dominate our reconstructions. Furthermore, in lieu of a comparison of modern data to paleorecords of variability, here we compare various intervals to each other to minimize potential biases inherent to both data sets.

RESULTS AND DISCUSSION

Although pCO_2 values were slightly elevated during the mid- to early Pliocene with respect to modern levels (Seki et al., 2010, Badger et al., 2013, *in press*), WEP SSTs did not exceed present day, and the long-term mean SST has been stable (~26-28 °C) since the early Pliocene (Figure 4.1, Wara et al., 2005). Our analysis of SST G-IG pairs indicates that, within calibration error, mean temperatures

were comparable to or cooler than Holocene values (SOM Table 1). Climate model ensemble analysis of the modern tropical response to future pCO_2 forcing indicates the WEP responds dynamically to reduce heating due to anthropogenic CO_2 inputs, through cloud albedo and evaporation feedbacks (DiNezio et al., 2009). Similar heat reduction feedbacks may have operated during the last four million years.

Some authors have argued that changes in the Mg/Ca of seawater may underestimate SST reconstructions for the mid- to early Pliocene (Medina-Elizalde et al., 2008). Medina-Elizalde et al., (2008) applied $Mg/Ca_{seawater}$ reconstructions based on $\delta^{44}Ca$, to estimate past weathering fluxes and ocean [Ca] (Fantle and DePaolo 2005), and deep-sea sediment pore fluid [Mg] and numerical modeling, to estimate past ocean [Mg] (Fantle and DePaolo, 2006). While $\delta^{44}Ca$ records are sparse and variable, during the early Pliocene, the [Ca] in the ocean may have been higher than present day (Fantle and DePaolo, 2005). In contrast, numerical modeling of Mg, Ca, and Sr cycling, with certain assumptions about calcite recrystallization, suggests during the early Pliocene [Mg] in the ocean may have been lower than present day (Higgins and Schrag, 2012). These [Ca] and [Mg] reconstructions combined suggest the $Mg/Ca_{seawater}$ may be lower than modern during the early Pliocene, which has been suggested to impact Mg/Ca derived temperatures such that temperature reconstructions during the early Pliocene may have a cold bias of ~1-3 °C (Medina-Elizalde et al., 2008). However, the application of $Mg/Ca_{seawater}$ corrections to SST reconstructions may be premature, particularly due to the uncertainty in these reconstructions. SST records from eastern equatorial Pacific ODP Site 847 based on

two independent proxies, the Mg/Ca of foraminifera and the alkenone unsaturation index (a temperature proxy independent of changes in Mg/Ca of seawater), have parallel trends in temperature and are within calibration error (Dekens et al., 2008). Furthermore, quantitative assessment of the errors in $Mg/Ca_{seawater}$ reconstructions suggest large uncertainties, and if take at face value, $Mg/Ca_{seawater}$ corrected bottom water temperature reconstructions imply unrealistic $\delta^{18}O$ of seawater values for the Pliocene (Dekens et al., *in prep*). Therefore, due to the uncertainty in $Mg/Ca_{seawater}$ through time and the similar trends in Mg/Ca and alkenone SST reconstructions at Site 847, we do not apply a $Mg/Ca_{seawater}$ correction in this study. While variations in $Mg/Ca_{seawater}$ over the last five million years may modestly affect our interpretation of long-term changes in surface and subsurface temperature, G-IG comparisons discussed below, including comparisons of temperature distribution, are not significantly impacted by changes in $Mg/Ca_{seawater}$ which occur over longer time scales (>1 Ma). We suggest our analyses, combined with previously generated records, indicate long-term warm pool SST stability, with G-IG fluctuations of ~1-2 °C since the early Pliocene.

The long-term subsurface temperature record indicates subsurface temperatures were ~6-8°C warmer during the early Pliocene in comparison to the Holocene and gradually cooled to present day values (Figure 4.1, Table 4.1). In the early Pliocene subsurface temperature appear warmer than SST; however, the surface and subsurface temperature reconstructions are within error of each other and these differences are likely due to choice of different calibrations (Anand et al., 2003 with a

depth correction by Regenberg et al., 2006 for *G. sacculifer* and Mohtadi et al., 2012, for *G tumida*) and calibration issues therein. Theoretically, warm subsurface temperatures during the Pliocene could be the result of a shallower depth habitat of *G. tumida* in comparison to present day; however, this is inconsistent with long-term $\delta^{13}C$ and subsurface temperature evidence from the equatorial Pacific. At ODP Site 851, located in the modern eastern Pacific cold tongue region, $\Delta^{13}C_{sac\text{-}tumida}$, the gradient in $\delta^{13}C$ values between *G. sacculifer* and *G. tumida,* is large during the Pliocene and decreases toward present day (Cannariato and Ravelo, 1997). If *G. tumida* had a shallower depth habitat during the Pliocene, a depth preference closer to that of *G. sacculifer*, the opposite trend would be expected: $\Delta^{13}C_{sac\text{-}tumida}$ would be smaller during the Pliocene, not larger. Furthermore, $\delta^{13}C$ values from *G. tumida* across the eastern Pacific are similarly inconsistent with a change in depth habitat and subsurface temperatures are also warm during the Pliocene to cool toward present day (Ford et al., 2012, Steph et al., 2006, Steph et al., 2010). Here, we interpret that this trend in long-term subsurface temperature across the equatorial Pacific represents an overall shoaling of the tropical thermocline from the early Pliocene to present.

In addition to basin-wide subsurface cooling (this study, Ford et al., 2012, Steph et al., 2006, Steph et al., 2010), $\delta^{18}O$ evidence and climate theory suggests the equatorial thermocline shoaled from the early Pliocene to present day. The $\Delta^{18}O_{sacc\text{-}tumida}$ gradient between *G. sacculifer* (mixed layer) and *G. tumida* (~100 m) can be used as a measure of upper ocean stratification and thermocline depth. At WEP Site 806 (LaRiviere et al., 2012) and EEP Site 1241 (Steph et al., 2006), the $\Delta^{18}O_{sacc\text{-}tumida}$

increased from the early Pliocene toward present day suggesting the ocean was less stratified and the thermocline was deep during the early Pliocene. Furthermore, using different species of foraminifera, a detailed upper ocean depth profile reconstruction during the Pliocene from Site 1241 indicates the mixed layer (*G. sacculifer*) and lower thermocline (*Globorotalia limbata*) were relatively stable (Steph et al., 2006). However, temperatures at the bottom of the photic zone (*G. tumida*) were warm during the early Pliocene and gradually cooled toward ~2 Ma suggesting a shoaling of the overall thermocline (Steph et al., 2006). This is further supported by $\delta^{18}O$ and faunal evidence from Site 847 suggesting the subsurface cooling from the early Pliocene to present day. Philander and Fedorov (2003) hypothesis a deep early Pliocene thermocline is a consequence of global warmth. The equilibrium of heat loss (high latitudes) and heat gain (low latitudes) by the ocean is balanced by the position of the thermocline (Boccaletti et al., 2004). As global climate gradually cooled over the last five million years, the thermocline shoaled (Philander and Fedorov, 2003). A deep basin-wide tropical thermocline during the Pliocene may be a vital component to various dynamic feedbacks, including vertical mixing, that are currently underestimated in climate models of Pliocene warmth (Fedorov et al., 2013). As the tropical thermocline shoaled, the global climate state gradually transitioned from the warm Pliocene to the cold Pleistocene (Fedorov et al., 2006).

Q-Q plots, which facilitate a qualitative comparison of the range and distribution of temperatures between populations of individual foraminifera, indicate the SST distribution is remarkably similar between G-IG pairs, with no change in

distribution but a uniform offset in temperatures (Figure 4.4). Similarly, all intervals compared to the Holocene indicate no change in SST distribution (Figure 4.5). This implies SST distribution has not changed since the early Pliocene. The mean G-IG shift in temperature amounts to ~0.7 to 2.0°C of cooling in glacials compared to the Holocene and ~1.3°C of cooling to ~0.6°C of warming in the interglacials compared to the Holocene (Figure 4.5). These shifts in mean G-IG SST are unlikely related to dynamic processes (e.g. upwelling). Dynamic forcing would likely impact SST distributions because processes that involve winds or upwelling tend to dominate in one season. However, it is conceivable a variety of dynamic feedbacks could balance each other and appear as a uniform change. Rather, the most parsimonious explanation is that the glacial-interglacial shifts in mean SST are likely related to process that would affect all seasons uniformly, as seen in the SST distributions. We infer this common forcing as a radiative effect due to changes in pCO_2 and associated feedbacks. A high-fidelity comparison of tropical Pacific mean SST and the Vostok pCO_2 record indicates the tropical Pacific mean SST has responded to pCO_2-radiative forcing over the last 350,000 years (Lea, 2004), and perhaps throughout late Pleistocene (Dyez and Ravelo, 2012; Medina-Elizalde and Lea, 2005). Although G-IG resolution pCO_2 records do not exist from the Pliocene, the mean shift in SSTs during both glacials and interglacials implies that the WEP warm pool has responded largely to pCO_2-radiative forcing and related feedbacks.

Amid the long-term subsurface temperature trend (Figure 4.1), subsurface temperature distributions may also suggest the WEP warm pool responded primarily

to pCO_2-radiative forcing on G-IG scales. Q-Q plots of subsurface temperature distribution indicate subsurface warming for all intervals relative to the Holocene, which is a reflection of long-term changes in the tropical thermocline from the Pliocene to present day (Figure 4.5). On G-IG scales, the mean subsurface temperature was offset by a comparable amount for each interval (~1.9°C, Figure 4.4), and the subsurface temperature distributions did not change. Due to the similar response of G-IG SST and subsurface temperature (Figure 4.4), we infer pCO_2-radiative forcing also controls subsurface temperature distributions on G-IG time scales. This *p*CO2 forcing may function locally or remotely, through radiative heating of the upper water column accompanied by changes in mixed layer depth or thourgh changes at mid-latitude source regions where water subducts and advects into the tropical thermocline. During the Pliocene, an expanded warm pool (Brierley et al., 2009) and warm mid-latitude source water regions (Karas et al., 2011) may have influenced the long-term mean thermocline state, but on G-IG time scales climate forcing remained largely pCO_2 driven.

Many factors arguably contributed to the long-term global climate state as it transitioned from the warm Pliocene to the cold Pleistocene, such as pCO_2 (Haywood and Valdes, 2004), reduced meridional and zonal gradients (Brierley et al., 2009), and ice sheets (Lunt et al., 2012). Since the late Pliocene, the WEP G-IG changes in mean climate were influenced by pCO_2 and related feedbacks as well as shoaling of the tropical thermocline. Although G-IG records of pCO_2 do not currently exist for the Pliocene, high-resolution pCO_2 records from mid-Pliocene warm period vary by ~55

ppm (Badger et al., 2013, *in press*) corresponding to a G-IG SST change of ~1.1°C observed here during the PRISM interval (Figure 4.4). This is roughly proportional in magnitude to the 100 ppm, ~2.4°C SST change observed between the Holocene and LGM, perhaps signifying a relatively constant tropical climate sensitivity throughout the Pliocene and Pleistocene.

Despite the fact that pCO_2 was only modestly higher than preindustrial values, global temperatures were 2-3°C warmer during the Pliocene warm period in comparison to modern (Haywood and Valdes, 2004). The response of the warm pool to pCO_2 forcing implies that radiative or dynamic feedbacks involving the mid- to high latitudes substantially contributed to Pliocene global warmth. For example, the changes in the long-term mean state of the tropical thermocline since the early Pliocene imply processes and mechanisms that influence mid-latitude regions where tropical subsurface and thermocline are sourced may have contributed the warm climate state. Today, warm pool SST rise related global warming may be balanced quickly by evaporative cooling (An et al., 2011). However, the delayed response of subsurface waters to global warming (An, 2008) implies that slower feedbacks involving the thermocline and vertical mixing have not yet responded to current temperature rise. Further paleoproxy and model studies focusing on climate evolution over the last four million will help identify processes and feedbacks, particularly those involving the subsurface, that are important to the climate system and will improve our ability to project future climate scenarios.

REFERENCES

An, S.-I., 2008, A review of interdecadal changes in the nonlinearity of the El Niño-Southern Oscillation: Theoretical and Applied Climatology, v. 97, no. 1-2, p. 29–40, doi: 10.1007/s00704-008-0071-z.

An, S.-I., Kim, J.-W., Im, S.-H., Kim, B.-M., and Park, J.-H., 2011, Recent and future sea surface temperature trends in tropical pacific warm pool and cold tongue regions: Climate Dynamics, v. 39, no. 6, p. 1373–1383, doi: 10.1007/s00382-011-1129-7.

Anand, P., Elderfield, H., and Conte, M., 2003, Calibration of Mg/Ca thermometry in planktonic foraminifera from a sediment trap time series: Paleoceanography, v. 18, no. 2, p. 1050, doi: 10.1029/2002KPA000846.

Bickert, T., Berger, W.H., Burke, S., Schmidt, H., and Wefer, G., 1993, 24. Late Quaternary Stable Isotope Records of Benthic Foraminifers: Sites 805 and 806 Ontong Java Plateau, *in* Proceedings of the Ocean Drilling Program, Scientific Results, Volume 130.

Boccaletti, G., Pacanowski, R., Philander, S. G., and Fedorov, A. V., 2004. The Thermal Structure of the Upper Ocean. Journal of Physical Oceanography, v. 34, p. 888–902.

Brierley, C.M., Fedorov, A.V., Liu, Z., Herbert, T.D., Lawrence, K.T., and Lariviere, J.P., 2009, Greatly Expanded Tropical Warm Pool and Weakened Hadley Circulation in the Early Pliocene: Science, v. 323, no. 5922, p. 1714–1718, doi: 10.1126/science.1167625.

Cannariato, K., and Ravelo, A., 1997, Plio-Pleistocene evolution of eastern tropical Pacific surface water circulation and thermocline depth. *Paleoceanography*, v. 12, p. 805–820.

Carton, J.A., and Giese, B.S., 2008, A Reanalysis of Ocean Climate Using Simple Ocean Data Assimilation (SODA): Monthly Weather Review, v. 136, no. 8, p. 2999–3017, doi: 10.1175/2007MWR1978.1.

Cravatte, S., Delcroix, T., Zhang, D., McPhaden, M., and Leloup, J., 2009, Observed freshening and warming of the western Pacific Warm Pool: Climate Dynamics, v. 33, no. 4, p. 565–589, doi: 10.1007/s00382-009-0526-7.

Dekens, P.S., Ravelo, A.C., Mccarthy, M.D., and Edwards, C.A., 2008, A 5 million year comparison of Mg/Ca and alkenone paleothermometers: Geochemistry Geophysics Geosystems, v. 9, no. 10, p. 18, doi: 10.1029/2007GC001931.

DiNezio, P.N., Clement, A.C., Vecchi, G.A., Soden, B.J., and Kirtman, B.P., 2009, Climate Response of the Equatorial Pacific to Global Warming: Journal of Climate, v. 22, no. 18, p. 4873–4892, doi: 10.1175/2009JCLI2982.1.

Dowsett, H.J., and Robinson, M., 2009, Mid-Pliocene equatorial Pacific sea surface temperature reconstruction: a multi-proxy perspective: Philosophical Transactions of the Royal Society A, v. 367, p. 109–125, doi: 10.1098/rsta.2008.0206.

Dyez, K.A., and Ravelo, A.C., 2012, Late Pleistocene tropical Pacific temperature sensitivity to radiative greenhouse gas forcing: Geology, v. 41, no. 1, p. 23–26, doi: 10.1130/G33425.1.

Eggins, S., Dedeckker, P., and Marshall, J., 2003, Mg/Ca variation in planktonic foraminifera tests: implications for reconstructing palaeo-seawater temperature and habitat migration: Earth and Planetary Science Letters, v. 212, no. 3-4, p. 291–306, doi: 10.1016/S0012-821X(03)00283-8.

Etourneau, J., Martinez, P., Blanz, T., and Schneider, R., 2009, Pliocene-Pleistocene variability of upwelling activity, productivity, and nutrient cycling in the Benguela region: Geology, v. 37, no. 10, p. 871–874, doi: 10.1130/G25733A.1.

Fairbanks, R.G., Sverdlove, M., Free, R., Wiebe, P.H., and Bé, A.W., 1982, Vertical distribution and isotopic fractionation of living planktonic foraminifera from the Panama Basin: Nature, v. 298, no. 5877, p. 841–844.

Fantle, M., and DePaolo, D., 2005. Variations in the marine Ca cycle over the past 20 million years. Earth and Planetary Science Letters, v. 237, p. 102–117. doi:10.1016/j.epsl.2005.06.024

Fantle, M. S., and DePaolo, D. J., 2006. Sr isotopes and pore fluid chemistry in carbonate sediment of the Ontong Java Plateau: Calcite recrystallization rates and evidence for a rapid rise in seawater Mg over the last 10 million years. Geochimica et Cosmochimica Acta, v. 70, p. 3883–3904. doi:10.1016/j.gca.2006.06.009

Fedorov, A.V., Brierley, C.M., Lawrence, K.T., Liu, Z., Dekens, P.S., and Ravelo, A.C., 2013, Patterns and mechanisms of early Pliocene warmth: Nature, v. 496, no. 7443, p. 43–49, doi: 10.1038/nature12003.

Fedorov, A.V., Dekens, P., McCarthy, M., Ravelo, A., deMenocal, P., Barreiro, M., Pacanowski, R., and Philander, G., 2006, The Pliocene Paradox (Mechanisms for a Permanent El Nino): Science, v. 312, no. 5779, p. 1485–1489, doi: 10.1126/science.1122666.

Ford, H., Ravelo, A., and Hovan, S., 2012, A deep Eastern Equatorial Pacific thermocline during the early Pliocene warm period: Earth and Planetary Science Letters, v. 355-356, p. 152–161.

Haywood, A., and Valdes, P., 2004, Modelling Pliocene warmth: contribution of atmosphere, oceans and cryosphere: Earth and Planetary Science Letters, v. 218, no. 3-4, p. 363–377, doi: 10.1016/S0012-821X(03)00685-X.

Haywood, A., Sellwood, B., and Valdes, P., 2000, Regional warming: Pliocene (3 Ma) paleoclimate of Europe and the Mediterranean: Geology, v. 28, p. 1063–1066.

Haywood, A.M., Hill, D.J., Dolan, A.M., Otto-Bliesner, B.L., Bragg, F., Chan, W.L., Chandler, M.A., Contoux, C., Dowsett, H.J., Jost, A., Kamae, Y., Lohmann, G., Lunt, D.J., Abe-Ouchi, A., et al., 2013, Large-scale features of Pliocene climate: results from the Pliocene Model Intercomparison Project: Climate Of The Past, v. 9, no. 1, p. 191–209, doi: 10.5194/cp-9-191-2013.

Higgins, J. A., and Schrag, D. P., 2012. Records of Neogene seawater chemistry and diagenesis in deep-sea carbonate sediments and pore fluids. Earth and Planetary Science Letters, v. 357-358, p. 386–396. doi:10.1016/j.epsl.2012.08.030

Karas, C., Nürnberg, D., Tiedemann, R., and Garbe-Schönberg, D., 2011, Pliocene climate change of the Southwest Pacific and the impact of ocean gateways: Earth and Planetary Science Letters, v. 301, p. 117–124, doi: 10.1016/j.epsl.2010.10.028.

Kawahata, H., Nishimura, A., and Gagan, M.K., 2002, Seasonal change in foraminiferal production in the western equatorial Pacific warm pool: evidence from sediment trap experiments: Deep-Sea Research Part Ii-Topical Studies In Oceanography, v. 49, no. 13-14, p. 2783–2800.

Key, R.M., Kozyr, A., Sabine, C.L., Lee, K., Wanninkhof, R., Bullister, J.L., Feely, R.A., Millero, F.J., Mordy, C., and Peng, T.H., 2004, A global ocean carbon climatology: Results from Global Data Analysis Project (GLODAP): Global Biogeochemical Cycles, v. 18, no. 4, p. n/a–n/a, doi: 10.1029/2004GB002247.

LaRiviere, J.P., Ravelo, A.C., Crimmins, A., Dekens, P.S., Ford, H.L., Lyle, M., and Wara, M.W., 2012, Late Miocene decoupling of oceanic warmth and atmospheric carbon dioxide forcing: Nature, v. 486, no. 7401, p. 97–100, doi: 10.1038/nature11200.

Lea, D.W., 2004, The 100 000-yr cycle in tropical SST, greenhouse forcing, and climate sensitivity: Journal of Climate, v. 17, no. 11, p. 2170–2179.

Lisiecki, L., and Raymo, M., 2005, A Pliocene-Pleistocene stack of 57 globally distributed benthic delta O-18 records: Paleoceanography, v. 20, no. 1, p. PA1003, doi: 10.1029/2004PA001071.

Locarnini, A.R., Mishonov, A.V., Antonov, J.I., Boyer, T.P., Garcia, H.E., Baranova, O.K., Zweng, M.M., and Johnson, D.R., 2010, *World Ocean Atlas 2009* (S. Levitus, Ed.): U.S. Government Printing Office, Washington, D.C.

Lunt, D.J., Haywood, A.M., Schmidt, G.A., Salzmann, U., Valdes, P.J., Dowsett, H.J., and Loptson, C.A., 2012, On the causes of mid-Pliocene warmth and polar amplification: Earth and Planetary Science Letters, v. 321-322, no. C, p. 128–138, doi: 10.1016/j.epsl.2011.12.042.

Martin, P.A., and Lea, D., 2002, A simple evaluation of cleaning procedures on fossil benthic foraminiferal Mg/Ca: Geochemistry Geophysics Geosystems, v. 3, no. 10, p. 8, doi: 10.1029/2001GC000280.

Martinez-Garcia, A., Rosell-Mele, A., McClymont, E.L., Gersonde, R., and Haug, G.H., 2010, Subpolar Link to the Emergence of the Modern Equatorial Pacific Cold Tongue: Science, v. 328, no. 5985, p. 1550–1553, doi: 10.1126/science.1184480.

Mayer, L., Jansen, E., Backman, J., and Takayama, T., 1993, 37. Climatic cyclicity at Site 806: The GRAPE record, *in* Berger, W.H., Kroenke, L.W., and Mayer, L. eds., Proceeding of the Ocean Drilling Program, Scientific Results, p. 623–639.

McPhaden, M.J., Busalacchi, A.J., Cheney, R., Donguy, J.-R., Gage, K.S., Halpern, D., Ji, M., Julian, P., Meyers, G., and Mitchum, G.T., 1998, The Tropical Ocean-Global Atmosphere observing system: A decade of progress: Journal of Geophysical Research: Oceans (1978–2012), v. 103, no. C7, p. 14169–14240.

Medina-Elizalde, M., and Lea, D., 2005, The Mid-Pleistocene Transition in the Tropical Pacific: Science, v. 310, no. 5750, p. 1009–1012, doi: 10.1126/science.1115933.

Medina-Elizalde, M., Lea, D., and Fantle, M., 2008, Implications of seawater Mg/Ca variability for Plio-Pleistocene tropical climate reconstruction: Earth and Planetary Science Letters, v. 269, no. 3-4, p. 585–595, doi: 10.1016/j.epsl.2008.03.014.

Mohtadi, M., oppo, D.W., Lückge, A., DePol-Holz, R., Steinke, S., Groeneveld, J., Hemme, N., and Hebbeln, D., 2011, Reconstructing the thermal structure of the upper ocean: Insights from planktic foraminifera shell chemistry and alkenones in modern sediments of the tropical eastern Indian Ocean: Paleoceanography, v. 26, no. 3, doi: 10.1029/2011PA002132.

Mudelsee, M., and Raymo, M., 2005, Slow dynamics of the Northern Hemisphere glaciation: Paleoceanography, v. 20, no. 4, p. PA4022, doi: 10.1029/2005PA001153.

Pagani, M., Liu, Z., Lariviere, J., and Ravelo, A.C., 2010, High Earth-system climate sensitivity determined from Pliocene carbon dioxide concentrations: Nature Geoscience, v. 3, no. 1, p. 27–30, doi: 10.1038/ngeo724.

Philander, S. G., and Fedorov, A. V., 2003. Role of tropics in changing the response to Milankovich forcing some three million years ago. Paleoceanography, v. 18. doi:10.1029/2002PA000837

Ravelo, A.C., and Fairbanks, R.G., 1992, Oxygen Isotopic Composition of Multiple Species of Planktonic Foraminifera: Recorders of the Modern Photic Zone Temperature Gradient: Paleoceanography, v. 7, no. 6, p. 815–831.

Regenberg, M., Nuernberg, D., Steph, S., Groeneveld, J., Garbe-Schoenberg, D., Tiedemann, R., and Dullo, W.-C., 2006, Assessing the effect of dissolution on planktonic foraminiferal Mg/Ca ratios: Evidence from Caribbean core tops: Geochemistry Geophysics Geosystems, v. 7, doi: 10.1029/2005GC001019.

Rincón-Martínez, D., Steph, S., Lamy, F., Mix, A., and Tiedemann, R., 2011, Tracking the equatorial front in the eastern equatorial Pacific Ocean by the isotopic and faunal composition of planktonic foraminifera. *Marine Micropaleontology*, v. 79, p. 24–40. doi:10.1016/j.marmicro.2011.01.001

Sadekov, A.Y., Eggins, S.M., Klinkhammer, G.P., and Rosenthal, Y., 2010, Effects of seafloor and laboratory dissolution on the Mg/Ca composition of Globigerinoides sacculifer and Orbulina universa tests — A laser ablation ICPMS microanalysis perspective: Earth and Planetary Science Letters, v. 292, no. 3-4, p. 312–324, doi: 10.1016/j.epsl.2010.01.039.

Seki, O., Foster, G.L., Schmidt, D.N., Mackensen, A., Kawamura, K., and Pancost, R.D., 2010, Alkenone and boron-based Pliocene pCO2 records: Earth and Planetary Science Letters, v. 292, no. 1-2, p. 201–211, doi: 10.1016/j.epsl.2010.01.037.

Steph, S., Tiedemann, R., Groeneveld, J., Sturm, A., and Nürnberg, A.D., 2006, 12. Pliocene Changes in Tropical East Pacific Upper Ocean Stratification: Response to Tropical Gateways?: Proceedings of the Ocean Drilling Program, Scientific Results, Volume 202,, p. 1–51.

Steph, S., Tiedemann, R., Prange, M., Groeneveld, J., Schulz, M., Timmermann, A., Nürnberg, D., Rühlemann, C., Saukel, C., and Haug, G.H., 2010, Early Pliocene increase in thermohaline overturning: A precondition for the development of the

modern equatorial Pacific cold tongue: Paleoceanography, v. 25, no. 2, p. PA2202, doi: 10.1029/2008PA001645.

Wara, M., Ravelo, A., and Delaney, M., 2005, Permanent El Nino-like conditions during the Pliocene warm period: Science, v. 309, no. 5735, p. 758–761, doi: 10.1126/science.1112596.

Wara, M.W., Anderson, L., Schellenberg, S., Franks, F., Ravelo, A., and Delaney, M., 2003, Application of a radially viewed inductively coupled plasma-optical emission spectrophotometer to simultaneous measurement of Mg/Ca, Sr/Ca, and Mn/Ca ratios in marine biogenic carbonates: Geochemistry Geophysics Geosystems, v. 4, no. 8, p. 14, doi: 10.1029/2003GC000525.

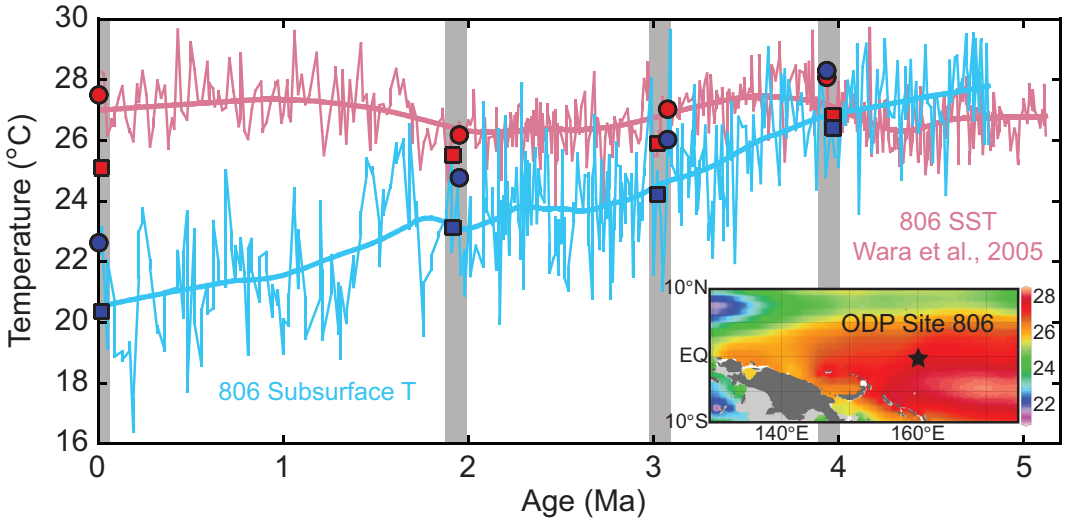

Figure 4.1: Long-term and G-IG SST and Subsurface Temperature Records Long-term records of SST (Wara et al., 2005, pink) and subsurface (this study, light blue) temperature from ODP Site 806. Intervals with individual foraminifera variability reconstructions are denoted in grey bars (Holocene-LGM, ~2 Ma, PRISM, ~4 Ma). Average individual foraminifera SST and subsurface temperature values for glacial (red, blue squares) and interglacial (red, blue circles) are plotted. Inset is a surface mean SST map of the WEP indicating the location of ODP Site 806 (Ocean Data Viewer, World Ocean Atlas, 2005). Long-term SST record suggests stability in the WEP warm pool. Subsurface temperatures in the early Pliocene were warm and gradually cooled to present day values indicating a long-term shoaling or cooling of the tropical thermocline.

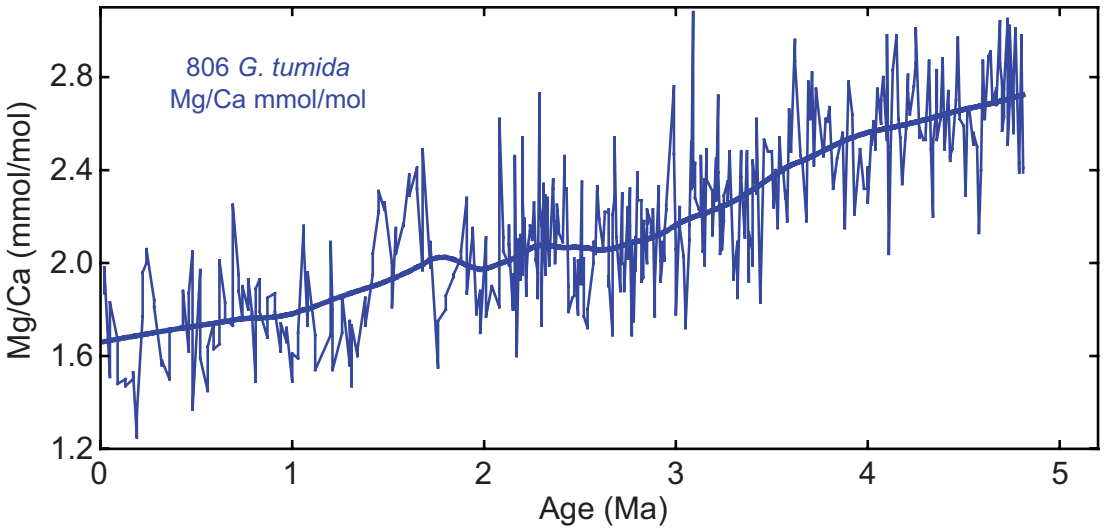

Figure 4.2: Long-term Mg/Ca values of *G. tumida*
Mg/Ca (mmol/mol) values from *G. tumida* from ODP Site 806 from ~5 Ma to present.

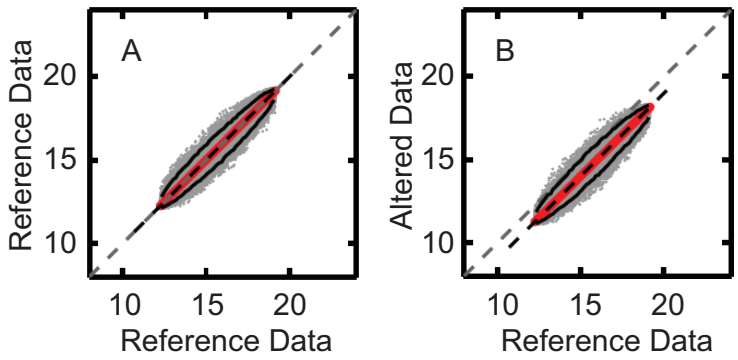

Figure 4.3: Schematics of Distribution Variation on Q-Q Plots
For all figures, the mean shifted one-to-one line (black dashed line), 90% confidence limits (black lines), monte carlo simulation (grey dots) and resampled pdf (red dots). Data with the same distribution (A) will plot on the one-to-one line (grey dashed line). Altered data with the same distribution, but the mean of the altered data is offset (B), will plot on a parallel one-to-one line.

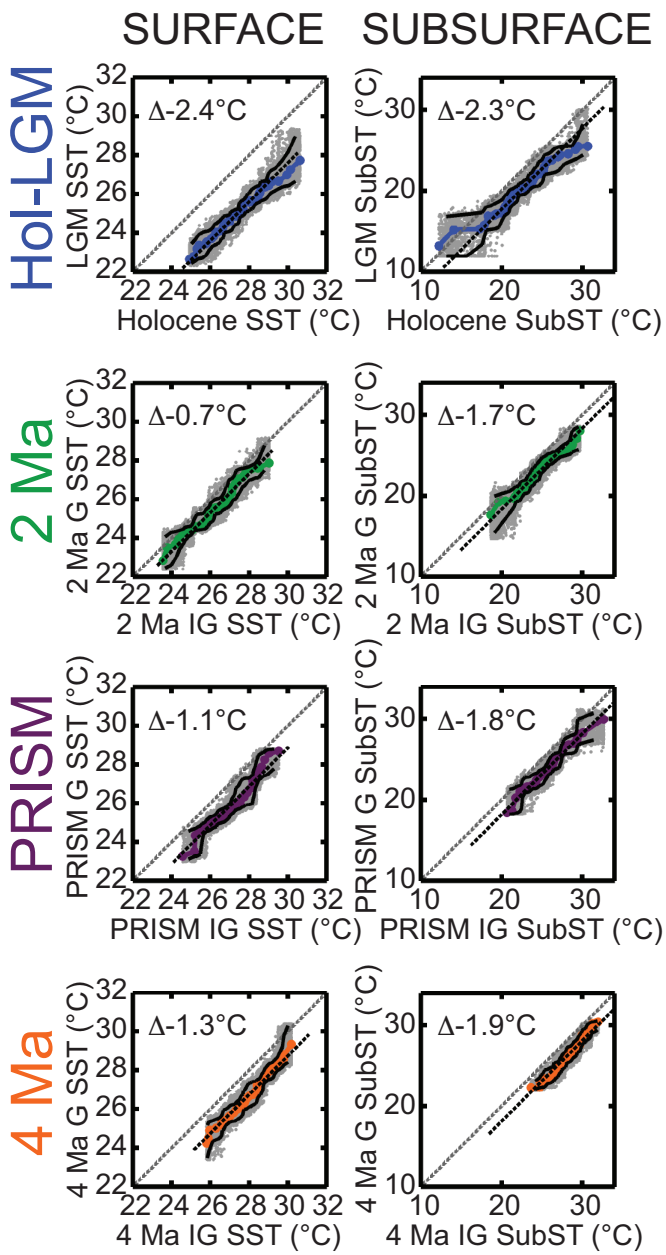

Figure 4.4: Q-Q Plots of surface and subsurface G-IG intervals
Temperature distributions plotted for Holocene-LGM (blue), 2 Ma (green), PRISM (purple), and 4 Ma (orange), with Monte Carlo simulation (grey dots) and 90% confidence limits (black lines). One-to-one line (grey dashed line) and parallel mean offset line (black dashed line) are plotted. The mean change from Holocene compared to the different intervals (example: DHol-LGM = -2.4˚C) is annotated in each plot. For the surface and subsurface, though the mean is offset, the distribution for different glacial-interglacial intervals compared to each other did not change. This suggests the mechanism and feedbacks responsible for glacial-interglacial SST and subsurface variability are similar and consistent through time.

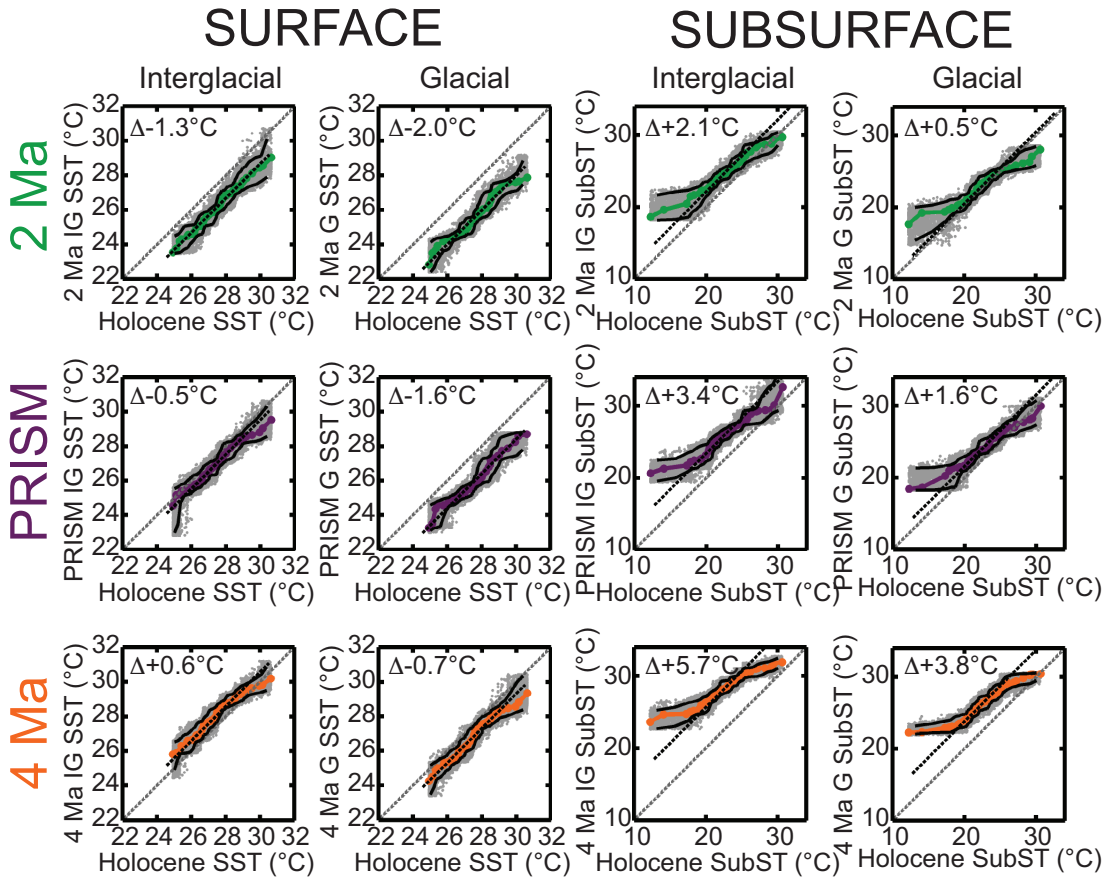

Figure 4.5: Q-Q Plots of surface and subsurface G-IG intervals compared to the Holocene

Temperature distributions plotted for 2 Ma (green), PRISM (purple), and 4 Ma (orange), with Monte Carlo simulation (grey dots) and 90% confidence limits (black lines). One-to-one line (grey dashed line) and parallel mean offset line (black dashed line) are plotted. The mean change from Holocene compared to the different intervals (example: DHol-2Ma IG = -1.3˚C) is annotated in each plot. For the surface, though the mean is offset, the distribution for different intervals compared to the Holocene did not change. For the subsurface, the mean for different intervals was warm compared to the Holocene. Additionally, the distribution for the different intervals was smaller, usually a warming of cold season temperatures, in comparison to the Holocene.

Table 4.1: Bulk and Individual *G. tumida* Mg/Ca (mmol/mol) and Temperature Values

Time Slice	*Interval*	*Leg*	*Site*	*Hole*	*Core*	*Type*	*Section*	*Top (cm)*	*Bot (cm)*	*Age (Ma)*	*Bulk Mg/Ca*	*Bulk Temperature*	*N*	*Average Mg/Ca*	*Average Temperature*	*Standard Dev.*	*Δ Relative to Holocene*	*Δ IG-G*
Hol	IG	130	806	A	1	H	1	0	2	0.003	2.005	23.34	70	1.981	22.64	4.0		
LGM	G	130	806	A	1	H	1	51	55	0.020	1.740	21.25	73	1.676	20.36	3.2	-2.3	2.3
2 Ma	IG	130	806	B	5	H	4	118	121	1.950	2.131	24.24	72	2.248	24.78	2.7	2.1	
2 Ma	G	130	806	B	5	H	4	15	19	1.917	2.033	23.55	72	2.007	23.13	2.6	0.5	1.6
Prism	IG	130	806	B	8	H	5	112	114	3.076	2.280	25.23	73	2.456	26.04	2.9	3.4	
Prism	G	130	806	B	8	H	4	92	94	3.021	1.923	22.72	71	2.164	24.22	2.7	1.6	1.8
4 Ma	IG	130	806	B	11	H	5	92	94	3.936	2.717	27.81	73	2.841	28.31	2.2	5.7	
4 Ma	G	130	806	B	11	H	6	92	94	3.971	2.438	26.22	72	2.502	26.41	2.4	3.8	1.9

Table 4.2: Bulk and Individual *G. sacculifer* Mg/Ca (mmol/mol) and Temperature Values

Time Slice	*Interval*	*Leg*	*Site*	*Hole*	*Core*	*Type*	*Section*	*Top (cm)*	*Bot (cm)*	*Age (Ma)*	*Bulk Mg/Ca*	*Bulk Temperature*	*N*	*Average Mg/Ca*	*Average Temperature*	*Standard Dev.*	*Δ Relative to Holocene*	*Δ IG-G*
Hol	IG	130	806	A	1	H	1	0	2	0.003	4.001	28.1	72	3.768	27.5	1.4		
LGM	G	130	806	A	1	H	1	51	53	0.019	3.177	26.1	69	2.878	25.1	1.3	-2.4	2.4
2 Ma	IG	130	806	B	5	H	4	118	121	1.950	3.571	27.1	83	3.258	26.2	1.4	-1.3	
2 Ma	G	130	806	B	5	H	4	15	19	1.917	3.011	25.6	82	3.018	25.5	1.3	-2.0	0.7
Prism	IG	130	806	B	8	H	5	112	114	3.076	3.865	27.8	82	3.576	27.0	1.3	-0.5	
Prism	G	130	806	B	8	H	4	92	94	3.021	3.152	26.0	74	3.154	25.9	1.3	-1.6	1.1
4 Ma	IG	130	806	B	11	H	5	92	94	3.936	3.957	28.0	83	4.003	28.1	1.2	0.6	
4 Ma	G	130	806	B	11	H	6	92	94	3.971	3.521	27.0	82	3.496	26.8	1.4	-0.7	1.3

Chapter 5: Conclusions

The projects in this dissertation aim to understand the dynamic and radiative processes that determine the tropical Pacific mean state and variability on various temporal and spatial scales. These projects provide new insight into the fundamental impact of the thermocline and high-resolution variability in determining tropical Pacific climate over the last five million years. In these projects I present subsurface temperature records across the tropical Pacific to explore the role of the thermocline on the mean state since the early Pliocene (Chapter 2 and 4), as well as the novel application of individual foraminifera to reconstruct high-resolution variability from glacial-interglacial intervals to study the radiative and dynamic forcing that influence the mean state (Chapter 3 and 4).

In Chapter 2, I present new subsurface temperature records from a latitudinal transect of sites from the eastern Pacific to determine the evolution of the thermocline within and outside the cold tongue region. During the early Pliocene the thermocline was deep and shoaled toward present day. Significant subsurface temperature cooling between 4.0-4.8 Ma, related to closure of the Panama Seaway, preconditioned sea surface temperature cooling that began 4.0 Ma. This initiated ocean-atmospheric feedbacks that influence the tightly coupled sea surface temperature-shallow thermocline cold tongue region today. Continued subsurface cooling from 4.0 Ma to present day may be related global processes by which heat loss in high latitudes is balanced by heat absorption at low latitude upwelling regions, tempered by the position of the thermocline. These high-latitude and low-latitude processes are

connected by their influence on mid-latitude equatorial thermocline source water regions. Additional records from these mid-latitude regions would aid in identifying the processes and feedbacks important to the transition from the warm Pliocene to the cold Pleistocene.

Chapter 3 uses individual surface and subsurface dwelling foraminifera to explore changes in high-resolution temperature variability related to radiative and dynamic forcing during the last glacial period in comparison to the Holocene. Though a single sediment sample integrates ~1000 years of variability, qualitative comparisons of samples using Q-Q plots are used to understand changes in the temperature range and temperature distribution to identify potential forcing mechanisms. Consistent with previous studies, the western Pacific warm pool responds primarily to radiative forcing as shown by a decrease in mean sea surface temperature accompanied by no change in individual foraminifera temperature distribution. However, the eastern Pacific cold tongue shows a significant dynamic response during the last glacial period. The change in individual foraminifera sea surface temperature distribution suggests a reduction in El Niño Southern Oscillation activity or amplitude, which is consistent with the balance of paleoproxy data that suggests El Niño Southern Oscillation is weak during glacial times. The different response between the warm pool and cold tongue to radiative and dynamic forcing during the glacial background state affects basin-wide zonal sea surface temperature reconstructions. Spatial heterogeneity in the mean temperature change between the Holocene and Last Glacial Maximum suggests the eastern Pacific warm pool

responded primarily to radiative forcing, similar to the western warm pool, and the cold tongue responded to radiative and dynamic forcing. Nevertheless, when comparing the western warm pool and the eastern cold tongue, reconstructions suggest the zonal sea surface temperature gradient was reduced during the last glacial maximum in comparison to the Holocene. Previous research combined with this study suggests the mean equatorial climate state during the Last Glacial Maximum included a weaker zonal temperature gradient, steeper equatorial thermocline tilt, and stronger Walker Circulation. Dynamic changes during the Last Glacial Maximum influenced the mean state and variability, particularly in the eastern Pacific, but the balance of the processes and feedbacks important to this climate state need to be explored further with climate models.

In Chapter 4, I present a long-term record of subsurface temperatures and individual surface and subsurface dwelling foraminifera high-resolution temperature variability from four discrete intervals over the last four million years to understanding the mean state and variability evolution of the western warm pool to different global boundary conditions (ice volume, pCO_2). Although pCO_2 during the early Pliocene was slightly elevated in comparison to the Holocene, sea surface temperatures are comparable to today. In the same vein as Chapter 2, subsurface temperatures in the warm pool were warm during the early Pliocene and gradually cooled toward present day. This trend in subsurface temperatures is further evidence that the equatorial thermocline gradually shoaled and is consistent with theories that the thermocline was an important component in the transition form the warm Pliocene

to the cold Pleistocene. High-resolution temperature variability from the surface and subsurface indicates there was no change in temperature distribution within glacial-interglacial intervals. Previous studies have suggested the warm pool responds primarily to radiative forcing during the mid-Pliocene and Pleistocene. Similarly, mean shifts in temperature at the sea surface documented in this study are consistent with direct pCO_2-radiative forcing for the warm pool throughout the last four million years. Although there is a long-term change in the mean state of the subsurface, glacial-interglacial mean shifts in subsurface temperature are inferred to respond to radiative forcing; however, identifying a specific mechanism is difficult, but may include processes that affect mid-latitude equatorial thermocline source water regions. Although no glacial-interglacial resolution pCO_2 reconstructions exist to accurately calculate climate sensitivity, glacial-interglacial changes in mean sea surface temperature and low-resolution pCO_2 variability for the mid-Pliocene may indicate tropical sensitivity may have been similar to Holocene-Last Glacial Maximum.

Many of the interpretations presented in this Chapter 4 are dependent on accurate reconstructions of the Mg/Ca of seawater through time and the temperature-Mg/Ca relationship remaining constant if there are secular changes in the Mg/Ca of seawater. As potential changes in Mg/Ca of seawater may alter the interpretation of the long-term trends, the within glacial-interglacial temperature distribution data remains robust because changes in the Mg/Ca of seawater occur over longer time scales. Additional robust records of the Mg and Ca concentrations in seawater over long-time scales are necessary, as well as laboratory culturing experiments verifying

the fidelity of Mg/Ca based temperature relationships under altered Mg/Ca of seawater scenarios.

This research contributes to the growing body of knowledge about the equatorial Pacific during the transition from the warm Pliocene period to the cold Pleistocene but many questions still remain. Over the last four million years it appears the thermocline was an important dynamic component in the mean state of the equatorial Pacific but the evolution of the mid-latitude equatorial thermocline source water regions are not well documented. While the early Pliocene equatorial Pacific is often characterized as a "permanent El Niño" because the mean sea surface temperature distribution resembles a modern El Niño, high-resolution temperature variability reconstructions in the eastern cold tongue remain elusive. The strong dynamic response in the cold tongue to Last Glacial Maximum forcing may suggest this region is sensitive to changes in the background mean state while the warm pool appears to remain relatively stable and respond primarily to radiative-pCO_2 forcing. As the early Pliocene warm period is the most recent period of sustained warmth, further paleoproxy and climate modeling may help identify some of the processes and mechanisms important in future climate change.

Appendix A: Site 848, 849, and 853 *G. tumida* $\delta^{13}C$, $\delta^{18}O$ and subsurface temperatures (Ford et al., 2012)

Depth mbsf (m)	Age (Ma)	δ13C *G. tumida*	δ18O *G. tumida*	Mg/Ca *G.tumida*	Subsurface Temp (C)	Notes
0.03	0.002	1.75	1.81	1.290	17.0	848B1H1 3-5
0.33	0.019			1.260	16.7	848B1H1 33-35
0.63	0.036	1.93	1.72	1.158	15.8	848B1H1 63-65
0.9	0.050	1.73	2.02	1.093	15.1	848B1H1 90-92
1.2	0.070	1.71	1.83	1.095	15.1	848B1H1 120-122
1.46	0.090	1.07	1.04	0.931	13.3	848B1H1 146-148
1.5	0.095	1.40	1.44	1.144	15.6	848B1H2 0-2
1.8	0.130	1.65	2.03	1.039	14.6	848B1H2 30-32
2.05	0.145	1.38	1.47	1.134	15.5	848B1H2 55-57
2.08	0.147	1.23	2.27	0.994	14.1	848B1HCC 0-2
2.2	0.155	1.29	1.91	1.272	16.8	848B2H1 0-2
2.5	0.174	1.43	1.93	1.069	14.9	848B2H1 30-32
2.76	0.200	1.68	1.69	1.156	15.8	848B2H1 56-58
3.1	0.244			1.463	18.4	848B2H1 90-92
3.42	0.264	1.66	1.72	1.166	15.8	848B2H1 122-124
3.65	0.276			1.712	20.1	848B2H1 145-147
3.7	0.280	1.58	2.19	1.168	15.9	848B2H2 0-2
4.01	0.311			1.092	15.1	848B2H2 31-33
4.26	0.330	1.48	1.77	1.205	16.2	848B2H2 56-58
4.64	0.346	1.88	1.74	1.214	16.3	848B2H2 94-96
4.92	0.359			1.315	17.2	848B2H2 122-124
5.2	0.372	1.62	1.30	1.290	17.0	848B2H3 0-2
5.51	0.388			1.605	19.4	848B2H3 31-33
5.8	0.414			1.061	14.8	848B2H3 60-62
6.1	0.428	1.21	1.46	1.104	15.2	848B2H3 90-92
6.43	0.442	1.48	1.41	1.118	15.4	848B2H3 123-125
6.7	0.455			1.273	16.8	848B2H4 0-2
7.02	0.470	1.47	1.83	1.324	17.3	848B2H4 32-34
7.36	0.488	0.83	2.44	1.191	16.1	848B2H4 66-68
7.6	0.502	1.24	1.62	1.146	15.7	848B2H4 90-92
7.93	0.528	1.32	1.13			848B2H4 123-125
7.93	0.528	1.60	1.51	1.182	16.0	848B2H4 123-125
8.15	0.539	0.73	0.94			848B2H4 145-147
8.15	0.539	1.09	1.33	1.252	16.6	848B2H4 145-147
8.2	0.541			1.297	17.0	848B2H5 0-2
8.51	0.556	1.66	1.89	1.250	16.6	848B2H5 31-33
8.8	0.570	1.40	2.19	1.308	17.1	848B2H5 60-62

9.1	0.592	1.25	2.51	1.215	16.3	848B2H5 90-92
9.42	0.619	1.43	2.08	0.946	13.5	848B2H5 122-124
9.66	0.629	1.33	1.46	1.186	16.0	848B2H5 146-148
9.7	0.631	1.21	1.47	1.173	15.9	848B2H6 0-2
10.01	0.644	1.50	2.25	1.060	14.8	848B2H6 31-33
10.26	0.655	1.45	2.22	1.167	15.9	848B2H6 56-58
10.6	0.671	1.42	0.94	1.607	19.4	848B2H6 90-92
11.2	0.708	1.11	2.46	1.054	14.7	848B2H7 0-2
11.52	0.727	1.09	1.51	1.054	14.7	848B2H7 32-34
11.7	0.737	1.44	1.05	1.223	16.4	848B3H1 0-2
11.76	0.741	1.22	1.69	1.174	15.9	848B2H7 56-58
12	0.758	1.34	1.39	1.248	16.6	848B3H1 30-32
12.05	0.762	0.78	1.53	1.257	16.7	848B2HCC 0-2
12.36	0.779	1.61	1.41	1.191	16.1	848B3H1 66-68
12.6	0.791	1.31	1.63	1.172	15.9	848B3H1 90-92
12.92	0.810	1.17	2.02	1.186	16.0	848B3H1 122-124
13.14	0.824	1.52	1.06	1.130	15.5	848B3H1 144-146
13.2	0.827	1.41	1.22	1.200	16.2	848B3H2 0-2
13.52	0.846			1.149	15.7	848B3H2 32-34
13.83	0.864	1.30	1.51	1.177	15.9	848B3H2 63-65
14.1	0.876	0.93	1.90	1.467	18.4	848B3H2 90-92
14.42	0.889	1.31	1.91	1.140	15.6	848B3H2 122-124
14.65	0.899	1.63	1.34	1.256	16.7	848B3H2 145-147
14.7	0.901	1.42	1.60	1.143	15.6	848B3H3 0-2
15	0.916	1.54	1.46	1.140	15.6	848B3H3 30-32
15.3	0.937	1.28	1.93	1.417	18.0	848B3H3 60-62
15.6	0.964	1.18	1.77	1.291	17.0	848B3H3 90-92
15.93	0.992	1.00	1.84	1.265	16.8	848B3H3 123-125
16.15	1.008	0.96	1.46	1.464	18.4	848B3H3 145-147
16.2	1.011	1.48	1.80	1.142	15.6	848B3H4 0-2
16.5	1.031	1.36	2.30	1.336	17.4	848B3H4 30-32
16.8	1.050	1.54	1.80	1.444	18.2	848B3H4 60-62
17.1	1.066	1.31	1.48	1.251	16.6	848B3H4 90-92
17.42	1.077	1.58	1.73	1.178	16.0	848B3H4 122-124
17.65	1.085	1.12	0.92	1.294	17.0	848B3H4 145-147
17.7	1.087	1.75	0.43	1.359	17.5	848B3H5 0-2
18	1.103	1.04	1.29	1.246	16.6	848B3H5 30-32
18.3	1.123	0.87	1.07	1.307	17.1	848B3H5 60-62
18.6	1.143	1.09	1.82	1.376	17.7	848B3H5 90-92
18.92	1.165	1.60	1.14	1.231	16.5	848B3H5 122-124
19.15	1.181	0.79	1.45	1.349	17.5	848B3H5 145-147
19.2	1.184	0.76	1.39	1.555	19.0	848B3H6 0-2
19.5	1.204	1.55	0.84	1.555	19.0	848B3H6 30-32
19.83	1.225	1.64	1.04	1.462	18.4	848B3H6 63-65
20.1	1.242	1.97	1.47	1.278	16.9	848B3H6 90-92
20.4	1.260	1.63	1.38	1.522	18.8	848B3H6 120-122
20.57	1.270	1.65	1.44	1.371	17.6	848B3H6 137-139

20.7	1.280	1.60	1.31	1.531	18.9	848B3H7 0-2
21.01	1.305	1.35	1.65	1.218	16.3	848B3H7 31-33
21.2	1.322			1.556	19.1	848B4H1 0-2
21.3	1.331			1.398	17.9	848B3H7 60-62
21.51	1.350	1.13	1.12	1.918	21.4	848B3HCC 0-2
21.51	1.350			1.349	17.5	848B4H1 31-33
21.8	1.374	1.46	1.57	1.242	16.5	848B4H1 60-62
22.1	1.388	1.52	2.70	1.127	15.5	848B4H1 90-92
22.96	1.439			1.258	16.7	848B4H2 26-28
23.3	1.473			1.137	15.6	848B4H2 60-62
23.6	1.504			1.163	15.8	848B4H2 90-92
23.9	1.535	1.41	1.28	1.520	18.8	848B4H2 120-122
24.15	1.556	1.10	1.46	1.335	17.4	848B4H2 145-147
24.22	1.562	1.07	1.79	1.236	16.5	848B4H3 2-4
24.5	1.613			1.521	18.8	848B4H3 30-32
24.8	1.646	1.26	1.63	1.169	15.9	848B4H3 60-62
25.1	1.678	1.57	1.90	1.299	17.0	848B4H3 90-92
25.4	1.706	1.71	1.31			848B4H3 120-122
25.4	1.706	1.72	0.92	1.508	18.7	848B4H3 120-122
25.65	1.741	1.34	1.26	1.462	18.4	848B4H3 145-147
25.72	1.752	1.41	1.21	1.613	19.5	848B4H4 2-4
26.33	1.804	1.40	1.03	1.632	19.6	848B4H4 63-65
26.6	1.832	1.38	1.32	1.393	17.8	848B4H4 90-92
26.92	1.866	0.95	2.04	1.551	19.0	848B4H4 122-124
27.14	1.894	1.78	0.93	1.294	17.0	848B4H4 144-146
27.2	1.902	1.69	0.69	1.393	17.8	848B4H5 0-2
27.46	1.950	1.49	0.83			848B4H5 26-28
27.46	1.950	1.70	0.47	1.677	19.9	848B4H5 26-28
27.83	2.016	1.28	1.75	1.338	17.4	848B4H5 63-65
28.1	2.054	1.41	1.11	1.216	16.3	848B4H5 90-92
28.43	2.087	1.56	1.67			848B4H5 123-126
28.43	2.087	1.51	1.60	1.263	16.7	848B4H5 123-126
28.65	2.110	1.37	1.48	1.299	17.0	848B4H5 145-147
28.7	2.124	1.45	1.49	1.192	16.1	848B4H6 0-2
28.96	2.188	1.26	1.44	1.187	16.0	848B4H6 26-28
29.3	2.285	1.37	1.34	1.309	17.1	848B4H6 60-62
29.6	2.347	1.40	1.15	1.191	16.1	848B4H6 90-92
29.92	2.391	1.35	0.80			848B4H6 122-124
30.16	2.441	1.66	0.92	1.149	15.7	848B4H6 146-148
30.2	2.448	1.51	1.45	1.283	16.9	848B4H7 0-2
30.46	2.493	1.42	1.40	1.319	17.2	848B4H7 26-28
30.7	2.534	1.48	1.54			848B5H1 0-2
30.7	2.534	1.41	1.20	1.315	17.2	848B5H1 0-2
30.84	2.560	1.21	1.13	1.289	17.0	848B4H7 64-66
30.96	2.582			1.223	16.4	848B5H1 26-28
30.97	2.584	1.40	1.15	1.550	19.0	848B4HCC 0-2
31.3	2.631	1.25	0.90	1.167	15.9	848B5H1 60-62

31.6	2.675	1.42	0.96	1.158	15.8	848B5H1 90-92
31.9	2.713	1.17	0.88			848B5H1 120-122
31.9	2.713	1.10	0.98	1.352	17.5	848B5H1 120-122
32.15	2.742	1.14	1.22	1.259	16.7	848B5H1 145-147
32.2	2.748	1.31	1.14			848B5H2 0-2
32.2	2.748	1.26	1.14	1.328	17.3	848B5H2 0-2
32.5	2.791	1.18	0.98	1.393	17.8	848B5H2 30-32
32.8	2.846	1.26	1.31	1.245	16.6	848B5H2 60-62
33.1	2.884	1.24	1.37	1.403	17.9	848B5H2 90-92
33.4	2.937	1.01	1.11	1.474	18.5	848B5H2 120-122
33.65	2.985	1.21	1.07	1.556	19.1	848B5H2 145-147
33.7	2.998	1.31	0.99	1.430	18.1	848B5H3 0-2
34	3.078			1.592	19.3	848B5H3 30-32
34.3	3.166			1.499	18.6	848B5H3 60-62
34.6	3.243	1.49	0.67	1.668	19.8	848B5H3 90-92
35.2	3.353			1.498	18.6	848B5H4 0-2
35.5	3.407			2.076	22.3	848B5H4 30-32
35.8	3.469	1.57	0.25	1.835	20.9	848B5H4 60-62
36.1	3.546	1.14	0.69	1.843	20.9	848B5H4 90-92
36.65	3.627			1.763	20.4	848B5H4 145-147
36.7	3.636			1.566	19.1	848B5H5 0-2
37	3.689			1.399	17.9	848B5H5 30-32
37.3	3.762	1.26	0.65	1.627	19.6	848B5H5 60-62
37.6	3.854	1.12	0.77	1.627	19.5	848B5H5 90-92
37.9	3.914			1.297	17.0	848B5H5 120-122
38.17	3.981			1.991	21.8	848B5H5 147-149
38.2	3.989			1.929	21.4	848B5H6 0-2
38.8	4.143			2.189	22.8	848B5H6 60-62
39.1	4.200			2.168	22.7	848B5H6 90-92
39.4	4.274			1.970	21.7	848B5H6 120-122
39.7	4.342			2.294	23.4	848B5H7 0-2
40.26	4.424			1.664	19.8	848B5HCC 0-2
40.5	4.461			1.639	19.6	848B6H1 30-32
40.8	4.505	1.21	0.72	1.924	21.4	848B6H1 60-62
41.1	4.543			1.909	21.3	848B6H1 90-92
41.4	4.575			1.564	19.1	848B6H1 120-122
41.65	4.590			1.828	20.8	848B6H1 145-147
41.7	4.591			1.461	18.4	848B6H2 0-2
42	4.603			2.026	22.0	848B6H2 30-32
42.6	4.639			1.877	21.1	848B6H2 90-92
42.9	4.657			2.059	22.2	848B6H2 120-122
43.15	4.673	1.14	0.73			848B6H2 145-147
43.15	4.673	1.27	0.51	1.791	20.6	848B6H2 145-147
43.2	4.676	1.27	0.70	1.583	19.2	848B6H3 0-2
43.8	4.714			1.651	19.7	848B6H3 60-62
44.1	4.733			2.008	21.9	848B6H3 90-92
44.65	4.763			2.643	24.9	848B6H3 145-147

44.7	4.765			2.537	24.5	848B6H4 0-2
45	4.791			1.657	19.8	848B6H4 30-32
45.9	4.860			1.424	18.1	848B6H4 120-122
46.15	4.877	1.14	0.08	2.310	23.4	848B6H4 145-147
46.5	4.906			2.143	22.6	848B6H5 30-32
46.8	4.932	1.48	0.67			848B6H5 60-62
46.8	4.932	1.47	0.71			848B6H5 60-62
47.1	4.958	1.46	0.65	2.489	24.3	848B6H5 90-92
47.4	4.983			2.537	24.5	848B6H5 120-122
48.9	5.120			2.573	24.6	848B6H6 120-122
51.17	5.260	1.46	0.70			848B7H1 147-149
51.2	5.261	1.56	0.49	2.294	23.4	848B7H2 0-2
51.5	5.275			2.027	22.0	848B7H2 30-32
52.4	5.317			2.624	24.9	848B7H2 120-122
52.7	5.330	1.60	0.50	2.571	24.6	848B7H3 0-2
53	5.345			2.054	22.1	848B7H3 30-32
54.5	5.424			2.590	24.7	848B7H4 30-32

Depth mbsf (m)	Age (Ma)	δ13C *G. tumida*	δ18O *G. tumida*	Mg/Ca *G.tumida*	Subsurface Temp (C)	Notes
0	0.000	1.93	0.89	1.021	14.4	849A1H1 0-3
0.58	0.015	1.78	1.73	1.182	16.0	849B1H1 58-60
0.87	0.027	2.12	1.93	0.934	13.4	849A1H1 87-89
1.58	0.052	1.80	1.48	1.009	14.2	849B1H2 8-10
1.78	0.058	1.67	1.28	1.046	14.6	849A1H2 28-30
2.08	0.067	1.76	1.48	0.908	13.1	849B1H2 58-61
2.58	0.082	1.96	1.36	1.061	14.8	849B1H2 108-111
1.88	0.084	1.98	1.00	0.873	12.6	849C1H1 88-91
2.68	0.086	2.07	0.78	0.925	13.3	849A1H2 118-120
2.74	0.112	1.58	1.03	1.027	14.4	849C1H2 38-41
3.65	0.117	1.75	0.84	0.977	13.9	849B1H3 65-67
4.42	0.139	1.79	2.15	0.980	13.9	849B1H3 142-144
4.24	0.155	1.36	1.76	1.116	15.4	849C1H3 38-41
4.74	0.169	1.53	1.24	1.067	14.9	849C1H3 88-91
5.23	0.181			1.146	15.7	849C1H3 137-140
5.73	0.196	1.72	0.83	1.137	15.6	849C1H4 37-40
6.23	0.212	1.71	0.54	1.209	16.2	849C1H4 87-90
6.75	0.227	1.59	1.42	1.205	16.2	849C1H4 139-142
4.21	0.227	1.40	1.53	1.053	14.7	849D1H1 21-24
4.7	0.240	1.36	1.37	1.295	17.0	849D1H1 70-75
5.21	0.255	1.48	1.43	1.055	14.7	849D1H1 121-124
5.7	0.278	1.78	1.23	1.000	14.1	849D1H2 20-25
6.2	0.298	1.72	0.80	1.037	14.5	849D1H2 70-75

6.71	0.322	1.54	0.51	1.164	15.8	849D1H2 121-124
6.99	0.330	1.60	0.37	1.274	16.8	849D1H3 20-25
7.49	0.339	1.17	2.08	1.407	17.9	849D1H3 70-75
7.96	0.348	1.54	1.30	1.113	15.3	849D1H3 117-120
9.58	0.357	1.72	1.62	1.084	15.0	849B2H2 138-141
10.08	0.374	1.91	0.86	1.136	15.5	849B2H3 38-41
10.58	0.390	1.84	0.86	1.205	16.2	849B2H3 88-91
12.08	0.451	1.43	1.62	0.995	14.1	849B2H4 88-91
12.58	0.469	1.92	1.01	1.173	15.9	849B2H4 138-141
11.57	0.471	1.83	1.29	1.196	16.1	849C2H1 107-110
12.07	0.486	1.92	0.95	1.369	17.6	849C2H2 7-10
12.57	0.500	1.94	1.16	1.192	16.1	849C2H2 57-60
13.07	0.514	1.78	1.27	1.331	17.3	849C2H2 107-110
13.57	0.531	1.50	1.23	1.114	15.3	849C2H3 7-10
14.07	0.557	1.72	0.68	1.105	15.2	849C2H3 57-60
14.57	0.582	1.59	1.12	1.141	15.6	849C2H3 107-110
15.09	0.606	1.72	1.25	1.132	15.5	849C2H4 9-12
15.58	0.628	1.41	1.40	1.083	15.0	849C2H4 58-61
15.07	0.642	1.57	1.89	1.311	17.1	849D2H2 7-10
16.03	0.644	1.48	1.90	1.024	14.4	849C2H4 103-106
15.57	0.658	1.57	1.15	1.130	15.5	849D2H2 57-60
16.07	0.673	1.49	1.46			849D2H2 107-110
16.07	0.673	1.62	0.96	1.112	15.3	849D2H2 107-110
16.57	0.689	1.60	1.10	1.062	14.8	849D2H3 7-10
17.07	0.705	1.06	1.31	0.984	14.0	849D2H3 57-60
17.57	0.722	1.22	1.89	1.096	15.2	849D2H3 107-110
18.57	0.760	1.66	1.11			849D2H4 57-60
19.07	0.782	1.14	1.58			849D2H4 107-110
19.57	0.813	1.23	1.52			849D2H5 7-10
20.07	0.832	1.45	1.16			849D2H5 57-60
20.57	0.850	1.23	0.85			849D2H5 107-110
21.07	0.865	1.42	1.35			849D2H6 7-10
21.14	0.871	0.98	1.86	0.954	13.6	849B3H4 44-47
21.51	0.879	1.52	1.45			849D2H6 51-54
21.58	0.888	1.18	1.73	1.049	14.7	849B3H4 88-91
22.08	0.907	1.23	1.54	1.012	14.3	849B3H4 138-141
22.28	0.915	1.15	1.57	0.961	13.7	849B3H5 8-11
22.72	0.932	1.51	0.85	1.158	15.8	849B3H5 52-55
20.38	0.933	1.55	0.70	1.113	15.3	849C3H1 38-41
20.87	0.953			1.203	16.2	849C3H1 87-90
21.37	0.983	1.63	1.21	1.115	15.3	849C3H1 137-140
21.87	0.999	1.63	1.13	1.155	15.7	849C3H2 37-40
22.37	1.021	1.63	0.95	1.197	16.1	849C3H2 87-90
22.87	1.043	1.25	1.22	1.161	15.8	849C3H2 137-140
26.86	1.081	1.52	1.35	1.131	15.5	849D3H3 112-114
28.35	1.142	1.81	1.43	0.982	13.9	849D3H4 111-113
29.85	1.212	1.36	1.37	0.928	13.3	849D3H5 111-113
30.86	1.244	1.20	1.09	1.312	17.1	849D3H6 62-64
31.27	1.257	1.50	1.49	1.072	14.9	849D3H6 103-105
31.54	1.265	1.76	1.28	1.066	14.8	849D3H6 130-132
31.84	1.271	1.83	1.38	0.989	14.0	849D3H7 10-12

32.07	1.277	1.81	1.01	1.153	15.7	849D3H7 33-35
32.52	1.288	1.38	1.29	1.304	17.1	849D3H7 78-80
29.82	1.305	1.57	1.06	1.290	17.0	849C4H1 32-34
30.3	1.320	1.49	0.88	1.152	15.7	849C4H2 8-10
30.74	1.334	1.42	1.79	1.194	16.1	849C4H2 52-54
31.19	1.344	1.76	1.42	0.931	13.3	849C4H2 97-99
31.64	1.353	1.60	0.87	1.237	16.5	849C4H2 142-144
32	1.361	1.71	1.48	1.093	15.1	849C4H3 28-30
33	1.372	1.75	1.28	1.109	15.3	849D4H1 50-52.5
33.33	1.388	1.54	1.19	1.255	16.7	849D4H1 83-85
33.72	1.412	1.51	1.13	1.163	15.8	849D4H1 122-124
34.09	1.435	1.80	0.86	1.159	15.8	849D4H2 9-11
34.52	1.454	1.31	1.03	1.248	16.6	849D4H2 52-54
34.99	1.479	1.95	0.67	1.190	16.1	849D4H2 99-101
35.32	1.496	1.56	0.98	1.410	18.0	849D4H2 132-134
35.68	1.510			1.126	15.4	849D4H3 18-20
36.08	1.525	1.89	0.57	1.338	17.4	849D4H3 58-60
36.51	1.540			1.501	18.6	849D4H3 101-103
36.9	1.554			1.225	16.4	849D4H3 140-142
37.3	1.568	2.01	1.04	1.428	18.1	849D4H4 30-32
37.71	1.584	1.73	1.04	1.515	18.7	849D4H4 71-73
38.11	1.598			1.140	15.6	849D4H4 111-113
38.53	1.617	1.77	1.29	1.151	15.7	849D4H5 3-5
38.93	1.638	1.76	1.26	1.141	15.6	849D4H5 43-45
39.3	1.652	1.64	1.21	1.359	17.5	849D4H5 80-82
39.7	1.666			1.233	16.5	849D4H5 120-122
40.03	1.690	1.59	1.11	1.300	17.0	849D4H6 3-5
40.43	1.702	1.50	1.03	1.227	16.4	849D4H6 43-45
40.83	1.709	1.22	0.88	1.523	18.8	849D4H6 83-85
39.37	1.712	1.67	1.32	1.524	18.8	849C5H1 37-39
41.22	1.716	1.54	1.27	1.143	15.6	849D4H6 122-124
39.72	1.718			1.260	16.7	849C5H1 72-74
40.1	1.737			1.218	16.3	849C5H1 110-112
40.42	1.749			1.204	16.2	849C5H1 142-144
40.73	1.759	1.65	1.02	1.185	16.0	849C5H2 23-25
41.08	1.781	1.47	1.13	1.192	16.1	849C5H2 58-60
41.39	1.791	1.27	1.25	1.109	15.3	849C5H2 89-91
41.73	1.802	1.53	1.37	1.106	15.3	849C5H2 123-125
42.03	1.811	1.96	1.14	1.175	15.9	849C5H3 3-5
42.32	1.824	1.81	1.08	1.221	16.3	849C5H3 32-34
42.68	1.836	1.65	1.34	1.068	14.9	849C5H3 68-70
42.98	1.844	1.54	1.24	1.354	17.5	849C5H3 98-100
42.82	1.847	1.47	0.98	1.202	16.2	849D5H1 82-84
43.42	1.863	1.95	0.97	1.107	15.3	849D5H1 142-144
43.72	1.870	1.70	1.07	1.156	15.7	849D5H2 22-24
44.07	1.880	1.99	1.00	1.047	14.6	849D5H2 57-59
44.37	1.887	1.83	0.93	1.200	16.2	849D5H2 87-89
44.72	1.896	1.61	0.77	1.185	16.0	849D5H2 122-124
45.03	1.905	1.55	1.26	0.843	12.2	849D5H3 3-5
45.42	1.915	1.64	1.15	1.110	15.3	849D5H3 42-44
45.67	1.927	1.90	0.96	1.118	15.4	849D5H3 67-69

45.97	1.944	1.88	1.09	1.239	16.5	849D5H3 97-99
46.27	1.950	1.66	0.46	1.289	16.9	849D5H3 127-129
46.52	1.953	1.46	0.92	1.320	17.2	849D5H4 2-4
46.81	1.957	1.56	1.01	1.178	16.0	849D5H4 31-33
47.12	1.963	1.88	1.02	1.166	15.8	849D5H4 62-64
47.43	1.970	2.05	1.05	1.029	14.5	849D5H4 93-95
47.73	1.978	2.02	0.62	1.037	14.5	849D5H4 123-125
48.03	1.985	1.93	0.78	1.122	15.4	849D5H5 3-5
48.32	1.992	1.76	0.72	1.071	14.9	849D5H5 32-34
48.63	2.000	1.78	0.95	1.180	16.0	849D5H5 63-65
48.93	2.007	1.73	1.06	1.001	14.1	849D5H5 93-95
49.23	2.016	1.92	0.73	1.048	14.7	849D5H5 123-125
49.53	2.024	2.06	0.67	1.172	15.9	849D5H6 3-5
49.82	2.030	1.99	0.71	1.090	15.1	849D5H6 32-34
50.12	2.037	1.73	1.06	1.149	15.7	849D5H6 62-64
50.43	2.044	1.81	1.32	1.030	14.5	849D5H6 93-95
50.74	2.051	1.68	1.13	1.138	15.6	849D5H6 124-126
51.03	2.059	1.67	1.05	1.061	14.8	849D5H7 3-5
51.33	2.067			1.220	16.3	849D5H7 33-35
51.63	2.075	1.44	1.39	1.137	15.6	849D5H7 63-65
54.12	2.219	1.48	0.70	1.351	17.5	849D6H2 112-114
55.62	2.283	1.03	0.55	1.280	16.9	849D6H3 112-114
57.12	2.341	1.63	0.56	1.341	17.4	849D6H4 112-114
58.62	2.405	1.84	0.87	1.138	15.6	849D6H5 112-114
60.11	2.453	1.64	0.77	1.169	15.9	849D6H6 111-113
60.61	2.469	1.71	0.36	1.384	17.7	849D6H7 11-13
66.62	2.716	1.43	0.89	1.297	17.0	849D7H4 112-114
68.1	2.765	1.46	0.79	1.354	17.5	849D7H5 110-112
69.6	2.833	1.59	0.48	1.475	18.5	849D7H6 110-112
70.65	2.935	1.50	0.88	1.192	16.1	849D8H1 15-17
72.08	2.997			1.485	18.5	849D8H2 8-10
72.44	3.013			1.213	16.3	849D8H2 44-46
72.73	3.022			1.289	17.0	849D8H2 73-75
73.03	3.029			1.254	16.6	849D8H2 103-105
73.93	3.063			1.338	17.4	849D8H3 43-45
74.23	3.075			1.123	15.4	849D8H3 73-75
74.53	3.087			1.525	18.8	849D8H3 103-105
74.8	3.099			1.330	17.3	849D8H3 130-132
75.13	3.113			1.353	17.5	849D8H4 13-15
75.43	3.125			1.436	18.2	849D8H4 43-45
75.73	3.137			1.417	18.0	849D8H4 73-75
76.04	3.147			1.428	18.1	849D8H4 104-106
76.38	3.158			1.276	16.8	849D8H4 138-140
76.73	3.172			1.546	19.0	849D8H5 23-25
77.63	3.200			1.232	16.5	849D8H5 113-115
77.93	3.210			1.213	16.3	849D8H5 143-145
78.23	3.219			1.308	17.1	849D8H6 23-25
78.53	3.229			1.292	17.0	849D8H6 53-55
78.83	3.238			1.112	15.3	849D8H6 83-85
77.54	3.245			1.191	16.1	849C9H1 54-56
77.84	3.255	1.77	0.59	1.425	18.1	849C9H1 84-86

78.13	3.266	1.60	0.69	1.148	15.7	849C9H1 113-115
78.43	3.276	1.77	0.91	1.468	18.4	849C9H1 143-145
78.73	3.287	1.46	0.68	1.423	18.0	849C9H2 23-25
78.73	3.287			1.430	18.1	849C9H2 23-25
79.1	3.297	1.48	1.23	1.213	16.3	849C9H2 60-62
79.42	3.312	1.43	0.59	1.499	18.6	849C9H2 92-94
79.72	3.325	1.50	0.93	1.342	17.4	849C9H2 122-124
80.03	3.337			1.406	17.9	849C9H3 3-5
80.23	3.354			1.224	16.4	849D9H1 23-25
80.52	3.362			1.314	17.2	849D9H1 52-54
80.82	3.376			1.350	17.5	849D9H1 82-84
81.12	3.392			1.214	16.3	849D9H1 112-114
81.42	3.397			1.360	17.5	849D9H1 142-144
81.72	3.405			1.275	16.8	849D9H2 22-24
82.02	3.419			1.299	17.0	849D9H2 52-54
82.32	3.432			1.421	18.0	849D9H2 82-84
82.62	3.446			1.360	17.6	849D9H2 112-114
82.92	3.459			1.419	18.0	849D9H2 142-144
83.13	3.466			1.433	18.1	849D9H3 13-15
83.42	3.474			1.512	18.7	849D9H3 42-44
83.72	3.482			1.455	18.3	849D9H3 72-74
84.02	3.491			1.400	17.9	849D9H3 102-104
84.32	3.500			1.397	17.8	849D9H3 132-134
84.82	3.523			1.283	16.9	849D9H4 32-34
85.12	3.536			1.323	17.2	849D9H4 62-64
85.41	3.548			1.463	18.4	849D9H4 91-93
85.73	3.562			1.583	19.2	849D9H4 123-125
86.32	3.577			1.367	17.6	849D9H5 32-34
86.63	3.584			1.475	18.5	849D9H5 63-65
86.92	3.591	1.77	1.00	1.314	17.2	849D9H5 92-94
87.23	3.605	1.45	0.46	1.379	17.7	849D9H5 123-125
87.83	3.631			1.570	19.1	849D9H6 33-35
88.13	3.643			1.213	16.3	849D9H6 63-65
88.44	3.655			1.445	18.2	849D9H6 94-96
88.73	3.663			1.333	17.3	849D9H6 123-125
89.03	3.672			1.594	19.3	849D9H7 3-5
88.22	3.694	1.71	0.53	1.404	17.9	849C10H2 22-24
88.53	3.706	1.42	1.25	1.263	16.7	849C10H2 53-55
88.81	3.715	1.24	1.05	1.409	17.9	849C10H2 81-83
89.13	3.725	1.46	1.10	1.091	15.1	849C10H2 113-115
89.42	3.746	1.62	1.01	1.253	16.6	849C10H2 142-144
89.72	3.753			1.448	18.2	849D10H1 22-24
90.02	3.763			1.546	19.0	849D10H1 52-54
90.33	3.773			1.324	17.3	849D10H1 83-85
90.63	3.782			1.149	15.7	849D10H1 113-115
90.93	3.788			1.223	16.4	849D10H1 143-145
91.23	3.795			1.242	16.5	849D10H2 23-25
91.53	3.801			1.254	16.6	849D10H2 53-55
91.82	3.815			1.394	17.8	849D10H2 82-84
92.15	3.829			1.630	19.6	849D10H2 115-117
92.57	3.841			1.448	18.2	849D10H3 7-9

93.17	3.863	1.52	0.78	1.338	17.4	849D10H3 67-69
93.78	3.890	1.47	0.85	1.321	17.2	849D10H3 128-130
94.17	3.905			1.518	18.8	849D10H4 17-19
94.52	3.919			1.289	17.0	849D10H4 52-54
94.97	3.934			1.294	17.0	849D10H4 97-99
95.27	3.946			1.587	19.3	849D10H4 127-129
95.67	3.962			1.499	18.6	849D10H5 17-19
95.97	3.972			1.592	19.3	849D10H5 47-49
96.31	3.985			1.639	19.6	849D10H5 81-83
97.58	4.034			1.235	16.5	849D10H6 58-60
99.11	4.109			1.205	16.2	849D11H1 11-13
100.62	4.163			1.261	16.7	849D11H2 12-14
102.12	4.214			1.679	19.9	849D11H3 12-14
103.6	4.265			1.544	19.0	849D11H4 10-12
105.12	4.317			1.703	20.1	849D11H5 12-14
106.61	4.353			1.639	19.6	849D11H6 11-13
108.12	4.403			1.614	19.4	849D11H7 12-14
115.12	4.579			1.584	19.2	849D12X5 62-64
119.08	4.669			1.986	21.8	849D13X3 58-60
129.18	4.826			2.080	22.3	849D14X3 108-110
135.37	5.038	0.99	0.13	1.845	20.9	849D15X1 57-59
138.37	5.106	1.14	0.58	1.872	21.1	849D15X3 57-59
139.88	5.147	1.20	0.38	2.008	21.9	849D15X4 58-60
142.87	5.206			1.890	21.2	849D15X6 57-59
144.62	5.276			2.073	22.2	849D16X1 12-14
150.57	5.334			2.105	22.4	849D16X5 7-9
155.29	5.423			2.350	23.6	849D17X1 119-121
156.79	5.459			2.043	22.1	849D17X2 119-121

Depth mbsf (m)	Age (Ma)	δ13C *G. tumida*	δ18O *G. tumida*	Mg/Ca *G.tumida*	Subsurface Temp (C)	Notes
0.2	0.000	1.94	0.76	1.343	17.4	853B1H1 20-22
0.35	0.040	1.49	1.37	1.390	17.7	853B1H1 35-37
0.5	0.085	1.87	1.21	1.390	17.7	853B1H1 50-52
0.66	0.134	1.47	1.45	1.252	16.6	853B1H1 66-68
0.83	0.186	1.66	0.95	1.123	15.4	853B1H1 83-85
0.97	0.229	1.31	1.50	1.296	17.0	853B1H1 97-99
0	0.269			1.256	16.6	853C1H1 0-2
1.12	0.275	1.35	1.85	1.226	16.3	853B1H1 112-114
0.15	0.314			1.273	16.8	853C1H1 15-17
1.27	0.320	2.09	1.40	1.510	18.7	853B1H1 127-129
0.3	0.360	1.42	1.08	1.247	16.5	853C1H1 30-32
1.42	0.366	1.76	1.68	1.565	19.1	853B1H1 142-144
1.5	0.391	1.62	1.06	1.426	18.0	853B1H2 0-2

0.45	0.406	1.46	1.35	1.269	16.7	853C1H1 45-47
1.7	0.452	1.69	1.37	1.371	17.6	853B1H2 20-22
0.6	0.452	1.43	1.39	1.343	17.4	853C1H1 60-62
0.73	0.491	1.37	1.52	1.438	18.1	853C1H1 73-75
1.86	0.500	1.71	0.89	1.329	17.2	853B1H2 36-38
2	0.541	1.61	0.69	1.822	20.8	853B1H2 50-52
0.9	0.541	1.76	1.00	1.168	15.8	853C1H1 90-92
2.15	0.586	1.39	2.04			853B1H2 65-67
2.15	0.586	1.40	2.02	1.251	16.6	853B1H2 65-67
1.05	0.586	1.55	1.34			853C1H1 105-107
1.05	0.586	1.58	1.37	1.194	16.1	853C1H1 105-107
2.3	0.630	1.31	1.10	1.279	16.8	853B1H2 80-82
1.2	0.630	1.67	0.37	1.424	18.0	853C1H1 120-122
2.45	0.675	1.41	0.74	1.917	21.3	853B1H2 95-97
1.35	0.675	1.48	1.54	1.299	17.0	853C1H1 135-137
2.61	0.710	1.43	1.57	1.481	18.4	853B1H2 111-113
2.75	0.739	1.05	1.71	1.245	16.5	853B1H2 125-127
2.9	0.770	1.21	1.71	1.184	16.0	853B1H2 140-142
3.01	0.794	1.35	1.80	1.731	20.2	853B1H3 1-3
3.17	0.831	1.37	1.43	1.373	17.6	853B1H3 17-19
3.3	0.862	1.13	2.00	1.261	16.7	853B1H3 30-32
3.47	0.901	1.22	1.22	1.195	16.1	853B1H3 47-49
3.58	0.927	1.37	1.12	1.269	16.7	853B1H3 58-60
3.78	0.974	1.54	0.82	1.226	16.4	853B1H3 78-80
3.93	1.009	1.35	0.92	1.344	17.4	853B1H3 93-95
4.07	1.042	1.25	1.28	1.771	20.4	853B1H3 107-109
4.31	1.084	1.35	1.54	1.661	19.7	853B2H1 1-3
4.45	1.111	1.46	1.19	1.854	21.0	853B2H1 15-17
4.6	1.140	1.48	1.24	1.350	17.4	853B2H1 30-32
4.75	1.169	1.27	1.45	1.290	16.9	853B2H1 45-47
4.88	1.194	1.42	0.77	1.506	18.6	853B2H1 58-60
5.03	1.223	1.05	1.71	1.357	17.5	853B2H1 73-75
5.19	1.254	1.35	1.20	1.527	18.8	853B2H1 89-91
5.35	1.285	1.31	1.16	1.309	17.1	853B2H1 105-107
5.49	1.312	1.26	1.16	1.172	15.9	853B2H1 119-121
5.65	1.343	1.34	1.21	1.614	19.4	853B2H1 135-137
5.81	1.374	1.46	1.03	1.651	19.7	853B2H2 1-3
5.95	1.402	1.47	1.38	1.446	18.2	853B2H2 15-17
6.12	1.435	1.39	1.07	1.546	18.9	853B2H2 32-34
6.25	1.460	1.51	1.04	1.417	18.0	853B2H2 45-47
6.38	1.485	1.30	0.39	1.284	16.9	853B2H2 58-60
6.54	1.516	1.50	0.71	1.429	18.1	853B2H2 74-76
6.68	1.543	1.59	0.79	1.480	18.4	853B2H2 88-90
6.85	1.576	1.61	0.84	1.565	19.1	853B2H2 105-107
6.98	1.601	1.40	0.54	1.752	20.3	853B2H2 118-120
7.15	1.634	1.24	0.98	1.570	19.1	853B2H2 135-137
7.31	1.665	1.19	1.06	1.748	20.3	853B2H3 1-3
7.45	1.692	1.30	1.00	1.204	16.1	853B2H3 15-17
7.45	1.692			1.204	16.1	853B2H3 15-17
7.75	1.751	1.28	0.84	1.608	19.4	853B2H3 45-47
7.88	1.777	1.25	1.06	2.131	22.5	853B2H3 58-60

8.03	1.812	1.10	1.35	1.421	18.0	853B2H3 73-75
8.17	1.845	1.35	1.36	1.706	20.0	853B2H3 87-89
8.35	1.887	1.51	1.02	1.455	18.3	853B2H3 105-107
8.48	1.917	1.43	1.46	1.170	15.8	853B2H3 118-120
8.65	1.955	1.53	0.91	1.455	18.3	853B2H3 135-137
8.81	1.984	1.35	1.27	1.392	17.8	853B2H4 1-3
9	2.018	1.59	0.43	1.379	17.7	853B2H4 20-22
9.1	2.036	1.60	0.09	1.474	18.4	853B2H4 30-32
9.25	2.063	1.20	1.01	1.372	17.6	853B2H4 45-47
9.38	2.087	1.52	0.68	1.357	17.5	853B2H4 58-60
9.55	2.117	1.47	0.52	1.538	18.9	853B2H4 75-77
9.67	2.139	1.37	0.80	1.481	18.5	853B2H4 87-89
9.86	2.173	1.22	0.85	1.550	19.0	853B2H4 106-108
10.02	2.202	1.28	0.14	2.106	22.4	853B2H4 122-124
10.15	2.225	1.50	0.56	1.451	18.2	853B2H4 135-137
10.3	2.252	1.39	0.57	1.508	18.6	853B2H5 0-2
10.74	2.332	1.65	0.52	1.676	19.8	853B2H5 44-46
10.89	2.359	1.55	0.34	1.588	19.2	853B2H5 59-61
11.04	2.386	1.64	0.67	1.384	17.7	853B2H5 74-76
11.16	2.407	1.77	0.42	1.268	16.7	853B2H5 86-88
11.37	2.445	1.27	0.19	1.558	19.0	853B2H5 107-109
11.48	2.465	1.50	0.38	1.695	19.9	853B2H5 118-120
11.66	2.497	1.28	0.36	1.448	18.2	853B2H5 136-138
11.81	2.524	1.19	0.04	1.572	19.1	853B2H6 1-3
12.25	2.603	1.55	-0.13	1.581	19.2	853B2H6 45-47
12.37	2.621	1.51	0.26	1.438	18.1	853B2H6 57-59
12.44	2.631	1.32	1.12			853B2H6 64-66
12.44	2.631	1.27	1.49	1.407	17.9	853B2H6 64-66
12.55	2.648	1.44	0.27	1.779	20.5	853B2H6 75-77
12.67	2.665	1.49	0.32	1.857	21.0	853B2H6 87-89
12.85	2.692	1.37	0.75	1.514	18.7	853B2H6 105-107
12.98	2.712	1.31	0.48			853B2H6 118-120
12.98	2.712	1.34	0.84	1.442	18.2	853B2H6 118-120
13.45	2.782	1.51	0.32			853B2H7 15-17
13.61	2.805	1.32	0.89	1.541	18.9	853B2H7 31-33
13.79	2.832	1.52	0.80	1.399	17.8	853B2H7 49-51
12.36	2.984	1.47	0.28	1.510	18.7	853B3H1 6-8
12.44	2.996	1.36	0.70	1.346	17.4	853B3H1 14-16
12.57	3.015	1.25	0.79			853B3H1 27-29
12.57	3.015	1.67	0.00	1.438	18.1	853B3H1 27-29
13.25	3.114	1.25	0.35	1.395	17.8	853B3H1 95-97
13.38	3.133	1.53	0.05	1.509	18.7	853B3H1 108-110
14.01	3.236	1.38	0.66	1.441	18.1	853B3H2 21-23
14.26	3.282	1.45	0.51	1.588	19.2	853B3H2 46-48
14.72	3.359	1.27	0.51	1.745	20.3	853B3H2 92-94
14.9	3.386	1.22	0.68	1.536	18.9	853B3H2 110-112
15.05	3.408	1.14	0.35	2.136	22.5	853B3H2 125-127
15.2	3.431	0.73	0.71	1.601	19.3	853B3H2 140-142
15.31	3.447	0.89	0.88	1.600	19.3	853B3H3 1-3
15.6	3.490	1.37	0.03	1.651	19.7	853B3H3 30-32
15.75	3.512	1.29	0.35	1.746	20.3	853B3H3 45-47

17	3.708	1.11	0.57	1.434	18.1	853B3H4 20-22
17.1	3.725	0.89	0.88	1.431	18.1	853B3H4 30-32
17.25	3.749	1.14	0.88	1.371	17.6	853B3H4 45-47
17.4	3.774	1.14	0.95	1.575	19.1	853B3H4 60-62
19.35	4.097	1.25	0.75	1.817	20.7	853B3H5 105-107
20.58	4.111	0.97	0.34	1.535	18.8	853B4H1 28-30
19.47	4.117	1.38	0.25	1.734	20.2	853B3H5 117-119
20.8	4.134	1.15	0.83	1.931	21.4	853B4H1 50-52
19.65	4.147	1.21	0.50	1.734	20.2	853B3H5 135-137
21.1	4.167	1.16	0.85	1.627	19.5	853B4H1 80-82
19.81	4.173	1.18	0.90	1.593	19.3	853B3H6 1-3
21.25	4.183	1.14	0.96	1.797	20.6	853B4H1 95-97
19.95	4.193	1.06	0.36	1.677	19.8	853B3H6 15-17
21.45	4.204	0.86	0.80	1.445	18.2	853B4H1 115-117
20.1	4.209	0.85	0.78	1.417	18.0	853B3H6 30-32
21.6	4.220	0.92	0.83	1.496	18.6	853B4H1 130-132
20.25	4.226	0.87	0.86	1.592	19.3	853B3H6 45-47
21.75	4.236	1.13	0.07	1.636	19.6	853B4H1 145-147
22.1	4.274	1.02	-0.82	1.755	20.3	853B4H2 30-32
20.8	4.285	1.09	0.50	1.765	20.4	853B3H6 100-102
22.25	4.290	1.29	-0.51	2.154	22.6	853B4H2 45-47
20.98	4.304	1.15	-0.20	2.036	22.0	853B3H6 118-120
22.41	4.307	1.28	-0.15	2.249	23.1	853B4H2 61-63
21.1	4.317			2.202	22.9	853B3H6 130-132
22.55	4.322	1.29	-0.21	2.125	22.5	853B4H2 75-77
22.68	4.332			2.113	22.4	853B4H2 88-90
22.85	4.345	1.25	0.02	1.600	19.3	853B4H2 105-107
22.98	4.355			1.785	20.5	853B4H2 118-120
23.15	4.368	1.44	0.23	1.814	20.7	853B4H2 135-137
23.45	4.391	1.34	0.08	1.687	19.9	853B4H3 15-17
23.6	4.403	1.35	-0.13	2.030	22.0	853B4H3 30-32
23.74	4.413	1.44	-0.72	1.799	20.6	853B4H3 44-46
24.65	4.534	1.19	-0.07	1.797	20.6	853B4H3 135-137
25.25	4.644	1.15	-0.22	1.994	21.8	853B4H4 45-47
25.85	4.725	1.44	-0.51	1.902	21.2	853B4H4 105-107
25.98	4.743			2.096	22.3	853B4H4 118-120
26.31	4.787			2.253	23.1	853B4H5 1-3
26.45	4.806			2.192	22.8	853B4H5 15-17
26.6	4.823	1.29	-0.78			853B4H5 30-32
26.91	4.858			1.890	21.2	853B4H5 61-63
27.48	4.933	1.63	-0.81			853B4H5 118-120
27.95	5.003			2.096	22.3	853B4H6 15-17
28.1	5.017	1.35	-0.33	1.837	20.8	853B4H6 30-32
28.25	5.031	1.31	-0.12	1.834	20.8	853B4H6 45-47
28.39	5.044	0.68	-0.51			853B4H6 59-61
28.67	5.070			2.030	22.0	853B4H6 87-89
28.6	5.289			2.072	22.2	853B5H1 30-32
28.75	5.303	1.58	-1.05	2.222	23.0	853B5H1 45-47
29.07	5.332	1.70	-1.11			853B5H1 77-79
29.19	5.342	1.70	-0.93	2.181	22.8	853B5H1 89-91
30.1	5.424	1.62	-0.64	2.258	23.1	853B5H2 30-32

30.4	5.451			2.073	22.2	853B5H2 60-62
31.01	5.506			1.827	20.8	853B5H2 121-123
31.15	5.518			1.945	21.5	853B5H2 135-137
31.45	5.545			2.237	23.0	853B5H3 15-17
31.92	5.588			1.818	20.7	853B5H3 62-64
32.33	5.624	1.82	-0.58	1.827	20.8	853B5H3 103-105
32.48	5.638	1.84	-0.66	2.251	23.1	853B5H3 118-120
32.64	5.652			2.115	22.4	853B5H3 134-136
33.76	5.753			1.969	21.6	853B5H4 96-98
35.18	5.880			1.913	21.3	853B5H5 88-90

Appendix B: Site 806 and 849 individual *G. sacculifer* SST and *G. tumida* subsurface temperature data

Holocene individual
G. sacculifer

Sample	Hole-Section	Interval	Sample #	avg Mg/Ca	std Mg/Ca	SST (C)
806A	1H1	0-2cm	1	3.789	0.19	27.6
806A	1H1	0-2cm	3	2.780	0.12	24.9
806A	1H1	0-2cm	5	2.922	0.19	25.3
806A	1H1	0-2cm	6	2.867	0.30	25.1
806A	1H1	0-2cm	7	3.799	0.19	27.7
806A	1H1	0-2cm	8	3.391	0.20	26.6
806A	1H1	0-2cm	9	4.208	0.08	28.6
806A	1H1	0-2cm	10	3.589	0.14	27.1
806A	1H1	0-2cm	11	3.942	0.11	28.0
806A	1H1	0-2cm	12	5.335	0.05	30.9
806A	1H1	0-2cm	13	4.928	0.06	30.1
806A	1H1	0-2cm	14	3.258	0.18	26.3
806A	1H1	0-2cm	15	4.150	0.48	28.5
806A	1H1	0-2cm	20	3.699	0.24	27.4
806A	1H1	0-2cm	21	4.342	0.58	28.9
806A	1H1	0-2cm	22	3.359	0.25	26.5
806A	1H1	0-2cm	23	2.810	0.11	25.0
806A	1H1	0-2cm	25	3.858	0.18	27.8
806A	1H1	0-2cm	26	4.124	0.25	28.4
806A	1H1	0-2cm	28	4.099	0.05	28.4
806A	1H1	0-2cm	29	3.962	0.22	28.1
806A	1H1	0-2cm	30	4.646	0.40	29.6
806A	1H1	0-2cm	31	4.977	0.31	30.2
806A	1H1	0-2cm	32	3.557	0.19	27.1
806A	1H1	0-2cm	33	4.888	0.39	30.0
806A	1H1	0-2cm	34	3.541	0.13	27.0
806A	1H1	0-2cm	35	3.195	0.86	26.1
806A	1H1	0-2cm	36	3.403	0.20	26.7
806A	1H1	0-2cm	37	3.293	0.03	26.4
806A	1H1	0-2cm	38	3.616	0.15	27.2
806A	1H1	0-2cm	39	3.868	0.21	27.8
806A	1H1	0-2cm	40	3.071	0.09	25.8
806A	1H1	0-2cm	41	3.118	0.08	25.9
806A	1H1	0-2cm	42	4.353	0.26	28.9

806A	1H1	0-2cm	43	4.212	0.08	28.6
806A	1H1	0-2cm	44	3.759	0.12	27.6
806A	1H1	0-2cm	45	2.924	0.17	25.3
806A	1H1	0-2cm	46	3.721	0.16	27.5
806A	1H1	0-2cm	49	4.044	0.02	28.2
806A	1H1	0-2cm	51	3.181	0.12	26.1
806A	1H1	0-2cm	52	4.614	0.14	29.5
806A	1H1	0-2cm	53	4.365	0.16	29.0
806A	1H1	0-2cm	54	3.827	0.13	27.7
806A	1H1	0-2cm	55	3.717	0.16	27.5
806A	1H1	0-2cm	56	2.609	0.07	24.3
806A	1H1	0-2cm	57	2.982	0.07	25.5
806A	1H1	0-2cm	58	3.419	0.09	26.7
806A	1H1	0-2cm	59	3.816	0.09	27.7
806A	1H1	0-2cm	60	3.743	0.09	27.5
806A	1H1	0-2cm	61	3.457	0.10	26.8
806A	1H1	0-2cm	62	3.874	0.14	27.9
806A	1H1	0-2cm	63	3.523	0.12	27.0
806A	1H1	0-2cm	64	3.952	0.05	28.0
806A	1H1	0-2cm	65	3.737	0.06	27.5
806A	1H1	0-2cm	66	3.416	0.07	26.7
806A	1H1	0-2cm	68	4.172	0.15	28.5
806A	1H1	0-2cm	69	4.156	0.19	28.5
806A	1H1	0-2cm	71	3.380	0.09	26.6
806A	1H1	0-2cm	72	3.072	0.13	25.8
806A	1H1	0-2cm	73	3.745	0.08	27.5
806A	1H1	0-2cm	74	3.672	0.09	27.4
806A	1H1	0-2cm	75	3.536	0.22	27.0
806A	1H1	0-2cm	76	4.433	0.17	29.1
806A	1H1	0-2cm	77	3.348	0.05	26.5
806A	1H1	0-2cm	78	3.705	0.09	27.4
806A	1H1	0-2cm	79	3.940	0.13	28.0
806A	1H1	0-2cm	80	3.480	0.15	26.9
806A	1H1	0-2cm	81	4.184	0.03	28.6
806A	1H1	0-2cm	82	5.350	0.23	30.9
806A	1H1	0-2cm	83	3.251	0.06	26.3
806A	1H1	0-2cm	84	4.470	0.10	29.2
806A	1H1	0-2cm	85	3.774	0.08	27.6

LGM individual
G. sacculifer

Sample	Hole-Section	Interval	Sample #	avg Mg/Ca	std Mg/Ca	SST (C)
806A	1H1	51-53cm	29	2.043	0.03	22.3
806A	1H1	51-53cm	32	2.117	0.06	22.6
806A	1H1	51-53cm	57	2.151	0.09	22.7
806A	1H1	51-53cm	36	2.175	0.06	22.8
806A	1H1	51-53cm	27	2.268	0.03	23.2
806A	1H1	51-53cm	50	2.326	0.03	23.4
806A	1H1	51-53cm	34	2.327	0.14	23.4
806A	1H1	51-53cm	38	2.353	0.04	23.5
806A	1H1	51-53cm	43	2.367	0.07	23.5
806A	1H1	51-53cm	49	2.419	0.06	23.7
806A	1H1	51-53cm	4	2.425	0.07	23.7
806A	1H1	51-53cm	23	2.458	0.09	23.8
806A	1H1	51-53cm	48	2.517	0.05	24.0
806A	1H1	51-53cm	59	2.519	0.05	24.0
806A	1H1	51-53cm	3	2.526	0.27	24.1
806A	1H1	51-53cm	17	2.535	0.07	24.1
806A	1H1	51-53cm	53	2.542	0.04	24.1
806A	1H1	51-53cm	54	2.543	0.02	24.1
806A	1H1	51-53cm	55	2.622	0.05	24.4
806A	1H1	51-53cm	19	2.636	0.11	24.4
806A	1H1	51-53cm	52	2.644	0.05	24.4
806A	1H1	51-53cm	51	2.666	0.06	24.5
806A	1H1	51-53cm	22	2.674	0.04	24.5
806A	1H1	51-53cm	12	2.690	0.08	24.6
806A	1H1	51-53cm	28	2.733	0.15	24.7
806A	1H1	51-53cm	46	2.743	0.06	24.8
806A	1H1	51-53cm	42	2.762	0.14	24.8
806A	1H1	51-53cm	31	2.771	0.06	24.8
806A	1H1	51-53cm	66	2.774	0.03	24.9
806A	1H1	51-53cm	35	2.779	0.05	24.9
806A	1H1	51-53cm	11	2.779	0.11	24.9
806A	1H1	51-53cm	10	2.788	0.08	24.9
806A	1H1	51-53cm	1	2.799	0.12	24.9
806A	1H1	51-53cm	63	2.846	0.03	25.1
806A	1H1	51-53cm	56	2.847	0.09	25.1
806A	1H1	51-53cm	47	2.851	0.07	25.1
806A	1H1	51-53cm	5	2.852	0.10	25.1

806A	1H1	51-53cm	26	2.881	0.08	25.2
806A	1H1	51-53cm	41	2.888	0.06	25.2
806A	1H1	51-53cm	15	2.889	0.06	25.2
806A	1H1	51-53cm	69	2.899	0.03	25.2
806A	1H1	51-53cm	2	2.997	0.16	25.5
806A	1H1	51-53cm	64	3.006	0.12	25.6
806A	1H1	51-53cm	25	3.007	0.10	25.6
806A	1H1	51-53cm	39	3.008	0.07	25.6
806A	1H1	51-53cm	18	3.009	0.03	25.6
806A	1H1	51-53cm	8	3.030	0.19	25.6
806A	1H1	51-53cm	60	3.041	0.06	25.7
806A	1H1	51-53cm	67	3.048	0.03	25.7
806A	1H1	51-53cm	45	3.056	0.06	25.7
806A	1H1	51-53cm	24	3.075	0.04	25.8
806A	1H1	51-53cm	9	3.106	0.22	25.8
806A	1H1	51-53cm	13	3.150	0.25	26.0
806A	1H1	51-53cm	16	3.172	0.08	26.0
806A	1H1	51-53cm	44	3.176	0.18	26.0
806A	1H1	51-53cm	20	3.208	0.08	26.1
806A	1H1	51-53cm	65	3.280	0.09	26.3
806A	1H1	51-53cm	7	3.293	0.15	26.4
806A	1H1	51-53cm	21	3.313	0.20	26.4
806A	1H1	51-53cm	14	3.314	0.21	26.4
806A	1H1	51-53cm	58	3.320	0.26	26.4
806A	1H1	51-53cm	40	3.395	0.12	26.6
806A	1H1	51-53cm	30	3.396	0.21	26.6
806A	1H1	51-53cm	37	3.406	0.05	26.7
806A	1H1	51-53cm	33	3.534	0.21	27.0
806A	1H1	51-53cm	62	3.626	0.06	27.2
806A	1H1	51-53cm	68	3.658	0.06	27.3
806A	1H1	51-53cm	61	3.983	0.25	28.1
806A	1H1	51-53cm	6	4.553	0.17	29.4

Holocene individual
G. sacculifer

Sample	Hole-Section	Interval	Sample #	avg Mg/Ca	std Mg/Ca	SST (C)
849A	1H1	6-8cm	12	1.683	0.06	24.2
849A	1H1	6-8cm	15	1.817	0.03	24.7
849A	1H1	6-8cm	18	1.843	0.07	24.8
849A	1H1	6-8cm	26	1.961	0.03	25.1
849A	1H1	6-8cm	10	1.989	0.11	25.2
849A	1H1	6-8cm	6	2.059	0.06	25.4
849A	1H1	6-8cm	23	2.070	0.09	25.5
849A	1H1	6-8cm	27	2.176	0.11	25.8
849A	1H1	6-8cm	25	2.239	0.16	25.9
849A	1H1	6-8cm	28	2.250	0.07	26.0
849A	1H1	6-8cm	17	2.296	0.07	26.1
849A	1H1	6-8cm	3	2.311	0.16	26.1
849A	1H1	6-8cm	19	2.313	0.07	26.1
849A	1H1	6-8cm	8	2.456	0.19	26.5
849A	1H1	6-8cm	4	2.472	0.05	26.6
849A	1H1	6-8cm	9	2.519	0.15	26.7
849A	1H1	6-8cm	5	2.577	0.20	26.9
849A	1H1	6-8cm	14	2.748	0.07	27.3
849A	1H1	6-8cm	20	2.750	0.05	27.3
849A	1H1	6-8cm	7	2.754	0.18	27.3
849A	1H1	6-8cm	24	2.924	0.12	27.7
849A	1H1	6-8cm	2	2.925	0.10	27.7
849A	1H1	6-8cm	11	2.986	0.02	27.9
849A	1H1	6-8cm	13	3.099	0.13	28.1
849A	1H1	6-8cm	16	3.548	0.33	29.1
849A	1H1	6-8cm	1	3.606	0.29	29.3
849A	1H1	6-8cm	21	3.610	0.40	29.3
849A	1H1	6-8cm	22	3.648	0.33	29.3
849B	1H1	15-18cm	8	1.762	0.12	24.5
849B	1H1	15-18cm	22	1.891	0.03	24.9
849B	1H1	15-18cm	5	1.912	0.09	25.0
849B	1H1	15-18cm	10	1.919	0.06	25.0
849B	1H1	15-18cm	3	1.993	0.16	25.2
849B	1H1	15-18cm	6	2.006	0.12	25.3
849B	1H1	15-18cm	4	2.057	0.11	25.4
849B	1H1	15-18cm	25	2.061	0.11	25.4
849B	1H1	15-18cm	12	2.093	0.08	25.5

849B	1H1	15-18cm	27	2.126	0.08	25.6
849B	1H1	15-18cm	14	2.189	0.11	25.8
849B	1H1	15-18cm	11	2.290	0.08	26.1
849B	1H1	15-18cm	20	2.309	0.05	26.1
849B	1H1	15-18cm	18	2.469	0.01	26.6
849B	1H1	15-18cm	17	2.532	0.10	26.7
849B	1H1	15-18cm	31	2.557	0.12	26.8
849B	1H1	15-18cm	26	2.568	0.07	26.8
849B	1H1	15-18cm	7	2.652	0.07	27.1
849B	1H1	15-18cm	28	2.686	0.15	27.1
849B	1H1	15-18cm	15	2.699	0.15	27.2
849B	1H1	15-18cm	19	2.700	0.06	27.2
849B	1H1	15-18cm	2	2.799	0.12	27.4
849B	1H1	15-18cm	24	2.987	0.09	27.9
849B	1H1	15-18cm	21	3.008	0.04	27.9
849B	1H1	15-18cm	30	3.096	0.11	28.1
849B	1H1	15-18cm	9	3.126	0.22	28.2
849B	1H1	15-18cm	13	3.186	0.19	28.3
849B	1H1	15-18cm	23	3.542	0.14	29.1
849B	1H1	15-18cm	1	3.909	0.24	29.9
849B	1H1	15-18cm	29	3.922	0.13	29.9

LGM individual
G. sacculifer

Sample	Hole-Section	Interval	Sample #	avg Mg/Ca	std Mg/Ca	SST (C)
849B	1H1	74-80cm	45	1.527	0.04	23.7
849B	1H1	74-80cm	3	1.635	0.08	24.1
849B	1H1	74-80cm	27	1.691	0.02	24.3
849B	1H1	74-80cm	1	1.719	0.09	24.4
849B	1H1	74-80cm	50	1.733	0.04	24.4
849B	1H1	74-80cm	60	1.740	0.03	24.4
849B	1H1	74-80cm	25	1.741	0.09	24.4
849B	1H1	74-80cm	14	1.761	0.04	24.5
849B	1H1	74-80cm	59	1.780	0.05	24.6
849B	1H1	74-80cm	52	1.790	0.05	24.6
849B	1H1	74-80cm	31	1.807	0.05	24.6
849B	1H1	74-80cm	15	1.832	0.02	24.7
849B	1H1	74-80cm	54	1.835	0.04	24.7
849B	1H1	74-80cm	7	1.846	0.03	24.8
849B	1H1	74-80cm	26	1.855	0.07	24.8
849B	1H1	74-80cm	32	1.856	0.06	24.8
849B	1H1	74-80cm	46	1.873	0.07	24.9
849B	1H1	74-80cm	44	1.902	0.03	24.9
849B	1H1	74-80cm	9	1.902	0.02	24.9
849B	1H1	74-80cm	47	1.905	0.04	25.0
849B	1H1	74-80cm	11	1.912	0.02	25.0
849B	1H1	74-80cm	63	1.937	0.02	25.0
849B	1H1	74-80cm	53	1.958	0.07	25.1
849B	1H1	74-80cm	40	1.959	0.07	25.1
849B	1H1	74-80cm	35	1.969	0.03	25.1
849B	1H1	74-80cm	58	1.973	0.06	25.2
849B	1H1	74-80cm	33	1.983	0.07	25.2
849B	1H1	74-80cm	19	1.986	0.07	25.2
849B	1H1	74-80cm	5	2.009	0.10	25.3
849B	1H1	74-80cm	62	2.013	0.16	25.3
849B	1H1	74-80cm	34	2.020	0.05	25.3
849B	1H1	74-80cm	38	2.033	0.08	25.3
849B	1H1	74-80cm	16	2.043	0.06	25.4
849B	1H1	74-80cm	42	2.078	0.04	25.5
849B	1H1	74-80cm	49	2.083	0.03	25.5
849B	1H1	74-80cm	17	2.085	0.04	25.5
849B	1H1	74-80cm	55	2.085	0.04	25.5

849B	1H1	74-80cm	41	2.103	0.02	25.5
849B	1H1	74-80cm	29	2.103	0.09	25.5
849B	1H1	74-80cm	2	2.115	0.08	25.6
849B	1H1	74-80cm	56	2.131	0.31	25.6
849B	1H1	74-80cm	20	2.134	0.16	25.6
849B	1H1	74-80cm	61	2.136	0.01	25.6
849B	1H1	74-80cm	36	2.138	0.04	25.6
849B	1H1	74-80cm	48	2.200	0.05	25.8
849B	1H1	74-80cm	13	2.218	0.05	25.9
849B	1H1	74-80cm	6	2.227	0.12	25.9
849B	1H1	74-80cm	43	2.238	0.04	25.9
849B	1H1	74-80cm	51	2.252	0.11	26.0
849B	1H1	74-80cm	8	2.287	0.08	26.1
849B	1H1	74-80cm	30	2.311	0.04	26.1
849B	1H1	74-80cm	18	2.333	0.04	26.2
849B	1H1	74-80cm	23	2.338	0.07	26.2
849B	1H1	74-80cm	28	2.372	0.12	26.3
849B	1H1	74-80cm	39	2.385	0.06	26.3
849B	1H1	74-80cm	4	2.404	0.07	26.4
849B	1H1	74-80cm	10	2.560	0.06	26.8
849B	1H1	74-80cm	12	2.645	0.10	27.0
849B	1H1	74-80cm	37	2.651	0.14	27.0
849B	1H1	74-80cm	21	2.891	0.12	27.6
849B	1H1	74-80cm	57	2.930	0.14	27.7
849B	1H1	74-80cm	24	2.941	0.06	27.8

Glacial individual
G. sacculifer

Sample	Hole-Section	Interval	Sample #	avg Mg/Ca	std Mg/Ca	SST (C)
849B	1H1	85-87cm	31	1.858	0.01	24.8
849B	1H1	85-87cm	32	1.986	0.05	25.2
849B	1H1	85-87cm	33	2.277	0.08	26.0
849B	1H1	85-87cm	34	2.093	0.08	25.5
849B	1H1	85-87cm	35	2.164	0.02	25.7
849B	1H1	85-87cm	36	2.083	0.02	25.5
849B	1H1	85-87cm	37	2.049	0.01	25.4
849B	1H1	85-87cm	38	1.978	0.11	25.2
849B	1H1	85-87cm	39	2.290	0.05	26.1
849B	1H1	85-87cm	40	1.973	0.03	25.2
849B	1H1	85-87cm	41	1.891	0.04	24.9
849B	1H1	85-87cm	42	2.029	0.08	25.3
849B	1H1	85-87cm	14	1.536	0.03	23.7
849B	1H1	85-87cm	4	1.677	0.16	24.2
849B	1H1	85-87cm	30	1.723	0.01	24.4
849B	1H1	85-87cm	10	1.810	0.01	24.7
849B	1H1	85-87cm	20	1.836	0.04	24.7
849B	1H1	85-87cm	17	1.854	0.06	24.8
849B	1H1	85-87cm	29	1.854	0.03	24.8
849B	1H1	85-87cm	1	1.910	0.04	25.0
849B	1H1	85-87cm	25	1.953	0.01	25.1
849B	1H1	85-87cm	18	1.953	0.11	25.1
849B	1H1	85-87cm	21	1.965	0.01	25.1
849B	1H1	85-87cm	19	2.010	0.03	25.3
849B	1H1	85-87cm	12	2.012	0.06	25.3
849B	1H1	85-87cm	2	2.013	0.09	25.3
849B	1H1	85-87cm	26	2.059	0.04	25.4
849B	1H1	85-87cm	13	2.060	0.10	25.4
849B	1H1	85-87cm	28	2.097	0.04	25.5
849B	1H1	85-87cm	6	2.134	0.02	25.6
849B	1H1	85-87cm	27	2.171	0.07	25.7
849B	1H1	85-87cm	16	2.183	0.04	25.8
849B	1H1	85-87cm	15	2.193	0.03	25.8
849B	1H1	85-87cm	5	2.246	0.01	26.0
849B	1H1	85-87cm	9	2.301	0.03	26.1
849B	1H1	85-87cm	11	2.310	0.07	26.1
849B	1H1	85-87cm	7	2.353	0.01	26.3

849B	1H1	85-87cm	24	2.397	0.04	26.4
849B	1H1	85-87cm	22	2.440	0.06	26.5
849B	1H1	85-87cm	3	2.474	0.03	26.6
849B	1H1	85-87cm	8	2.568	0.04	26.8
849B	1H1	85-87cm	23	3.236	0.01	28.5

Holocene individual
G. tumida

Sample	Hole-Section	Interval	Sample #	Mg/Ca	Subsurface T (C)
806A	1H1	0-2cm	1	0.862	10.94
806A	1H1	0-2cm	2	1.746	21.31
806A	1H1	0-2cm	3	1.430	18.37
806A	1H1	0-2cm	4	2.062	23.75
806A	1H1	0-2cm	5	1.377	17.82
806A	1H1	0-2cm	6	2.293	25.32
806A	1H1	0-2cm	7	1.653	20.50
806A	1H1	0-2cm	8	1.516	19.23
806A	1H1	0-2cm	9	2.279	25.22
806A	1H1	0-2cm	10	1.822	21.93
806A	1H1	0-2cm	11	2.239	24.97
806A	1H1	0-2cm	12	1.724	21.12
806A	1H1	0-2cm	13	0.898	11.54
806A	1H1	0-2cm	14	3.114	29.81
806A	1H1	0-2cm	15	2.007	23.36
806A	1H1	0-2cm	16	1.587	19.90
806A	1H1	0-2cm	17	1.839	22.07
806A	1H1	0-2cm	18	1.926	22.75
806A	1H1	0-2cm	19	1.826	21.97
806A	1H1	0-2cm	20	1.691	20.83
806A	1H1	0-2cm	21	2.600	27.16
806A	1H1	0-2cm	22	1.644	20.43
806A	1H1	0-2cm	23	1.636	20.35
806A	1H1	0-2cm	24	2.597	27.15
806A	1H1	0-2cm	25	2.120	24.16
806A	1H1	0-2cm	26	1.625	20.26
806A	1H1	0-2cm	27	2.193	24.66
806A	1H1	0-2cm	28	2.151	24.37
806A	1H1	0-2cm	29	2.356	25.72
806A	1H1	0-2cm	30	1.966	23.05
806A	1H1	0-2cm	31	1.919	22.70
806A	1H1	0-2cm	32	2.238	24.96
806A	1H1	0-2cm	33	1.758	21.41
806A	1H1	0-2cm	34	1.533	19.40
806A	1H1	0-2cm	35	1.314	17.12
806A	1H1	0-2cm	36	2.270	25.16
806A	1H1	0-2cm	37	2.981	29.17

806A	1H1	0-2cm	38	1.683	20.77
806A	1H1	0-2cm	39	3.612	32.00
806A	1H1	0-2cm	40	1.809	21.83
806A	1H1	0-2cm	41	2.439	26.22
806A	1H1	0-2cm	42	2.023	23.47
806A	1H1	0-2cm	43	3.021	29.37
806A	1H1	0-2cm	44	1.634	20.33
806A	1H1	0-2cm	45	2.337	25.59
806A	1H1	0-2cm	46	1.816	21.88
806A	1H1	0-2cm	47	1.707	20.97
806A	1H1	0-2cm	48	1.026	13.49
806A	1H1	0-2cm	49	1.698	20.90
806A	1H1	0-2cm	50	2.012	23.39
806A	1H1	0-2cm	51	2.002	23.32
806A	1H1	0-2cm	52	1.781	21.60
806A	1H1	0-2cm	53	1.855	22.20
806A	1H1	0-2cm	54	2.065	23.77
806A	1H1	0-2cm	55	1.085	14.31
806A	1H1	0-2cm	56	1.994	23.26
806A	1H1	0-2cm	58	2.270	25.17
806A	1H1	0-2cm	59	2.785	28.17
806A	1H1	0-2cm	60	1.381	17.86
806A	1H1	0-2cm	61	3.414	31.17
806A	1H1	0-2cm	62	2.037	23.57
806A	1H1	0-2cm	63	2.034	23.55
806A	1H1	0-2cm	64	1.711	21.01
806A	1H1	0-2cm	65	1.831	22.01
806A	1H1	0-2cm	66	1.793	21.70
806A	1H1	0-2cm	67	2.096	23.99
806A	1H1	0-2cm	68	2.189	24.64
806A	1H1	0-2cm	69	2.804	28.27
806A	1H1	0-2cm	70	2.437	26.21
806A	1H1	0-2cm	71	1.492	19.00

LGM individual
G. tumida

Sample	Hole-Section	Interval	Sample #	Mg/Ca	Subsurface T (C)
806A	1H1	51-53cm	1	1.537	19.4
806A	1H1	51-53cm	2	1.851	22.2
806A	1H1	51-53cm	3	1.660	20.6
806A	1H1	51-53cm	4	2.045	23.6
806A	1H1	51-53cm	5	2.113	24.1
806A	1H1	51-53cm	6	1.428	18.4
806A	1H1	51-53cm	7	1.637	20.4
806A	1H1	51-53cm	8	1.625	20.2
806A	1H1	51-53cm	9	1.657	20.5
806A	1H1	51-53cm	10	1.289	16.8
806A	1H1	51-53cm	11	1.849	22.2
806A	1H1	51-53cm	12	1.745	21.3
806A	1H1	51-53cm	13	1.323	17.2
806A	1H1	51-53cm	14	1.377	17.8
806A	1H1	51-53cm	15	1.153	15.2
806A	1H1	51-53cm	16	1.215	16.0
806A	1H1	51-53cm	17	1.527	19.3
806A	1H1	51-53cm	18	1.841	22.1
806A	1H1	51-53cm	19	1.550	19.6
806A	1H1	51-53cm	20	1.467	18.8
806A	1H1	51-53cm	21	3.204	30.2
806A	1H1	51-53cm	22	2.152	24.4
806A	1H1	51-53cm	23	0.924	12.0
806A	1H1	51-53cm	24	1.589	19.9
806A	1H1	51-53cm	25	1.854	22.2
806A	1H1	51-53cm	26	1.160	15.3
806A	1H1	51-53cm	27	1.349	17.5
806A	1H1	51-53cm	28	1.569	19.7
806A	1H1	51-53cm	30	1.992	23.2
806A	1H1	51-53cm	31	1.841	22.1
806A	1H1	51-53cm	32	1.890	22.5
806A	1H1	51-53cm	33	1.610	20.1
806A	1H1	51-53cm	34	1.604	20.1
806A	1H1	51-53cm	35	1.395	18.0
806A	1H1	51-53cm	36	1.299	17.0
806A	1H1	51-53cm	37	2.076	23.9
806A	1H1	51-53cm	38	1.452	18.6

806A	1H1	51-53cm	39	0.924	12.0
806A	1H1	51-53cm	40	1.331	17.3
806A	1H1	51-53cm	41	2.286	25.3
806A	1H1	51-53cm	42	1.467	18.7
806A	1H1	53-55cm	1	1.908	22.6
806A	1H1	53-55cm	2	1.315	17.1
806A	1H1	53-55cm	3	1.407	18.1
806A	1H1	53-55cm	4	1.644	20.4
806A	1H1	53-55cm	5	2.205	24.7
806A	1H1	53-55cm	6	1.661	20.6
806A	1H1	53-55cm	7	1.833	22.0
806A	1H1	53-55cm	8	2.035	23.6
806A	1H1	53-55cm	9	1.445	18.5
806A	1H1	53-55cm	10	2.060	23.7
806A	1H1	53-55cm	11	1.650	20.5
806A	1H1	53-55cm	12	1.163	15.3
806A	1H1	53-55cm	13	1.541	19.5
806A	1H1	53-55cm	14	1.143	15.1
806A	1H1	53-55cm	15	1.682	20.8
806A	1H1	53-55cm	16	1.804	21.8
806A	1H1	53-55cm	17	2.316	25.5
806A	1H1	53-55cm	18	1.633	20.3
806A	1H1	53-55cm	19	1.693	20.9
806A	1H1	53-55cm	20	1.546	19.5
806A	1H1	53-55cm	21	2.175	24.5
806A	1H1	53-55cm	22	1.597	20.0
806A	1H1	53-55cm	23	1.489	19.0
806A	1H1	53-55cm	24	2.323	25.5
806A	1H1	53-55cm	25	1.660	20.6
806A	1H1	53-55cm	26	2.327	25.5
806A	1H1	53-55cm	27	2.161	24.4
806A	1H1	53-55cm	28	1.709	21.0
806A	1H1	53-55cm	29	1.305	17.0
806A	1H1	53-55cm	30	1.752	21.4
806A	1H1	53-55cm	31	1.730	21.2
806A	1H1	53-55cm	32	1.614	20.1

Holocene individual
G. tumida

Sample	Hole-Section	Interval	Sample #	Mg/Ca	Subsurface T (C)
849A	1H1	6-8cm	1	1.076	14.2
849A	1H1	6-8cm	2	0.890	11.4
849A	1H1	6-8cm	3	1.280	16.7
849A	1H1	6-8cm	4	1.426	18.3
849A	1H1	6-8cm	5	1.208	15.9
849A	1H1	6-8cm	6	1.424	18.3
849A	1H1	6-8cm	7	1.140	15.0
849A	1H1	6-8cm	8	1.396	18.0
849A	1H1	6-8cm	9	0.911	11.7
849A	1H1	6-8cm	10	1.086	14.3
849A	1H1	6-8cm	11	1.338	17.4
849A	1H1	6-8cm	12	1.061	14.0
849A	1H1	6-8cm	13	0.920	11.9
849A	1H1	6-8cm	14	1.109	14.6
849A	1H1	6-8cm	15	1.451	18.6
849A	1H1	6-8cm	16	1.072	14.1
849A	1H1	6-8cm	17	1.121	14.8
849A	1H1	6-8cm	18	0.870	11.1
849A	1H1	6-8cm	19	1.229	16.1
849A	1H1	6-8cm	20	1.438	18.5
849A	1H1	6-8cm	21	1.110	14.6
849A	1H1	6-8cm	22	1.047	13.8
849A	1H1	6-8cm	23	1.110	14.6
849A	1H1	6-8cm	24	1.463	18.7
849A	1H1	6-8cm	25	0.735	8.6
849A	1H1	6-8cm	26	1.254	16.4
849A	1H1	6-8cm	27	1.225	16.1
849A	1H1	6-8cm	28	0.995	13.0
849A	1H1	6-8cm	29	0.885	11.3
849A	1H1	6-8cm	30	1.309	17.1
849A	1H1	6-8cm	31	0.993	13.0
849A	1H1	6-8cm	32	1.146	15.1
849A	1H1	6-8cm	33	0.878	11.2
849A	1H1	6-8cm	34	1.139	15.0
849A	1H1	6-8cm	35	1.190	15.7
849A	1H1	6-8cm	36	1.584	19.9
849A	1H1	6-8cm	37	1.283	16.8

849A	1H1	6-8cm	38	1.129	14.9
849A	1H1	6-8cm	39	0.887	11.4
849A	1H1	6-8cm	40	1.255	16.5
849A	1H1	6-8cm	41	1.747	21.3
849A	1H1	6-8cm	42	0.996	13.0
849A	1H1	6-8cm	43	0.921	11.9
849A	1H1	6-8cm	44	0.945	12.3
849B	1H1	15-18cm	1	1.143	15.1
849B	1H1	15-18cm	2	0.970	12.7
849B	1H1	15-18cm	3	1.213	16.0
849B	1H1	15-18cm	4	1.079	14.2
849B	1H1	15-18cm	5	0.988	12.9
849B	1H1	15-18cm	6	1.258	16.5
849B	1H1	15-18cm	7	1.234	16.2
849B	1H1	15-18cm	8	1.127	14.9
849B	1H1	15-18cm	9	0.960	12.5
849B	1H1	15-18cm	10	0.791	9.7
849B	1H1	15-18cm	11	1.006	13.2
849B	1H1	15-18cm	12	1.103	14.6
849B	1H1	15-18cm	13	1.057	13.9
849B	1H1	15-18cm	14	1.204	15.8
849B	1H1	15-18cm	15	1.159	15.3
849B	1H1	15-18cm	16	0.887	11.4
849B	1H1	15-18cm	17	1.190	15.7
849B	1H1	15-18cm	18	1.488	19.0
849B	1H1	15-18cm	19	0.977	12.8
849B	1H1	15-18cm	21	1.078	14.2
849B	1H1	15-18cm	22	0.682	7.5
849B	1H1	15-18cm	23	1.035	13.6
849B	1H1	15-18cm	24	0.917	11.8
849B	1H1	15-18cm	25	1.028	13.5
849B	1H1	15-18cm	26	1.322	17.2
849B	1H1	15-18cm	27	0.958	12.5

LGM individual *G. tumida*

Sample	Hole-Section	Interval	Sample #	Mg/Ca	Subsurface T (C)
849B	1H1	74-80cm	1	1.658	20.5
849B	1H1	74-80cm	2	0.912	11.8
849B	1H1	74-80cm	3	0.841	10.6
849B	1H1	74-80cm	4	1.312	17.1
849B	1H1	74-80cm	5	1.017	13.4
849B	1H1	74-80cm	6	1.059	14.0
849B	1H1	74-80cm	7	0.846	10.7
849B	1H1	74-80cm	8	0.901	11.6
849B	1H1	74-80cm	9	0.963	12.6
849B	1H1	74-80cm	10	1.028	13.5
849B	1H1	74-80cm	11	0.935	12.1
849B	1H1	74-80cm	12	1.132	14.9
849B	1H1	74-80cm	13	1.245	16.3
849B	1H1	74-80cm	14	1.065	14.0
849B	1H1	74-80cm	15	1.409	18.2
849B	1H1	74-80cm	16	1.977	23.1
849B	1H1	74-80cm	17	0.827	10.3
849B	1H1	74-80cm	18	0.775	9.4
849B	1H1	74-80cm	19	1.007	13.2
849B	1H1	74-80cm	20	1.114	14.7
849B	1H1	74-80cm	21	1.115	14.7
849B	1H1	74-80cm	22	1.122	14.8
849B	1H1	74-80cm	23	1.410	18.2
849B	1H1	74-80cm	24	0.679	7.4
849B	1H1	74-80cm	25	0.618	6.0
849B	1H1	74-80cm	26	0.718	8.2
849B	1H1	74-80cm	27	1.363	17.7
849B	1H1	74-80cm	28	1.596	20.0
849B	1H1	74-80cm	29	1.187	15.6
849B	1H1	74-80cm	30	1.332	17.3
849B	1H1	74-80cm	31	0.946	12.3
849B	1H1	74-80cm	32	1.080	14.2
849B	1H1	74-80cm	33	1.392	18.0
849B	1H1	74-80cm	34	1.096	14.5
849B	1H1	74-80cm	35	1.200	15.8
849B	1H1	74-80cm	36	1.127	14.9

849B	1H1	74-80cm	37	0.774	9.4
849B	1H1	74-80cm	38	1.299	17.0
849B	1H1	74-80cm	39	1.301	17.0
849B	1H1	74-80cm	40	0.921	11.9
849B	1H1	74-80cm	41	1.000	13.1
849B	1H1	74-80cm	42	0.826	10.3
849B	1H1	74-80cm	43	0.855	10.8
849B	1H1	74-80cm	44	1.220	16.0
849B	1H1	74-80cm	45	1.066	14.0
849B	1H1	74-80cm	46	0.840	10.5
849B	1H1	74-80cm	47	0.883	11.3
849B	1H1	74-80cm	48	1.679	20.7
849B	1H1	74-80cm	49	0.757	9.0
849B	1H1	74-80cm	50	1.005	13.2
849B	1H1	74-80cm	51	1.531	19.4
849B	1H1	74-80cm	52	0.925	12.0
849B	1H1	74-80cm	53	1.253	16.4
849B	1H1	74-80cm	54	0.643	6.6
849B	1H1	74-80cm	55	0.727	8.4
849B	1H1	74-80cm	56	1.064	14.0
849B	1H1	74-80cm	57	0.847	10.7
849B	1H1	74-80cm	58	1.020	13.4
849B	1H1	74-80cm	59	0.738	8.6
849B	1H1	74-80cm	60	1.917	22.7
849B	1H1	74-80cm	61	0.705	8.0
849B	1H1	74-80cm	62	1.173	15.5
849B	1H1	74-80cm	63	1.029	13.5
849B	1H1	74-80cm	64	0.907	11.7
849B	1H1	74-80cm	65	0.959	12.5
849B	1H1	74-80cm	66	0.997	13.1
849B	1H1	74-80cm	67	0.877	11.2
849B	1H1	74-80cm	68	1.222	16.1
849B	1H1	74-80cm	69	1.428	18.4
849B	1H1	74-80cm	70	1.347	17.5

Glacial individual *G. tumida*

Sample	Hole-Section	Interval	Sample #	Mg/Ca	Subsurface T (C)
849B	1H1	85-87cm	1	1.239	16.3
849B	1H1	85-87cm	2	0.893	11.4
849B	1H1	85-87cm	3	0.976	12.7
849B	1H1	85-87cm	4	0.922	11.9
849B	1H1	85-87cm	5	1.034	13.6
849B	1H1	85-87cm	6	1.025	13.5
849B	1H1	85-87cm	7	1.190	15.7
849B	1H1	85-87cm	8	0.736	8.6
849B	1H1	85-87cm	9	1.618	20.2
849B	1H1	85-87cm	10	1.006	13.2
849B	1H1	85-87cm	11	1.175	15.5
849B	1H1	85-87cm	12	1.394	18.0
849B	1H1	85-87cm	13	1.044	13.7
849B	1H1	85-87cm	14	1.341	17.4
849B	1H1	85-87cm	15	0.989	12.9
849B	1H1	85-87cm	16	0.795	9.7
849B	1H1	85-87cm	17	0.907	11.7
849B	1H1	85-87cm	18	1.153	15.2
849B	1H1	85-87cm	19	0.797	9.8
849B	1H1	85-87cm	20	1.160	15.3
849B	1H1	85-87cm	21	1.238	16.2
849B	1H1	85-87cm	22	0.958	12.5
849B	1H1	85-87cm	23	1.005	13.2
849B	1H1	85-87cm	24	0.859	10.9
849B	1H1	85-87cm	25	1.541	19.5
849B	1H1	85-87cm	26	1.044	13.8
849B	1H1	85-87cm	27	0.917	11.8
849B	1H1	85-87cm	28	1.055	13.9
849B	1H1	85-87cm	29	1.062	14.0
849B	1H1	85-87cm	30	1.134	15.0
849B	1H1	85-87cm	31	1.054	13.9
849B	1H1	85-87cm	33	0.780	9.4
849B	1H1	85-87cm	34	1.670	20.7
849B	1H1	85-87cm	35	1.731	21.2
849B	1H1	85-87cm	36	1.771	21.5
849B	1H1	85-87cm	40	1.246	16.3
849B	1H1	85-87cm	41	1.611	20.1
849B	1H1	85-87cm	42	1.435	18.4

849B	1H1	85-87cm	43	1.229	16.1
849B	1H1	85-87cm	44	1.635	20.3
849B	1H1	85-87cm	45	1.399	18.0
849B	1H1	85-87cm	47	1.043	13.7
849B	1H1	85-87cm	48	1.211	15.9
849B	1H1	85-87cm	49	1.456	18.6
849B	1H1	85-87cm	50	0.738	8.6
849B	1H1	85-87cm	53	1.056	13.9
849B	1H1	85-87cm	54	1.590	19.9
849B	1H1	85-87cm	55	1.033	13.6
849B	1H1	85-87cm	56	1.516	19.2
849B	1H1	85-87cm	57	1.297	16.9
849B	1H1	85-87cm	58	1.243	16.3
849B	1H1	85-87cm	59	1.274	16.7
849B	1H1	85-87cm	60	1.555	19.6
849B	1H1	85-87cm	61	1.194	15.7
849B	1H1	85-87cm	62	1.137	15.0
849B	1H1	85-87cm	63	1.280	16.7
849B	1H1	85-87cm	64	0.910	11.7
849B	1H1	85-87cm	65	0.960	12.5
849B	1H1	85-87cm	66	0.755	9.0
849B	1H1	85-87cm	67	0.854	10.8
849B	1H1	85-87cm	68	0.715	8.2
849B	1H1	85-87cm	69	0.893	11.4
849B	1H1	85-87cm	70	1.903	22.6
849B	1H1	85-87cm	71	0.878	11.2
849B	1H1	85-87cm	72	1.087	14.3
849B	1H1	85-87cm	73	1.790	21.7
849B	1H1	85-87cm	75	1.074	14.2
849B	1H1	85-87cm	76	1.041	13.7
849B	1H1	85-87cm	77	0.788	9.6
849B	1H1	85-87cm	78	0.897	11.5
849B	1H1	85-87cm	79	1.066	14.1
849B	1H1	85-87cm	80	0.900	11.6
849B	1H1	85-87cm	81	0.808	10.0
849B	1H1	85-87cm	82	1.055	13.9
849B	1H1	85-87cm	83	1.183	15.6

Appendix C: Site 806 *G. sacculifer* SST and *G. tumida* subsurface temperature

2 Ma Glacial individual
G. sacculifer

Sample	Hole-Section	Interval	Sample #	avg Mg/Ca	std Mg/Ca	SST (C)
806B	5H4	15-19cm	1	3.573	0.06	27.1
806B	5H4	15-19cm	2	3.731	0.20	27.5
806B	5H4	15-19cm	3	2.897	0.05	25.2
806B	5H4	15-19cm	4	2.778	0.08	24.9
806B	5H4	15-19cm	5	2.677	0.04	24.6
806B	5H4	15-19cm	6	2.636	0.07	24.4
806B	5H4	15-19cm	7	3.115	0.13	25.9
806B	5H4	15-19cm	8	3.473	0.03	26.9
806B	5H4	15-19cm	9	2.914	0.11	25.3
806B	5H4	15-19cm	10	3.839	0.10	27.8
806B	5H4	15-19cm	11	2.947	0.06	25.4
806B	5H4	15-19cm	12	3.745	0.09	27.5
806B	5H4	15-19cm	13	2.118	0.08	22.6
806B	5H4	15-19cm	14	2.656	0.16	24.5
806B	5H4	15-19cm	16	3.011	0.12	25.6
806B	5H4	15-19cm	17	3.782	0.15	27.6
806B	5H4	15-19cm	18	2.414	0.02	23.7
806B	5H4	15-19cm	19	2.793	0.09	24.9
806B	5H4	15-19cm	20	3.021	0.03	25.6
806B	5H4	15-19cm	21	2.961	0.04	25.4
806B	5H4	15-19cm	22	2.740	0.12	24.8
806B	5H4	15-19cm	23	2.607	0.15	24.3
806B	5H4	15-19cm	24	3.156	0.07	26.0
806B	5H4	15-19cm	25	2.732	0.02	24.7
806B	5H4	15-19cm	26	2.625	0.02	24.4
806B	5H4	15-19cm	27	3.248	0.01	26.2
806B	5H4	15-19cm	28	4.034	0.06	28.2
806B	5H4	15-19cm	29	2.602	0.09	24.3
806B	5H4	15-19cm	30	2.846	0.01	25.1
806B	5H4	15-19cm	31	2.655	0.11	24.5
806B	5H4	15-19cm	32	2.646	0.02	24.5
806B	5H4	15-19cm	33	3.762	0.12	27.6
806B	5H4	15-19cm	34	2.400	0.02	23.6
806B	5H4	15-19cm	35	2.622	0.07	24.4

806B	5H4	15-19cm	36	2.695	0.05	24.6
806B	5H4	15-19cm	37	3.385	0.01	26.6
806B	5H4	15-19cm	39	2.565	0.06	24.2
806B	5H4	15-19cm	40	2.587	0.09	24.3
806B	5H4	15-19cm	41	3.286	0.13	26.4
806B	5H4	15-19cm	42	3.051	0.30	25.7
806B	5H4	15-19cm	43	3.798	0.07	27.7
806B	5H4	15-19cm	44	3.386	0.14	26.6
806B	5H4	15-19cm	45	3.540	0.03	27.0
806B	5H4	15-19cm	46	2.062	0.01	22.4
806B	5H4	15-19cm	47	2.899	0.03	25.2
806B	5H4	15-19cm	48	3.452	0.04	26.8
806B	5H4	15-19cm	49	2.647	0.09	24.5
806B	5H4	15-19cm	50	3.295	0.16	26.4
806B	5H4	15-19cm	51	3.009	0.17	25.6
806B	5H4	15-19cm	52	2.895	0.03	25.2
806B	5H4	15-19cm	53	2.699	0.05	24.6
806B	5H4	15-19cm	54	3.173	0.07	26.0
806B	5H4	15-19cm	55	2.984	0.08	25.5
806B	5H4	15-19cm	56	3.680	0.09	27.4
806B	5H4	15-19cm	57	2.992	0.04	25.5
806B	5H4	15-19cm	58	3.117	0.17	25.9
806B	5H4	15-19cm	59	2.891	0.06	25.2
806B	5H4	15-19cm	60	3.586	0.02	27.1
806B	5H4	15-19cm	61	2.759	0.04	24.8
806B	5H4	15-19cm	62	3.004	0.05	25.6
806B	5H4	15-19cm	63	3.514	0.07	27.0
806B	5H4	15-19cm	64	2.630	0.02	24.4
806B	5H4	15-19cm	65	3.030	0.05	25.6
806B	5H4	15-19cm	66	3.178	0.13	26.1
806B	5H4	15-19cm	67	3.564	0.11	27.1
806B	5H4	15-19cm	68	2.591	0.16	24.3
806B	5H4	15-19cm	69	2.347	0.07	23.4
806B	5H4	15-19cm	70	3.061	0.02	25.7
806B	5H4	15-19cm	71	2.457	0.04	23.8
806B	5H4	15-19cm	72	3.149	0.05	26.0
806B	5H4	15-19cm	73	2.751	0.07	24.8
806B	5H4	15-19cm	74	2.766	0.08	24.8
806B	5H4	15-19cm	75	4.471	0.10	29.2
806B	5H4	15-19cm	76	3.767	0.11	27.6

806B	5H4	15-19cm	77	3.002	0.01	25.6
806B	5H4	15-19cm	78	3.555	0.13	27.1
806B	5H4	15-19cm	79	3.141	0.06	25.9
806B	5H4	15-19cm	80	2.520	0.03	24.0
806B	5H4	15-19cm	81	3.186	0.04	26.1
806B	5H4	15-19cm	82	2.704	0.09	24.6
806B	5H4	15-19cm	83	2.229	0.07	23.0
806B	5H4	15-19cm	84	2.694	0.02	24.6

2 Ma Interglacial individual *G. sacculifer*

Sample	Hole-Section	Interval	Sample #	avg Mg/Ca	std Mg/Ca	SST (C)
806B	5H4	118-121cm	1	3.512	0.12	27.0
806B	5H4	118-121cm	2	3.112	0.05	25.9
806B	5H4	118-121cm	3	2.685	0.13	24.6
806B	5H4	118-121cm	4	3.072	0.05	25.8
806B	5H4	118-121cm	5	2.900	0.05	25.2
806B	5H4	118-121cm	6	2.846	0.03	25.1
806B	5H4	118-121cm	7	3.018	0.02	25.6
806B	5H4	118-121cm	8	3.012	0.05	25.6
806B	5H4	118-121cm	9	3.554	0.03	27.1
806B	5H4	118-121cm	10	2.369	0.05	23.5
806B	5H4	118-121cm	11	3.237	0.05	26.2
806B	5H4	118-121cm	12	3.151	0.03	26.0
806B	5H4	118-121cm	13	3.578	0.07	27.1
806B	5H4	118-121cm	14	3.800	0.13	27.7
806B	5H4	118-121cm	15	2.991	0.07	25.5
806B	5H4	118-121cm	16	2.732	0.05	24.7
806B	5H4	118-121cm	17	3.329	0.14	26.5
806B	5H4	118-121cm	18	3.485	0.10	26.9
806B	5H4	118-121cm	19	3.104	0.07	25.8
806B	5H4	118-121cm	20	2.453	0.03	23.8
806B	5H4	118-121cm	21	2.653	0.28	24.5
806B	5H4	118-121cm	22	3.599	0.09	27.2
806B	5H4	118-121cm	23	4.407	0.06	29.1
806B	5H4	118-121cm	24	3.126	0.06	25.9
806B	5H4	118-121cm	25	3.758	0.09	27.6
806B	5H4	118-121cm	26	3.177	0.12	26.1
806B	5H4	118-121cm	27	3.874	0.03	27.9
806B	5H4	118-121cm	28	2.355	0.02	23.5
806B	5H4	118-121cm	29	3.375	0.03	26.6
806B	5H4	118-121cm	30	3.451	0.05	26.8
806B	5H4	118-121cm	31	2.855	0.07	25.1
806B	5H4	118-121cm	32	3.137	0.07	25.9
806B	5H4	118-121cm	33	4.129	0.07	28.4
806B	5H4	118-121cm	34	3.396	0.08	26.6
806B	5H4	118-121cm	35	3.078	0.12	25.8
806B	5H4	118-121cm	36	2.861	0.04	25.1
806B	5H4	118-121cm	37	2.699	0.03	24.6
806B	5H4	118-121cm	38	2.863	0.23	25.1

806B	5H4	118-121cm	39	3.582	0.04	27.1
806B	5H4	118-121cm	40	2.630	0.06	24.4
806B	5H4	118-121cm	41	3.128	0.22	25.9
806B	5H4	118-121cm	42	4.201	0.05	28.6
806B	5H4	118-121cm	43	3.867	0.03	27.8
806B	5H4	118-121cm	44	3.490	0.09	26.9
806B	5H4	118-121cm	45	3.675	0.24	27.4
806B	5H4	118-121cm	46	3.651	0.20	27.3
806B	5H4	118-121cm	47	2.828	0.03	25.0
806B	5H4	118-121cm	48	2.694	0.06	24.6
806B	5H4	118-121cm	49	3.258	0.25	26.3
806B	5H4	118-121cm	50	2.571	0.07	24.2
806B	5H4	118-121cm	51	3.777	0.08	27.6
806B	5H4	118-121cm	52	2.381	0.05	23.6
806B	5H4	118-121cm	53	3.219	0.07	26.2
806B	5H4	118-121cm	54	2.440	0.02	23.8
806B	5H4	118-121cm	55	2.743	0.04	24.8
806B	5H4	118-121cm	56	3.514	0.09	27.0
806B	5H4	118-121cm	57	3.976	0.05	28.1
806B	5H4	118-121cm	58	3.499	0.07	26.9
806B	5H4	118-121cm	59	5.256	0.11	30.7
806B	5H4	118-121cm	60	2.839	0.03	25.1
806B	5H4	118-121cm	61	2.576	0.13	24.2
806B	5H4	118-121cm	62	3.194	0.06	26.1
806B	5H4	118-121cm	63	4.133	0.02	28.5
806B	5H4	118-121cm	64	3.161	0.05	26.0
806B	5H4	118-121cm	65	3.284	0.07	26.3
806B	5H4	118-121cm	66	3.577	0.11	27.1
806B	5H4	118-121cm	67	3.063	0.05	25.7
806B	5H4	118-121cm	68	2.868	0.04	25.1
806B	5H4	118-121cm	69	3.366	0.04	26.6
806B	5H4	118-121cm	70	3.457	0.07	26.8
806B	5H4	118-121cm	71	3.108	0.10	25.9
806B	5H4	118-121cm	72	3.700	0.02	27.4
806B	5H4	118-121cm	73	3.687	0.07	27.4
806B	5H4	118-121cm	75	3.125	0.06	25.9
806B	5H4	118-121cm	76	3.091	0.07	25.8
806B	5H4	118-121cm	77	3.640	0.07	27.3
806B	5H4	118-121cm	78	2.683	0.09	24.6
806B	5H4	118-121cm	79	3.239	0.09	26.2

806B	5H4	118-121cm	80	4.391	0.07	29.0
806B	5H4	118-121cm	81	2.860	0.09	25.1
806B	5H4	118-121cm	82	3.440	0.09	26.8
806B	5H4	118-121cm	83	4.002	0.07	28.2
806B	5H4	118-121cm	84	2.845	0.01	25.1

2 Ma Glacial individual
G. tumida

Sample	Hole-Section	Interval	Sample #	Mg/Ca	Subsurface T (C)
806B	5H4	15-19cm	1	1.729	21.2
806B	5H4	15-19cm	2	1.811	21.8
806B	5H4	15-19cm	3	2.436	26.2
806B	5H4	15-19cm	4	1.985	23.2
806B	5H4	15-19cm	5	2.418	26.1
806B	5H4	15-19cm	8	2.075	23.8
806B	5H4	15-19cm	9	2.470	26.4
806B	5H4	15-19cm	10	2.144	24.3
806B	5H4	15-19cm	11	2.142	24.3
806B	5H4	15-19cm	12	1.808	21.8
806B	5H4	15-19cm	13	1.727	21.1
806B	5H4	15-19cm	15	2.380	25.9
806B	5H4	15-19cm	16	2.297	25.3
806B	5H4	15-19cm	17	1.690	20.8
806B	5H4	15-19cm	18	2.791	28.2
806B	5H4	15-19cm	19	2.023	23.5
806B	5H4	15-19cm	20	1.625	20.2
806B	5H4	15-19cm	21	1.952	22.9
806B	5H4	15-19cm	22	1.571	19.8
806B	5H4	15-19cm	23	1.744	21.3
806B	5H4	15-19cm	24	1.523	19.3
806B	5H4	15-19cm	25	1.587	19.9
806B	5H4	15-19cm	26	2.029	23.5
806B	5H4	15-19cm	27	1.821	21.9
806B	5H4	15-19cm	28	2.203	24.7
806B	5H4	15-19cm	29	1.701	20.9
806B	5H4	15-19cm	30	1.994	23.3
806B	5H4	15-19cm	31	2.166	24.5
806B	5H4	15-19cm	32	1.630	20.3
806B	5H4	15-19cm	33	2.353	25.7
806B	5H4	15-19cm	34	2.222	24.9
806B	5H4	15-19cm	35	2.309	25.4
806B	5H4	15-19cm	36	1.964	23.0
806B	5H4	15-19cm	37	1.540	19.5
806B	5H4	15-19cm	38	1.798	21.7
806B	5H4	15-19cm	39	2.211	24.8
806B	5H4	15-19cm	40	2.314	25.4

806B	5H4	15-19cm	41	2.864	28.6
806B	5H4	15-19cm	42	1.718	21.1
806B	5H4	15-19cm	43	2.194	24.7
806B	5H4	15-19cm	44	1.640	20.4
806B	5H4	15-19cm	45	1.947	22.9
806B	5H4	15-19cm	46	2.082	23.9
806B	5H4	15-19cm	47	2.333	25.6
806B	5H4	15-19cm	48	2.076	23.9
806B	5H4	15-19cm	49	2.317	25.5
806B	5H4	15-19cm	51	2.275	25.2
806B	5H4	15-19cm	52	1.725	21.1
806B	5H4	15-19cm	53	1.529	19.4
806B	5H4	15-19cm	54	1.944	22.9
806B	5H4	15-19cm	55	2.268	25.2
806B	5H4	15-19cm	56	1.795	21.7
806B	5H4	15-19cm	57	1.888	22.5
806B	5H4	15-19cm	58	1.811	21.8
806B	5H4	15-19cm	59	1.441	18.5
806B	5H4	15-19cm	60	1.656	20.5
806B	5H4	15-19cm	61	2.120	24.2
806B	5H4	15-19cm	62	1.915	22.7
806B	5H4	15-19cm	63	2.229	24.9
806B	5H4	15-19cm	64	2.089	23.9
806B	5H4	15-19cm	65	2.153	24.4
806B	5H4	15-19cm	66	1.797	21.7
806B	5H4	15-19cm	67	1.293	16.9
806B	5H4	15-19cm	68	2.032	23.5
806B	5H4	15-19cm	69	2.175	24.5
806B	5H4	15-19cm	70	1.111	14.7
806B	5H4	15-19cm	71	2.717	27.8
806B	5H4	15-19cm	72	2.239	25.0
806B	5H4	15-19cm	73	2.264	25.1
806B	5H4	15-19cm	74	2.244	25.0
806B	5H4	15-19cm	75	2.565	27.0
806B	5H4	15-19cm	76	1.840	22.1

2 Ma Interglacial individual
G. tumida

Sample	Hole-Section	Interval	Sample #	Mg/Ca	Subsurface T (C)
806B	5H4	118-121cm	1	1.742	21.3
806B	5H4	118-121cm	2	1.891	22.5
806B	5H4	118-121cm	3	1.925	22.7
806B	5H4	118-121cm	4	2.061	23.7
806B	5H4	118-121cm	5	2.442	26.2
806B	5H4	118-121cm	6	2.141	24.3
806B	5H4	118-121cm	8	2.560	26.9
806B	5H4	118-121cm	9	2.331	25.6
806B	5H4	118-121cm	10	2.027	23.5
806B	5H4	118-121cm	11	2.425	26.1
806B	5H4	118-121cm	12	1.777	21.6
806B	5H4	118-121cm	13	2.224	24.9
806B	5H4	118-121cm	14	2.320	25.5
806B	5H4	118-121cm	15	1.919	22.7
806B	5H4	118-121cm	16	2.341	25.6
806B	5H4	118-121cm	17	1.522	19.3
806B	5H4	118-121cm	18	2.249	25.0
806B	5H4	118-121cm	19	2.839	28.5
806B	5H4	118-121cm	20	1.843	22.1
806B	5H4	118-121cm	21	2.028	23.5
806B	5H4	118-121cm	22	1.926	22.8
806B	5H4	118-121cm	23	3.023	29.4
806B	5H4	118-121cm	24	2.156	24.4
806B	5H4	118-121cm	25	2.198	24.7
806B	5H4	118-121cm	26	2.042	23.6
806B	5H4	118-121cm	27	1.873	22.3
806B	5H4	118-121cm	28	2.400	26.0
806B	5H4	118-121cm	29	1.788	21.7
806B	5H4	118-121cm	30	2.601	27.2
806B	5H4	118-121cm	31	3.160	30.0
806B	5H4	118-121cm	32	2.899	28.8
806B	5H4	118-121cm	33	2.105	24.1
806B	5H4	118-121cm	34	2.272	25.2
806B	5H4	118-121cm	35	1.978	23.1
806B	5H4	118-121cm	36	2.876	28.6
806B	5H4	118-121cm	37	1.565	19.7
806B	5H4	118-121cm	38	1.883	22.4

806B	5H4	118-121cm	39	2.281	25.2
806B	5H4	118-121cm	40	2.287	25.3
806B	5H4	118-121cm	41	2.530	26.8
806B	5H4	118-121cm	42	2.619	27.3
806B	5H4	118-121cm	43	2.185	24.6
806B	5H4	118-121cm	44	2.344	25.6
806B	5H4	118-121cm	45	2.133	24.3
806B	5H4	118-121cm	46	2.066	23.8
806B	5H4	118-121cm	47	2.133	24.3
806B	5H4	118-121cm	48	2.866	28.6
806B	5H4	118-121cm	49	3.266	30.5
806B	5H4	118-121cm	50	2.528	26.8
806B	5H4	118-121cm	51	2.596	27.1
806B	5H4	118-121cm	52	2.040	23.6
806B	5H4	118-121cm	53	2.081	23.9
806B	5H4	118-121cm	54	1.410	18.2
806B	5H4	118-121cm	55	2.350	25.7
806B	5H4	118-121cm	56	2.471	26.4
806B	5H4	118-121cm	57	2.523	26.7
806B	5H4	118-121cm	58	2.203	24.7
806B	5H4	118-121cm	59	2.009	23.4
806B	5H4	118-121cm	60	1.873	22.3
806B	5H4	118-121cm	61	2.907	28.8
806B	5H4	118-121cm	62	2.688	27.7
806B	5H4	118-121cm	63	2.238	25.0
806B	5H4	118-121cm	64	1.421	18.3
806B	5H4	118-121cm	65	2.770	28.1
806B	5H4	118-121cm	66	1.621	20.2
806B	5H4	118-121cm	67	2.036	23.6
806B	5H4	118-121cm	68	1.796	21.7
806B	5H4	118-121cm	69	2.184	24.6
806B	5H4	118-121cm	70	2.696	27.7
806B	5H4	118-121cm	71	2.256	25.1
806B	5H4	118-121cm	72	3.005	29.3
806B	5H4	118-121cm	73	2.083	23.9

3 Ma Glacial individual
G. sacculifer

Sample	Hole-Section	Interval	Sample #	avg Mg/Ca	std Mg/Ca	SST (C)
806B	8H4	92-94cm	1	2.970	0.06	25.5
806B	8H4	92-94cm	2	3.230	0.07	26.2
806B	8H4	92-94cm	3	2.810	0.05	25.0
806B	8H4	92-94cm	4	2.810	0.05	25.0
806B	8H4	92-94cm	5	3.240	0.04	26.2
806B	8H4	92-94cm	6	3.960	0.07	28.1
806B	8H4	92-94cm	7	2.697	0.01	24.6
806B	8H4	92-94cm	8	3.130	0.05	25.9
806B	8H4	92-94cm	9	4.187	0.22	28.6
806B	8H4	92-94cm	10	3.481	0.08	26.9
806B	8H4	92-94cm	11	3.095	0.05	25.8
806B	8H4	92-94cm	12	2.767	0.02	24.8
806B	8H4	92-94cm	13	2.967	0.12	25.4
806B	8H4	92-94cm	14	3.003	0.11	25.6
806B	8H4	92-94cm	15	3.641	0.09	27.3
806B	8H4	92-94cm	16	2.829	0.04	25.0
806B	8H4	92-94cm	17	3.104	0.17	25.8
806B	8H4	92-94cm	18	2.301	0.04	23.3
806B	8H4	92-94cm	19	2.640	0.03	24.4
806B	8H4	92-94cm	20	4.291	0.09	28.8
806B	8H4	92-94cm	21	3.652	0.13	27.3
806B	8H4	92-94cm	22	2.924	0.13	25.3
806B	8H4	92-94cm	23	3.152	0.07	26.0
806B	8H4	92-94cm	24	3.630	0.06	27.3
806B	8H4	92-94cm	25	2.888	0.13	25.2
806B	8H4	92-94cm	26	2.927	0.05	25.3
806B	8H4	92-94cm	27	3.517	0.07	27.0
806B	8H4	92-94cm	28	2.827	0.04	25.0
806B	8H4	92-94cm	29	2.585	0.04	24.3
806B	8H4	92-94cm	30	3.136	0.04	25.9
806B	8H4	92-94cm	32	3.764	0.28	27.6
806B	8H4	92-94cm	33	4.094	0.15	28.4
806B	8H4	92-94cm	34	2.742	0.07	24.8
806B	8H4	92-94cm	35	3.708	0.04	27.4
806B	8H4	92-94cm	37	3.166	0.12	26.0
806B	8H4	92-94cm	39	3.139	0.10	25.9
806B	8H4	92-94cm	40	3.849	0.05	27.8

806B	8H4	92-94cm	41	3.009	0.03	25.6
806B	8H4	92-94cm	42	3.397	0.09	26.7
806B	8H4	92-94cm	43	4.189	0.18	28.6
806B	8H4	92-94cm	44	2.297	0.05	23.3
806B	8H4	92-94cm	45	2.960	0.03	25.4
806B	8H4	92-94cm	46	3.880	0.05	27.9
806B	8H4	92-94cm	47	2.828	0.02	25.0
806B	8H4	92-94cm	48	2.794	0.05	24.9
806B	8H4	92-94cm	49	3.033	0.06	25.6
806B	8H4	92-94cm	50	3.023	0.02	25.6
806B	8H4	92-94cm	51	3.135	0.05	25.9
806B	8H4	92-94cm	52	3.064	0.20	25.7
806B	8H4	92-94cm	53	2.800	0.12	24.9
806B	8H4	92-94cm	54	3.601	0.05	27.2
806B	8H4	92-94cm	55	3.450	0.04	26.8
806B	8H4	92-94cm	56	2.860	0.10	25.1
806B	8H4	92-94cm	57	2.753	0.06	24.8
806B	8H4	92-94cm	58	2.374	0.06	23.5
806B	8H4	92-94cm	59	2.871	0.06	25.2
806B	8H4	92-94cm	60	2.686	0.04	24.6
806B	8H4	92-94cm	61	2.733	0.04	24.7
806B	8H4	92-94cm	62	3.275	0.04	26.3
806B	8H4	92-94cm	63	3.279	0.03	26.3
806B	8H4	92-94cm	64	3.089	0.15	25.8
806B	8H4	92-94cm	65	2.223	0.09	23.0
806B	8H4	92-94cm	66	3.648	0.04	27.3
806B	8H4	92-94cm	67	3.055	0.06	25.7
806B	8H4	92-94cm	68	3.312	0.02	26.4
806B	8H4	92-94cm	69	3.694	0.08	27.4
806B	8H4	92-94cm	70	3.063	0.18	25.7
806B	8H4	92-94cm	72	2.679	0.04	24.6
806B	8H4	92-94cm	73	2.682	0.10	24.6
806B	8H4	92-94cm	74	4.287	0.09	28.8
806B	8H4	92-94cm	75	2.868	0.04	25.1
806B	8H4	92-94cm	76	2.914	0.06	25.3
806B	8H4	92-94cm	77	3.715	0.10	27.5
806B	8H4	92-94cm	78	3.039	0.09	25.7

3 Ma Interglacial individual
G. sacculifer

Sample	Hole-Section	Interval	Sample #	avg Mg/Ca	std Mg/Ca	SST (C)
806B	8H5	112-114cm	1	3.793	0.12	27.7
806B	8H5	112-114cm	2	4.051	0.17	28.3
806B	8H5	112-114cm	3	3.526	0.11	27.0
806B	8H5	112-114cm	4	3.004	0.02	25.6
806B	8H5	112-114cm	5	5.205	0.18	30.6
806B	8H5	112-114cm	6	3.532	0.04	27.0
806B	8H5	112-114cm	7	3.100	0.07	25.8
806B	8H5	112-114cm	8	3.647	0.06	27.3
806B	8H5	112-114cm	9	3.388	0.13	26.6
806B	8H5	112-114cm	10	3.617	0.15	27.2
806B	8H5	112-114cm	11	3.477	0.08	26.9
806B	8H5	112-114cm	12	4.017	0.15	28.2
806B	8H5	112-114cm	13	3.655	0.06	27.3
806B	8H5	112-114cm	14	2.957	0.03	25.4
806B	8H5	112-114cm	15	3.280	0.18	26.3
806B	8H5	112-114cm	16	4.560	0.13	29.4
806B	8H5	112-114cm	17	3.015	0.10	25.6
806B	8H5	112-114cm	18	3.088	0.16	25.8
806B	8H5	112-114cm	19	3.743	0.04	27.5
806B	8H5	112-114cm	20	3.165	0.06	26.0
806B	8H5	112-114cm	21	3.413	0.12	26.7
806B	8H5	112-114cm	23	3.483	0.18	26.9
806B	8H5	112-114cm	24	3.943	0.04	28.0
806B	8H5	112-114cm	25	3.844	0.19	27.8
806B	8H5	112-114cm	26	2.943	0.04	25.4
806B	8H5	112-114cm	27	3.530	0.15	27.0
806B	8H5	112-114cm	28	3.472	0.09	26.8
806B	8H5	112-114cm	29	3.049	0.24	25.7
806B	8H5	112-114cm	30	4.029	0.09	28.2
806B	8H5	112-114cm	31	2.872	0.05	25.2
806B	8H5	112-114cm	32	3.072	0.04	25.8
806B	8H5	112-114cm	33	3.656	0.20	27.3
806B	8H5	112-114cm	34	4.050	0.15	28.3
806B	8H5	112-114cm	35	3.279	0.07	26.3
806B	8H5	112-114cm	36	4.422	0.03	29.1
806B	8H5	112-114cm	37	4.797	0.08	29.9
806B	8H5	112-114cm	38	3.874	0.06	27.9

806B	8H5	112-114cm	39	3.494	0.04	26.9
806B	8H5	112-114cm	40	3.750	0.11	27.6
806B	8H5	112-114cm	41	3.313	0.09	26.4
806B	8H5	112-114cm	42	3.164	0.05	26.0
806B	8H5	112-114cm	43	3.008	0.03	25.6
806B	8H5	112-114cm	44	4.169	0.10	28.5
806B	8H5	112-114cm	45	3.389	0.18	26.6
806B	8H5	112-114cm	46	3.776	0.13	27.6
806B	8H5	112-114cm	47	3.574	0.09	27.1
806B	8H5	112-114cm	48	3.981	0.11	28.1
806B	8H5	112-114cm	49	3.612	0.06	27.2
806B	8H5	112-114cm	50	3.619	0.06	27.2
806B	8H5	112-114cm	51	4.018	0.08	28.2
806B	8H5	112-114cm	52	2.810	0.03	25.0
806B	8H5	112-114cm	53	3.305	0.06	26.4
806B	8H5	112-114cm	54	3.281	0.07	26.3
806B	8H5	112-114cm	55	3.267	0.09	26.3
806B	8H5	112-114cm	56	4.097	0.16	28.4
806B	8H5	112-114cm	57	3.230	0.11	26.2
806B	8H5	112-114cm	58	3.169	0.05	26.0
806B	8H5	112-114cm	59	4.062	0.17	28.3
806B	8H5	112-114cm	60	3.326	0.05	26.5
806B	8H5	112-114cm	61	3.576	0.05	27.1
806B	8H5	112-114cm	62	4.280	0.24	28.8
806B	8H5	112-114cm	63	4.234	0.08	28.7
806B	8H5	112-114cm	64	3.493	0.13	26.9
806B	8H5	112-114cm	65	4.184	0.13	28.6
806B	8H5	112-114cm	66	2.170	0.04	22.8
806B	8H5	112-114cm	67	3.439	0.22	26.8
806B	8H5	112-114cm	68	4.102	0.10	28.4
806B	8H5	112-114cm	69	2.884	0.08	25.2
806B	8H5	112-114cm	70	3.093	0.06	25.8
806B	8H5	112-114cm	71	2.386	0.08	23.6
806B	8H5	112-114cm	72	4.209	0.04	28.6
806B	8H5	112-114cm	73	3.277	0.13	26.3
806B	8H5	112-114cm	74	4.019	0.08	28.2
806B	8H5	112-114cm	75	3.732	0.03	27.5
806B	8H5	112-114cm	76	2.892	0.11	25.2
806B	8H5	112-114cm	77	3.802	0.28	27.7
806B	8H5	112-114cm	78	4.104	0.07	28.4

806B	8H5	112-114cm	79	3.564	0.05	27.1
806B	8H5	112-114cm	80	3.075	0.10	25.8
806B	8H5	112-114cm	81	4.000	0.05	28.1
806B	8H5	112-114cm	83	3.412	0.08	26.7
806B	8H5	112-114cm	84	4.345	0.12	28.9

3 Ma Glacial individual
G. tumida

Sample	Hole-Section	Interval	Sample #	Mg/Ca	Subsurface T (C)
806B	8H4	92-94cm	1	1.748	21.3
806B	8H4	92-94cm	2	2.566	27.0
806B	8H4	92-94cm	3	2.522	26.7
806B	8H4	92-94cm	4	2.334	25.6
806B	8H4	92-94cm	5	2.655	27.5
806B	8H4	92-94cm	6	1.751	21.4
806B	8H4	92-94cm	7	1.996	23.3
806B	8H4	92-94cm	8	1.985	23.2
806B	8H4	92-94cm	9	1.934	22.8
806B	8H4	92-94cm	10	2.004	23.3
806B	8H4	92-94cm	11	2.221	24.8
806B	8H4	92-94cm	12	1.928	22.8
806B	8H4	92-94cm	13	1.456	18.6
806B	8H4	92-94cm	14	2.105	24.1
806B	8H4	92-94cm	15	2.773	28.1
806B	8H4	92-94cm	16	1.769	21.5
806B	8H4	92-94cm	17	2.184	24.6
806B	8H4	92-94cm	19	1.814	21.9
806B	8H4	92-94cm	20	2.677	27.6
806B	8H4	92-94cm	21	1.415	18.2
806B	8H4	92-94cm	22	2.395	26.0
806B	8H4	92-94cm	23	1.599	20.0
806B	8H4	92-94cm	25	2.359	25.7
806B	8H4	92-94cm	26	2.376	25.8
806B	8H4	92-94cm	27	2.081	23.9
806B	8H4	92-94cm	28	1.784	21.6
806B	8H4	92-94cm	29	2.313	25.4
806B	8H4	92-94cm	30	2.175	24.5
806B	8H4	92-94cm	31	1.933	22.8
806B	8H4	92-94cm	32	2.015	23.4
806B	8H4	92-94cm	33	2.050	23.7
806B	8H4	92-94cm	34	2.097	24.0
806B	8H4	92-94cm	35	2.370	25.8
806B	8H4	92-94cm	36	2.184	24.6
806B	8H4	92-94cm	37	2.481	26.5
806B	8H4	92-94cm	38	2.411	26.1
806B	8H4	92-94cm	39	2.776	28.1

806B	8H4	92-94cm	40	2.358	25.7
806B	8H4	92-94cm	41	1.974	23.1
806B	8H4	92-94cm	42	1.456	18.6
806B	8H4	92-94cm	43	1.967	23.1
806B	8H4	92-94cm	44	1.802	21.8
806B	8H4	92-94cm	45	2.023	23.5
806B	8H4	92-94cm	46	1.878	22.4
806B	8H4	92-94cm	47	1.416	18.2
806B	8H4	92-94cm	48	2.749	28.0
806B	8H4	92-94cm	49	2.319	25.5
806B	8H4	92-94cm	50	1.799	21.7
806B	8H4	92-94cm	51	3.128	29.9
806B	8H4	92-94cm	53	2.064	23.8
806B	8H4	92-94cm	54	1.704	20.9
806B	8H4	92-94cm	56	2.059	23.7
806B	8H4	92-94cm	57	1.832	22.0
806B	8H4	92-94cm	58	3.161	30.0
806B	8H4	92-94cm	59	2.361	25.7
806B	8H4	92-94cm	60	2.034	23.6
806B	8H4	92-94cm	61	2.545	26.8
806B	8H4	92-94cm	63	1.981	23.2
806B	8H4	92-94cm	64	1.888	22.5
806B	8H4	92-94cm	65	2.314	25.5
806B	8H4	92-94cm	66	2.142	24.3
806B	8H4	92-94cm	67	2.269	25.2
806B	8H4	92-94cm	68	2.583	27.1
806B	8H4	92-94cm	69	2.489	26.5
806B	8H4	92-94cm	70	1.704	20.9
806B	8H4	92-94cm	71	1.752	21.4
806B	8H4	92-94cm	72	2.322	25.5
806B	8H4	92-94cm	73	2.568	27.0
806B	8H4	92-94cm	74	3.426	31.2
806B	8H4	92-94cm	76	2.077	23.9
806B	8H4	92-94cm	77	2.264	25.1

3 Ma Interglacial
individual *G. tumida*

Sample	Hole-Section	Interval	Sample #	Mg/Ca	Subsurface T (C)
806B	8H5	112-114cm	1	3.050	29.5
806B	8H5	112-114cm	2	2.414	26.1
806B	8H5	112-114cm	3	1.791	21.7
806B	8H5	112-114cm	4	2.265	25.1
806B	8H5	112-114cm	5	2.466	26.4
806B	8H5	112-114cm	6	1.533	19.4
806B	8H5	112-114cm	7	2.058	23.7
806B	8H5	112-114cm	8	1.745	21.3
806B	8H5	112-114cm	9	2.408	26.0
806B	8H5	112-114cm	11	1.605	20.1
806B	8H5	112-114cm	12	2.174	24.5
806B	8H5	112-114cm	13	2.640	27.4
806B	8H5	112-114cm	14	2.653	27.5
806B	8H5	112-114cm	21	2.645	27.4
806B	8H5	112-114cm	22	1.803	21.8
806B	8H5	112-114cm	23	2.467	26.4
806B	8H5	112-114cm	24	2.553	26.9
806B	8H5	112-114cm	25	2.038	23.6
806B	8H5	112-114cm	26	2.129	24.2
806B	8H5	112-114cm	27	2.485	26.5
806B	8H5	112-114cm	28	1.883	22.4
806B	8H5	112-114cm	29	2.308	25.4
806B	8H5	112-114cm	30	2.390	25.9
806B	8H5	112-114cm	31	2.195	24.7
806B	8H5	112-114cm	32	2.650	27.4
806B	8H5	112-114cm	33	2.978	29.2
806B	8H5	112-114cm	34	2.672	27.6
806B	8H5	112-114cm	35	2.422	26.1
806B	8H5	112-114cm	36	2.886	28.7
806B	8H5	112-114cm	37	3.142	29.9
806B	8H5	112-114cm	38	2.601	27.2
806B	8H5	112-114cm	39	3.015	29.3
806B	8H5	112-114cm	40	2.185	24.6
806B	8H5	112-114cm	41	2.682	27.6
806B	8H5	112-114cm	42	2.665	27.5
806B	8H5	112-114cm	43	2.215	24.8
806B	8H5	112-114cm	44	1.874	22.4

806B	8H5	112-114cm	45	3.038	29.5
806B	8H5	112-114cm	46	2.133	24.3
806B	8H5	112-114cm	47	2.478	26.5
806B	8H5	112-114cm	48	3.783	32.7
806B	8H5	112-114cm	49	1.737	21.2
806B	8H5	112-114cm	50	2.480	26.5
806B	8H5	112-114cm	51	2.507	26.6
806B	8H5	112-114cm	52	2.350	25.7
806B	8H5	112-114cm	53	1.921	22.7
806B	8H5	112-114cm	54	2.698	27.7
806B	8H5	112-114cm	55	3.755	32.6
806B	8H5	112-114cm	56	3.017	29.4
806B	8H5	112-114cm	57	2.291	25.3
806B	8H5	112-114cm	58	2.622	27.3
806B	8H5	112-114cm	59	2.930	28.9
806B	8H5	112-114cm	60	2.741	27.9
806B	8H5	112-114cm	61	1.884	22.4
806B	8H5	112-114cm	62	2.345	25.6
806B	8H5	112-114cm	63	2.319	25.5
806B	8H5	112-114cm	64	2.460	26.4
806B	8H5	112-114cm	65	4.725	35.9
806B	8H5	112-114cm	66	3.024	29.4
806B	8H5	112-114cm	67	2.650	27.4
806B	8H5	112-114cm	68	2.574	27.0
806B	8H5	112-114cm	69	2.122	24.2
806B	8H5	112-114cm	70	1.904	22.6
806B	8H5	112-114cm	71	2.284	25.3
806B	8H5	112-114cm	72	2.230	24.9
806B	8H5	112-114cm	73	2.700	27.7
806B	8H5	112-114cm	74	2.352	25.7
806B	8H5	112-114cm	75	2.421	26.1
806B	8H5	112-114cm	76	2.614	27.2
806B	8H5	112-114cm	77	1.914	22.7
806B	8H5	112-114cm	78	2.366	25.8
806B	8H5	112-114cm	79	2.057	23.7
806B	8H5	112-114cm	80	2.179	24.6

4 Ma Glacial individual
G. sacculifer

Sample	Hole-Section	Interval	Sample #	avg Mg/Ca	std Mg/Ca	SST (C)
806B	11H6	92-94cm	1	2.65	0.09	24.5
806B	11H6	92-94cm	2	3.70	0.08	27.4
806B	11H6	92-94cm	3	3.65	0.04	27.3
806B	11H6	92-94cm	4	3.43	0.11	26.7
806B	11H6	92-94cm	5	3.93	0.06	28.0
806B	11H6	92-94cm	6	3.28	0.11	26.3
806B	11H6	92-94cm	7	4.17	0.11	28.5
806B	11H6	92-94cm	8	3.50	0.07	26.9
806B	11H6	92-94cm	9	5.09	0.05	30.4
806B	11H6	92-94cm	10	3.89	0.05	27.9
806B	11H6	92-94cm	11	3.96	0.14	28.0
806B	11H6	92-94cm	12	4.11	0.04	28.4
806B	11H6	92-94cm	13	3.38	0.26	26.6
806B	11H6	92-94cm	14	2.98	0.15	25.5
806B	11H6	92-94cm	15	3.41	0.07	26.7
806B	11H6	92-94cm	16	3.80	0.08	27.7
806B	11H6	92-94cm	17	3.64	0.11	27.3
806B	11H6	92-94cm	18	2.87	0.05	25.2
806B	11H6	92-94cm	19	4.19	0.03	28.6
806B	11H6	92-94cm	20	2.93	0.06	25.3
806B	11H6	92-94cm	21	2.86	0.06	25.1
806B	11H6	92-94cm	22	4.87	0.13	30.0
806B	11H6	92-94cm	23	3.43	0.07	26.7
806B	11H6	92-94cm	24	3.02	0.26	25.6
806B	11H6	92-94cm	25	3.66	0.19	27.3
806B	11H6	92-94cm	26	3.75	0.05	27.5
806B	11H6	92-94cm	27	3.92	0.10	28.0
806B	11H6	92-94cm	28	3.21	0.03	26.1
806B	11H6	92-94cm	29	2.96	0.06	25.4
806B	11H6	92-94cm	30	2.79	0.04	24.9
806B	11H6	92-94cm	31	3.75	0.10	27.6
806B	11H6	92-94cm	32	4.22	0.03	28.6
806B	11H6	92-94cm	33	3.93	0.04	28.0
806B	11H6	92-94cm	34	3.47	0.09	26.8
806B	11H6	92-94cm	35	4.12	0.07	28.4
806B	11H6	92-94cm	36	3.00	0.08	25.5
806B	11H6	92-94cm	37	3.74	0.07	27.5

806B	11H6	92-94cm	38	3.14	0.10	25.9
806B	11H6	92-94cm	39	3.87	0.26	27.9
806B	11H6	92-94cm	40	3.15	0.04	26.0
806B	11H6	92-94cm	41	2.63	0.03	24.4
806B	11H6	92-94cm	42	3.65	0.07	27.3
806B	11H6	92-94cm	43	3.37	0.08	26.6
806B	11H6	92-94cm	44	3.75	0.10	27.6
806B	11H6	92-94cm	45	3.70	0.04	27.4
806B	11H6	92-94cm	46	4.07	0.05	28.3
806B	11H6	92-94cm	47	3.26	0.07	26.3
806B	11H6	92-94cm	48	3.84	0.06	27.8
806B	11H6	92-94cm	49	4.04	0.15	28.2
806B	11H6	92-94cm	50	3.24	0.07	26.2
806B	11H6	92-94cm	51	3.52	0.09	27.0
806B	11H6	92-94cm	52	2.33	0.09	23.4
806B	11H6	92-94cm	53	3.52	0.08	27.0
806B	11H6	92-94cm	54	3.70	0.04	27.4
806B	11H6	92-94cm	55	3.04	0.05	25.7
806B	11H6	92-94cm	56	4.00	0.04	28.2
806B	11H6	92-94cm	57	2.79	0.07	24.9
806B	11H6	92-94cm	58	4.40	0.17	29.0
806B	11H6	92-94cm	59	3.12	0.11	25.9
806B	11H6	92-94cm	60	3.03	0.06	25.6
806B	11H6	92-94cm	61	3.19	0.05	26.1
806B	11H6	92-94cm	62	3.65	0.04	27.3
806B	11H6	92-94cm	63	4.01	0.05	28.2
806B	11H6	92-94cm	64	3.20	0.10	26.1
806B	11H6	92-94cm	65	3.88	0.06	27.9
806B	11H6	92-94cm	66	2.72	0.02	24.7
806B	11H6	92-94cm	67	3.71	0.07	27.5
806B	11H6	92-94cm	68	3.07	0.07	25.7
806B	11H6	92-94cm	69	3.24	0.03	26.2
806B	11H6	92-94cm	70	3.31	0.09	26.4
806B	11H6	92-94cm	71	2.44	0.05	23.8
806B	11H6	92-94cm	72	3.73	0.25	27.5
806B	11H6	92-94cm	73	3.20	0.11	26.1
806B	11H6	92-94cm	74	2.92	0.03	25.3
806B	11H6	92-94cm	75	3.16	0.08	26.0
806B	11H6	92-94cm	76	3.79	0.08	27.7
806B	11H6	92-94cm	77	3.43	0.09	26.7

806B	11H6	92-94cm	78	4.09	0.05	28.4
806B	11H6	92-94cm	79	4.32	0.14	28.9
806B	11H6	92-94cm	80	2.94	0.09	25.4
806B	11H6	92-94cm	81	2.94	0.05	25.4
806B	11H6	92-94cm	82	3.26	0.09	26.3

4 Ma Interglacial
individual *G. sacculifer*

Sample	Hole-Section	Interval	Sample #	avg Mg/Ca	std Mg/Ca	SST (C)
806B	11H5	92-94cm	13	3.80	0.19	27.7
806B	11H5	92-94cm	14	4.10	0.20	28.4
806B	11H5	92-94cm	15	3.84	0.14	27.8
806B	11H5	92-94cm	16	4.62	0.59	29.5
806B	11H5	92-94cm	17	3.77	0.05	27.6
806B	11H5	92-94cm	18	4.50	0.04	29.2
806B	11H5	92-94cm	19	4.29	0.15	28.8
806B	11H5	92-94cm	20	4.50	0.24	29.2
806B	11H5	92-94cm	21	4.05	0.05	28.3
806B	11H5	92-94cm	22	4.71	0.26	29.7
806B	11H5	92-94cm	23	4.54	0.16	29.3
806B	11H5	92-94cm	24	3.51	0.15	26.9
806B	11H5	92-94cm	25	3.77	0.21	27.6
806B	11H5	92-94cm	26	3.12	0.05	25.9
806B	11H5	92-94cm	27	3.90	0.28	27.9
806B	11H5	92-94cm	28	3.11	0.04	25.9
806B	11H5	92-94cm	29	4.34	0.13	28.9
806B	11H5	92-94cm	30	4.55	0.05	29.4
806B	11H5	92-94cm	31	4.37	0.04	29.0
806B	11H5	92-94cm	32	3.40	0.07	26.7
806B	11H5	92-94cm	33	4.78	0.06	29.8
806B	11H5	92-94cm	34	4.62	0.07	29.5
806B	11H5	92-94cm	35	3.44	0.16	26.8
806B	11H5	92-94cm	36	3.81	0.05	27.7
806B	11H5	92-94cm	37	4.94	0.15	30.1
806B	11H5	92-94cm	38	4.14	0.10	28.5
806B	11H5	92-94cm	39	3.90	0.04	27.9
806B	11H5	92-94cm	40	5.01	0.47	30.3
806B	11H5	92-94cm	41	3.12	0.08	25.9
806B	11H5	92-94cm	42	2.64	0.04	24.4
806B	11H5	92-94cm	43	4.22	0.11	28.6
806B	11H5	92-94cm	44	4.29	0.34	28.8
806B	11H5	92-94cm	45	4.27	0.17	28.7
806B	11H5	92-94cm	46	3.74	0.28	27.5
806B	11H5	92-94cm	47	4.35	0.34	28.9
806B	11H5	92-94cm	48	4.27	0.10	28.8
806B	11H5	92-94cm	49	4.16	0.17	28.5

806B	11H5	92-94cm	50	3.69	0.01	27.4
806B	11H5	92-94cm	52	4.52	0.10	29.3
806B	11H5	92-94cm	53	4.57	0.13	29.4
806B	11H5	92-94cm	54	4.11	0.07	28.4
806B	11H5	92-94cm	55	4.17	0.08	28.5
806B	11H5	92-94cm	56	3.50	0.14	26.9
806B	11H5	92-94cm	57	4.76	0.09	29.8
806B	11H5	92-94cm	58	4.11	0.07	28.4
806B	11H5	92-94cm	59	4.17	0.10	28.5
806B	11H5	92-94cm	61	3.65	0.16	27.3
806B	11H5	92-94cm	62	3.37	0.12	26.6
806B	11H5	92-94cm	63	3.37	0.08	26.6
806B	11H5	92-94cm	64	4.16	0.08	28.5
806B	11H5	92-94cm	65	3.96	0.48	28.1
806B	11H5	92-94cm	72	4.41	0.11	29.1
806B	11H5	92-94cm	73	4.78	0.20	29.8
806B	11H5	92-94cm	74	4.27	0.11	28.8
806B	11H5	92-94cm	75	4.00	0.05	28.2
806B	11H5	92-94cm	76	3.81	0.10	27.7
806B	11H5	92-94cm	77	4.45	0.26	29.1
806B	11H5	92-94cm	78	5.52	0.03	31.2
806B	11H5	92-94cm	79	3.15	0.07	26.0
806B	11H5	92-94cm	80	3.32	0.11	26.4
806B	11H5	92-94cm	81	4.34	0.08	28.9
806B	11H5	92-94cm	82	3.94	0.10	28.0
806B	11H5	92-94cm	83	4.25	0.10	28.7
806B	11H5	92-94cm	84	4.67	0.07	29.6
806B	11H5	92-94cm	85	3.35	0.05	26.5
806B	11H5	92-94cm	86	4.25	0.17	28.7
806B	11H5	92-94cm	87	3.80	0.07	27.7
806B	11H5	92-94cm	88	3.51	0.11	27.0
806B	11H5	92-94cm	89	3.57	0.06	27.1
806B	11H5	92-94cm	90	3.85	0.05	27.8
806B	11H5	92-94cm	91	2.99	0.12	25.5
806B	11H5	92-94cm	92	4.31	0.06	28.8
806B	11H5	92-94cm	93	4.07	0.05	28.3
806B	11H5	92-94cm	94	3.67	0.08	27.4
806B	11H5	92-94cm	95	3.63	0.04	27.2
806B	11H5	92-94cm	96	4.23	0.12	28.7
806B	11H5	92-94cm	97	3.81	0.07	27.7

806B	11H5	92-94cm	98	3.19	0.07	26.1
806B	11H5	92-94cm	99	3.98	0.16	28.1
806B	11H5	92-94cm	100	3.39	0.05	26.6
806B	11H5	92-94cm	101	4.22	0.06	28.7
806B	11H5	92-94cm	102	3.41	0.04	26.7
806B	11H5	92-94cm	103	3.54	0.11	27.0

4 Ma Glacial individual
G. tumida

Sample	Hole-Section	Interval	Sample #	Mg/Ca	Subsurface T (C)
806B	11H6	92-94cm	1	3.243	30.4
806B	11H6	92-94cm	2	2.174	24.5
806B	11H6	92-94cm	3	2.933	28.9
806B	11H6	92-94cm	5	3.235	30.4
806B	11H6	92-94cm	6	2.532	26.8
806B	11H6	92-94cm	7	2.384	25.9
806B	11H6	92-94cm	8	3.286	30.6
806B	11H6	92-94cm	9	2.593	27.1
806B	11H6	92-94cm	10	1.873	22.3
806B	11H6	92-94cm	11	2.511	26.7
806B	11H6	92-94cm	12	2.613	27.2
806B	11H6	92-94cm	13	2.449	26.3
806B	11H6	92-94cm	14	1.949	22.9
806B	11H6	92-94cm	15	2.211	24.8
806B	11H6	92-94cm	16	2.739	27.9
806B	11H6	92-94cm	18	2.303	25.4
806B	11H6	92-94cm	19	2.708	27.8
806B	11H6	92-94cm	20	2.727	27.9
806B	11H6	92-94cm	21	2.648	27.4
806B	11H6	92-94cm	22	2.281	25.2
806B	11H6	92-94cm	23	2.373	25.8
806B	11H6	92-94cm	24	1.870	22.3
806B	11H6	92-94cm	25	2.150	24.4
806B	11H6	92-94cm	26	3.215	30.3
806B	11H6	92-94cm	27	3.097	29.7
806B	11H6	92-94cm	28	2.311	25.4
806B	11H6	92-94cm	29	2.068	23.8
806B	11H6	92-94cm	30	2.224	24.9
806B	11H6	92-94cm	31	1.990	23.2
806B	11H6	92-94cm	32	3.174	30.1
806B	11H6	92-94cm	33	2.086	23.9
806B	11H6	92-94cm	34	2.325	25.5
806B	11H6	92-94cm	35	1.976	23.1
806B	11H6	92-94cm	36	2.098	24.0
806B	11H6	92-94cm	38	1.943	22.9
806B	11H6	92-94cm	39	2.213	24.8
806B	11H6	92-94cm	40	2.301	25.4

806B	11H6	92-94cm	41	2.628	27.3
806B	11H6	92-94cm	42	2.421	26.1
806B	11H6	92-94cm	43	2.468	26.4
806B	11H6	92-94cm	45	2.162	24.4
806B	11H6	92-94cm	46	2.987	29.2
806B	11H6	92-94cm	47	2.030	23.5
806B	11H6	92-94cm	49	1.820	21.9
806B	11H6	92-94cm	50	2.204	24.7
806B	11H6	92-94cm	52	2.949	29.0
806B	11H6	92-94cm	54	2.797	28.2
806B	11H6	92-94cm	55	3.249	30.4
806B	11H6	92-94cm	56	2.803	28.3
806B	11H6	92-94cm	57	2.490	26.5
806B	11H6	92-94cm	58	2.909	28.8
806B	11H6	92-94cm	59	2.337	25.6
806B	11H6	92-94cm	61	2.173	24.5
806B	11H6	92-94cm	62	2.951	29.0
806B	11H6	92-94cm	63	2.526	26.7
806B	11H6	92-94cm	64	2.886	28.7
806B	11H6	92-94cm	65	2.435	26.2
806B	11H6	92-94cm	66	2.031	23.5
806B	11H6	92-94cm	67	2.522	26.7
806B	11H6	92-94cm	68	2.340	25.6
806B	11H6	92-94cm	69	3.041	29.5
806B	11H6	92-94cm	70	1.864	22.3
806B	11H6	92-94cm	71	2.960	29.1
806B	11H6	92-94cm	72	2.782	28.2
806B	11H6	92-94cm	73	2.553	26.9
806B	11H6	92-94cm	74	2.664	27.5
806B	11H6	92-94cm	75	1.960	23.0
806B	11H6	92-94cm	76	3.019	29.4
806B	11H6	92-94cm	77	2.623	27.3
806B	11H6	92-94cm	78	2.656	27.5
806B	11H6	92-94cm	79	2.851	28.5
806B	11H6	92-94cm	80	2.213	24.8

4 Ma Interglacial individual
G. tumida

Sample	Hole-Section	Interval	Sample #	Mg/Ca	Subsurface T (C)
806B	11H5	92-94cm	2	2.576	27.0
806B	11H5	92-94cm	3	3.155	30.0
806B	11H5	92-94cm	4	3.091	29.7
806B	11H5	92-94cm	5	2.646	27.4
806B	11H5	92-94cm	6	3.289	30.6
806B	11H5	92-94cm	7	3.399	31.1
806B	11H5	92-94cm	8	3.043	29.5
806B	11H5	92-94cm	9	2.258	25.1
806B	11H5	92-94cm	10	3.288	30.6
806B	11H5	92-94cm	11	2.872	28.6
806B	11H5	92-94cm	12	2.586	27.1
806B	11H5	92-94cm	13	2.996	29.2
806B	11H5	92-94cm	14	3.136	29.9
806B	11H5	92-94cm	15	2.766	28.1
806B	11H5	92-94cm	16	3.231	30.4
806B	11H5	92-94cm	17	2.728	27.9
806B	11H5	92-94cm	18	3.580	31.9
806B	11H5	92-94cm	19	2.605	27.2
806B	11H5	92-94cm	20	2.542	26.8
806B	11H5	92-94cm	21	3.628	32.1
806B	11H5	92-94cm	22	3.142	29.9
806B	11H5	92-94cm	23	3.403	31.1
806B	11H5	92-94cm	24	3.805	32.8
806B	11H5	92-94cm	25	2.813	28.3
806B	11H5	92-94cm	26	2.761	28.0
806B	11H5	92-94cm	27	3.018	29.4
806B	11H5	92-94cm	28	2.214	24.8
806B	11H5	92-94cm	29	2.637	27.4
806B	11H5	92-94cm	30	3.229	30.3
806B	11H5	92-94cm	31	2.683	27.6
806B	11H5	92-94cm	32	3.016	29.3
806B	11H5	92-94cm	33	2.266	25.1
806B	11H5	92-94cm	34	2.199	24.7
806B	11H5	92-94cm	35	3.082	29.7
806B	11H5	92-94cm	36	1.979	23.2
806B	11H5	92-94cm	37	3.020	29.4
806B	11H5	92-94cm	38	2.445	26.3

806B	11H5	92-94cm	39	3.096	29.7
806B	11H5	92-94cm	40	2.997	29.3
806B	11H5	92-94cm	41	2.758	28.0
806B	11H5	92-94cm	42	3.128	29.9
806B	11H5	92-94cm	43	2.936	28.9
806B	11H5	92-94cm	44	2.588	27.1
806B	11H5	92-94cm	45	2.393	25.9
806B	11H5	92-94cm	46	2.793	28.2
806B	11H5	92-94cm	47	2.461	26.4
806B	11H5	92-94cm	48	2.509	26.6
806B	11H5	92-94cm	49	3.361	30.9
806B	11H5	92-94cm	50	3.108	29.8
806B	11H5	92-94cm	51	2.643	27.4
806B	11H5	92-94cm	52	2.133	24.3
806B	11H5	92-94cm	53	2.486	26.5
806B	11H5	92-94cm	54	2.875	28.6
806B	11H5	92-94cm	55	2.467	26.4
806B	11H5	92-94cm	56	2.464	26.4
806B	11H5	92-94cm	57	3.132	29.9
806B	11H5	92-94cm	58	3.395	31.1
806B	11H5	92-94cm	59	2.852	28.5
806B	11H5	92-94cm	60	2.876	28.6
806B	11H5	92-94cm	61	1.905	22.6
806B	11H5	92-94cm	62	2.660	27.5
806B	11H5	92-94cm	63	2.316	25.5
806B	11H5	92-94cm	64	2.723	27.8
806B	11H5	92-94cm	65	2.308	25.4
806B	11H5	92-94cm	66	2.203	24.7
806B	11H5	92-94cm	67	3.127	29.9
806B	11H5	92-94cm	68	3.551	31.7
806B	11H5	92-94cm	69	2.688	27.7
806B	11H5	92-94cm	70	3.466	31.4
806B	11H5	92-94cm	71	2.754	28.0
806B	11H5	92-94cm	72	2.718	27.8
806B	11H5	92-94cm	73	3.403	31.1
806B	11H5	92-94cm	74	2.965	29.1

Appendix D: Site 806 *G. tumida* subsurface temperatures

Sample	top (cm)	bottom (cm)	mbsf	mcd	Mg/Ca	Age (Ma)	Subsurface Temperature (C)
806A1H1	5	7	0.05	0.35	1.865	0.024	22.3
806A1H1	5	7	0.05	0.35	1.979	0.024	23.1
806A1H1	58	60	0.58	0.88	1.508	0.051	19.2
806A1H1	58	60	0.58	0.88	1.835	0.051	22.0
806A1H1	137	139	1.37	1.67	1.674	0.090	20.7
806A1H1	137	139	1.37	1.67	1.480	0.090	18.9
806A1H2	68	70	2.18	2.48	1.497	0.132	19.0
806A1H2	68	70	2.18	2.48	1.469	0.132	18.8
806A1H2	147	149	2.97	3.27	1.499	0.168	19.1
806A1H2	147	149	2.97	3.27	1.529	0.168	19.4
806A1H3	39	41	3.39	3.69	1.253	0.188	16.4
806A1H3	39	41	3.39	3.69	1.345	0.188	17.5
806A1H3	112	114	4.12	4.42	1.768	0.222	21.5
806A1H3	112	114	4.12	4.42	1.960	0.222	23.0
806A1H4	6	8	4.56	4.86	2.000	0.242	23.3
806A1H4	6	8	4.56	4.86	2.062	0.242	23.8
806A1H4	87	89	5.37	5.67	1.838	0.277	22.1
806A1H4	87	89	5.37	5.67	1.808	0.277	21.8
806A1H5	6	8	6.06	6.36	1.564	0.322	19.7
806A1H5	6	8	6.06	6.36	1.583	0.322	19.9
806A1H5	87	89	6.87	7.17	1.500	0.362	19.1
806A1H5	87	89	6.87	7.17	1.714	0.362	21.0
806A2H1	45	47	8.15	8.46	1.729	0.428	21.2
806A2H1	45	47	8.15	8.46	1.875	0.428	22.4
806A2H1	126	128	8.96	9.27	1.618	0.464	20.2
806A2H1	126	128	8.96	9.27	1.870	0.464	22.3
806A2H2	15	17	9.35	9.66	2.048	0.482	23.7
806A2H2	15	17	9.35	9.66	1.368	0.482	17.7
806A2H2	96	98	10.16	10.47	1.965	0.521	23.0
806A2H2	96	98	10.16	10.47	1.594	0.521	20.0
806A2H3	27	29	10.97	11.28	1.451	0.559	18.6
806A2H3	27	29	10.97	11.28	1.645	0.559	20.4
806A2H3	105	107	11.75	12.06	1.741	0.588	21.3
806A2H3	105	107	11.75	12.06	1.631	0.588	20.3
806A2H4	36	38	12.56	12.87	1.649	0.618	20.5
806A2H4	36	38	12.56	12.87	2.007	0.618	23.4

806A2H4	117	119	13.37	13.68	1.831	0.652	22.0
806A2H4	117	119	13.37	13.68	1.759	0.652	21.4
806A2H5	47	49	14.17	14.48	1.734	0.689	21.2
806A2H5	47	49	14.17	14.48	2.247	0.689	25.0
806A2H5	125	127	14.95	15.26	1.954	0.725	23.0
806A2H5	125	127	14.95	15.26	1.881	0.725	22.4
806A2H6	15	17	15.35	15.66	1.756	0.743	21.4
806A2H6	15	17	15.35	15.66	1.896	0.743	22.5
806A2H6	105	107	16.25	16.56	1.801	0.767	21.8
806A2H6	105	107	16.25	16.56	1.930	0.767	22.8
806A2H7	25	27	16.95	17.26	1.788	0.792	21.7
806A2H7	25	27	16.95	17.26	1.778	0.792	21.6
806A2H7	53	55	17.23	17.54	1.486	0.809	18.9
806A2H7	53	55	17.23	17.54	1.885	0.809	22.4
806A3H1	5	7	17.25	17.89	1.928	0.829	22.8
806A3H1	5	7	17.25	17.89	1.792	0.829	21.7
806A3H1	85	87	18.05	18.69	1.676	0.875	20.7
806A3H1	85	87	18.05	18.69	1.849	0.875	22.1
806A3H2	15	17	18.85	19.49	1.872	0.910	22.3
806A3H2	15	17	18.85	19.49	1.793	0.910	21.7
806A3H2	95	97	19.65	20.29	1.621	0.943	20.2
806A3H2	95	97	19.65	20.29	1.737	0.943	21.2
806A3H3	25	27	20.45	21.09	1.664	0.974	20.6
806A3H3	25	27	20.45	21.09	1.716	0.974	21.1
806A3H3	105	107	21.25	21.89	1.489	1.001	19.0
806A3H3	105	107	21.25	21.89	1.607	1.001	20.1
806A3H4	35	37	22.05	22.69	1.587	1.029	19.9
806A3H4	35	37	22.05	22.69	1.700	1.029	20.9
806A3H4	115	117	22.85	23.49	2.155	1.062	24.4
806A3H4	115	117	22.85	23.49	2.085	1.062	23.9
806A3H5	5	7	23.25	23.89	1.726	1.081	21.1
806A3H5	5	7	23.25	23.89	1.963	1.081	23.0
806A3H5	85	87	24.05	24.69	1.691	1.122	20.8
806A3H5	85	87	24.05	24.69	1.543	1.122	19.5
806A3H6	15	17	24.85	25.49	1.685	1.197	20.8
806A3H6	15	17	24.85	25.49	2.095	1.197	24.0
806A3H6	105	107	25.75	26.39	1.798	1.210	21.7
806A3H6	105	107	25.75	26.39	1.539	1.210	19.5
806A4H1	5	7	26.75	26.48	1.705	1.256	21.0
806A4H1	5	7	26.75	26.48	1.859	1.256	22.2

806A3H7	25	27	26.45	27.09	1.560	1.296	19.6
806A3H7	25	27	26.45	27.09	1.745	1.296	21.3
806A4H1	85	87	27.55	27.28	1.497	1.305	19.0
806A4H1	85	87	27.55	27.28	1.474	1.305	18.8
806A3H7	65	67	26.85	27.49	1.570	1.315	19.7
806A3H7	65	67	26.85	27.49	1.729	1.315	21.2
806A4H2	15	17	28.35	28.08	1.597	1.341	20.0
806A4H2	15	17	28.35	28.08	1.629	1.341	20.3
806A4H2	95	97	29.15	28.88	1.851	1.380	22.2
806A4H2	95	97	29.15	28.88	1.729	1.380	21.2
806A4H3	25	27	29.95	29.68	1.951	1.417	22.9
806A4H3	25	27	29.95	29.68	2.043	1.417	23.6
806A4H3	105	107	30.75	30.48	2.219	1.450	24.8
806A4H3	105	107	30.75	30.48	2.309	1.450	25.4
806A4H4	35	37	31.55	31.28	2.233	1.485	24.9
806A4H4	35	37	31.55	31.28	2.261	1.485	25.1
806A4H4	118	120	32.38	32.11	1.998	1.523	23.3
806A4H4	118	120	32.38	32.11	1.812	1.523	21.9
806A4H5	5	7	32.75	32.48	2.148	1.539	24.4
806A4H5	5	7	32.75	32.48	2.036	1.539	23.6
806A4H5	85	87	33.55	33.28	2.169	1.579	24.5
806A4H5	85	87	33.55	33.28	2.161	1.579	24.4
806A4H6	15	17	34.35	34.08	2.384	1.614	25.9
806A4H6	15	17	34.35	34.08	2.287	1.614	25.3
806A4H6	105	107	35.25	34.98	2.407	1.652	26.0
806A4H6	105	107	35.25	34.98	2.324	1.652	25.5
806A4H7	25	27	35.95	35.68	1.971	1.682	23.1
806A4H7	25	27	35.95	35.68	2.490	1.682	26.5
806A5H1	7	9	36.27	36.42	1.982	1.719	23.2
806A5H1	7	9	36.27	36.42	2.089	1.719	23.9
806A5H1	85	87	37.05	37.2	1.552	1.761	19.6
806A5H1	85	87	37.05	37.2	1.747	1.761	21.3
806A5H2	15	17	37.85	38	1.800	1.802	21.8
806A5H2	15	17	37.85	38	1.857	1.802	22.2
806A5H2	95	97	38.65	38.8	1.939	1.840	22.9
806A5H2	95	97	38.65	38.8	1.953	1.840	23.0
806A5H3	25	27	39.45	39.6	2.022	1.875	23.5
806A5H3	25	27	39.45	39.6	2.048	1.875	23.7
806A5H3	105	107	40.25	40.4	2.280	1.910	25.2
806A5H3	105	107	40.25	40.4	1.874	1.910	22.3

806A5H4	35	37	41.05	41.2	2.132	1.937	24.2
806A5H4	35	37	41.05	41.2	2.153	1.937	24.4
806A5H4	115	117	41.85	42	1.780	1.965	21.6
806A5H4	115	117	41.85	42	1.790	1.965	21.7
806A5H5	5	7	42.25	42.4	1.878	1.981	22.4
806A5H5	5	7	42.25	42.4	1.697	1.981	20.9
806A5H5	85	87	43.05	43.2	2.114	2.013	24.1
806A5H5	85	87	43.05	43.2	1.773	2.013	21.5
806A5H6	15	17	43.85	44	1.898	2.044	22.5
806A5H6	105	107	44.75	44.9	1.812	2.076	21.9
806A5H6	105	107	44.75	44.9	2.617	2.076	27.3
806A5H7	25	27	45.45	45.6	2.111	2.104	24.1
806A5H7	25	27	45.45	45.6	2.052	2.104	23.7
806B6H1	2	4	44.52	45.38	1.988	2.130	23.2
806B6H1	2	4	44.52	45.38	2.082	2.130	23.9
806A6H1	5	7	45.75	45.48	2.156	2.134	24.4
806A6H1	5	7	45.75	45.48	2.075	2.134	23.8
806B6H1	42	44	44.92	45.78	1.799	2.145	21.7
806B6H1	42	44	44.92	45.78	1.948	2.145	22.9
806B6H1	83	85	45.33	46.19	1.801	2.159	21.8
806B6H1	83	85	45.33	46.19	1.830	2.159	22.0
806A6H1	85	87	46.55	46.28	2.170	2.162	24.5
806A6H1	85	87	46.55	46.28	2.463	2.162	26.4
806B6H1	123	125	45.73	46.59	1.596	2.173	20.0
806B6H1	123	125	45.73	46.59	1.612	2.173	20.1
806B6H2	2	4	46.02	46.88	1.998	2.183	23.3
806B6H2	2	4	46.02	46.88	2.097	2.183	24.0
806A6H2	15	17	47.35	47.08	1.928	2.190	22.8
806A6H2	15	17	47.35	47.08	2.117	2.190	24.1
806B6H2	42	44	46.42	47.28	1.949	2.196	22.9
806B6H2	42	44	46.42	47.28	2.018	2.196	23.4
806A6H2	55	57	47.75	47.48	1.972	2.203	23.1
806A6H2	55	57	47.75	47.48	2.538	2.203	26.8
806A6H2	55	57	47.75	47.48	2.299	2.203	25.4
806B6H2	83	85	46.83	47.69	2.051	2.210	23.7
806B6H2	83	85	46.83	47.69	2.188	2.210	24.6
806A6H2	95	97	48.15	47.88	1.867	2.216	22.3
806A6H2	95	97	48.15	47.88	1.863	2.216	22.3
806B6H2	123	125	47.23	48.09	2.008	2.224	23.4
806B6H2	123	125	47.23	48.09	1.940	2.224	22.9

806A6H2	135	137	48.55	48.28	2.077	2.230	23.9
806A6H2	135	137	48.55	48.28	2.082	2.230	23.9
806B6H3	12	14	47.62	48.48	2.144	2.237	24.3
806B6H3	12	14	47.62	48.48	2.158	2.237	24.4
806B6H3	52	54	48.02	48.88	2.109	2.251	24.1
806B6H3	52	54	48.02	48.88	2.096	2.251	24.0
806A6H3	65	67	49.35	49.08	2.259	2.258	25.1
806B6H3	92	94	48.42	49.28	2.023	2.266	23.5
806B6H3	92	94	48.42	49.28	2.011	2.266	23.4
806B6H3	132	134	48.82	49.68	1.959	2.280	23.0
806B6H3	132	134	48.82	49.68	1.846	2.280	22.1
806A6H3	145	147	50.15	49.88	2.732	2.288	27.9
806A6H3	145	147	50.15	49.88	2.251	2.288	25.0
806B6H4	22	24	49.22	50.08	2.164	2.295	24.5
806B6H4	22	24	49.22	50.08	2.193	2.295	24.7
806A6H4	35	37	50.55	50.28	1.727	2.303	21.1
806A6H4	35	37	50.55	50.28	1.889	2.303	22.5
806B6H4	64	66	49.64	50.5	2.339	2.311	25.6
806B6H4	64	66	49.64	50.5	2.133	2.311	24.3
806B6H4	101	103	50.01	50.87	1.946	2.324	22.9
806B6H4	101	103	50.01	50.87	2.288	2.324	25.3
806B6H4	113	115	50.13	50.99	2.193	2.328	24.7
806B6H4	113	115	50.13	50.99	2.064	2.328	23.8
806A6H4	115	117	51.35	51.08	2.276	2.331	25.2
806A6H4	115	117	51.35	51.08	2.107	2.331	24.1
806B6H5	2	4	50.52	51.38	1.992	2.341	23.2
806B6H5	42	44	50.92	51.78	2.362	2.355	25.8
806B6H5	42	44	50.92	51.78	2.319	2.355	25.5
806B6H5	83	85	51.33	52.19	1.997	2.368	23.3
806B6H5	123	125	51.73	52.59	2.180	2.382	24.6
806B6H5	123	125	51.73	52.59	2.252	2.382	25.0
806B6H6	2	4	52.02	52.88	2.158	2.391	24.4
806B6H6	2	4	52.02	52.88	2.133	2.391	24.3
806B6H6	42	44	52.42	53.28	2.092	2.405	24.0
806B6H6	83	85	52.83	53.69	2.462	2.418	26.4
806B6H6	83	85	52.83	53.69	2.320	2.418	25.5
806B6H6	123	125	53.23	54.09	2.322	2.432	25.5
806B6H7	2	4	53.52	54.38	1.902	2.441	22.6
806B6H7	2	4	53.52	54.38	1.787	2.441	21.6
806B6H7	42	44	53.92	54.78	1.845	2.455	22.1

806B6H7	84	86	54.34	55.2	1.863	2.470	22.3
806B6H7	84	86	54.34	55.2	2.023	2.470	23.5
806B7H1	42	44	54.42	54.49	1.780	2.493	21.6
806B7H1	42	44	54.42	54.49	2.008	2.493	23.4
806A6H7	25	27	54.95	54.68	1.910	2.501	22.6
806B7H1	82	84	54.82	54.89	2.349	2.508	25.7
806B7H1	82	84	54.82	54.89	1.910	2.508	22.6
806B7H1	122	124	55.22	55.29	2.015	2.524	23.4
806B7H1	122	124	55.22	55.29	1.766	2.524	21.5
806B7H2	2	4	55.52	55.59	1.719	2.535	21.1
806B7H2	2	4	55.52	55.59	1.805	2.535	21.8
806B7H2	82	84	56.32	56.39	2.003	2.566	23.3
806B7H2	82	84	56.32	56.39	2.086	2.566	23.9
806B7H2	122	124	56.72	56.79	2.083	2.581	23.9
806B7H2	122	124	56.72	56.79	2.045	2.581	23.6
806B7H2	132	134	56.82	56.89	2.335	2.585	25.6
806B7H3	22	24	57.22	57.29	2.191	2.600	24.6
806B7H3	62	64	57.62	57.69	2.066	2.616	23.8
806B7H3	102	104	58.02	58.09	2.223	2.631	24.9
806B7H3	142	144	58.42	58.49	2.215	2.646	24.8
806B7H3	142	144	58.42	58.49	2.231	2.646	24.9
806B7H4	2	4	58.52	58.59	1.904	2.650	22.6
806B7H4	2	4	58.52	58.59	1.936	2.650	22.8
806B7H4	42	44	58.92	58.99	1.687	2.665	20.8
806B7H4	42	44	58.92	58.99	2.210	2.665	24.8
806B7H4	82	84	59.32	59.39	2.284	2.679	25.3
806B7H4	82	84	59.32	59.39	2.544	2.679	26.8
806B7H4	122	124	59.72	59.79	2.105	2.694	24.1
806B7H5	2	4	60.02	60.09	1.883	2.705	22.4
806B7H5	2	4	60.02	60.09	1.998	2.705	23.3
806B7H5	32	34	60.32	60.39	2.300	2.715	25.4
806B7H5	32	34	60.32	60.39	2.005	2.715	23.3
806B7H5	82	84	60.82	60.89	1.986	2.732	23.2
806B7H5	82	84	60.82	60.89	1.878	2.732	22.4
806B7H5	122	124	61.22	61.29	2.237	2.745	25.0
806B7H5	122	124	61.22	61.29	2.022	2.745	23.5
806B7H6	2	4	61.52	61.59	2.320	2.755	25.5
806B7H6	2	4	61.52	61.59	2.160	2.755	24.4
806B7H6	42	44	61.92	61.99	1.687	2.768	20.8
806B7H6	42	44	61.92	61.99	2.082	2.768	23.9

806B7H6	82	84	62.32	62.39	1.828	2.780	22.0
806B7H6	82	84	62.32	62.39	1.751	2.780	21.4
806B7H6	122	124	62.72	62.79	2.105	2.793	24.1
806B7H6	122	124	62.72	62.79	1.971	2.793	23.1
806B7H7	2	4	63.02	63.09	2.393	2.803	25.9
806B7H7	2	4	63.02	63.09	2.274	2.803	25.2
806B7H7	42	44	63.42	63.49	2.270	2.816	25.2
806B7H7	42	44	63.42	63.49	1.921	2.816	22.7
806B7HCC	2	4	63.79	63.86	1.940	2.828	22.9
806B7HCC	2	4	63.79	63.86	2.182	2.828	24.6
806B8H1	42	44	63.92	63.99	1.998	2.852	23.3
806B8H1	42	44	63.92	63.99	2.183	2.852	24.6
806B8H1	42	44	63.92	63.99	2.168	2.852	24.5
806B8H1	42	44	63.92	63.99	2.228	2.852	24.9
806B8H1	82	84	64.32	64.39	2.173	2.867	24.5
806B8H1	82	84	64.32	64.39	2.134	2.867	24.3
806B8H1	122	124	64.72	64.79	2.112	2.882	24.1
806B8H1	122	124	64.72	64.79	2.227	2.882	24.9
806B8H2	2	4	65.02	65.09	1.774	2.893	21.5
806B8H2	2	4	65.02	65.09	1.913	2.893	22.7
806B8H2	42	44	65.42	65.49	2.333	2.906	25.6
806B8H2	42	44	65.42	65.49	2.199	2.906	24.7
806B8H2	82	84	65.82	65.89	2.007	2.919	23.4
806B8H2	82	84	65.82	65.89	1.919	2.919	22.7
806B8H2	122	124	66.22	66.29	2.024	2.932	23.5
806B8H2	122	124	66.22	66.29	2.088	2.932	23.9
806B8H3	2	4	66.52	66.59	2.013	2.941	23.4
806B8H3	2	4	66.52	66.59	2.134	2.941	24.3
806B8H3	42	44	66.92	66.99	2.226	2.954	24.9
806B8H3	42	44	66.92	66.99	2.249	2.954	25.0
806B8H4	2	4	68.02	68.09	2.760	2.990	28.0
806B8H4	2	4	68.02	68.09	2.468	2.990	26.4
806B8H4	42	44	68.42	68.49	2.064	3.004	23.8
806B8H4	42	44	68.42	68.49	1.780	3.004	21.6
806B8H4	82	84	68.82	68.89	2.239	3.018	25.0
806B8H4	82	84	68.82	68.89	2.155	3.018	24.4
806B8H5	2	4	69.52	69.59	2.032	3.041	23.5
806B8H5	2	4	69.52	69.59	2.032	3.041	23.5
806B8H5	42	44	69.92	69.99	1.780	3.054	21.6
806B8H5	42	44	69.92	69.99	1.716	3.054	21.1

806B8H5	82	84	70.32	70.39	2.104	3.067	24.0
806B8H5	82	84	70.32	70.39	2.160	3.067	24.4
806B8H5	122	124	70.72	70.79	2.521	3.080	26.7
806B8H5	122	124	70.72	70.79	2.322	3.080	25.5
806B8H6	2	4	71.02	71.09	3.080	3.089	29.7
806B8H6	2	4	71.02	71.09	2.331	3.089	25.6
806B8H6	42	44	71.42	71.49	2.432	3.102	26.2
806B8H6	42	44	71.42	71.49	2.275	3.102	25.2
806B8H6	82	84	71.82	71.89	2.227	3.115	24.9
806B8H6	122	124	72.22	72.29	2.219	3.128	24.8
806B8H6	142	144	72.42	72.49	2.462	3.134	26.4
806B8H7	2	4	72.52	72.59	2.047	3.138	23.6
806B8H7	42	44	72.92	72.99	2.087	3.151	23.9
806B8H7	42	44	72.92	72.99	2.360	3.151	25.7
806B9H1	2	4	73.02	73.09	2.291	3.154	25.3
806B9H1	2	4	73.02	73.09	1.991	3.154	23.2
806B8HCC	2	4	73.14	73.21	2.488	3.158	26.5
806B8HCC	2	4	73.14	73.21	2.360	3.158	25.7
806B9H1	42	44	73.42	73.43	2.314	3.193	25.5
806B9H1	42	44	73.42	73.43	2.119	3.193	24.2
806B9H1	82	84	73.82	73.83	2.449	3.206	26.3
806B9H1	82	84	73.82	73.83	2.270	3.206	25.2
806B9H1	122	124	74.22	74.23	2.719	3.219	27.8
806B9H1	122	124	74.22	74.23	2.385	3.219	25.9
806B9H2	2	4	74.52	74.53	2.160	3.228	24.4
806B9H2	2	4	74.52	74.53	2.039	3.228	23.6
806B9H2	42	44	74.92	74.93	2.254	3.241	25.1
806B9H2	42	44	74.92	74.93	2.060	3.241	23.7
806B9H2	82	84	75.32	75.33	2.181	3.254	24.6
806B9H2	82	84	75.32	75.33	2.291	3.254	25.3
806B9H2	122	124	75.72	75.73	2.352	3.267	25.7
806B9H2	122	124	75.72	75.73	2.267	3.267	25.2
806B9H3	2	4	76.02	76.03	2.483	3.277	26.5
806B9H3	82	84	76.82	76.83	1.992	3.303	23.2
806B9H3	82	84	76.82	76.83	1.925	3.303	22.7
806B9H4	2	4	77.52	77.53	2.092	3.322	24.0
806B9H4	2	4	77.52	77.53	1.850	3.322	22.2
806B9H4	82	84	78.32	78.33	2.478	3.344	26.5
806B9H4	82	84	78.32	78.33	2.366	3.344	25.8
806B9H5	2	4	79.02	79.03	2.110	3.362	24.1

806B9H5	2	4	79.02	79.03	2.212	3.362	24.8
806B9H5	42	44	79.42	79.43	2.484	3.373	26.5
806B9H5	82	84	79.82	79.83	1.922	3.384	22.7
806B9H5	82	84	79.82	79.83	2.127	3.384	24.2
806B9H5	122	124	80.22	80.23	2.052	3.395	23.7
806B9H5	122	124	80.22	80.23	1.988	3.395	23.2
806B9H6	2	4	80.52	80.53	2.416	3.403	26.1
806B9H6	2	4	80.52	80.53	2.444	3.403	26.3
806B9H6	82	84	81.32	81.33	2.304	3.424	25.4
806B9H6	82	84	81.32	81.33	2.619	3.424	27.3
806B9H7	2	4	82.02	82.03	1.826	3.442	22.0
806B9H7	82	84	82.82	82.83	2.532	3.464	26.8
806B10H1	52	54	83.02	83.44	2.477	3.481	26.4
806B10H1	132	134	83.82	84.24	2.482	3.502	26.5
806B10H2	2	4	84.02	84.44	2.237	3.507	25.0
806B10H2	42	44	84.42	84.84	2.396	3.518	26.0
806B10H2	82	84	84.82	85.24	2.148	3.529	24.4
806B10H2	122	124	85.22	85.64	2.540	3.539	26.8
806B10H3	2	4	85.52	85.94	2.390	3.547	25.9
806B10H3	42	44	85.92	86.34	2.387	3.558	25.9
806B10H3	82	84	86.32	86.74	2.277	3.568	25.2
806B10H3	82	84	86.32	86.74	2.305	3.568	25.4
806B10H3	122	124	86.72	87.14	2.184	3.578	24.6
806B10H4	2	4	87.02	87.44	2.656	3.586	27.5
806B10H4	42	44	87.42	87.84	2.476	3.596	26.4
806B10H4	122	124	88.22	88.64	2.962	3.616	29.1
806B10H5	2	4	88.52	88.94	2.868	3.623	28.6
806B10H5	82	84	89.32	89.74	2.457	3.645	26.3
806B10H6	2	4	90.02	90.44	2.434	3.664	26.2
806B10H6	42	44	90.42	90.84	2.187	3.676	24.6
806B10H6	42	44	90.42	90.84	2.175	3.676	24.5
806B10H6	82	84	90.82	91.24	2.784	3.687	28.2
806B10H6	122	124	91.22	91.64	2.624	3.699	27.3
806B10H7	2	4	91.52	91.94	2.816	3.707	28.3
806B10H7	42	44	91.92	92.34	2.421	3.719	26.1
806B10HCC	2	4	92.15	92.57	2.750	3.725	28.0
806B11H1	62	64	92.62	93.04	2.460	3.769	26.4
806B11H1	102	104	93.02	93.44	2.616	3.781	27.3
806B11H1	142	144	93.42	93.84	2.607	3.792	27.2
806B11H2	3	5	93.53	93.95	2.668	3.795	27.5

806B11H2	82	84	94.32	94.74	2.324	3.819	25.5
806B11H3	3	5	95.03	95.45	2.451	3.840	26.3
806B11H3	132	134	96.32	96.74	2.562	3.874	26.9
806B11H4	12	14	96.62	97.04	2.153	3.881	24.4
806B11H4	92	94	97.42	97.84	2.781	3.901	28.2
806B11H5	22	24	98.22	98.64	2.641	3.920	27.4
806B11H5	62	64	98.62	99.04	2.214	3.929	24.8
806B11H6	62	64	100.12	100.54	2.495	3.964	26.6
806B11H6	142	144	100.92	101.34	2.317	3.983	25.5
806B11H7	72	74	101.72	102.14	2.318	4.002	25.5
806B12H1	22	24	101.72	102.14	2.412	4.002	26.1
806B12H1	22	24	101.72	102.14	2.265	4.002	25.1
806B12H1	102	104	102.52	102.94	2.560	4.016	26.9
806B12H1	102	104	102.52	102.94	2.511	4.016	26.6
806B12H2	32	34	103.32	103.74	2.609	4.031	27.2
806B12H2	32	34	103.32	103.74	2.604	4.031	27.2
806B12H2	112	113	104.12	104.54	2.492	4.045	26.5
806B12H2	112	113	104.12	104.54	2.531	4.045	26.8
806B12H3	2	4	104.52	104.94	2.747	4.052	28.0
806B12H3	82	84	105.32	105.74	2.596	4.066	27.1
806B12H3	82	84	105.32	105.74	2.701	4.066	27.7
806B12H4	22	24	106.22	106.64	2.804	4.082	28.3
806B12H4	102	104	107.02	107.44	2.535	4.096	26.8
806B12H4	102	104	107.02	107.44	2.975	4.096	29.1
806B12H5	22	24	107.72	108.14	2.039	4.109	23.6
806B12H5	102	104	108.52	108.94	2.497	4.123	26.6
806B12H6	2	4	109.02	109.44	2.834	4.132	28.4
806B12H6	82	84	109.82	110.24	2.984	4.146	29.2
806B12H7	12	14	110.62	111.04	2.622	4.160	27.3
806B13H1	2	4	111.02	111.44	2.541	4.167	26.8
806B13H1	82	84	111.82	112.24	2.340	4.182	25.6
806B13H2	12	14	112.62	113.04	2.582	4.196	27.1
806B13H2	92	94	113.42	113.84	2.812	4.210	28.3
806B13H2	92	94	113.42	113.84	2.731	4.210	27.9
806B13H3	22	24	114.22	114.64	2.642	4.224	27.4
806B13H3	102	104	115.02	115.44	2.756	4.239	28.0
806B13H4	31	33	115.81	116.23	2.856	4.253	28.5
806B13H4	31	33	115.81	116.23	3.013	4.253	29.3
806B13H4	112	114	116.62	117.04	2.538	4.267	26.8
806B13H5	2	4	117.02	117.44	2.582	4.274	27.1

806B13H5	82	84	117.82	118.24	2.533	4.288	26.8
806B13H6	22	24	118.72	119.14	2.531	4.304	26.8
806B13H6	102	104	119.52	119.94	2.872	4.319	28.6
806B13H7	32	34	120.32	120.74	2.490	4.333	26.5
806B14H1	32	34	120.82	121.24	2.202	4.342	24.7
806B14H1	32	34	120.82	121.24	2.520	4.342	26.7
806B14H1	123	125	121.73	122.15	2.673	4.358	27.6
806B14H1	123	125	121.73	122.15	2.828	4.358	28.4
806B14H2	2	4	122.02	122.44	2.525	4.363	26.7
806B14H2	82	84	122.82	123.24	2.622	4.377	27.3
806B14H3	2	4	123.52	123.94	2.877	4.390	28.7
806B14H3	82	84	124.32	124.74	2.489	4.404	26.5
806B14H4	33	35	125.33	125.75	2.738	4.422	27.9
806B14H4	102	104	126.02	126.44	2.443	4.434	26.2
806B14H4	102	104	126.02	126.44	2.462	4.434	26.4
806B14H5	2	4	126.52	126.94	2.488	4.443	26.5
806B14H5	82	84	127.32	127.74	2.699	4.457	27.7
806B14H6	2	4	128.02	128.44	2.974	4.470	29.1
806B14H6	82	84	128.82	129.24	2.636	4.484	27.4
806B14H6	82	84	128.82	129.24	2.618	4.484	27.3
806B14H7	18	20	129.68	130.1	2.587	4.499	27.1
806B15H1	42	44	130.42	130.84	2.289	4.512	25.3
806B15H1	102	104	131.02	131.44	2.666	4.523	27.5
806B15H2	2	4	131.52	131.94	2.663	4.532	27.5
806B15H2	82	84	132.32	132.74	2.507	4.546	26.6
806B15H2	82	84	132.32	132.74	2.560	4.546	26.9
806B15H3	42	44	133.42	133.84	2.504	4.566	26.6
806B15H3	123	125	134.23	134.65	2.127	4.580	24.2
806B15H4	2	4	134.52	134.94	2.397	4.585	26.0
806B15H4	82	84	135.32	135.74	2.873	4.599	28.6
806B15H5	2	4	136.02	136.44	2.621	4.612	27.3
806B15H5	82	84	136.82	137.24	2.892	4.626	28.7
806B15H6	2	4	137.52	137.94	2.907	4.638	28.8
806B15H6	82	84	138.32	138.74	2.694	4.653	27.7
806B15H7	2	4	139.02	139.44	2.752	4.665	28.0
806B16H1	2	4	139.52	139.94	2.685	4.674	27.6
806B16H1	82	84	140.32	140.74	3.044	4.688	29.5
806B16H1	82	84	140.32	140.74	2.855	4.688	28.5
806B16H2	2	4	141.02	141.44	2.766	4.701	28.1
806B16H2	2	4	141.02	141.44	2.575	4.701	27.0

806B16H2	82	84	141.82	142.24	2.632	4.715	27.3
806B16H2	82	84	141.82	142.24	2.754	4.715	28.0
806B16H3	2	4	142.52	142.94	3.052	4.727	29.5
806B16H3	2	4	142.52	142.94	2.513	4.727	26.7
806B16H3	82	84	143.32	143.74	2.682	4.742	27.6
806B16H3	82	84	143.32	143.74	3.017	4.742	29.4
806B16H4	62	64	144.62	145.04	2.565	4.765	27.0
806B16H4	62	64	144.62	145.04	2.792	4.765	28.2
806B16H4	102	104	145.02	145.44	3.010	4.772	29.3
806B16H4	102	104	145.02	145.44	3.005	4.772	29.3
806B16H5	42	44	145.92	146.34	2.389	4.788	25.9
806B16H5	42	44	145.92	146.34	2.425	4.788	26.1
806B16H5	123	125	146.73	147.15	2.887	4.802	28.7
806B16H5	123	125	146.73	147.15	2.981	4.802	29.2
806B16H6	2	4	147.02	147.44	2.410	4.807	26.0
806B16H6	2	4	147.02	147.44	2.388	4.807	25.9